VULNERABILITY OF COASTAL ARCHAEOLOGICAL SITES OF TURKEY TO SEA LEVEL RISE

A THESIS SUBMITTED TO
THE GRADUATE SCHOOL OF NATURAL AND APPLIED SCIENCES
OF
MIDDLE EAST TECHNICAL UNIVERSITY

BY

İREMNAZ KÖSEM

IN PARTIAL FULFILLMENT OF THE REQUIREMENTS
FOR
THE DEGREE OF MASTER OF SCIENCE
IN
CIVIL ENGINEERING

APRIL 2025

Approval of the thesis:

VULNERABILITY OF COASTAL ARCHAEOLOGICAL SITES OF TURKEY TO SEA LEVEL RISE

submitted by **İREMNAZ KÖSEM** in partial fulfillment of the requirements for the degree of **Master of Science** i**n Civil Engineering, Middle East Technical University** by,

Prof. Dr. Naci Emre Altun
Dean, **Graduate School of Natural and Applied Sciences** _____

Prof. Dr. Erdem Canbay
Head of the Department, **Civil Engineering** _____

Assist. Prof. Dr. Gülizar Özyurt Tarakcıoğlu
Supervisor, **Civil Engineering, METU** _____

Examining Committee Members:

Assoc. Prof. Dr. Elif Oğuz
Civil Engineering, METU _____

Assist. Prof. Dr. Gülizar Özyurt Tarakcıoğlu
Civil Engineering, METU _____

Assist. Prof. Dr. Cüneyt Baykal
Civil Engineering, METU _____

Assist. Prof. Dr. Hasan Gökhan Güler
Civil Engineering, METU _____

Assist. Prof. Dr. Doğan Kısacık
Civil Engineering, IZTECH _____

Date: 09.04.2025

I hereby declare that all information in this document has been obtained and presented in accordance with academic rules and ethical conduct. I also declare that, as required by these rules and conduct, I have fully cited and referenced all material and results that are not original to this work.

Name Last name : İremnaz Kösem

Signature :

ABSTRACT

VULNERABILITY OF COASTAL ARCHAEOLOGICAL SITES OF TURKEY TO SEA LEVEL RISE

Kösem, İremnaz
Master of Science, Civil Engineering
Supervisor : Assist. Prof. Dr. Gülizar Özyurt Tarakcıoğlu

April 2025, 244 pages

Coasts have always been the centers of cultural exchange and trade, which can be seen clearly by the cultural heritage sites left behind. Those sites hold the essence of a society with its art and history, in addition to providing significant resources for the land's economic and social development. With its 8333 km long coastline, Türkiye is one of the countries with numerous coastal cultural heritage sites, and it is expected that the rise of sea levels due to climate change will negatively affect those sites at different levels.

This study aims to assess the vulnerability of archaeological heritage sites protected by law along the coasts of Türkiye to sea level rise and its impacts (coastal erosion, flooding, and permanent loss of land caused by extreme water levels). For this purpose, a coastal cultural heritage vulnerability assessment model (CCHVAM) is developed and utilized. It is found that over 35% of the coastal cultural heritage sites of Turkey have high vulnerability to sea level rise based on both the SSP2-4.5 and the SSP5-8.5 scenarios. Furthermore, coastal erosion analysis is performed using the

Digital Shoreline Analysis System (DSAS) and the Shoreline Simulation (ShorelineS) Model on two of the assessed heritage sites. The analyses performed on the shorelines of the Anemurium Ancient City and the Soli-Pompeiopolis Ancient City revealed that there are many ancient buildings on the beach in these sites, and they are threatened by coastal erosion. Finally, it is found by the projections made that in these two sites, the average coastline movement is over 20 m landward by 2050.

Keywords: Vulnerability Assessment, Climate Change, Coastal Erosion, Cultural Heritage, Sea Level Rise.

ÖZ

TÜRKİYE KIYILARINDA BULUNAN ARKEOLOJİK ALANLARIN DENİZ SEVİYESİ YÜKSELMESİNE OLAN KIRILGANLIĞI

Kösem, İremnaz
Yüksek Lisans, İnşaat Mühendisliği
Tez Yöneticisi: Dr. Öğr. Üye. Gülizar Özyurt Tarakcıoğlu

Nisan 2025, 244 sayfa

Kıyılar, tarih boyunca kültürel etkileşimin ve ticaretin merkezleri olmuştur, günümüze ulaşan kültürel miras alanları da bunu açıkça göstermektedir. Bu alanlar, sanatsal ve tarihi nitelikleriyle toplumun özünü yansıtırken aynı zamanda da ekonomik ve sosyal kalkınma için önemli kaynaklar sağlıyor. 8333 km uzunluğundaki kıyı şeridiyle Türkiye, çok sayıda kültürel miras alanına sahip ülkelerden biridir. Ancak iklim değişikliği sebebiyle deniz seviyesinin yükselmesi ve bu alanları olumsuz etkilemesi öngörülmektedir.

Çalışma kapsamında, Türkiye kıyılarında bulunan ve ilgili yasalarla koruma altına alınmış olan arkeolojik miras alanlarının deniz seviyesinin yükselmesi ve etkilerine (kıyı erozyonu, su baskını ve ekstrem su seviyeleri sebebiyle kalıcı arazi kaybı) karşı kırılganlığı değerlendirilmiştir. Bu amaçla, miras alanlarının bulunduğu kıyıların kırılganlığını, bu alanların hassasiyetleri ve uyum kapasiteleri ile bütünleştiren bir Kültürel Miras Kırılganlık Değerlendirme Modeli (CCHVAM) geliştirilmiş ve kullanılmıştır. Yapılan analizler sonucunda, Türkiye'deki kıyısal kültürel miras alanlarının %35'ten fazlasının, hem SSP2-4.5 hem de SSP5-8.5 senaryolarına göre,

deniz seviyesi yükselmesine karşı yüksek kırılganlığa sahip olduğu belirlenmiştir. Ayrıca değerlendirilen alanlardan iki tanesi için kıyı erozyonu analizi da yapılarak model çıktılarının tutarlılığı kontrol edilmiştir. Anemurium Antik Kenti ve Soli-Pompeiopolis Antik Kenti kıyılarında DSAS ve ShorelineS Modeli ile yapılan analizler, bu alanlardaki birçok antik yapının doğrudan sahilde bulunduğunu ve kıyı erozyonu tehdidi altında olduğunu ortaya koymuştur. Son olarak, yapılan projeksiyonlar, bu iki bölgede 2050 yılına kadar kıyı çizgisinin kıyı yönünde 20 metreden fazla ilerleyeceğini göstermiştir.

Anahtar Kelimeler: Kırılganlık Analizi, İklim Değişikliği, Kıyı Erozyonu, Kültürel Miras, Deniz Seviyesi Yükselmesi.

Dedicated to those who never lose hope and to the great blue

ACKNOWLEDGMENTS

To begin with, I want to extend my heartfelt thanks to Mustafa Kemal Atatürk. His boundless hope, remarkable intellect, exceptional leadership, and vision have truly inspired millions. As a young woman striving to make a difference, regardless of how big or small, I am truly grateful for his groundbreaking reforms that created pathways for everyone in this country to aspire and achieve. His commitment to science, art, the humanities, and education will forever act as my guiding light.

I want to express my gratitude to my mom, my grandma, my brother, and my aunt wholeheartedly. Achieving this would not have been possible without your support. I truly appreciate your constant encouragement to persevere. You have always had faith in me, even during times when I struggled to believe in myself. I also want to thank my dear little boy, Şaşkın. You have been more than just a cute cat. Thanks for allowing me to pet you whenever I need emotional support.

I want to sincerely thank my supervisor, Dr. Gülizar Özyurt Tarakcıoğlu, for her unwavering support and guidance during this long and challenging journey. Her discipline, expertise, inspiring curiosity, and patient mentorship encouraged me and influenced both this research and my development as a scholar. It has been a genuine honor to study alongside her and gain insights from her.

I want to thank Prof. Dr. Ayşen Ergin for inspiring me to explore coastal engineering and enjoy life each and every day. Her knowledge, her love for art, and her enthusiasm to celebrate life are truly unmatched and inspiring. Thank you, professor, for helping me get to know the waves and you. I feel so lucky to be one of your students.

I wish to extend my heartfelt gratitude to my wonderful professors: Prof. Dr. Ahmet Cevdet Yalçıner, Assist. Dr. Cüneyt Baykal, Assist. Dr. Hasan Gökhan Güler, and Dr. Işıkhan Güler. Their relentless dedication to working, learning, and sharing their

knowledge with students has continually inspired and motivated me during my academic experience with them.

I would like to thank my great friend, İlayda Demir. Thank you for asking for that pencil on the very first day of school. I cannot even think how boring and sad my life would be without you. Thank you for never letting me feel alone, especially when I am suffering from my anxiety.

I would love to thank Arif Çağatay Uysal, my precious friend and confidante, yes, I call you that, too. Thank you for always being by my side. From prep school to this day, you have always been with me, literally, in my best and worst moments. Thanks for encouraging me to move forward and for making fun of me when it is absolutely needed. I want to thank Elif Ayşe Öztürk Çambal for being such an amazing friend. Your attitude, your support, and your friendship are truly unmatched. I feel so lucky to have you in my life.

I would like to express my sincere gratitude to all the amazing people that I met during this journey: Ayşenur Gökdağ, Bilge Karakütük, Setenay Özaslan, Alperen Korkmaz, Akdeniz İnce, Mustafa Erdoğan, Furkan Demir, Barış Ufuk Şentürk, Görkem Kılıç, Cem Sevindik, Doğaç Sayar, Günay Gazaloğlu, Mert Yaman, Can Albayrak, and Semih Can. You guys made this challenging process so much fun and enjoyable. I have so many things to say and thank you for. Thanks for making every moment with you in this lab, at the conferences, and our great parties priceless.

I would like to thank everyone at Prota Software, my great friends and managers. Thank you for supporting and motivating me throughout this entire journey. Thanks for tolerating a sleepless and tired version of me on many days.

Lastly, I want to appreciate the help of Prof. Dr. Mehmet Tekocak (Head of Anemurium Archaeology Team), Prof. Dr. Musa Kadıoğlu (Head of Teos Archaeology Team), and Prof. Dr. Deniz Kaplan (Head of Soli-Pompeipolis Archaeology Team) during our visits to the sites. Also, I want to highlight that this thesis is partially funded by TÜBİTAK ARDEB Project 122M613.

TABLE OF CONTENTS

ABSTRACT v

ÖZ vii

ACKNOWLEDGMENTS x

TABLE OF CONTENTS xii

LIST OF TABLES xvi

LIST OF FIGURES xxi

LIST OF ABBREVIATIONS xxxii

CHAPTERS

1 INTRODUCTION 1

2 LITERATURE REVIEW 5

2.1 Observed Impacts of Climate Change 5

2.2 Projections For Future Sea Level Rise 8

2.3 Impact of Climate Change-Induced Sea Level Rise on Coastal Cultural Heritage Sites 11

2.4 Vulnerability Assessment of Cultural Heritage Sites 13

2.5 Impacts of Coastal Erosion on Coastal Cultural Heritage Sites 19

3 VULNERABILITY ASSESSMENT OF COASTAL CULTURAL HERITAGE SITES OF TÜRKİYE TO SEA LEVEL RISE 23

3.1 Framework of the Coastal Cultural Heritage Vulnerability Assessment Model… 24

3.1.1 Geographical Definitions of Coastal Cultural Heritage Site 25

3.1.2 Components of CCHVAM 26

3.2 Data Utilized in the Vulnerability Assessment 43

3.2.1 Coastal Archaeological Heritage Sites of Türkiye 44
3.2.2 Data Utilized for the Exposure Component 46
3.2.3 Data Utilized for the Sensitivity Component 52
3.2.4 Data Utilized for the Adaptive Capacity Component 58
3.3 Discussions About Methodology and Data 61
3.3.1 Class Limits of Sensitivity Indicators 62
3.3.2 The Impact of Weights on the Computation of Sensitivity Value .. 62
3.3.3 Limit Values of the Sensitivity Classes 64
4 SHORELINE EVOLUTION MODELING WITH THE DIGITAL SHORELINE ANALYSIS SYSTEM (DSAS) 71
4.1 Computation Process in DSAS 72
4.2 Study Area 75
4.2.1 Anemurium Ancient City 76
4.2.2 Soli-Pompeiopolis Ancient City 80
4.3 Input Data 84
4.3.1 Shoreline Data 86
4.3.2 Baseline Data 88
4.3.3 Transects 89
5 SHORELINE EVOLUTION MODELING WITH THE SHORELINE SIMULATION (ShorelineS) MODEL 93
5.1 Input Data 94
5.1.1 Shoreline Data 95
5.1.2 Structures Along the Coastline 96
5.1.3 Wave Conditions 99

5.1.4 Foreshore Orientation 104
5.1.5 Offshore Depth and Nearshore Depth 105
5.1.6 Active Profile Height 108
5.1.7 Boundary Conditions 110
5.1.8 Climate Change Parameters 111
5.2 Calibration of the Longshore Sediment Transport Formula 112
6 RESULTS & DISCUSSIONS 117
6.1 Vulnerability Assessment of the Coastal Archaeological Heritage Sites of Türkiye 117
6.1.1 Sensitivity Values of the Assessed Heritage Sites 118
6.1.2 Adaptive Capacity of the Coastal Archaeological Sites of Türkiye….. 124
6.1.3 Vulnerability Assessment for the Conditions of SSP2-4.5 Scenario…… 126
6.1.4 Vulnerability Assessment for the Conditions of SSP5-8.5 132
6.1.5 Vulnerability Assessment with the Coastal Erosion Impact Scores Based on SSP2-4.5 Scenario 137
6.1.6 Vulnerability Assessment with the Coastal Erosion Impact Scores Based on SSP5-8.5 Scenario 142
6.1.7 Comparison of the Vulnerability Classes Determined Based on SSP2-4.5 and SSP5-8.5 Scenarios 147
6.2 Shoreline Evolution with the DSAS 152
6.2.1 Anemurium Ancient City 153
6.2.2 Soli-Pompeiopolis Ancient City 176

6.3 Shoreline Evolution Modeling with the Shoreline Simulation (ShorelineS) Model 200
6.3.1 Projected Shoreline for the Year 2050 201
6.3.2 Projected Shoreline Evolution by 2050 Considering the Impact of Climate Change 203
6.4 Discussions on the 2050 Projections 207
7 CONCLUSION 211
REFERENCES 217
8 APPENDICES 225
A. Assessment of the Impact of Weights Through the Schematic View 225
B. Wave Climate Data 227
C. Properties of Each Sensitivity Class 229
D. Results of Shoreline Evolution Modeling with DSAS Using Transects with Spacings of 100 m 233

LIST OF TABLES

TABLES

Table 2.1. SLR and RSLR values projected in SSP scenarios with ranges and median values (IPCC AR6 WGI, Chapter 9, Table 9.9, 2021). 11
Table 3.1. Physical and human influence parameters that are utilized to obtain the vulnerability indices to each impact of sea level rise (Ozyurt, 2010; Ince, 2024). . 29
Table 3.2. Limiting CVI values of the exposure classes. 30
Table 3.3. Sensitivity classes of each sensitivity indicator. 33
Table 3.4. Limiting values of the sensitivity classes. 34
Table 3.5. Standard Preference Scale used in AHP (Saaty, T. L., 1990). 36
Table 3.6. The judgment matrix formed to perform the pairwise comparison for the sensitivity indicators. 37
Table 3.7. Computation of the weights of sensitivity indicators. 38
Table 3.8. Adaptive capacity classes of each indicator. 40
Table 3.9. Adaptive capacity classes and their limiting values. 41
Table 3.10. Regional distribution of the sites based on CVI values obtained for the SSP2-4.5 emission scenario (Ince, 2024). 48
Table 3.11. Regional distribution of the sites based on CVI values obtained for the SSP5-8.5 emission scenario (Ince, 2024). 49
Table 3.12. Regional distribution of the sites based on erosion impact scores obtained for the SSP2-4.5 emission scenario (Ince, 2024). 50
Table 3.13. Regional distribution of the sites based on erosion impact scores values obtained for the SSP5-8.5 emission scenario (Ince, 2024). 51
Table 3.14. Land use/land cover classes assessed in the scope of Copernicus' Land Cover/Land Use Change dataset. 59
Table 3.15. Computation of the sensitivity values of Site-31 and Site-38. 64
Table 3.16. Elevation and proximity indicator sensitivity classes observed in sites assigned to each sensitivity class. 66

Table 3.17. Elevation and proximity indicator sensitivity classes observed in sites assigned to each sensitivity class. 69
Table 3.18. Distribution of the assessed sites based on old and new sensitivity class limits. 70
Table 4.1. Dates of the shoreline data utilized in the assessment of Anemurium and Soli-Pompeiopolis shorelines. 85
Table 5.1. Parameters of the equation of sediment conservation. 94
Table 5.2. The deep-water wave parameters and the depth-of-closure values computed for each direction. 107
Table 5.3. Frequency table showing the frequency (in hours) and significant wave height observed in each direction over the last 50 years. 107
Table 5.4. The biascm, RMSE, and the average value of the absolute distances between the generated and observed shorelines along the transects, which are obtained using the given calibration factors. 114
Table 6.1. Regional distribution of the assessed heritage sites with sensitivity levels ranging from very high to very low. 119
Table 6.2. Regional distribution of the assessed heritage sites that are located directly on the shoreline, where the shortest distance to the shoreline (x) is equal to zero for each of these sites. 120
Table 6.3. The regional distribution of the sites grouped by their adaptive capacity classes. 126
Table 6.4. Regional distribution of the assessed heritage sites grouped by their potential impact classes obtained by using the CVI values based on the data of the SSP2-4.5 scenario. 128
Table 6.5. The regional distribution of the coastal archaeological sites of Türkiye grouped by their vulnerability classes obtained by using the data of the SSP2-4.5 scenario. 130
Table 6.6. Regional distribution of the coastal archaeological sites of Türkiye grouped by their potential impact classes determined by the CCHVAM using the CVI values obtained from the data of the SSP5-8.5 scenario. 133

Table 6.6. Regional distribution of the coastal archaeological sites of Türkiye grouped by their potential impact classes determined by the CCHVAM using the CVI values obtained from the data of the SSP5-8.5 scenario. 134
Table 6.7. Regional distribution of the coastal archaeological sites of Türkiye grouped by their vulnerability classes determined by the CCHVAM using the CVI values obtained from the data of the SSP5-8.5 scenario. 135
Table 6.8. Regional distribution of the coastal archaeological sites of Türkiye grouped by their potential impact classes determined by the CCHVAM using the erosion impact scores obtained from the data of the SSP2-4.5 scenario. 139
Table 6.9. Regional distribution of the coastal archaeological sites of Türkiye grouped by their vulnerability classes determined by the CCHVAM using the erosion impact scores obtained from the data of the SSP2-4.5 scenario. 140
Table 6.10. Regional distribution of the coastal archaeological sites of Türkiye based on their potential impact classes determined by the CCHVAM using the coastal erosion impact scores obtained from the data of the SSP5-8.5 scenario... 144
Table 6.11. Regional distribution of the coastal archaeological sites of Türkiye based on their vulnerability classes determined by the CCHVAM using the coastal erosion impact scores obtained from the data of the SSP5-8.5 scenario. 146
Table 6.12. Comparison of the number of sites in each potential impact class obtained when the SSP2-4.5 and SSP5-8.5 scenarios are followed in the computation of CVI values. 148
Table 6.13. Comparison of the number of sites in each vulnerability class obtained when the SSP2-4.5 and SSP5-8.5 scenarios are followed for the CVI values. 149
Table 6.14. Comparison of the number of sites in each potential impact class obtained when the SSP2-4.5 and SSP5-8.5 scenarios are followed for the erosion impact scores. 150
Table 6.15. Comparison of the number of sites in each vulnerability class obtained when the SSP2-4.5 and SSP5-8.5 scenarios are followed for the erosion impact scores. 151

Table 6.16. The distribution of sites based on their vulnerability classes determined by the CCHVAM using CVI values and the coastal erosion impact scores as exposure values, separately. 152
Table 6.17. The CVI values and the coastal erosion impact scores obtained from the FCVAM and utilized as the exposure component of the CCHVAM..... 153
Table 6.18. The indicator values assessed to obtain the sensitivity component of the CCHVAM. 154
Table 6.19. The indicator values assessed to obtain the adaptive capacity component of the CCHVAM. 154
Table 6.20. Values obtained from the CCHVAM for each vulnerability component and the final vulnerability value of Anemurium Ancient City. 155
Table 6.21. Shoreline change envelope values obtained from both transects with 50 m spacing and transects with a spacing of 100 m. 157
Table 6.22. Net shoreline movement values obtained from both transects with 50 m spacing and transects with a spacing of 100 m. 157
Table 6.23. Statistical values of the endpoint rate at each transect obtained from both the transects with a spacing of 50 meters and the transects with a spacing of 100 meters. 160
Table 6.24. Statistical values of the linear regression rate at each transect obtained from both the transects with a spacing of 50 meters and the transects with a spacing of 100 meters. 161
Table 6.25. The coastal vulnerability indices obtained from the FCVAM and utilized as the exposure component of the CCHVAM. 177
Table 6.26. The indicator values assessed to obtain the sensitivity component of the CCHVAM. 177
Table 6.27. The indicator values assessed to obtain the adaptive capacity component of the CCHVAM. 178
Table 6.28. Values obtained from the CCHVAM for each vulnerability component and the final vulnerability value of Soli-Pompeiopolis Ancient City. 179

Table 6.29. Shoreline change envelope values obtained from both transects with 50 m spacing and transects with a spacing of 100 m. 180
Table 6.30. Net shoreline movement values obtained from both transects with 50 m spacing and transects with a spacing of 100 m. 181
Table 6.31. Statistical values of the endpoint rate at each transect obtained from both the transects with a spacing of 50 meters and the transects with a spacing of 100 meters. 183
Table 6.32. Statistical values of the linear regression rate at each transect obtained from both the transects with a spacing of 50 meters and the transects with a spacing of 100 meters. 184
Table 6.33. The average net shoreline movement, average erosional and accretional shoreline movement, and the total areas where erosional and accretional changes are projected by the LRR values and the simulations performed with the ShorelineS Model. 209
Table 8.1. Computation matrix utilized to determine the sensitivity value of Site 33, assuming that each indicator has equal weight. 225
Table 8.2. The sensitivity value of each site shown in Figure 7.5 is computed as described above. 226

LIST OF FIGURES

FIGURES

Figure 2.1. Geographical distribution of the massive natural disasters that occurred in the first half of 2024 (WTW, July 2024). 6
Figure 2.2. Annual global mean temperature anomalies recorded between 1850 and 2024 relative to 1850-1900 obtained from six datasets (WMO, 2024). 7
Figure 2.3. Global mean sea level recorded between 1993 and 2023 (WMO, 2024). 8
Figure 2.4. The effective radiative forcings of GHGs in five SSPs are compared (IPCC AR6-WGI, 2021). 10
Figure 2.5. Cultural sites on the World Heritage List of UNESCO in Europe (UNESCO World Heritage Online Map, December 2024). 12
Figure 2.6. Comparison of the terms given in the 4th (AR4) and 5th (AR5) Assessment Reports of the IPCC. 15
Figure 2.7. The CVI framework proposed by the ICOMOS (Day et al., 2020). 18
Figure 3.1. Sample sites that are in the scope of the CCHVAM based on the defined criteria. 26
Figure 3.2. The flowchart followed by the CCHVAM to obtain the vulnerability of the OUV (Day et al., 2020). 27
Figure 3.3. Decision hierarchy for the sensitivity component of the CCHVAM. .. 35
Figure 3.4. Decision-matrix of potential impact utilized in the CCHVAM. 42
Figure 3.5. Vulnerability Matrix utilized in the CCHVAM. 43
Figure 3.6. Registered archaeological sites in Türkiye as shown in the GIS layer obtained from the Ministry of Culture and Tourism (2023). 44
Figure 3.7. The archaeological sites assessed by utilizing the CCHVAM in this study. 45
Figure 3.8. The GIS layer providing the exposure data. 47
Figure 3.9. Distribution of the assessed coastline segments along the coastline of Türkiye. 48

Figure 3.10. Distribution of the assessed coastline segments along the coastline of Türkiye. 49
Figure 3.11. Distribution of the assessed coastline segments along the coastline of Türkiye grouped by their exposure classes. 50
Figure 3.12. Distribution of the assessed coastline segments along the coastline of Türkiye grouped by their exposure classes. 51
Figure 3.13. The heritage polygon of Side Ancient City and the polygon that shows the part of the heritage polygon below 10 meters elevation. 53
Figure 3.14. Heritage sites and the number of those in elevation indicator classes. 53
Figure 3.15. Heritage sites and the number of those in area indicator classes. 54
Figure 3.16. The shortest distance of each heritage site is measured between the boundary of the heritage polygon and the closest shoreline segment. 55
Figure 3.17. Heritage sites and the number of those in proximity indicator classes. 56
Figure 3.18. The coastline segment directly interacting with the Anemurium Ancient City, which is determined in the scope of this study. 57
Figure 3.19. Heritage sites and the number of those in interaction length indicator classes. 57
Figure 3.20. Geographical distribution of the sites based on the degree of protection indicator. 58
Figure 3.21. a. Land use in the region of Side Ancient City, b. Side Ancient City heritage polygon and the buffer zone, c. The urban area around the Ancient City, d. The urban area intersecting with the heritage site polygon and the buffer. 60
Figure 3.22. Heritage sites and the number of those in urbanization indicator classes. 61
Figure 3.23. Schematic view where representative heritage sites with different positions along the coastline are shown. 63
Figure 3.24. Distribution of sites based on their proximity and elevation indicator classes, and they are grouped based on their overall sensitivity values. 65

Figure 3.25. Grouped scatter plot showing the distribution of sites based on their proximity parameter and sensitivity values, and grouped by their elevation indicator. 67
Figure 3.26. Distribution of sites based on their overall sensitivity values and their proximity parameter value after the class limits are modified. 68
Figure 4.1. The interface of DSAS v6.0.168 with the input data for the analysis of the shoreline segment interacting with the Soli-Pompeiopolis Ancient City loaded. 73
Figure 4.2. The illustration describing how the values of net shoreline movement, shoreline change envelope and end point rate are computed (Himmelstoss, E.A., et al., 2021. Digital Shoreline Analysis System (DSAS) Version 5.1 User Guide). .. 74
Figure 4.3. a. The Mediterranean coastline of Türkiye where Mersin and the assessed sites are highlighted. b. Location of Anemurium Ancient City in Anamur, Mersin. c. Location of Soli-Pompeiopolis Ancient City in Mezitli, Mersin (Google Earth, 2024). 75
Figure 4.4. Necropolis and acropolis of Anemurium Ancient City (Tekocak, M., 2021). 76
Figure 4.5. Top view of the Anemurium Ancient City captured by a UAV on September 21, 2024, during the site visit. 77
Figure 4.6. Some of the structures located on the beach of Anemurium Ancient City, photo taken by İremnaz Kösem during the site visit on September 21, 2024. 78
Figure 4.7. Some parts of the structures where the coastal material is taken away by the waves leaving gaps in the bottom parts of the structures, photo taken by İremnaz Kösem during the site visit on September 21, 2024. 79
Figure 4.8. The ancient harbor of the Soli-Pompeiopolis Ancient City captured on September 20, 2024, by a UAV during the site visit. 80
Figure 4.9. The Colonnade Street of the Soli-Pompeiopolis Ancient City, photo taken by İremnaz Kösem during the site visit on September 20, 2024. 81
Figure 4.10. The breakwater in the eastern part of the harbor, photo taken by İremnaz Kösem during the site visit on September 20, 2024. 82

Figure 4.11. The breakwater in the western part of the harbor, photo taken by İremnaz Kösem during the site visit on September 20, 2024. 82
Figure 4.12. Top of the western breakwater of the harbor, photo taken by İremnaz Kösem during the site visit on September 20, 2024. 83
Figure 4.13. Excavation site on the beach of Soli-Pompeiopolis (IHA, November 2023). 84
Figure 4.14. SENTINEL-2 satellite images of the Soli region from the years 2024 and 2016. The control points are shown with yellow points on these images. 86
Figure 4.15. Satellite images of Anemurium Ancient City acquired in the years 2024 and 2016. The purple points in those show the control points utilized for georeferencing. 86
Figure 4.16. Layers obtained throughout the data preparation process. 88
Figure 4.17. The baselines and the latest shorelines obtained for both study areas are shown. 89
Figure 4.18. ID numbers and locations of the transects along the assessed coastline of Anemurium Ancient City. 90
Figure 4.19. ID numbers and locations of the transects along the assessed coastline of Soli-Pompeiopolis Ancient City. 91
Figure 5.1. Points of which the coordinates are utilized as the input for the shoreline observed on September 29, 2024. 96
Figure 5.2. a. The jetty on the west edge of the large canal, b. Jetties on both edges of the narrow canal, c. The angled groin located in the middle of the assessed shoreline segment. 97
Figure 5.3. The structures located along the assessed shoreline, and the close-up view of Groin-3. 98
Figure 5.4. The point at which the data of wave conditions is acquired from the Copernicus database. 99
Figure 5.5. The monthly mean significant wave height observed in each month from September 2016 to September 2024, and the trendline with a slope of -0.0007. 100

Figure 5.6. The wave rose obtained by utilizing the wave conditions observed between September 2016 and September 2024. 101
Figure 5.7. The distribution of the waves in wave direction bins with equal total energy flux with a wave height class per direction. 103
Figure 5.8. Wave rose created by using the hourly significant wave height data with the temporal coverage between January 1974 and November 2024, obtained at (36 N, 33E) from the Copernicus database (https://cds.climate.copernicus.eu). 104
Figure 5.9. The contour lines generated using bathymetry data across the foreshore area, and the transect line showing the orientation angle, determined as 140 degrees from the North. 105
Figure 5.10. The relation of deep-water significant wave height and cumulative exceedance probability in each direction, determined by the LTWS. 108
Figure 5.11. The transects along which the profile views are created in ArcGIS Pro. 109
Figure 5.12. a. The elevation plots generated along the transects numbered 0, 1, and 2 in ArcGIS Pro. b. The elevation plots generated along the transects numbered 6, 7, and 8 in ArcGIS Pro. 110
Figure 5.13. Maximum hourly significant wave heights observed in each year between January 1, 1974 and November 11, 2024. 112
Figure 5.14. The transect layer utilized to check the consistency of the generated shoreline with the calibration factor of b=2.5e4 with the shoreline observed in September 2024 (ArcGIS Pro). 113
Figure 5.15. Shorelines generated by using the following values of the calibration factor; 1e5, 4.5e4, and 2e4, and the shoreline observed on September 29, 2024 (ArcGIS Pro). 115
Figure 6.1. Distribution of the heritage sites with very high, high, moderate, low, and very low sensitivity along the coastline of Türkiye. 119
Figure 6.2. Regional distribution of the sites located on the shoreline. 121
Figure 6.3. Histograms of the sites with very high sensitivity based on proximity, elevation, area, and interaction length indicators. 124

Figure 6.4. The distribution of the coastal archaeological sites of Türkiye based on their adaptive capacity classes. 125
Figure 6.5. Distribution of the coastal archaeological sites based on their potential impact classes. 127
Figure 6.6. Distribution of the coastal archaeological sites of Türkiye based on their vulnerability classes. 129
Figure 6.7. Distribution of the coastal archaeological sites of Türkiye based on vulnerability classes and proximity indicator values. 131
Figure 6.8. Distribution of the coastal archaeological sites of Türkiye based on their potential impact classes determined by the CCHVAM for the SSP5-8.5 scenario. 133
Figure 6.9. Distribution of the coastal archaeological sites of Türkiye based on their vulnerability classes, when the exposure data is obtained from the CVI values based on the SSP5-8.5 scenario. 135
Figure 6.10. The shortest distances of the assessed coastal archaeological sites of Türkiye in each vulnerability class, assigned by the CCHVAM. 136
Figure 6.11. Distribution of the coastal archaeological sites of Türkiye based on their potential impact classes determined by the CCHVAM for the SSP2-4.5 scenario. 138
Figure 6.12. Distribution of the coastal archaeological sites of Türkiye based on their vulnerability classes, when the exposure values are the erosion impact scores obtained from the data of the SSP2-4.5 scenario. 140
Figure 6.13. The shortest distances of the assessed coastal archaeological sites of Türkiye in each vulnerability class, assigned by the CCHVAM. 142
Figure 6.14. Distribution of the coastal archaeological sites of Türkiye based on their potential impact classes determined by the CCHVAM using the coastal erosion impact scores obtained from the data of the SSP5-8.5 scenario. 143
Figure 6.15. Distribution of the coastal archaeological sites of Türkiye based on their vulnerability classes, when the coastal erosion impact scores are obtained from the data of the SSP5-8.5 scenario. 145

Figure 6.16. The shortest distances of the assessed coastal archaeological sites of Türkiye in each vulnerability class, assigned by the CCHVAM. 147
Figure 6.17. The transect layer with 50-m spacings exported from the DSAS, providing the analysis results, and grouped based on the LRR values computed at each of them. 156
Figure 6.18. The shorelines observed in 2016 and 2024 obtained from the SENTINEL-2 satellite imagery in ArcGIS Pro. 159
Figure 6.19. The linear regression rate of shoreline movement observed between the years 2016 and 2024, obtained from the transects with equal spacings of 50 m. 163
Figure 6.20. The shoreline observed in 2024 and the one projected by using the LRR values computed at the transects with 50 m spacing. 164
Figure 6.21. Comparison of the net shoreline movement measured and the net shoreline movement between the projected 2024 shoreline and the 2016 shoreline, where the transects overlaying the heritage site area are highlighted with the red area. 165
Figure 6.22. Distance between the shoreline observed in 2024 and the projected one by using the LRR values at transects with 50 m spacing. 166
Figure 6.23. Comparison of the actual and projected shoreline movements between 2016 and 2024. 167
Figure 6.24. The projected 2050 shoreline (purple) and the shoreline observed in September 2024 (red) along the Anemurium Ancient City, obtained from the transects with equal spacings of 50 m. 169
Figure 6.25. The shoreline positions projected to be observed by 2050 by using the LRR values obtained from the transects with 50 m-spacing and the transects with equal spacings of 100 m. 170
Figure 6.26. Projected shorelines for the year 2050 by utilizing the LRR and the EPR are compared with each other and the shoreline observed in 2024. 171

Figure 6.27. The parts of the assessed shoreline that are projected to be eroded and accreted by the year 2050 are based on the rates computed by utilizing the transects with 50-meter spacing. 172
Figure 6.28. The projected 2100 shoreline (purple) and the shoreline observed in September 2024 (red) along the Anemurium Ancient City, obtained from the transects with equal spacings of 50 m. 174
Figure 6.29. The parts of the assessed shoreline that are projected to be eroded and accreted by the year 2100 are based on the rates computed by utilizing the transects with 50-meter spacing. 175
Figure 6.30. The shorelines observed in 2016 and 2024, and the projected one for the year 2050 by using the transects with 50-meter spacings. 176
Figure 6.31. The shoreline positions observed in 2016 and 2024. 182
Figure 6.32. The linear regression rate of shoreline movement observed between the years 2016 and 2024, obtained from the transects with equal spacings of 50 m. 186
Figure 6.33. The shoreline position observed in 2024 and the projected one using the LRR values computed at transects with 50 m of spacing. 187
Figure 6.34. Comparison of the net shoreline movement measured and the net shoreline movement between the projected 2024 shoreline and the 2016 shoreline, where the transects overlaying the heritage site area are highlighted as the red area. 188
Figure 6.35. The distance between the original shoreline and the projected shoreline for the year 2024 is calculated at each transect. The heritage site area along the analyzed shoreline is highlighted with the red rectangle. 189
Figure 6.36. Comparison of the projected shoreline movement between 2016 and 2024 by using the LRR values of the transects with spacing values of 50 m and 100 m. 190
Figure 6.37. Comparison of the actual and projected shoreline movements between the years 2016 and 2024. 191

Figure 6.38. The projected 2050 shoreline (blue) and the shoreline observed in 2024 (red) along the Soli-Pompeiopolis Ancient City, obtained from the transects with equal spacings of 50 m. 192
Figure 6.39. The parts of the assessed shoreline that are projected to be eroded and accreted by the year 2050 are based on the rates computed by utilizing the transects with 50-meter spacing. 193
Figure 6.40. The shorelines projected for the year 2050 by using the LRR values at the transects with the spacing values of 50 m (blue) and 100 m (red). 194
Figure 6.41. Projected shorelines for the year 2050 by utilizing the LRR and the EPR are compared with each other and the shoreline observed in 2024. 195
Figure 6.42. The projected 2100 shoreline (blue) and the shoreline observed in 2024 (red) along the Soli-Pompeiopolis Ancient City, obtained from the transects with equal spacings of 50 m. 197
Figure 6.43. The parts of the assessed shoreline that are projected to be eroded and accreted by the year 2100 are based on the rates computed by utilizing the transects with 50-meter spacing. 198
Figure 6.44. Comparison of projected shorelines for the years 2100 and 2050 to the shoreline recorded in 2024 along the assessed shoreline and over the heritage site (red). 199
Figure 6.45. Shoreline resulting from the simulated shoreline evolution by 2050 and the shoreline observed on September 29, 2024 (ArcGIS Pro). 201
Figure 6.46. Based on the 2050 projection, the areas where the erosional and accretional changes are measured. 202
Figure 6.47. Shoreline resulting from the simulated shoreline evolution by 2050 with the RSLR input parameter (ccSLR), and the shoreline observed on September 29, 2024 (ArcGIS Pro). 204
Figure 6.48. Based on the 2050 projection with the RSLR input parameter, the areas where the erosional and accretional changes are measured. 205

Figure 6.49. Shoreline resulting from the simulated shoreline evolution by 2050 with the RSLR (ccSLR) and rate of change in wave height (ccHS) input parameters, and the shoreline observed on September 29, 2024 (ArcGIS Pro). ... 206
Figure 6.50. Based on the 2050 projection with the RSLR (ccSLR) and rate of change in wave height (ccHS) input parameters, the areas where the erosional and accretional changes are measured. ... 207
Figure 6.51. The shorelines obtained from the 2050 projections performed by using the results of the DSAS and the simulations performed with the ShorelineS Model. ... 208
Figure 6.52. The remainings of the Anemurium Ancient City located on the shore where erosional change is projected in the ShorelineS Model simulation with the RSLR input. ... 210
Figure 8.1. Schematic view where representative heritage sites with different positions along the coastline are shown. ... 225
Figure 8.2. Distribution of the sites with very low sensitivity based on indicator values. ... 229
Figure 8.3. Distribution of the sites with low sensitivity based on indicator values. ... 230
Figure 8.4. Distribution of the sites with moderate sensitivity based on indicator values. ... 231
Figure 8.5. Distribution of the sites with high sensitivity based on indicator values. ... 232
Figure 8.6. The linear regression rate of shoreline movement observed between the years 2016 and 2024, obtained from the transects with equal spacings of 100 m. 233
Figure 8.7. The shoreline observed in 2024 and the one projected by using the LRR values computed at the transects with 100 m spacing. ... 234
Figure 8.8. The projected 2050 shoreline (blue) and the shoreline observed in September 2024 (red) along the Anemurium Ancient City, obtained from the transects with equal spacings of 100 m. ... 235

Figure 8.9. The parts of the assessed shoreline that are projected to be eroded and accreted by the year 2050 are based on the rates computed by utilizing the transects with 100-meter spacing. 236
Figure 8.10. The projected 2100 shoreline (blue) and the shoreline observed in September 2024 (red) along the Anemurium Ancient City, obtained from the transects with equal spacings of 100 m. 237
Figure 8.11. The parts of the assessed shoreline that are projected to be eroded and accreted by the year 2100 are based on the rates computed by utilizing the transects with 100-meter spacing. 238
Figure 8.12. The linear regression rate of shoreline movement observed between the years 2016 and 2024, obtained from the transects with equal spacings of 100 m. 239
Figure 8.13. The shoreline position observed in 2024 and the projected one using the LRR values computed at transects with 100 m of spacing. 240
Figure 8.14. The projected 2050 shoreline (blue) and the shoreline observed in 2024 (red) along the Soli-Pompeiopolis Ancient City, obtained from the transects with equal spacings of 100 m. 241
Figure 8.15. The parts of the assessed shoreline that are projected to be eroded and accreted by the year 2050 are based on the rates computed by utilizing the transects with 100-meter spacing. 242
Figure 8.16. The projected 2100 shoreline (blue) and the shoreline observed in 2024 (red) along the Soli-Pompeiopolis Ancient City, obtained from the transects with equal spacings of 100 m. 243
Figure 8.17. The parts of the assessed shoreline that are projected to be eroded and accreted by the year 2100 are based on the rates computed by utilizing the transects with 100-meter spacing. 244

LIST OF ABBREVIATIONS

ABBREVIATIONS

AC	Adaptive Capacity
CCHVAM	Coastal Cultural Heritage Vulnerability Assessment Model
CRVI	Cultural Resource Vulnerability Index
CVI	Coastal Vulnerability Index
DoP	Degree of Protection
EM-DAT	Emergency Events Database
DSAS	Digital Shoreline Analysis System
FCVAM	Fuzzy Coastal Vulnerability Assessment Model
GHGs	Greenhouse gases
ICOMOS	International Council on Monuments and Sites
IPCC	Intergovernmental Panel on Climate Change
OMC	Open Method of Coordination
OUV	Outstanding Universal Value
PI	Potential Impact
RCM	Regional Climate Model
RCP	Representative Concentration Pathways
RSLR	Rate of Sea Level Rise
SSP	Shared Socioeconomic Pathways
WMO	World Meteorological Organization

CHAPTER 1

INTRODUCTION

Humanity has always chosen to live close to the water. Big cities and harbors have been built along the coastlines, taking advantage of the life and opportunities provided by the sea. Throughout the ages, the coastal areas have become the centers of cultural exchange and trade, which can be seen clearly by the archaeological and historical sites left behind. These sites hold the essence of their local societies with their art, history, and the implications of their lifestyles, in addition to providing essential resources for the lands' economic and social development.

Although the coastal areas are rich in heritage for humanity, they are under a major risk of destruction due to various threats. One of those is the rise in sea levels due to thermal expansion in surface waters resulting from the increase in global temperature as a result of climate change. This is because rising sea levels lead to coastal erosion, inundation of land, and flooding due to increased storm surges.

Although these changes threaten mainly small islands in oceans and low-lying coastal areas, along the 8333 km shoreline, many coastal heritage sites in Türkiye are also expected to be threatened by the impacts. Hence, Türkiye is one of the countries in Europe that needs immediate and effective adaptation measures while participating in mitigation efforts. However, there are significant limitations, including the availability of data on cultural heritage sites in Türkiye. Also, there is not much research investigating the threats caused by the impacts of climate change on the coastal cultural heritage sites of Türkiye and assessing the risk of them being harmed irreversibly. Thus, the TÜBİTAK ARDEB-funded project 122M613 aims to investigate the vulnerability of coastal cultural and natural sites in Türkiye by

developing and utilizing a new assessment model integrating both the site characteristics and the physical properties of the coastal areas.

This study aims to develop and utilize an assessment model to investigate the vulnerability of those sites to sea level rise and its impacts, considering both the characteristics of the sites affecting their vulnerability and the interaction with the vulnerability of the shoreline on which they are located. The goals of the developed assessment model are listed below.

- Rank the cultural heritage sites based on their vulnerability to sea level rise and its impacts.
- Provide a prioritization for the planning of the adaptation efforts,
- Provide knowledge on the main threats to the coastal archaeological heritage sites of Türkiye.

In addition to the assessment of all the coastal archaeological heritage sites of Türkiye, the vulnerability of two selected sites to coastal erosion (one of the main impacts for Turkish coastlines) is investigated in detail using geographical information systems (GIS) and numerical models. The aim of coastal erosion assessment is to discuss the possible use of simpler shoreline prediction models for coastal cultural heritage sites in Türkiye as part of the local area management practices.

To achieve these goals, the parameters that provide adequate insight into the sites and the physical conditions indicating the impacts of sea level rise are identified, their relationships to each other are investigated, and a parametric coastal heritage vulnerability model is developed and applied. Furthermore, coastal erosion analysis is performed for selected sites by utilizing the Digital Shoreline Analysis System (DSAS) and the Shoreline Simulation (ShorelineS) model to predict the shoreline change for the selected sites for 2050.

In Chapter 2, the findings of the literature review about the observed and projected impacts of climate, the impacts of climate change on coastal cultural heritage sites, the concept of vulnerability assessment of the coastal heritage sites, the impacts of

coastal erosion resulting from sea level rise on the heritage sites, and use of shoreline models are introduced.

In Chapter 3, the framework of the Coastal Cultural Heritage Vulnerability Assessment Model (CCHVAM) is described, and the indicators, which describe the interaction of coastal cultural heritage sites with the shoreline and are utilized for the assessment, are introduced. Furthermore, the data used for the assessment performed in this study is described in detail. Also, discussions about the development of the CCHVAM are given in this chapter.

The shoreline evolution analyses are performed on two of the assessed heritage sites with the Digital Shoreline Analysis System (DSAS) and the Shoreline Simulation Model (ShorelineS).

In Chapter 4, the workflow followed during the analysis performed with the DSAS and the data utilized are described. Furthermore, the selected sites, Anemurium Ancient City and Soli-Pompeiopolis Ancient City, are introduced in detail.

In Chapter 5, the process of shoreline evolution modeling performed by utilizing the ShorelineS Model is described, and the input data prepared and used for this process is introduced. In both analyses, the projected movement of the shoreline is also studied, in addition to the observed movement between 2016 and 2024.

In Chapter 6, the results of the vulnerability assessment of the coastal archaeological sites of Türkiye and the coastal erosion analyses performed on the sample sites are presented. Also, the discussions about the results are provided in this chapter.

In Chapter 7, conclusions and recommendations for future studies on the vulnerability of coastal cultural heritage sites are given, in addition to discussions about the limitations of this study.

CHAPTER 2

LITERATURE REVIEW

This study primarily aims to develop a vulnerability assessment model to investigate the vulnerability of archaeological heritage sites located in coastal areas to sea level rise and its impacts. Also, coastal erosion analyses on two archaeological heritage sites on the Mediterranean coast of Türkiye are performed in the scope of this study. Hence, a literature review is done to understand the observed impacts of climate change on cultural heritage sites, methods to assess the vulnerability of cultural heritage sites to climate change, and the impacts of coastal erosion resulting from the climate change-induced sea level rise on coastal heritage sites. The findings of this review are presented in this chapter.

2.1 Observed Impacts of Climate Change

Based on the data shared by the Emergency Events Database (EM-DAT), the natural disasters that have happened in the 21st century so far have resulted in more than 1.6 million deaths, 4.6 billion people affected, and more than US$ 4.5 billion worth of damage. It is also stated in the same report that floods are the most frequent and they affect the largest number of people, whereas storms are the costliest disasters. Only in the spring of 2024, devastating flood hazards were reported from various parts of the world, including Brazil, China, Dubai, Germany, and East Africa. The geographical distribution of some major natural disasters recorded in the first half of 2024 is provided in Figure 2.1. The increase in the frequency and the impact of these hazards can be explained by acknowledging the mechanism and the current process of climate change.

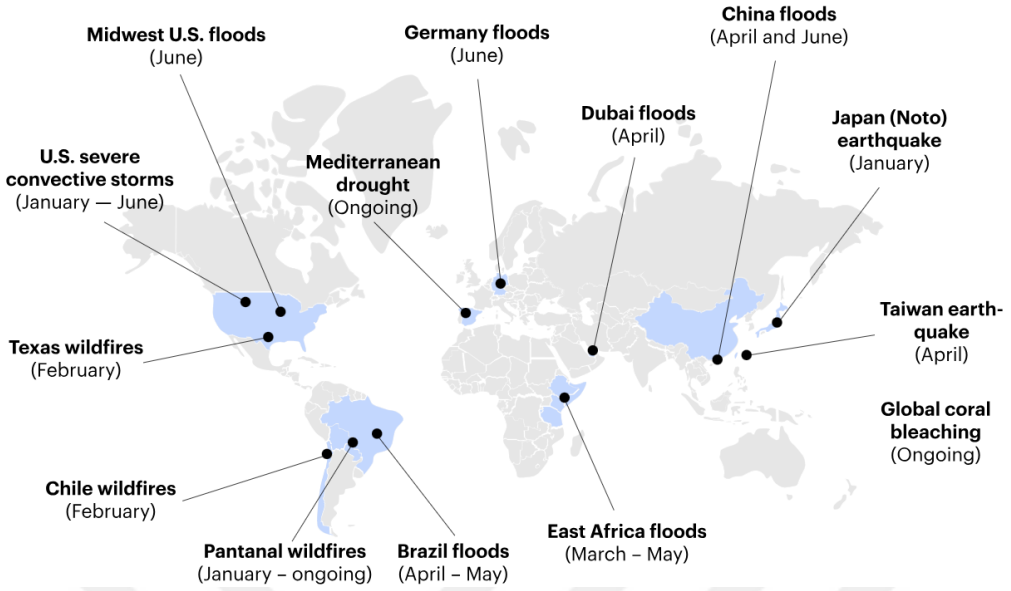


Figure 2.1. Geographical distribution of the massive natural disasters that occurred in the first half of 2024 (WTW, July 2024).

The mechanism of climate change can be explained simply as the increase in the concentrations of greenhouse gases blocking both heat and radiation in the atmosphere and causing an increase in surface air temperature globally (European Commission, n.d.). The increase in temperature leads to glacier loss and thermal expansion in surface waters, causing a rise in sea levels globally.

The World Meteorological Organization (WMO) published a report titled “State of the Climate 2024 – Update for COP29” and shared data about the changes in the global climate and the impacts of these changes. It is reported that a significant increase is observed in the concentrations of the three major greenhouse gases in the atmosphere; the concentrations of carbon dioxide, methane, and nitrous oxide are determined to be 151%, 265%, and 124% of the pre-industrial levels, respectively. Although some natural processes are also sources of the emissions of these gases, human emissions have the highest contribution. Especially, the emissions resulting from fossil fuels have had a major impact on the increase in the concentration of greenhouse gases since the 1950s. The impacts of this increase in emissions are seen

clearly when the global mean temperature anomalies are checked. In the same report, the WMO provides a figure showing the anomalies between the late 1800s and 2020 obtained from six datasets, which can be seen in Figure 2.2. It is highlighted that the impacts of El Nino led 2023 and 2024 to be the warmest years on record.

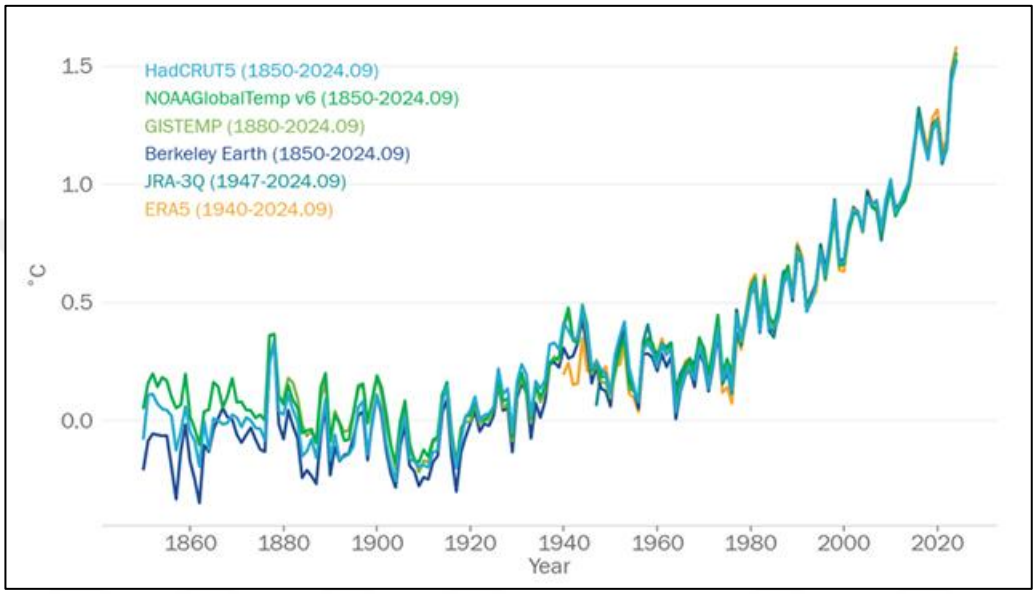


Figure 2.2. Annual global mean temperature anomalies recorded between 1850 and 2024 relative to 1850-1900 obtained from six datasets (WMO, 2024).

The global mean sea level data recorded between 1993 and 2023 is also consistent with the description of the mechanism given above, as shown in Figure 2.3. The AVISO CNES (CLS, https://www.aviso.altimetry.fr/) data shows that the global mean sea level in 2023 is above 110 mm when the value in 1993 is taken as zero, meaning that a 1.10 cm increase in the global mean sea level is recorded from 1993 to 2023.

In the report published by the World Meteorological Organization (2024), it is stated that the rate of sea level rise is recorded as 4.77 mm/year between 2014 and 2023, which was recorded as 2.13 mm/year between 1993 and 2002.

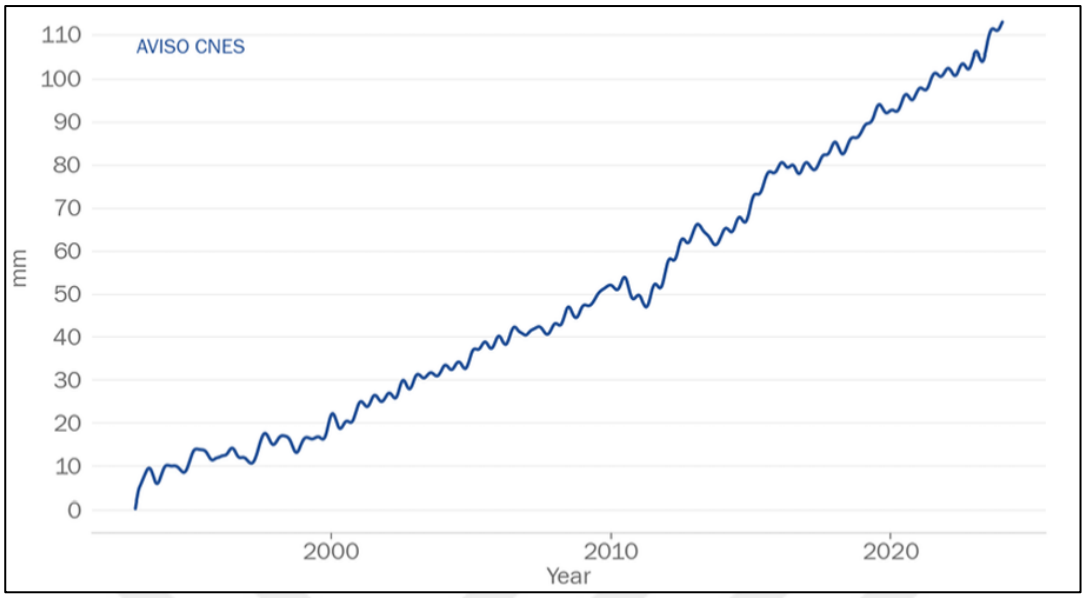


Figure 2.3. Global mean sea level recorded between 1993 and 2023 (WMO, 2024).

In the Sixth Assessment Report of IPCC (AR6), it is stated that the melting land ice contributed to approximately 45% of the observed rise in global mean sea level, while the contribution of seawater expansion was approximately 39% between the years 2006 and 2018.

2.2 Projections For Future Sea Level Rise

Greenhouse gas emissions (GHGs) are produced by highly complex dynamic systems affected by demographic changes, developing socio-economic conditions, and technological developments. Hence, climate change involves a high level of uncertainty (IPCC, 2000). To account for this uncertainty, a set of scenarios is developed to predict future changes in climate based on various conditions of the driving forces of the emissions. In the IPCC AR6, future sea level rise is assessed under five GHG emissions and socioeconomic scenarios. These scenarios are based on Shared Socio-economic Pathways (SSPs). Each pathway describes a different narrative with different conditions and impacts on the climate as listed below.

- SSP1 – Sustainability: Low challenges to mitigation and adaptation
- SSP2 – Middle of the Road: Medium challenges to mitigation and adaptation
- SSP3 – Regional Rivalry: High challenges to mitigation and adaptation
- SSP4 – Inequality: Low challenges to mitigation, high challenges to adaptation
- SSP5 – Fossil-fueled Development: High challenges to mitigation, low challenges to adaptation

In addition to different socio-economic developments, different driving forces are also considered while structuring these SSPs. The main focus while assessing the driving forces is the amount of CO2 emission in these scenarios. As presented in Figure 2.4, the forcing resulting from the CO2 emission ranges from very low in SSP1-1.9 to very high in SSP5-8.5.

As expected, the global mean air surface temperature, the global mean precipitation, the global mean sea level, and other impacts get worse in scenarios from SSP1 to SSP5.

Note that it is not quite right to compare the current Shared Socio-economic Pathways (SSP) scenarios to Representative Concentration Pathways (RCP). It is because the concentrations of each gas in greenhouse gas compositions are different, and overall effective radiative forcings considered are different from each other, as stated in Chapter 1 of the IPCC AR6 Working Group 1 Report (IPCC, 2021). Also, another significant difference between SSPs and RCPs is the emphasis put on the socio-economic conditions; SSPs pay more attention to those.

SSP1-1.9 is the lowest emissions scenario, leading to 1.4℃ of warming at the end of the century, in 2100, whereas SSP5-8.5 is the highest emissions scenario, leading to 4.4℃ of warming at the end of the century. As expected, these scenarios result in different projections for sea level rise. SSP1-1.9 predicts the global mean SLR to reach 18 cm by 2050 and 38 cm by 2100, while SSP5-8.5 projects an increase in global mean sea level of 23 cm by 2050 and 77 cm by 2100.

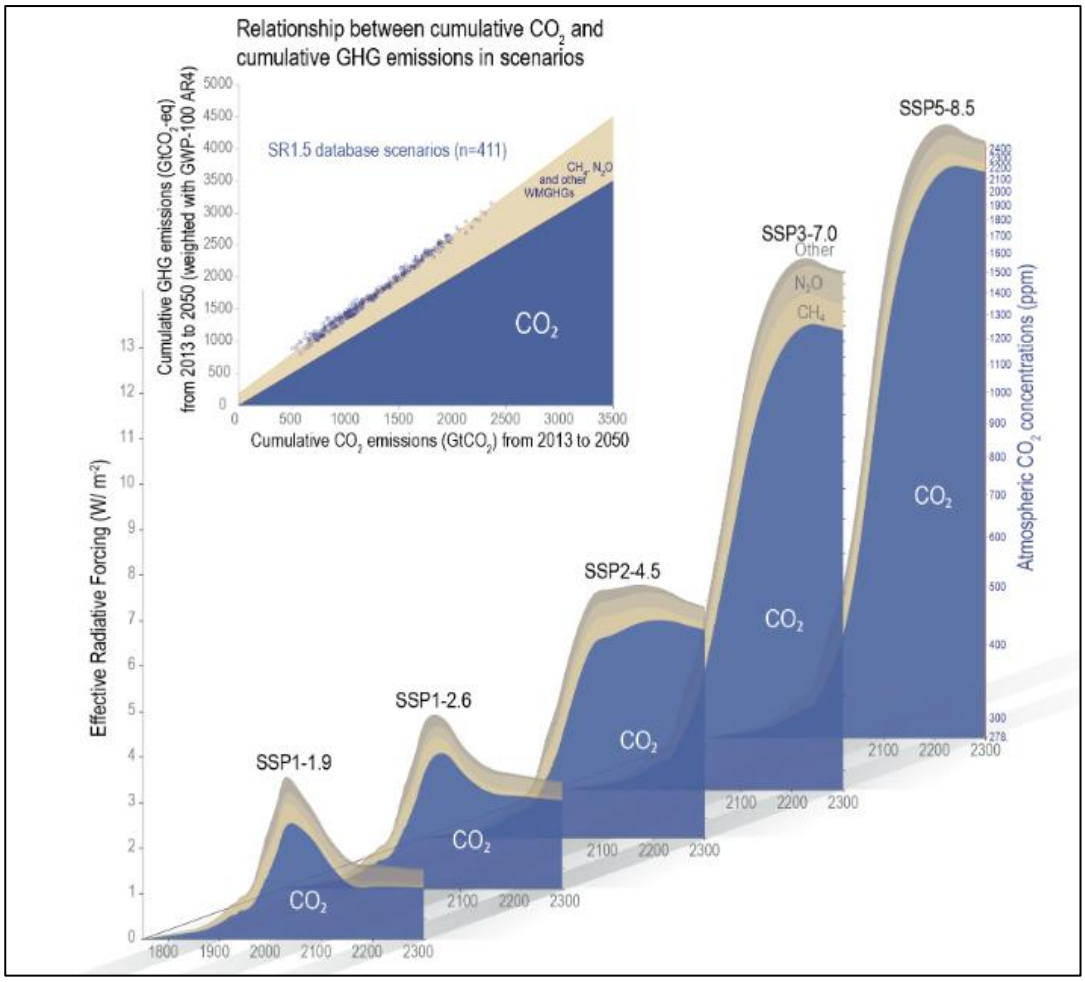


Figure 2.4. The effective radiative forcings of GHGs in five SSPs are compared (IPCC AR6-WGI, 2021).

Projected values of SLR relative to 1995-2014 and rates of SLR under each SSP scenario are assessed in the IPCC AR6. The projected ranges of SLR and median values are given in Table 2.1 below for each SSP scenario.

In the same report, it is also stated that the increased RSLR has the potential to reshape coastlines throughout the 21st century, and it poses significant threats to the low-elevation coastal zones around the globe, which are defined as both continental and island areas below 10 meters elevation above mean sea level. These threats include the increase in frequency and anomalies of "climate-driven coastal hazards"

such as coastal flooding, saltwater intrusion into groundwater, coastal erosion, inundation, and loss of coastal ecosystems.

Table 2.1. SLR and RSLR values projected in SSP scenarios with ranges and median values (IPCC AR6 WGI, Chapter 9, Table 9.9, 2021).

SLR (m)	*SSP1-1.9*	*SSP1-2.6*	*SSP2-4.5*	*SSP3-7.0*	*SSP5-8.5*
by 2030	0.09	0.09	0.09	0.09	0.10
	[0.08-0.12]	[0.08-0.12]	[0.08-0.12]	[0.08-0.12]	[0.09-0.12]
by 2050	0.18	0.19	0.20	0.22	0.23
	[0.15-0.23]	[0.16-0.25]	[0.17-0.26]	[0.18-0.27]	[0.20-0.29]
by 2100	0.38	0.44	0.56	0.68	0.77
	[0.28-0.55]	[0.32-0.62]	[0.44-0.76]	[0.55-0.90]	[0.63-1.01]
RSLR (mm/yr)					
2040-2060	4.1 [2.8-6.0]	4.8 [3.5-6.8]	5.8 [4.4-8.0]	6.4 [5.0-8.7]	7.2 [5.6-9.7]
2080-2100	4.2 [2.4-6.6]	5.2 [3.2-8.0]	7.7 [5.2-11.6]	10.4 [7.4-14.8]	12.1 [8.6-17.6]

2.3 Impact of Climate Change-Induced Sea Level Rise on Coastal Cultural Heritage Sites

Coastal areas are complex and dynamic spaces where air, water, and land meet along the coastline. Hence, the cultural heritage sites located in coastal areas are in exacerbating danger of getting damaged as the impacts of climate change are getting more and more serious every day. Although climate change has been studied for decades, the impact of this process on cultural heritage sites is a relatively new research topic. To be more specific, the first major step taken towards investigating the impacts of climate change on outdoor cultural heritage is the European

Commission, which was launched in 2003. Then, the Fifth Assessment Report (AR5) of the Intergovernmental Panel on Climate Change (IPCC), published in 2014, was the first time that this topic had ever been addressed (Sesana et al., 2018).

Reimann et al. (2018) conducted a comprehensive study on the sites located along the Mediterranean coastlines threatened by coastal flooding and coastal erosion resulting from sea-level rise. In this study, they found that there are 49 cultural World Heritage sites located in low-elevation coastal zones of the Mediterranean, 37 of which are at significant risk from a 100-year flood, and 42 of the sites are at a high risk from coastal erosion. This study was done in 2018, when the total number of cultural and natural sites on the World Heritage List was 1092. Today, the number of World Heritage Sites stated on the website of UNESCO as of December 2024 is 1223 globally, and 77.8% of those (952) are cultural heritage sites. Based on the statistics provided by UNESCO and as presented in Figure 2.5, the majority of these cultural World Heritage sites are located in Europe and North America, and there is a significant number of sites located in coastal areas.



Figure 2.5. Cultural sites on the World Heritage List of UNESCO in Europe (UNESCO World Heritage Online Map, December 2024).

The majority of the cultural heritage sites are directly exposed to the impacts of climate change without a barrier or a cover, preventing them from getting damaged by the changing climate. As a result, the change in freezing and thawing cycles, humidity, and salt crystallization affects the weathering process and damages the earthen material of most sites. Also, the changing patterns of wind and wind-driven rain lead to material erosion. On the other hand, sea level rise combined with a higher frequency of storm surges causes inundation, coastal flooding, and coastal erosion in heritage sites, which can lead to the destruction of those.

Marzeion and Levermann (2014) investigated the impacts of sea level rise on the Cultural World Heritage sites defined by the United Nations Educational, Scientific and Cultural Organization (UNESCO). They utilized "spatially explicit sea-level estimates for the next 2000 years" and topography data, and they found that 19% of the UNESCO World Heritage Sites could be at risk of destruction due to inundation driven by sea level rise for the 3℃ warming scenario. In addition to inundation, the rise in sea levels also increases coastal erosion, which results in the reshaping of the coasts. Both coastal retreat and sediment accumulation may lead to the destruction of heritage sites because they could either collapse or be destroyed by the accumulated or moved material.

2.4 Vulnerability Assessment of Cultural Heritage Sites

Vulnerability is defined as the sensitivity of geophysical, biological, and socio-economic systems to the destructive impacts of the changing climate and extremes and their ability to endure in the Fourth Assessment Report of the Intergovernmental Panel on Climate Change (AR4, 2014). This definition comprehends both the properties of the vulnerable site, which make it sensitive to harmful impacts and external factors. Based on this definition, vulnerability has three main components: exposure, sensitivity, and adaptive capacity. The exposure gives information about how harmful the external stressor is, while the sensitivity expresses how open the site is to getting damaged due to internal factors. The adaptive capacity, on the other

hand, provides information about the ability of the site to adapt and endure the changing climate.

After many scientific studies had been done throughout the years, the IPCC has redefined vulnerability in the Fifth Assessment Report (AR5). The new approach introduced focuses on the concept of risk from a disaster risk assessment perspective, and it considers vulnerability as a component of risk. Within this framework, risk is the potential for an outcome to be uncertainly endangered, acknowledging the various values that carry significance. The risk is defined by three components: Hazard, exposure, and vulnerability.

Exposure in this approach is defined as "the presence of people, livelihoods, species or ecosystems, environmental functions, services, and resources, infrastructure, or economic, social, or cultural assets in places and settings which could be harmed". Vulnerability expresses the predisposition to be adversely affected, comprehending the concepts of sensitivity (susceptibility to harm) and adaptive capacity introduced in the previous report, AR4. Hazard is a new term, defined as "the potential of physical impact of a natural or human-induced physical event or trend that may cause loss of life, injury, or other health impacts, as well as damage and loss to property, infrastructure, livelihoods, service provision, ecosystems, and environmental resources.".

Although the definitions of vulnerability given in AR4 and AR5 differ from each other, the fundamental concept expresses the potential for hazard and the resilience of a system that is known to be valuable under the impacts of climate change. In both perspectives, the concepts of vulnerability and risk consist of the following components:

1. External Elements: This component considers climate-related stressors, represented by "exposure" in AR4 and by "hazard" in AR5. These elements include factors like extreme weather events that pose a potential threat.
2. Internal Elements: This component consists of regulatory properties within a system. These properties affect how the system responds to climate-related

stressors or hazards, and they can be socio-economic, physical, or environmental. These elements are represented by “sensitivity” and “adaptive capacity” in AR4 and by “exposure” and “vulnerability” in AR5.

Consequently, the vulnerability approach defined up to AR5 and the risk approach introduced in AR5 fundamentally seek to answer similar questions. A clear comparison of the concepts introduced in AR4 and AR5 can be seen in Figure 2.6 below.

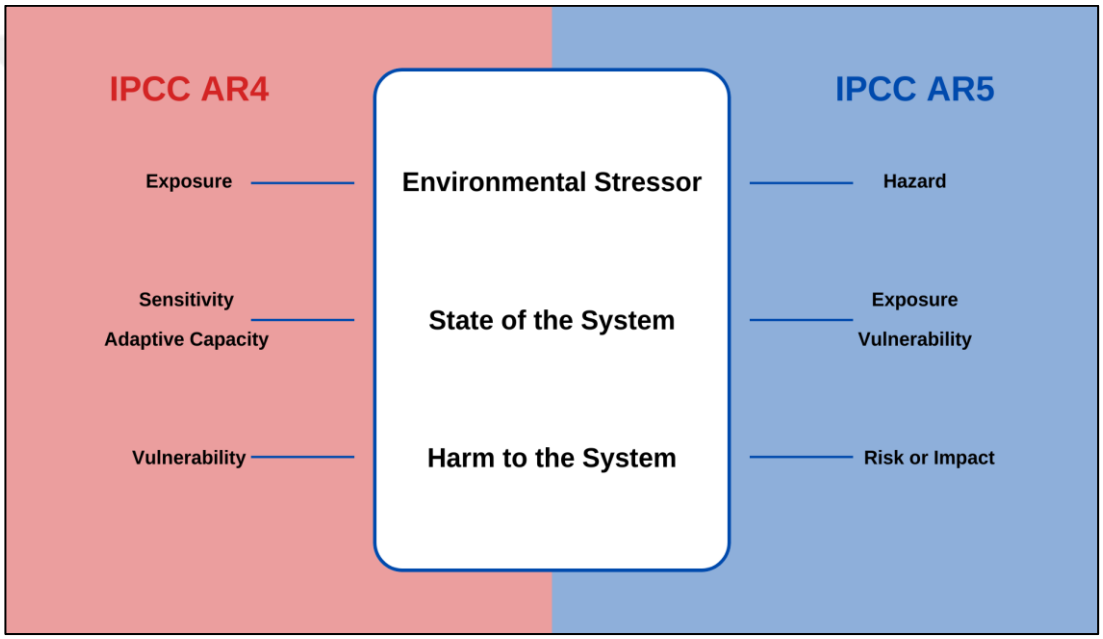


Figure 2.6. Comparison of the terms given in the 4th (AR4) and 5th (AR5) Assessment Reports of the IPCC.

As stated in the report presenting the findings of the European Union Open Method of Coordination (OMC) done with the participation of experts from the member states, one of the major gaps in the European Green Deal is the lack of a standardized methodology providing reliable information and quantitative data about the vulnerability of tangible heritage (European Commission, 2022). Hence, there are various methods utilized in different studies investigating the vulnerability.

Daly (2014) proposed a six-step framework to assess the vulnerability of archaeological heritage sites to the outcomes of climate change. It is stated that this method can be utilized for the assessment of landscapes, monuments, and buried archaeology. This framework uses the same vulnerability components as the IPCC defined in AR4 and AR5, which are exposure (E), sensitivity (S), and adaptive capacity (AC). The works done in each step of this framework are explained below.

- **Step 1 -** The heritage sites to be assessed are selected, and the spatial extent of the assessment subjects is determined.
- **Step 2 -** The vulnerability components are obtained. For this step, the sites are visited in different seasons to understand their exposure, sensitivity, and adaptive capacity through observation. Future climate conditions are recommended to be obtained from the Regional Climate Model (RCM), and interviews with stakeholders and experts are conducted.
- **Step 3** – The hazards likely to adversely affect the selected sites under the future climate scenarios are identified.
- **Step 4** – The indicators providing insights into each vulnerability component are defined.
- **Step 5** – The vulnerability is assessed by entering all the values for exposure, sensitivity, and adaptive capacity into the causal model.
- **Step 6** – The feedback of stakeholders is taken to refine the results.

In this framework, at every stage of the framework except the fifth step, there is a consultation with stakeholders and experts.

Zarley et al. (2016) developed a "cultural resource vulnerability index (CRVI)" to assess the vulnerability of coastal archaeological sites in Florida to sea level rise and hurricanes. Utilizing Geographic Information Systems (GIS), they created the index evaluating the following indicators:

- Proximity to the coastline (D)
- Average elevation of the site (E)

- Modern land use in the interacting area (LU)
- Shoreline vulnerability (SV)

The shoreline vulnerability indicator that they consider is obtained from the assessment of several parameters, including geomorphology, coastal slope, relative sea level rise, wave height, shoreline retreat, and tidal range.

They computed the final CRVI values by using Equation 2.1.

$$CRVI = \frac{2(D+E) + 3(SV) + 2(LU)}{3} \quad [2.1]$$

Sesana et al. (2020) presented a different method that provides a vulnerability value through a qualitative assessment, an "integrated approach" for the vulnerability assessment of World Heritage Sites to sea level rise. They developed a five-step assessment framework. The first step is the identification of the Outstanding Universal Value (OUV) of the selected site. The impacts of climate change causing stress on the area where the site is located are identified in the second step, and the exposure of the site and its sensitivity are also assessed at this stage. In the third step, the adaptive capacity is introduced to the framework. In the fourth step, a qualitative assessment is done to obtain vulnerability. Then, it is stated in their paper that the fifth step is repeating this assessment periodically because the components affecting the vulnerability change over time.

The International Council on Monuments and Sites (ICOMOS), a major non-governmental organization working for the conservation and protection of cultural heritage sites, proposes the Climate Vulnerability Index (CVI). In their report published in 2019, it is stated that the CVI is a robust assessment tool providing comprehensive results rapidly. Furthermore, it has been developed to assess all types of heritage sites, including cultural, natural, and mixed. Day et al. (2020) list the benefits of the CVI as given below.

- It assesses both the physical and ecological impacts of the changing climate on the OUV of a property.
- It is a systematic and comprehensive method, but it is not too complex to make it challenging to understand and apply.
- It is an easily repeatable process.
- It provides significant insights that can be utilized to define adaptation strategies.

In addition to stating its advantages, Day et al. (2020) applied CVI on several natural and cultural heritage sites. The CVI utilizes a risk assessment approach and follows the framework presented in Figure 2.7.

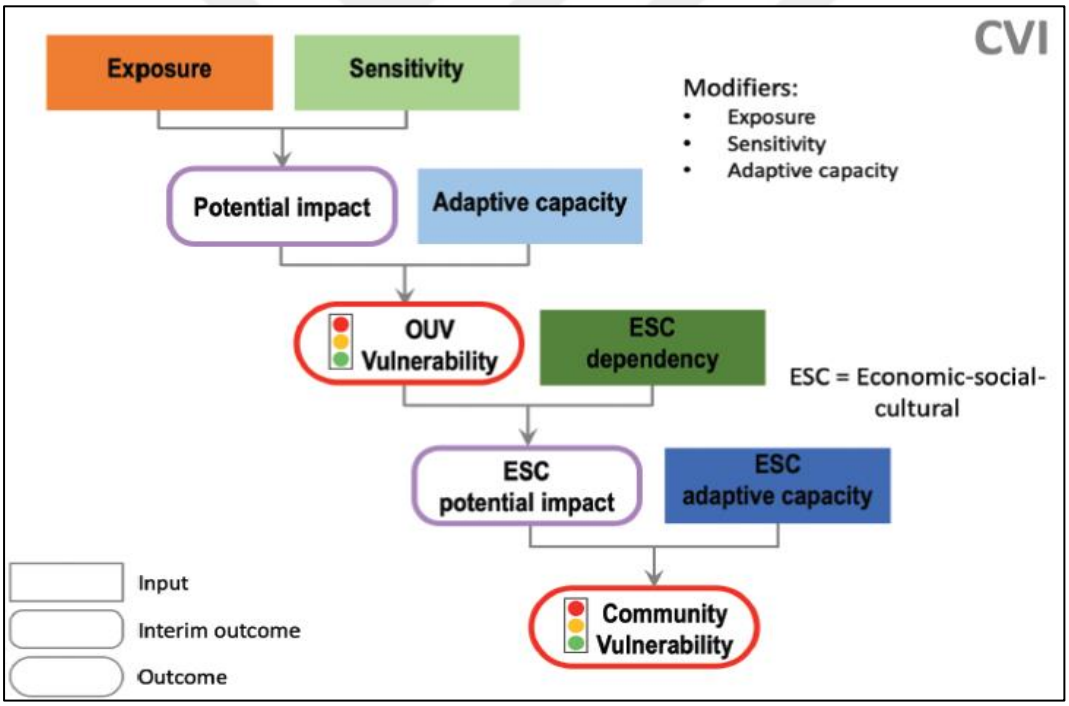


Figure 2.7. The CVI framework proposed by the ICOMOS (Day et al., 2020).

As can be seen in the above figure, the CVI consists of two main stages:

- **The OUV Vulnerability** – The identified climatic stressors and the vulnerability of the key values of the assessed site to those are investigated.
- **Community Vulnerability** – The dependency of the interacting community on the assessed property and the adaptive capacity of the community to climate change are investigated based on the economic, social, and cultural interactions between the community and the heritage property.

2.5 Impacts of Coastal Erosion on Coastal Cultural Heritage Sites

Coastal erosion is a critical process threatening coastal zones and all the population, resources, and heritage sites located on them. The U.S. Climate Resilience defines it as a process by which the rise in sea levels and strong wave action move coastal material like sand, rocks, and soil along the shore. The movement of the material results in a change in shoreline position.

The increase observed in global temperature accelerates sea level rise, and eventually, it accelerates the coastal erosion process in many regions of the globe. Hence, especially in recent years, there have been numerous studies investigating the impact of coastal erosion and measures that can be taken to preserve the coastal zones, especially over the last thirty years.

In the 1990s, archaeologists reported that heritage sites in Scotland, including remains from the Iron Age, were endangered due to coastal erosion (Ashmore, 1994). In the 2010s, the same warning about the coastal heritage sites threatened by coastal erosion was made by French researchers (Daire et al., 2012). Furthermore, climate researchers from Alexandria report that over 40% of the beach area in Alexandria was lost in the past 25 years to a combination of coastal erosion and human intervention. Another study, done by Sánchez et al. (2020), revealed that there are a number of coastal heritage sites under threat from coastal erosion. One of them is the Castle of San Cristóbal, and the study revealed that there is a high risk of getting

damaged by coastal erosion and coastal flooding for the castle, based on the exposure data collected by Losada et al. (2014) and Fraile et al. (2014).

On the other hand, Reimann et al. (2018) assessed 49 UNESCO World Heritage Sites in the Mediterranean at risk from coastal flooding and coastal erosion utilizing an index-based approach. They assessed the risk from coastal erosion by evaluating a set of indicators, including distance from the coastline, coastal material, mean wave height, and sediment supply. They found that 42 of the assessed sites are threatened by coastal erosion.

The risk is getting serious as global climate change proceeds, so there is a growing need for precautions. However, for determining the required adaptation and mitigation actions, the threat and possible scenarios should be well understood. For this purpose, a number of methodologies and tools have been developed over the last decades, but it is a challenging process to model coastal erosion. Toimil et al. (2020) summarized the challenges in this modeling process as follows:

- The coastline evolution over long periods is affected by a complex mechanism of interacting short-to-long term coastal processes, and there is no established way of modeling such complex and long-term interactions and mechanisms longer than a few years.
- The coastal processes affecting the coastal evolution are getting affected by climate change, as well. The impact of climate change adds uncertainty to this process. Although a set of assumptions can be made or projection scenarios can be utilized for each of the mean wave height, storm surge, or river discharge, evaluating their combination while considering the uncertainty is a challenge.
- All the uncertainties and assumptions affecting the emission scenarios, climate models, and erosion models combine and accumulate in the final output.

Overall, this literature review showed that there is a need for a standardized vulnerability assessment model to identify the level of risk of destruction at coastal heritage sites resulting from the impacts of sea level rise and accelerate the planning phase of protective actions. Additionally, it is seen that there are only a limited number of studies on the vulnerability of the heritage sites along the coastlines of Türkiye. Hence, in the scope of this study, a new vulnerability assessment model is introduced, which utilizes and provides quantitative data, and which can provide a vulnerability assessment on a national scale, instead of a site-specific assessment. Also, this model is utilized on the coastal archaeological sites to get some insights into the vulnerability of those to sea level rise and its impacts, and the results are presented in Chapter 6.

Furthermore, the findings of this literature review showed that among all the impacts of sea level rise, coastal erosion and coastal flooding are the most critical ones, especially along the Mediterranean coastlines. Hence, these impacts should also be investigated in detail. Considering this, assessment of coastal erosion is focused on in this study, and the performance of different methodologies in analyzing the coastal erosion along the shorelines directly interacting with the heritage sites is investigated.

CHAPTER 3

VULNERABILITY ASSESSMENT OF COASTAL CULTURAL HERITAGE SITES OF TÜRKİYE TO SEA LEVEL RISE

Technological developments and the changing lifestyle of the world population accelerate the process of climate change scenarios turning into reality. As stated in the previous chapter, even for the year 2050, the expected rise in sea levels is concerning, highlighting the immediate need for adaptive and preventive efforts. Hence, the risk in the low-lying areas should be investigated well, and the planning stage for applying preventive actions should be accelerated. Although many studies on climate change have been performed globally in recent years, unfortunately, there are a limited number of studies focusing on the impacts of climate change on the coasts of Türkiye and the vulnerability of the country's coastal cultural heritage sites.

The majority of the existing studies on the cultural heritage of Türkiye focus mostly on the sites in urban areas and the risks resulting from natural disasters, namely fire and earthquake. The gap in the research on the impacts of climate change on the coastal cultural heritage in Türkiye and the vulnerability of those sites can be explained by considering certain limitations. The major limitation in this regard is data availability. Unfortunately, there are either limited or no datasets on the national scale providing detailed information about both the parameters that define the physical processes along the coasts of the country and the characteristics of cultural heritage sites.

This chapter presents the Coastal Cultural Heritage Vulnerability Assessment Model (CCHVAM) through its development process. The model is utilized for the vulnerability assessment of coastal cultural heritage sites of Türkiye to sea level rise in the scope of this study as a part of the research project (Vulnerability of Coastal Cultural Heritage Areas to Sea Level Rise and Its Impacts) funded by TUBITAK, and the data used for the assessment is also introduced in this chapter.

3.1 Framework of the Coastal Cultural Heritage Vulnerability Assessment Model

The susceptibility of a system to be affected by external and internal impacts resulting from the changing climatic conditions is explained by the term "vulnerability" in AR4 (IPCC, 2007) and "risk" in AR5 (IPCC, 2014), as stated in Chapter 2. Although the terminology has evolved over time, the main goal remains the same. Vulnerability assessment of a site aims to understand the changing physical conditions due to climate change that are likely to cause destructive impacts on the site and the properties of the site or the available conditions that make the site susceptible to being adversely affected.

As stated in the previous chapter, the majority of the studies investigating the vulnerability of heritage sites to the impacts of climate change are site-specific studies. In these studies, it is stated that there is no global model established to be utilized for multiple sites with various characteristics simultaneously. The absence of such a model results in an inability to provide a ranking of sites, which can accelerate the adaptation planning process. Hence, taking the method proposed in the ICOMOS report (2019) as a reference, this study aims to develop a model which can;

- Assess the vulnerability of a heritage site by considering both the threats resulting from the existing conditions along the coast and the properties of the site, making it sensitive to those threats
- Assess multiple sites at a national scale rapidly and save time
- Provide a ranking of heritage sites based on their vulnerabilities by assessing each site based on the same indicators

Considering the goals targeted with this model, the scope and main components of the model are defined, and the flowchart is structured.

3.1.1 Geographical Definitions of Coastal Cultural Heritage Site

The scope of the CCHVAM is defined based on the term “coastal cultural heritage”. The model assesses the impacts of sea level rise and those that affect not only the coastline but also the land behind it, so the sites to which the term refers are usually selected based on proximity and elevation criteria. In this study, the criteria to define coastal cultural heritage are decided after the evaluation of similar studies in the literature. Karaca and Nicholls (2008) defined the area that is expected to be affected directly by a one-meter rise in sea level as the area below a 100-meter elevation and within a kilometer distance to the shoreline. On the other hand, Kuleli (2010) defined the area that is expected to be affected by the sea level rise as the area below a 10-meter elevation. In addition to studies on Mediterranean basin, some international studies are reviewed, and it is seen that in those, various limit values of elevation and proximity are utilized; the elevation limit between 1 to 100 m and the proximity limit between 0.5 to 200 km (Ezcurra et al., 2018; Anderson et al., 2017; Reimann et al., 2018).

Considering these findings of the literature review, the CCHVAM is developed to assess the sites satisfying either one or both of the following criteria:

- Area below 10-meter elevation
- Area within 1 km distance to the shoreline

After checking these criteria for the Turkish cultural heritage dataset, three groups of heritage sites are obtained as described in Figure 3.1.

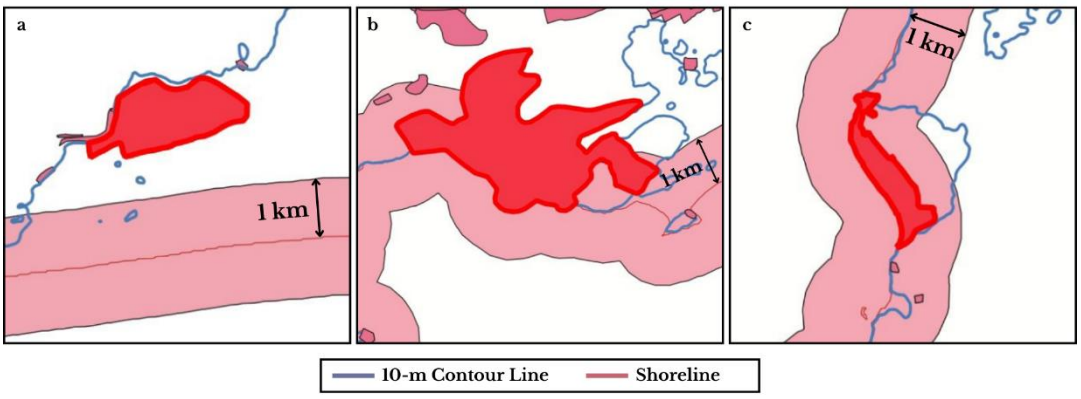


Figure 3.1. Sample sites that are in the scope of the CCHVAM based on the defined criteria.

The three groups of heritage sites that the CCHVAM assesses are the sites that have no parts within a kilometer distance to the shoreline but have parts below 10-m elevation as shown in Figure 3.1a, the sites that have no parts below 10-m elevation but have some parts within a kilometer distance to the shoreline as shown in Figure 3.1b, and the sites that parts lower than 10 meters and located within a kilometer distance to the shoreline.

3.1.2 Components of CCHVAM

The main components of the Coastal Cultural Heritage Vulnerability Assessment Model (CCHVAM) are exposure, sensitivity, and adaptive capacity. They are introduced briefly below, and further details are provided in the following parts of this chapter.

The exposure component of the model provides insights into the threat that a site faces posed by the vulnerability of the coastline segment, with which the site directly interacts. The exposure component considers sea level rise and its impacts, including coastal erosion, inundation, and coastal flooding due to storm surge. The sensitivity component describes the interaction between the site and the shoreline based on the

physical properties of the site and the shoreline. Finally, the adaptive capacity describes the properties or conditions of the site that may enhance its resilience against destruction due to sea level rise and its impacts.

These components are combined to obtain a value of vulnerability based on the climate vulnerability index (Day et al., 2020), as given in Figure 3.2. First, sensitivity and exposure values are combined to determine the potential impact by using a decision matrix. Here, exposure describes the threat, while sensitivity provides insights about the properties making the site open to getting harmed by the existing threat. Then, the potential impact and the adaptive capacity components are combined by utilizing another decision matrix to determine the vulnerability value. In other words, vulnerability is obtained as a combination of threats resulting from both external and internal factors and the capacity of the site to withstand those destructive impacts resulting from sea level rise.

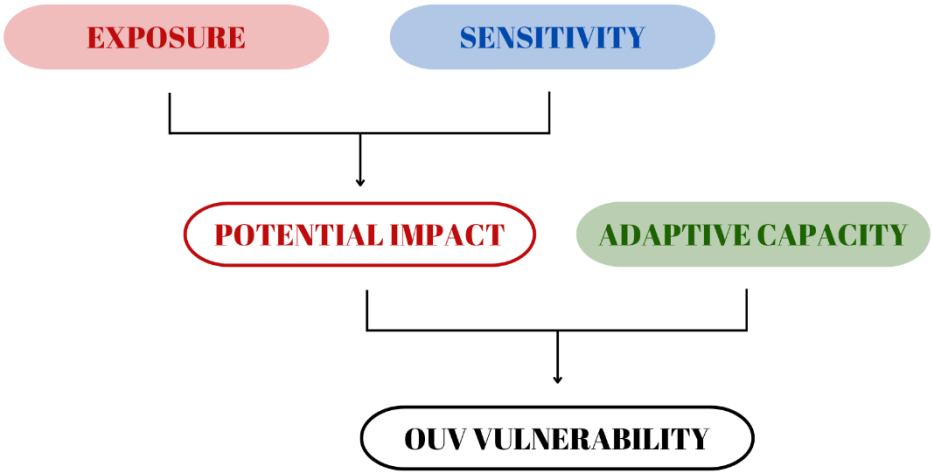


Figure 3.2. The flowchart followed by the CCHVAM to obtain the vulnerability of the OUV (Day et al., 2020).

3.1.2.1 Exposure Component of the CCHVAM

The IPCC refers to exposure as the physical conditions that are likely to affect the coastal area negatively when defining climate vulnerability. Based on this definition, the exposure component of the newly developed CCHVAM is obtained from a modified version of the Fuzzy Coastal Vulnerability Assessment Model (Özyurt, 2010). The results of the FCVAM model utilized in this study are provided by Ince (2024), and the details on the FCVAM model and the coastal vulnerability can be found. However, a summary is given here to provide a comprehensive presentation of the CCHVAM model developed in this thesis.

The FCVAM model provides separate vulnerability indices for the physical impacts of sea level rise, and it also computes an overall vulnerability score (CVI) based on the results of those indices. The separate vulnerability indices computed by the model are listed below.

- Coastal Erosion
- Flooding due to Storm Surge
- Inundation

Each index is obtained from the assessment of both physical and human influence parameters using fuzzy logic inference systems. The outputs of the FCVAM are separate vulnerability indices for the impacts listed above and the overall vulnerability index of the assessed coastline segment, which is called the coastal vulnerability index (CVI). The physical and human influence parameters assessed for the vulnerability to each impact are presented in Table 3.1.

Table 3.1. Physical and human influence parameters that are utilized to obtain the vulnerability indices to each impact of sea level rise (Ozyurt, 2010; Ince, 2024).

Impact	***Physical***	***Human Influence***
Coastal Erosion	Rate of Sea Level Rise	River Flow Regulation
	Geomorphology	Engineered Frontage
	Coastal Slope	Natural Protection Degradation
	Significant Wave Height	Coastal Protection Structures
	Sediment Budget	
	Tidal Range	
Flooding due to Storm Surge	Rate of Sea Level Rise	Engineered Frontage
	Coastal Slope	Natural Protection Degradation
	Significant Wave Height	Coastal Protection Structures
	Tidal Range	
Inundation	Rate of Sea Level Rise	Natural Protection Degradation
	Coastal Slope	Coastal Protection Structures

In the FCVAM, two sets of input parameters are assessed for each impact, then the defuzzified output values determine the vulnerability value of the coastline segment for the specific impact of the sea level rise. Finally, the overall vulnerability value is obtained from fuzzy arithmetic, and it is called the Coastal Vulnerability Index (CVI). The exposure component of the CCHVAM is obtained from CVI values of the updated version of the FCVAM (Ince, 2024). Both individual impact CVI values as well as the overall CVI values are used to determine the exposure of a site based on the level of assessment.

The assessed heritage sites are divided into several exposure classes based on their CVI values. For this classification process, the limit values presented in Table 3.2 are used.

Table 3.2. Limiting CVI values of the exposure classes.

Limit Values	Exposure Class
$0.0 < CVI < 1.5$	Very Low Exposure
$1.5 \leq CVI < 2.5$	Low Exposure
$2.5 \leq CVI < 3.5$	Moderate Exposure
$3.5 \leq CVI < 4.25$	High Exposure
$4.25 \leq CVI$	Very High Exposure

3.1.2.2 Sensitivity Component of the CCHVAM

The sensitivity component of the CCHVAM aims to describe the interaction between the assessed heritage site and the coastline, which is expected to be vulnerable to sea level rise and its impacts. The interaction described by this component indicates how likely the site is will be affected by the vulnerability of the shoreline.

As discussed in the previous chapter, Zarley et al. (2016) studied a vulnerability assessment model using a similar approach to this study. Their method consists of a shoreline vulnerability value separately. It is obtained from the assessment of several indicators similar to the FCVAM, including relative sea level rise, geomorphology, wave height, tidal range, and shoreline erosion. The method includes distance, elevation, and land use parameters, additionally. For the elevation indicator, the method utilizes the normalized average elevation of each site on a scale of one to five, where one is the highest elevation. For the distance indicator, "the shortest planar distance from the edges of each site polygon to the coastline" is determined. For the land use indicator, the method assigns a different value to each of the five land use categories, which are presented in the following parts.

On the other hand, Reimann et al. (2018) employed the following indicators to compute coastal erosion risk in addition to distance from the coastline: coastal

material, mean wave height, and sediment supply in their study on the coastal flooding and coastal erosion risk of Mediterranean UNESCO World Heritage.

However, Cassar (2016) introduces a whole new set of indicators, including the material of the remnants in the site, the size of the heritage site, the spread of the site, the state of conservation, and degrees of intervention.

Overall, a similar set of indicators is utilized in most studies on vulnerability assessment of coastal heritage sites (European Commission, 2014; Ciantelli et al., 2018; Forino et al., 2016). During the development of the CCHVAM, the possible indicators of sensitivity are reviewed based on these studies, among which several of them (materials of the elements of the heritage site (stone, ceramics, metals, etc.), states of conservation (pristine and ruins), degree of intervention (touched or restored)) are not included in the final model due to the unavailability of data for the majority of the sites in Türkiye.

As a result, four indicators are identified to determine the sensitivity of a coastal cultural heritage site in the CCHVAM, which are described below.

- **Elevation:** The percentage of the area that is below 10 meters elevation is defined as the elevation indicator. The elevation limit is selected as 10 meters based on the reviewed studies presented in the previous part. The model fundamentally acknowledges that a coastal area below a 10-meter elevation is at risk of being adversely affected by the impacts threatening the interacting coastline segment. Hence, the part of a heritage site below a 10-meter elevation is the part primarily susceptible to being affected. For this indicator, a single elevation value, such as the mean elevation of the site and the maximum or minimum elevation of the site, is not considered since a single value might misrepresent the elevation characteristics. For example, if only a small part of the site has a very high elevation and most parts have moderate elevation, the mean elevation value is likely to be high, but this mean elevation would not be representative of the whole site.

- **Area:** For the area indicator, the percentage of the area that is located within 100 meters distance to the shoreline is used. Similar to the elevation indicator, for the area indicator, a single value like the total area would not be representative of the whole site for a vulnerability assessment. Instead, it is decided that when the area of the part of a site that is close to the threatened coastline segment is used as the parameter, it would better represent the sensitivity of the heritage site to the vulnerability of the coastline.
- **Proximity:** For the proximity indicator, the closest distance to the shoreline from the edge of the site (in meters) is used. The other parameter suggested is the shortest distance measured from the centroid, however this definition could give the same proximity value to two different sites where one of them is directly on the coastline and covers a large area landward while the other one is a small site not located on the coastline but its centroid is in the same distance to the shoreline. To differentiate cases like this, the actual distance from the closest border of the cultural heritage site is used as an indicator so that direct interaction of the shoreline and the cultural heritage site can be represented accurately.
- **Interaction with the coastline:** This indicator aims to rank sites located on the same coast by comparing the length of the coastline segment with which the sites are interacting directly. In other words, this indicator expresses for each site how much of the threatened coastline is interacting with the site directly. For the interaction indicator, the length of the coastline segment with which the site directly interacts is used, in meters. The interaction length is the length of the coastline segment that intersects with the buffer area, of which the width is one kilometer, generated around the heritage site polygon in the ArcGIS Pro environment.

Similar to the exposure classes, sensitivity classes are defined for both the sensitivity indicators and the final sensitivity value. Five sensitivity classes defined for each sensitivity indicator are very high sensitivity (VH), high sensitivity (H), moderate sensitivity (M), low sensitivity (L), and very low sensitivity (VL). Each class also

has a numerical value from one to five, where the value of "very high sensitivity" is 5 and the value of "very low sensitivity" is 1. The limiting values of the sensitivity classes of each indicator and their numeric values are presented in Table 3.3 below. The class limits for each indicator are selected by utilizing the "Natural Breaks Classification (Jenks)" method in the ArcGIS Pro environment on the heritage site data, which is explained in Section 3.3.1.

Table 3.3. Sensitivity classes of each sensitivity indicator.

	VL (1)	**L (2)**	**M (3)**	**H (4)**	**VH (5)**
Elevation Percentage of area below 10-meter elevation (%)	0 - 10	10 - 30	30 - 50	50 - 80	80 - 100
Area Percentage of area within 100-meter distance to the shoreline (%)	0 - 10	10 - 25	25 - 50	50 - 75	75 - 100
Proximity to the coastline Shortest distance to the shoreline (m)	2000 - 750	750 - 500	500 - 250	250 - 100	100 - 0
Interaction with the coastline Length of the shoreline segment directly interacting with the heritage site (m)	0 - 1500	1500 - 3000	3000 - 5000	5000 - 10000	> 10000

The sensitivity component of the CCHVAM is aggregated by a weighted sum approach utilizing the numerical values of the indicator sensitivity classes. The weight of each indicator value is obtained from the Analytical Hierarchy Process (AHP), which is explained in detail in the following part of this section. Utilizing the weights calculated with the AHP, the formula of the sensitivity component of CCHVAM is obtained as given below.

$$\text{Sensitivity} = (0.51*\text{Proximity}) + (0.31*\text{Elevation}) + (0.15*\text{Area}) + (0.03*\text{Interaction}) \quad [3.1]$$

Similar to the exposure classes, five sensitivity classes are defined from "Very High Sensitivity" to "Very Low Sensitivity", with numerical values from 5 to 1, respectively. The classes and their limiting sensitivity scores are presented in Table 3.4.

Table 3.4. Limiting values of the sensitivity classes.

Limit Value	Sensitivity Class
$0.00 \leq$ Sensitivity Score < 1.50	Very Low Sensitivity
$1.50 \leq$ Sensitivity Score < 2.50	Low Sensitivity
$2.50 \leq$ Sensitivity Score < 3.25	Moderate Sensitivity
$3.25 \leq$ Sensitivity Score < 4.25	High Sensitivity
$4.25 \leq$ Sensitivity Score	Very High Sensitivity

3.1.2.2.1 Parameter Weights of Sensitivity Components by AHP

The AHP is a multi-criteria decision-making method assessing the relative importance of various criteria in pursuit of a specific objective. It offers a structured framework for deconstructing complex decisions into a hierarchy of factors, which

enables a thorough evaluation of their contributions to the solution. The methodology of the AHP involves three main steps, which are outlined below.

A. Establishing the hierarchical structure of the problem

In this step, the problem is defined and the components contributing to the decision-making process are identified. These components are then organized into a hierarchical structure. As presented in Figure 3.3, in this hierarchy, the goal is placed at the top and followed by criteria and sub-criteria, if applicable, with potential alternatives at the lowest level.

For this study, the problem involves determining the weight of each sensitivity indicator of the CCHVAM based on its expected effects on the sensitivity score. Indicators are organized hierarchically based on expert input and literature review.

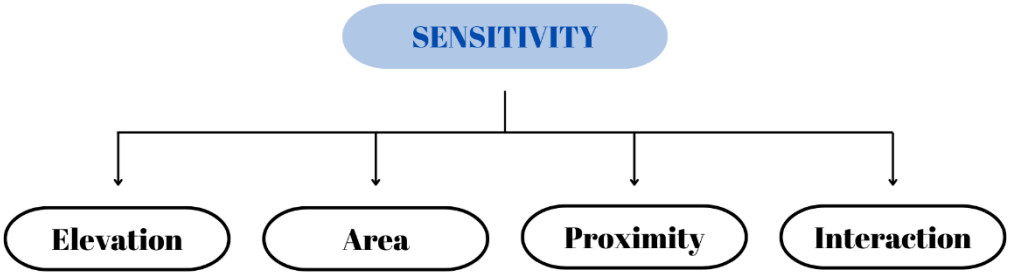


Figure 3.3. Decision hierarchy for the sensitivity component of the CCHVAM.

B. Pairwise Comparison

In the AHP, the relative importance of criteria is assessed through pairwise comparisons. Each criterion is compared against every other criterion, and their relative importance is rated on a scale from 1 to 9, as shown in the standard preference scale in Table 3.5.

Table 3.5. Standard Preference Scale used in AHP (Saaty, T. L., 1990).

Rate	**Indication**	**Meaning**
1	Equally important	Equal contribution to the solution
3	Slightly more important	Based on experience and judgment, one is slightly more preferred than the other
5	Considerably more important	Based on experience, one is more preferred than the other.
7	More Important	The importance of one over the other is proved in practice
9	Definitely more important	The validation of the preference of one over the other is confirmed in the highest possible order.
2, 4, 6, 8	Intermediate values	Existence of compromise between the rates listed above.

The following assumptions are made while describing the relative dominancy of each indicator over the sensitivity:

- A site that is closer to the shoreline is affected more by the threats posed at the corresponding coastline segment. It is simply because the outcomes of sea level rise, including inundation, coastal erosion, and coastal flooding, affect the coastal region starting from the shoreline and propagating landward.
- When two sites that are located in the same proximity to the shoreline are assessed, then the elevation indicator would be critical to provide a ranking among those. It is because in this case, the site that has more parts below 10 meters elevation is more sensitive to the impacts of sea level rise. The reason why the elevation indicator is more critical than the area and interaction length indicators is based on the assumption that a site can have higher values

for these indicators but if it is located on a high land, then the site is less sensitive than the other site with the same properties but located on a lower land.

- The area and the interaction length indicators provide insight into the shape of the site. It is assumed that if most parts of a site are located within 100-meter distance of the shoreline, then this site is significantly more sensitive than another site with the same proximity and elevation indicator values but having a narrower area at the coast.
- It is assumed that the interaction length indicator should have less impact on the sensitivity when compared to the other indicators. This is because this indicator does not provide direct information about the sensitivity, like proximity and the elevation indicators do. It only gives information about the length of the coastline segment with which the site is directly interacting, and the longer the coastline segment is, the variations in the coastline properties along the segment increase.

During the pairwise comparison, if the rate of a criterion is "x", the rate of the other criterion for the same pairwise comparison is "1/x". The pairwise comparison is performed on a judgment matrix shown in Table 3.6.

Table 3.6. The judgment matrix formed to perform the pairwise comparison for the sensitivity indicators.

	Proximity	Elevation	Area	Interaction
Proximity	1	5	7	9
Elevation	1/5	1	5	7
Area	1/7	1/5	1	5
Interaction	1/9	1/7	1/5	1

C. Defining the Priorities and Calculating Weights

After the judgment matrix is formed, the weight of each criterion is calculated by summing all the rates given for the criteria along the row and normalizing this value. This process is shown in Table 3.7.

Table 3.7. Computation of the weights of sensitivity indicators.

	Prox.	Elev.	Area	Interaction	Sum	Weight
Proximity	1	5	7	9	22.0	**0.51**
Elevation	1/5	1	5	7	6.34	**0.31**
Area	1/7	1/5	1	5	13.2	**0.15**
Interaction	1/9	1/7	1/5	1	1.45	**0.03**
				Total	43	1.00

3.1.2.3 Adaptive Capacity Component of the CCHVAM

The adaptive capacity component of the model is developed based on the definition by the IPCC, which is the ability of a system to adapt to the impacts of climate change, taking advantage of the opportunities or coping with the consequences (IPCC, 2007). The adaptive capacity component of the CCHVAM aims to provide insights into the conditions and the properties of a site that enhance its resilience against sea level rise and its impacts.

For assessing adaptive capacity, mostly qualitative indicators such as the awareness of local authorities, the awareness of local communities, and policies on conservation are considered in the literature (Daly, 2014). However, one of the goals targeted while developing the CCHVAM is to structure a model that can be utilized on a national scale, especially for qualitative indicators, such a database providing nationwide information may be hard to find. Hence, considering the data availability,

the two indicators given below are utilized to obtain the adaptive capacity component of the CCHVAM:

- Degree of Protection (DoP)
- Urbanization

The "Degree of Protection" indicator evaluates the legal action taken to protect the heritage sites. The higher the protection level is, the more protected and has stronger restrictions on the use. Hence, it can be assumed that there will be less pressure on the utilization of the area, as well as there will be a higher level of management plans and activities that would increase the resilience of the site. Although these activities might not be directly focused on sea level rise or its impacts, the site would still have a higher capacity to provide adaptation measures against the destructive effects of sea-level rise and its impact on the coastal area where the site is located.

In the scope of this study, the parameters for this indicator are defined based on the degrees of protection stated by Turkish Law 2863, "Protection of Cultural and Natural Assets" and assigned to each site by the local governmental bodies and the Ministry of Culture. The law defines three degrees of protection and their definitions are given below.

- 1st Degree Protection: All actions on the heritage site except for scientific studies and conservation measures are strictly forbidden.
- 2nd Degree Protection: In addition to scientific studies, restricted and controlled urbanization and maintenance are allowed.
- 3rd Degree Protection: New arrangements and the construction of new buildings are permitted as long as they are in line with the conservation use rules stated by the law.

The "Urbanization" indicator evaluates the percentage of built area within the interacting area around the assessed heritage site. The interacting area is defined as the area within a one-kilometer distance of the heritage. This area is determined by defining a buffer zone around the heritage site polygon with a width of 1 km in the

ArcGIS Pro environment. Then, the land use and land cover data are utilized to determine the built area in the buffer zone. The final parameter value is obtained from the percentage of the built area in the area of the heritage site and the buffer area. The adaptive capacity classes for this indicator are created by using the classes of the percentage values obtained from the Jenks method, similar to the indicator classes of exposure and sensitivity components.

The limiting values of the adaptive capacity classes of each indicator and their numeric values are presented in Table 3.8. Similar to the exposure and sensitivity components, five classes are defined for the adaptive capacity component. They are "Very High Adaptive Capacity (VH)", "High Adaptive Capacity (H)", "Moderate Adaptive Capacity (M)", "Low Adaptive Capacity (L), and "Very Low Adaptive Capacity (VL)". The numerical values of these classes are again on a scale from 1 to 5, where 5 is VH, and 1 is VL.

Table 3.8. Adaptive capacity classes of each indicator.

Indicator	**VL (1)**	**L (2)**	**M (3)**	**H (4)**	**VH (5)**
Degree of Protection (DoP) Degree of protection assigned by the ministry	3		2		1
Urbanization Percentage of built area within 1-km distance to the heritage site (%)	100 - 60	60 - 35	35 - 20	20 - 5	5 - 0

The overall "Adaptive Capacity (AC)" value is determined by normalizing the average of the two parameters, Equation 3.2 given below, after obtaining the indicator values.

$$AC = \frac{0.5 * (\text{DoP} + \text{Urbanization})}{5} \quad [3.2]$$

Similar to the other components of the CCHVAM, adaptive capacity classes are defined based on the computed AC values. In Table 3.9, these classes and the class limits are presented.

Table 3.9. Adaptive capacity classes and their limiting values.

Adaptive Capacity Values	Adaptive Capacity Classes
0.5 > AC	Low Adaptive Capacity
0.5 < AC < 0.7	Moderate Adaptive Capacity
AC > 0.7	High Adaptive Capacity

3.1.2.4 Potential Impact

Vulnerability assessment evaluates the conditions that make the site open to damage under climatic stressors and the opportunities that make it resilient against them. The parameters that enhance the resilience are assessed in the scope of the adaptive capacity component as described above, whereas the conditions that enhance the threat are assessed as potential impact in the last step of this methodology, providing the overall vulnerability.

As presented in Figure 3.2 in the previous part, after determining the sensitivity and exposure values of a site, the first major step is obtaining the potential impact.

Following the method utilized by Day et al. (2020), a decision matrix is created and used to determine the value of potential impact.

The classes assigned in the previous step, as explained earlier for sensitivity and exposure, are used in the matrix presented in Figure 3.4. It consists of various potential impact classes and assigns them to each site based on its sensitivity and exposure classes. The matrix assigns the potential impact classes to the sites with "Very Low" and "Low" sensitivity classes, applying a more conservative approach.

	Sensitivity				
Exposure	**Very Low**	**Low**	**Moderate**	**High**	**Very High**
Very Low	Very Low	Very Low	Very Low	Low	Low
Low	Very Low	Low	Low	Moderate	Moderate
Moderate	Very Low	Low	Moderate	High	High
High	Low	Moderate	Moderate	High	Very High
Very High	Low	Moderate	High	Very High	Very High

Figure 3.4. Decision-matrix of potential impact utilized in the CCHVAM.

Overall, the numeric values of exposure and sensitivity are converted to classes introduced in the sections 3.1.2.1 and 3.1.2.2, respectively. These classes are utilized in the matrix. The class of sensitivity is chosen on the second row, the class of exposure is chosen on the first column, and the class of potential impact is determined by the cell located at their intersection. Similar to the two components considered here, the potential impact is scaled over five classes. The class of potential impact indicates the level of threat resulting from both external and internal factors.

3.1.2.5 Vulnerability Matrix

The final result of the CCHVAM is the vulnerability class of each heritage site. It is determined by using another decision matrix similar to the one introduced in the previous part. This matrix is called the Vulnerability Matrix in the scope of this study, and it is presented in Figure 3.5. It takes the classes of adaptive capacity and potential impact as inputs. In other words, this matrix assesses the overall threat and the resilience available for a site, and it assigns a vulnerability class.

	Adaptive Capacity		
Potential Impact	**High**	**Moderate**	**Low**
Very Low	Very Low	Very Low	Low
Low	Low	Low	Moderate
Moderate	Moderate	High	High
High	Moderate	High	Very High
Very High	High	Very High	Very High

Figure 3.5. Vulnerability Matrix utilized in the CCHVAM.

This matrix is designed following a conservative approach and considering the properties of each model component, their classes, and the indicator classes.

3.2 Data Utilized in the Vulnerability Assessment

The heritage dataset utilized for this study and the data used for each component of the CCHVAM are described separately below.

3.2.1 Coastal Archaeological Heritage Sites of Türkiye

The archaeological heritage sites that are assessed in this study are the sites protected by Law 2863 “Protection of Cultural and Natural Assets” and assigned a degree of protection on the scale of one to three, where the first degree is the highest level of protection, as explained in Section 3.1.3. The data about the heritage sites is obtained from the Ministry of Culture and Tourism in the form of GIS layers via WMS servers. The raw data, the GIS layer, consists of 22898 archeological sites as polygons, presented in Figure 3.6.



Figure 3.6. Registered archaeological sites in Türkiye as shown in the GIS layer obtained from the Ministry of Culture and Tourism (2023).

These sites include all the archeological sites with 1st, 2nd, and 3rd degrees of protection in the mainland and the islands of Türkiye. However, the CCHVAM assesses only the sites satisfying either one or both of the model criteria regarding elevation and proximity to the shoreline, as explained in Section 3.1.1.

The sites satisfying these criteria are determined by generating a contour line and a buffer. The contour line separates the areas below and above 10 meters of elevation,

where the elevation along the shoreline is taken as zero, and it is obtained by utilizing the Digital Elevation Model (DEM) data with a spatial resolution of 25 m (EU-DEMv1.1, 2022). The shoreline is obtained as a line layer in the ArcGIS Pro environment. Then, the buffer is generated on both sides of the shoreline with a width of 1 km by utilizing the "Buffer" command of the ArcGIS Pro.

The archaeological site polygons that do not intersect with the buffer or the area between the contour line and the shoreline are eliminated from the layer. Also, in the scope of this study, only the sites located on the mainland are assessed. Hence, the heritage site layer consists of 1176 archaeological site polygons. It is determined that there are 467 sites located within 1 km distance to the shoreline but have no parts below 10 m elevation, and 709 sites located closer than 1 km to the shoreline and have some parts lower than 10 m. In Figure 3.7, the archaeological sites assessed in this study are presented.

The GIS layer provides information about the location, area, and degree of protection of each site protected by the law.

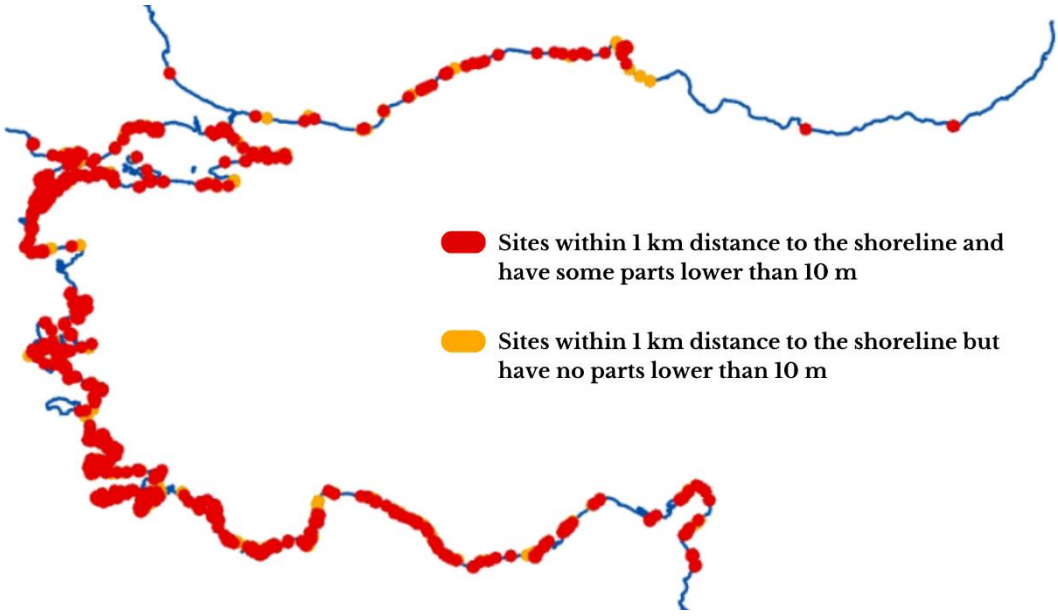


Figure 3.7. The archaeological sites assessed by utilizing the CCHVAM in this study.

3.2.2 Data Utilized for the Exposure Component

In the scope of this study, the results obtained by Ince (2024) from the application of the modified version of FCVAM are used as the input for the exposure component of the CCHVAM. Ince applied the model by using the sea level rise projections based on all emission scenarios presented in AR6 (2023); however, in this study, only the results obtained for the SSP2-4.5 “Likely Future” and SSP5-8.5 “the Worst-Case Scenario” are utilized as exposure data.

As explained in Section 3.1.2.1, Ince (2024) computed separate impact scores for inundation, flooding due to storm surge, and coastal erosion, and obtained a coastal vulnerability index (CVI) by the aggregation of these impact scores. In the scope of this study, two sets of assessments are done with the CCHVAM: in the first set, the overall CVI values are used, and in the second set, the coastal erosion impact scores are used as the exposure component values. Both sets of assessments are performed by using the values obtained from the data of SSP2-4.5 and SSP5-8.5 scenarios, separately.

The data is obtained as a line layer because the FCVAM provides the vulnerability score of shoreline segments. The vulnerability of the shoreline segment directly interacting with each heritage site is provided in this GIS layer; the shoreline segments are called “Interaction Line”, and the layer is shown in Figure 3.8. In order to provide a clearer view, the coastline of Muğla is also shown in Figure 3.8a.

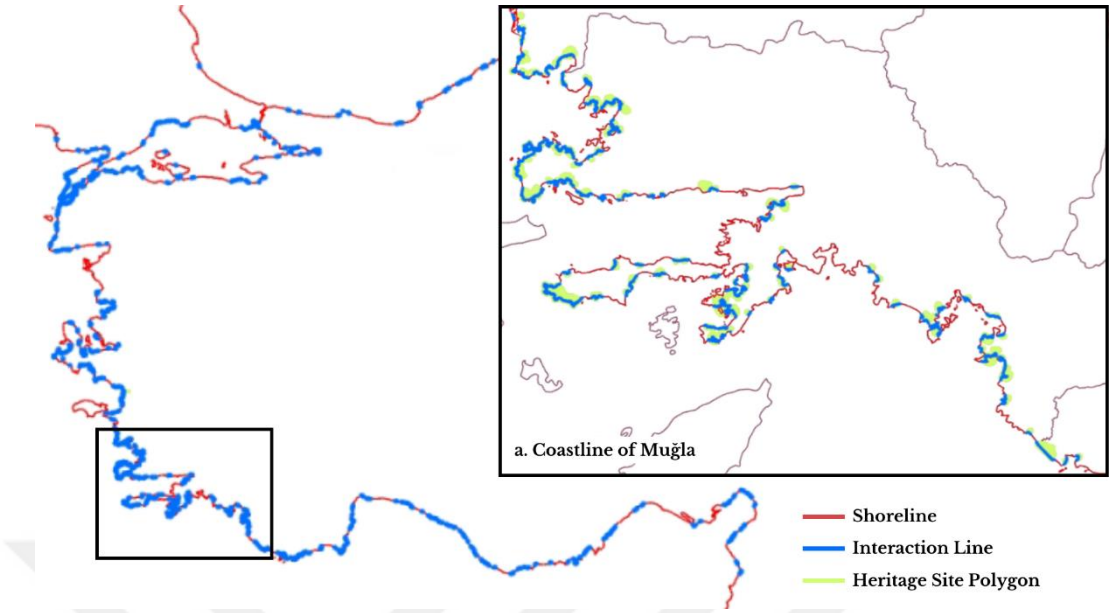


Figure 3.8. The GIS layer providing the exposure data.

3.2.2.1 CVI Values Based on SSP2-4.5

The results, obtained from the application of the modified FCVAM on the coastline segments interacting with the coastal archaeological heritage sites of Türkiye, revealed that the majority of the assessed coastline segments have low and moderate vulnerability to sea level rise and its impacts. Also, it is seen that the majority the sites with low and moderate vulnerability are located along the coastlines in the Mediterranean and Aegean regions, as presented in Table 3.10 and Figure 3.9.

Table 3.10. Regional distribution of the sites based on CVI values obtained for the SSP2-4.5 emission scenario (Ince, 2024).

CVI	Mediterranean	Aegean	Marmara	Black Sea
Very Low (0.0, 1.5)	0	0	0	0
Low [1.5, 2.5)	341(29%)	281(23.9%)	77(6.5%)	95(8.1%)
Moderate [2.5, 3.5)	91(7.7%)	195(16.6%)	84(7.1%)	11(0.9%)
High [3.5, 4.25)	0	0	0	1(0.2%)
Very High [4.25, 5)	0	0	0	0

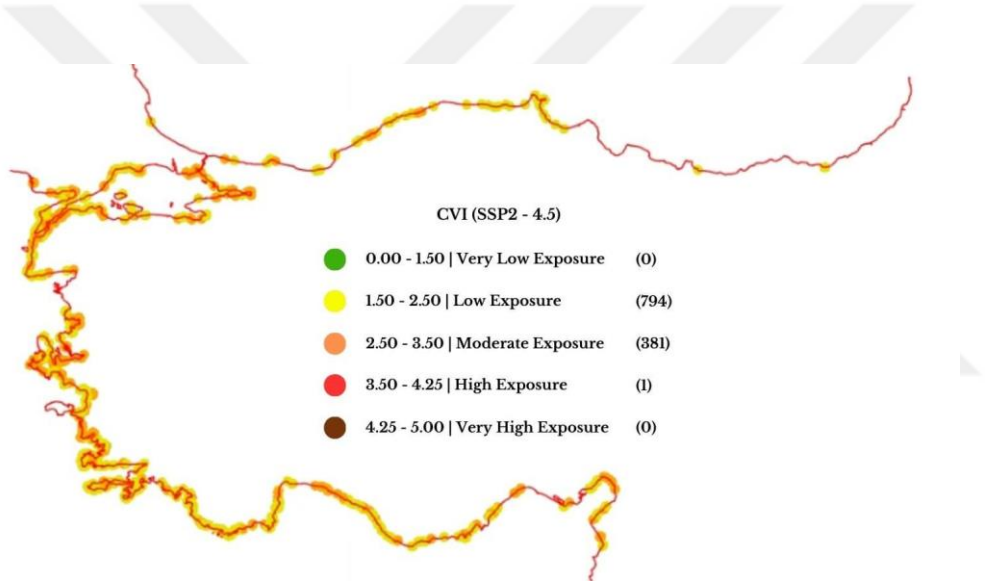


Figure 3.9. Distribution of the assessed coastline segments along the coastline of Türkiye.

3.2.2.2 CVI Values Based on SSP5-8.5

The same assessment is made with the modified FCVAM by utilizing the data based on the SSP5-8.5 emission scenario. As presented in Table 3.11, the number of sites in each region assigned to each exposure class is not significantly different from the ones obtained from the assessment based on the SSP2-4.5 scenario. Again, the

majority of the sites have low exposure, and the majority of these sites are located along the Mediterranean and Aegean coastlines, as shown in Figure 3.10.

Table 3.11. Regional distribution of the sites based on CVI values obtained for the SSP5-8.5 emission scenario (Ince, 2024).

CVI		Mediterranean	Aegean	Marmara	Black Sea
Very Low	**(0.0, 1.5)**	0	0	0	0
Low	**[1.5, 2.5)**	323 (27.5%)	273(23.2%)	75 (6.4%)	93 (7.9%)
Moderate	**[2.5, 3.5)**	109 (9.3%)	203(17.3%)	86 (7.3%)	13 (1.0%)
High	**[3.5, 4.25)**	0	0	0	1 (0.1%)
Very High	**[4.25, 5)**	0	0	0	0

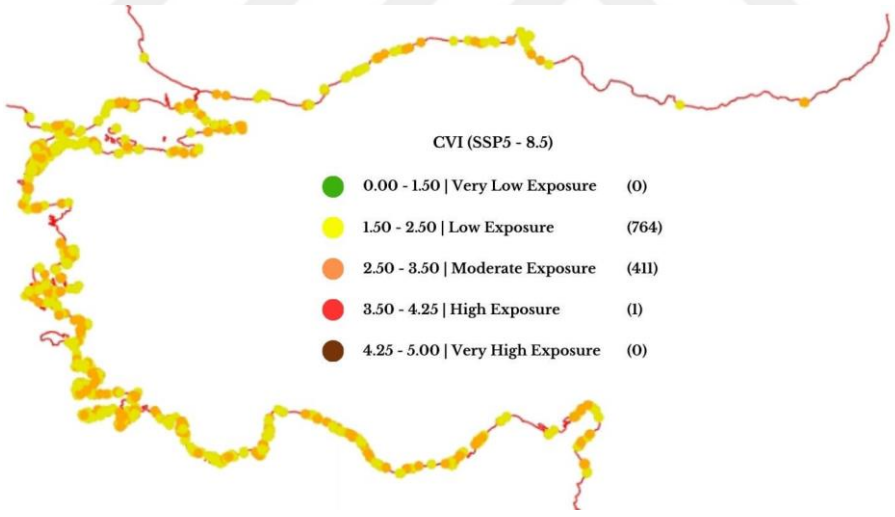


Figure 3.10. Distribution of the assessed coastline segments along the coastline of Türkiye.

3.2.2.3 Erosion Impact Score Based on SSP2-4.5

The erosion impact score integrates physical parameters with human parameters. As presented in Table 3.12, 69.4% of the coastal cultural heritage sites of Türkiye have low exposure to coastal erosion based on the impact scores computed by utilizing the data of the SSP2-4.5 emission scenario. The highest level of exposure to coastal erosion determined in this assessment is moderate, and in Figure 3.11, it can be seen that 47.5% of these sites are located along the Aegean coastline of Türkiye.

Table 3.12. Regional distribution of the sites based on erosion impact scores obtained for the SSP2-4.5 emission scenario (Ince, 2024).

Erosion Imp. Score	Mediterranean	Aegean	Marmara	Black Sea
Very Low (0.0, 1.5)	3 (0.22%)	1(0.08%)	0	0
Low [1.5, 2.5)	329 (28%)	306(26%)	101(8.6%)	80(6.8%)
Moderate [2.5, 3.5)	100 (8.5%)	169(14.4%)	60(5.1%)	27(2.3%)
High [3.5, 4.25)	0	0	0	0
Very High [4.25, 5)	0	0	0	0

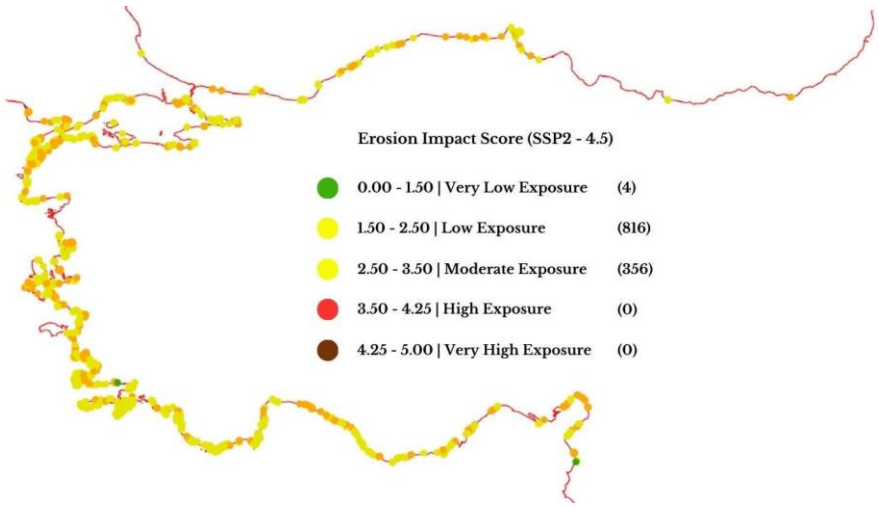


Figure 3.11. Distribution of the assessed coastline segments along the coastline of Türkiye grouped by their exposure classes.

3.2.2.4 Erosion Impact Scores Based on SSP5-8.5

The erosion impact score of each coastal cultural heritage site is obtained by combining the physical and human impact scores computed by using the data of the SSP5-8.5 emission scenario. As presented in Table 3.13 and Figure 3.12, based on this scenario, 52.8% of the assessed sites have moderate exposure.

Table 3.13. Regional distribution of the sites based on erosion impact scores values obtained for the SSP5-8.5 emission scenario (Ince, 2024).

Erosion Imp. Score		Mediterranean	Aegean	Marmara	Black Sea
Very Low	**(0.0, 1.5)**	2 (0.13%)	1 (0.07%)	0	0
Low	**[1.5, 2.5)**	208 (17.7%)	196(16.7%)	74(6.3%)	74 (6.3%)
Moderate	**[2.5, 3.5)**	222 (18.9%)	279(23.7%)	87(7.4%)	33 (2.8%)
High	**[3.5, 4.25)**	0	0	0	0
Very High	**[4.25, 5)**	0	0	0	0

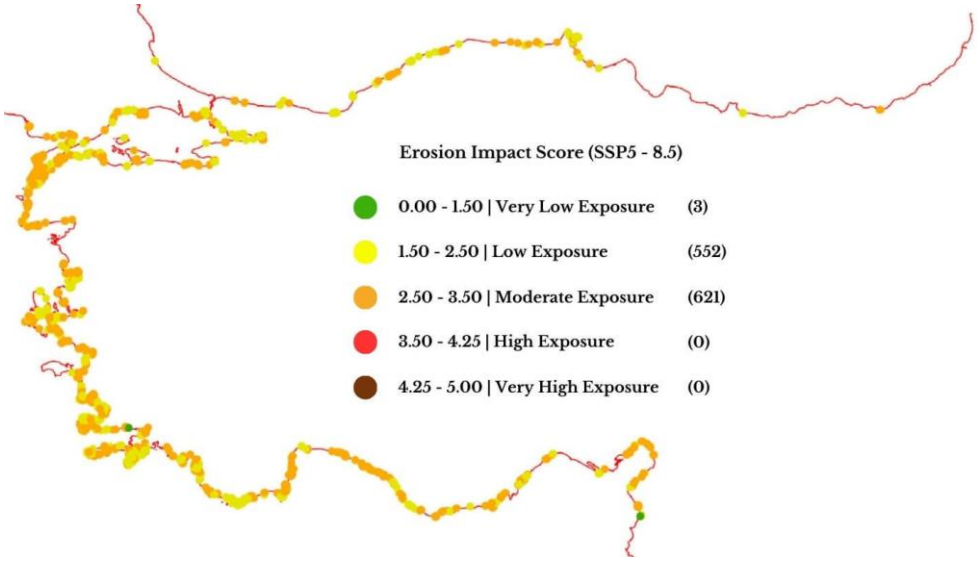


Figure 3.12. Distribution of the assessed coastline segments along the coastline of Türkiye grouped by their exposure classes.

3.2.3 Data Utilized for the Sensitivity Component

A set of indicators are assessed to obtain the sensitivity value including the elevation, area, interaction length, and proximity. The data about them is obtained as explained below.

Elevation

As described in the previous part, the elevation indicator expresses the percentage of the area of a heritage site that is lower than 10 m. This value is obtained by utilizing a series of commands in the ArcGIS Pro environment. First, a polygon layer is generated by the "Features to Polygon" tool, which shows the area between the contour line and the shoreline. Then, the area of a site that is below 10-meter elevation is determined by using the "Intersect" tool of ArcGIS Pro, which generates a polygon layer showing the intersecting area between the heritage polygon area and the generated polygon. The heritage polygon of Side Ancient City and the polygon showing the area lower than 10 m are shown in Figure 3.13, as an example. Finally, the area of each heritage polygon and the area of each polygon that shows the area within the heritage polygon and lower than 10 meters are determined by using the "Calculate Geometry" command of ArcGIS Pro.

When the percentage of heritage site area lower than 10 m is computed for each heritage site, it is seen that 30% of the heritage sites have more than 50% of their areas below 10 m elevation. The sites that are divided into elevation indicator classes and the number of those in each class are presented in Figure 3.14 below.



Figure 3.13. The heritage polygon of Side Ancient City and the polygon that shows the part of the heritage polygon below 10 meters elevation.

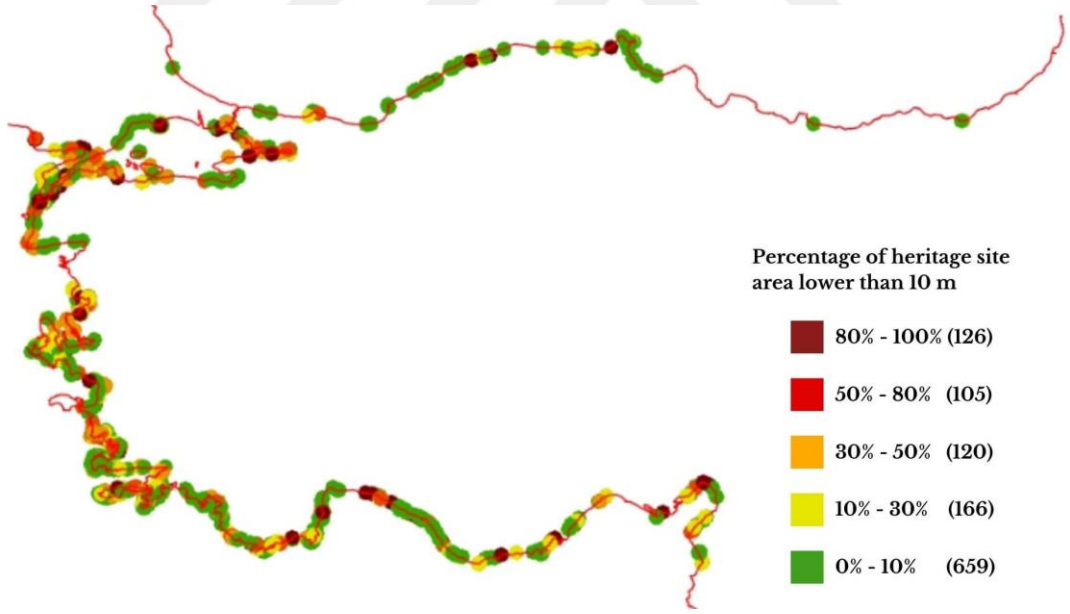


Figure 3.14. Heritage sites and the number of those in elevation indicator classes.

Area

The area indicator assesses the percentage of heritage site area that is within 100 m of the shoreline for each heritage site. This percentage value for each heritage site is obtained by utilizing a series of tools and commands in ArcGIS Pro, similar to the process applied for the elevation indicator. For this indicator, a buffer zone with a width of 100 m is generated on both sides of the shoreline. Then, the "Intersect" tool is used to generate a polygon layer consisting of the polygons showing the areas over the intersections of the buffer and the heritage polygons.

After computing the percentage of area within 100-m distance of the shoreline for each site, it is found that 173 sites have more than 50% of their areas closer than 100 m to the shoreline. The sites that are divided into five area indicator classes and the number of those in each class are presented in Figure 3.15.

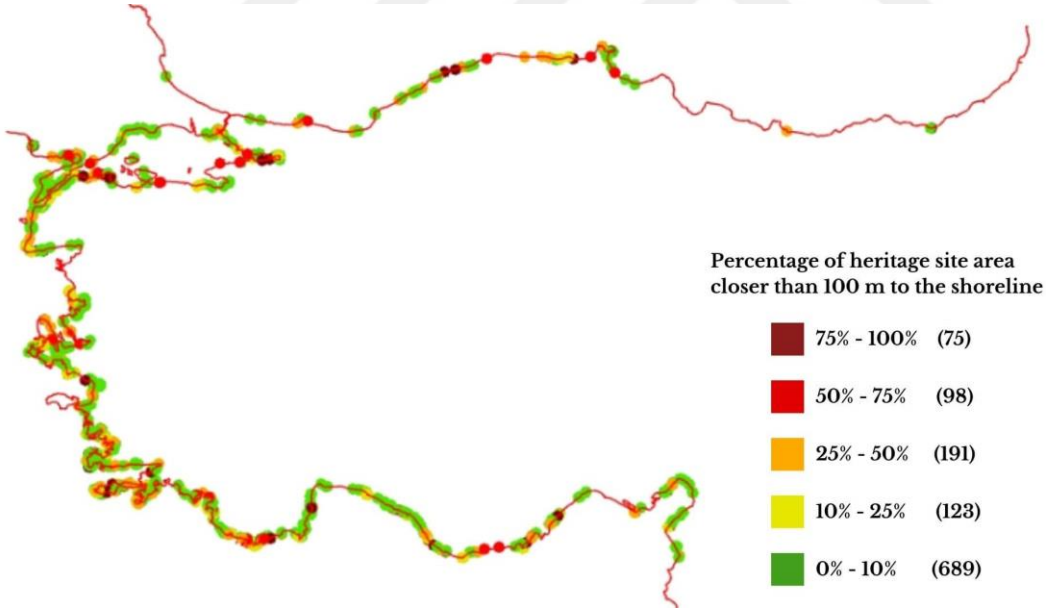


Figure 3.15. Heritage sites and the number of those in area indicator classes.

Proximity

This sensitivity indicator assesses the heritage sites based on their shortest distances to the shoreline, as shown in Figure 3.16. The shortest distance of each site is obtained by using the "Near" tool of ArcGIS Pro. After obtaining the shortest distance of each site in the layer, it is found that there are 468 sites located directly on the shoreline, which is 40% of all the archaeological sites assessed in this study by using the CCHVAM.

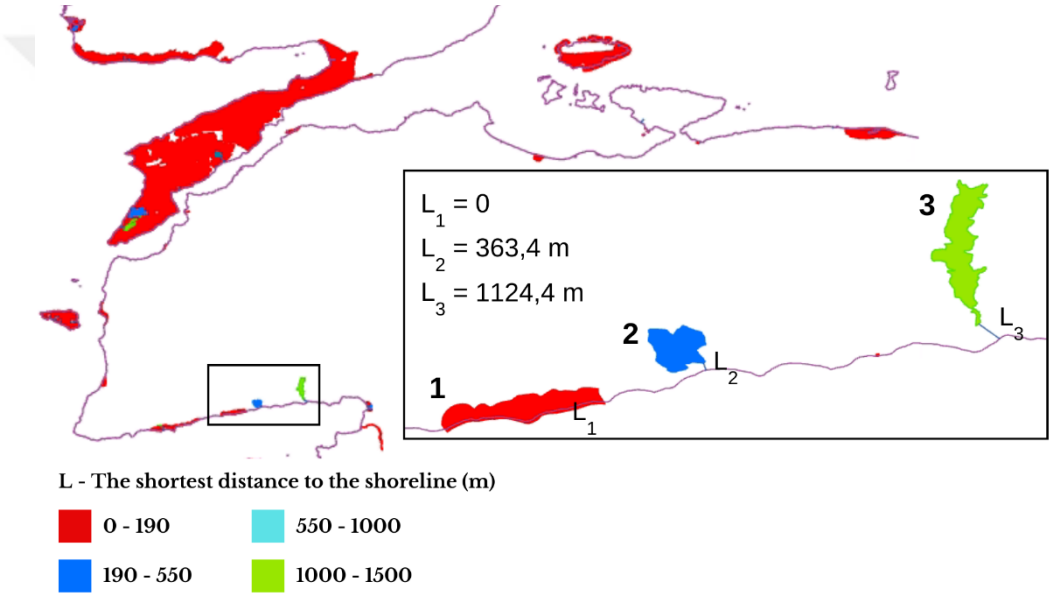


Figure 3.16. The shortest distance of each heritage site is measured between the boundary of the heritage polygon and the closest shoreline segment.

The sites that are divided into five proximity indicator classes and the number of those in each class are presented in Figure 3.17.

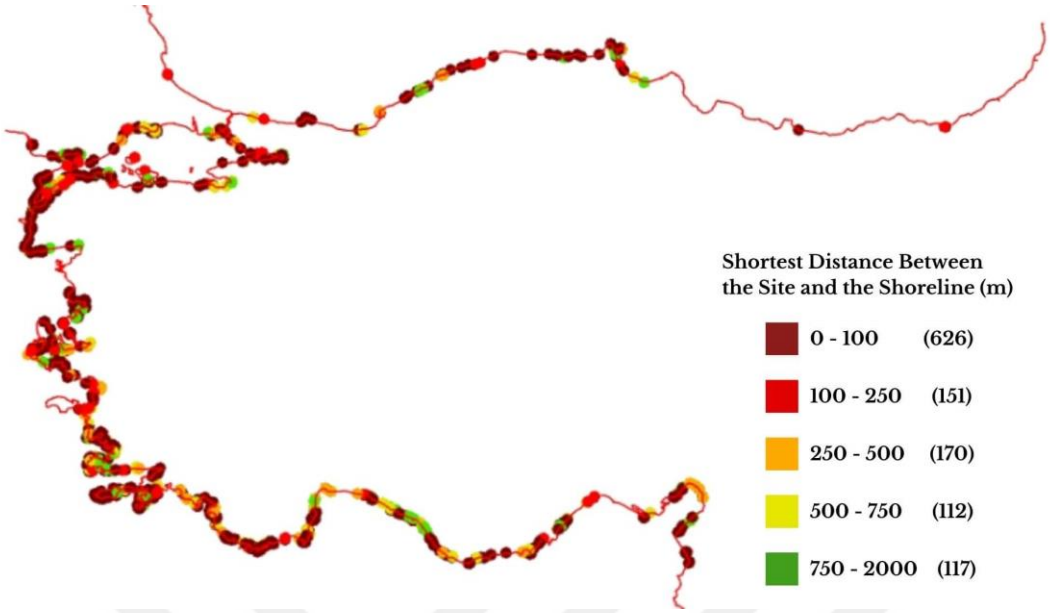


Figure 3.17. Heritage sites and the number of those in proximity indicator classes.

Interaction Length

This sensitivity indicator assesses the length of a shoreline segment that the heritage site is or could be interacted with under the coastal processes. The interacting shoreline segment with a heritage site is determined by simply generating a buffer with a width of 1 km from the boundary of the site polygon, as shown in Figure 3.18. Then, the line along which the length is measured and used for this indicator is generated by using the "Intersect" tool with a line output.

After obtaining the interaction length of each heritage site, it is found that 43% of the heritage sites have interaction lengths between 1.5 and 3 km. Furthermore, it is seen that 166 sites are interacting with coastline segments longer than 5 km, which have either "High" or "Very High" sensitivity based on the interaction length indicator.

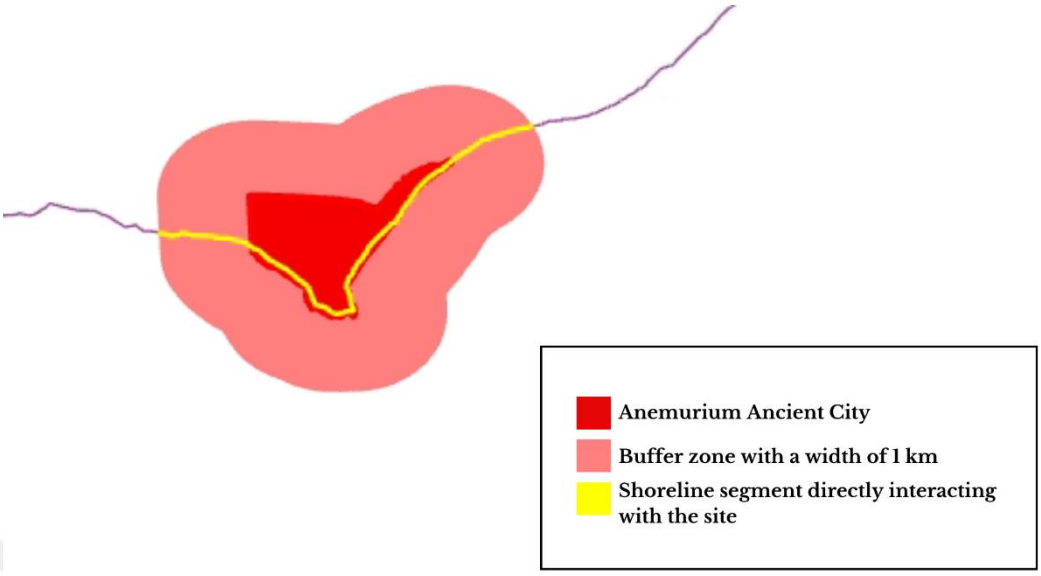


Figure 3.18. The coastline segment directly interacting with the Anemurium Ancient City, which is determined in the scope of this study.

The sites that are divided into five interaction length indicator classes and the number of those in each class are presented in Figure 3.19.

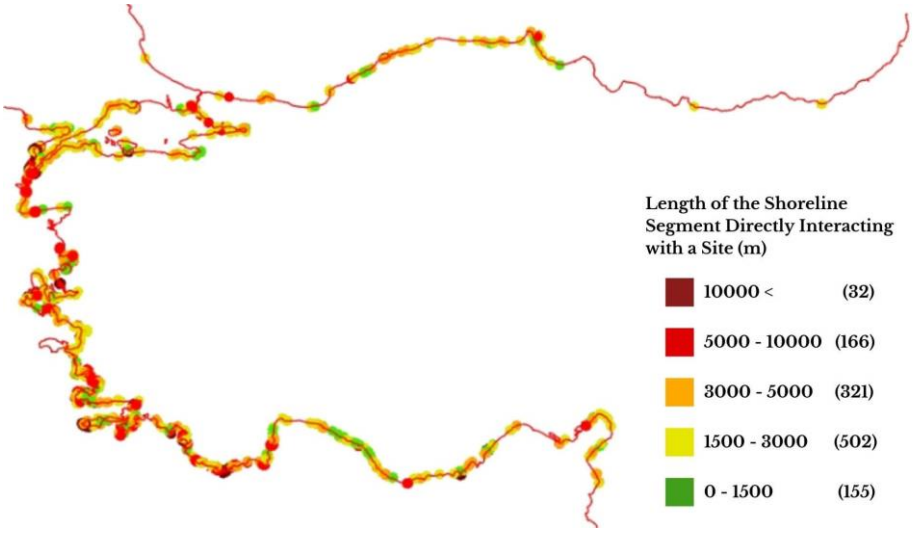


Figure 3.19. Heritage sites and the number of those in interaction length indicator classes.

3.2.4 Data Utilized for the Adaptive Capacity Component

For this component value of the CCHVAM, the degree of protection and urbanization indicators are assessed, and the data utilized for these assessments are introduced below.

Degree of Protection

The degrees of protection are assigned to the heritage sites by the ministry, hence, the data for this indicator is obtained from the raw layer accessed through the WMS server provided by the Ministry of Culture of Tourism. The challenge encountered while working on this data is that the protection degree information is not provided in the raw layer for most of the sites. For those, a conservative approach is applied, and an assumption is made, and they are assumed to be under 3rd-degree protection. In the raw layer, it is seen that there are 333 sites with a 1st degree of protection, which is 28.3% of all the assessed heritage sites. The sites that have the protection degree information provided in the raw layer are shown in Figure 3.20. In this figure, it can be seen that the majority of the sites under 1st-degree protection are located along the coasts of the Aegean and the Mediterranean, and unfortunately, for the majority of the sites, no information is provided in the raw data.

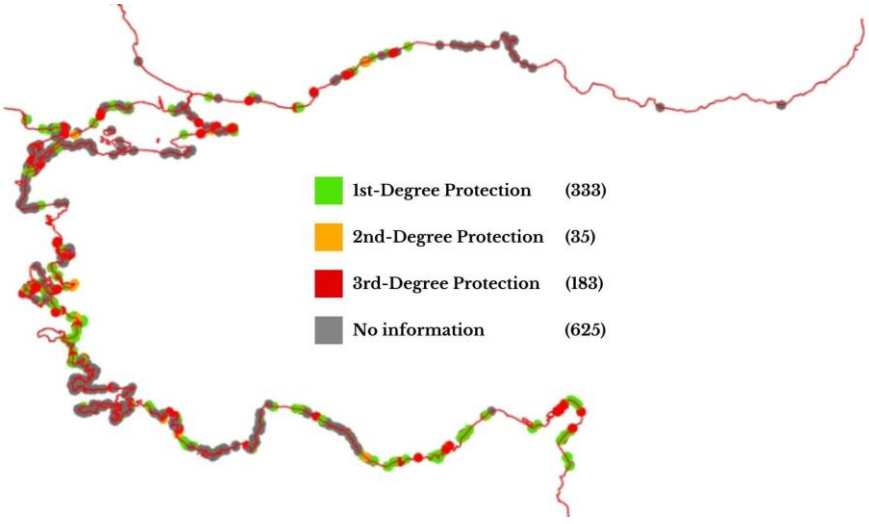


Figure 3.20. Geographical distribution of the sites based on the degree of protection indicator.

Urbanization

The deterioration in the natural urban tissue in the area that directly interacts with a heritage site is expected to enhance the vulnerability of the heritage site. Hence, as an adaptive capacity indicator, a low amount of urbanization is taken as a high adaptive capacity. In the scope of this model, this indicator assesses the percentage of built area within a one-kilometer distance of the heritage site.

The data on the built area is obtained from the "2012-2018 Coastal Zones Land Cover/Land Use Change" dataset of Copernicus (EU Copernicus Land Monitoring Service, 2021). The dataset with the spatial extent of "Europe" has a spatial resolution of 10 m. This dataset consists of three main GIS layers, and in this study, the most recent one, which provides data from the year 2018, is utilized.

The data in this layer is obtained from satellite images recorded between the years 2017 and 2019, and it consists of information about eight different land use classes, presented in Table 3.14.

Table 3.14. Land use/land cover classes assessed in the scope of Copernicus' Land Cover/Land Use Change dataset.

	1 Urban
	2 Cropland
	3 Woodland and Forest
	4 Grassland
	5 Heathland and Scrub
	6 Open Spaces with Little or No Vegetation
	7 Wetland
	8 Water

The land use class “1 (Urban)” includes the areas with urban fabric; industrial, commercial, public, and military units; transport infrastructure; mineral extraction, dump and construction sites, land without current use; green urban, sports, and leisure facilities.

The percentage value is obtained for each heritage site by generating a buffer with a width of one kilometer around the heritage site polygon. Then, the features with a land use attribute class of “1 (Urban)” of the land use layer are exported as a separate layer. Finally, the intersecting area of the exported land use layer polygons and the heritage site polygons is determined by using the “Intersect” command of ArcGIS Pro, as shown in Figure 3.21a to Figure 3.21d, and the area of the overlaying land use polygon is divided by the total area of the heritage site and the buffer.

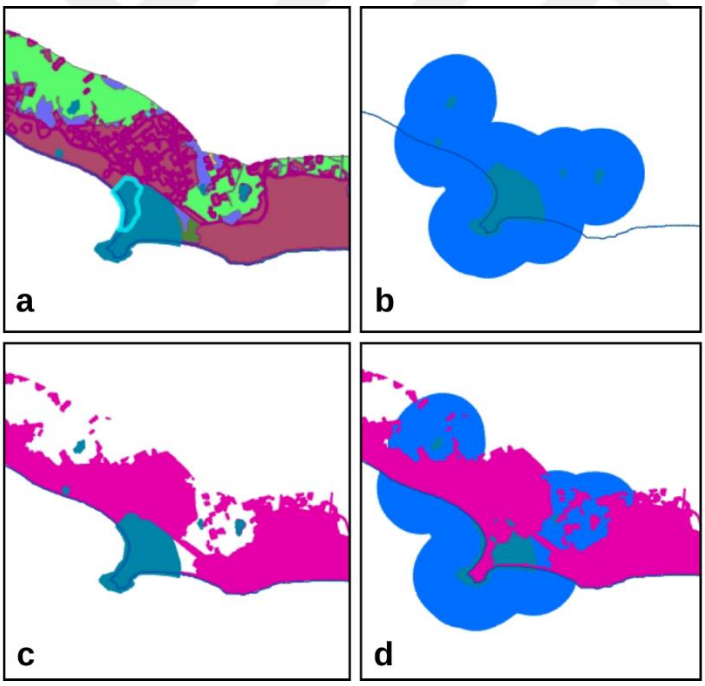


Figure 3.21. a. Land use in the region of Side Ancient City, b. Side Ancient City heritage polygon and the buffer zone, c. The urban area around the Ancient City, d. The urban area intersecting with the heritage site polygon and the buffer.

It is found that there are 170 coastal archaeological sites along the coastline of Türkiye that have urbanized land in more than 35% of their interacting area. Also, it is seen that 42% of all the assessed heritage sites have built areas in less than 5% of their interacting areas, of which the geographic distribution along Türkiye's coastline can be seen in Figure 3.22.

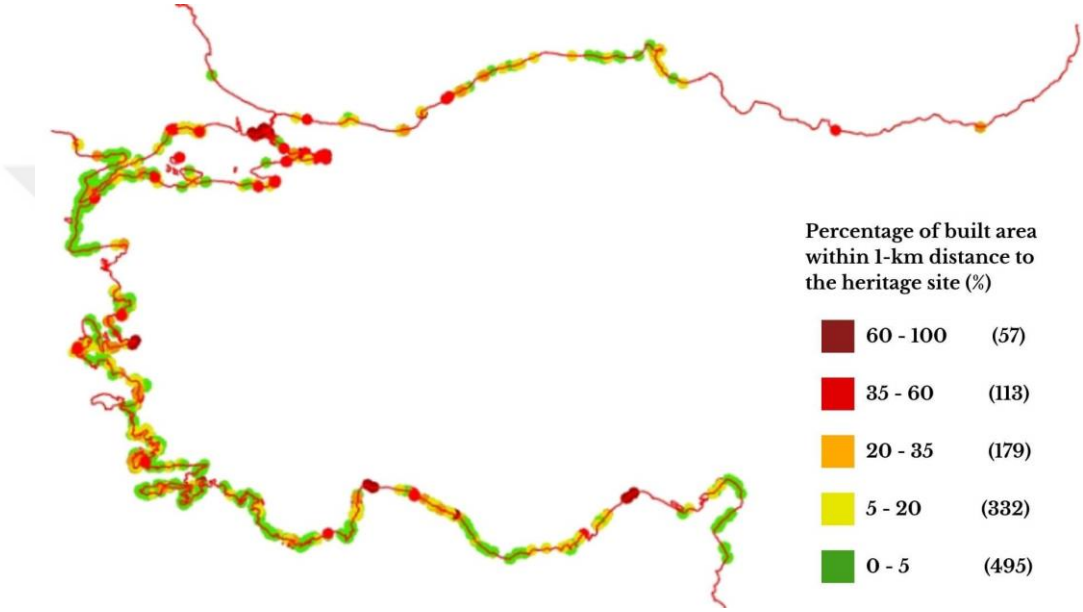


Figure 3.22. Heritage sites and the number of those in urbanization indicator classes.

After obtaining and processing the data that are introduced above, the process described in the previous part is followed, and the coastal archaeological heritage sites along the coastline of Türkiye are assessed by using the CCHVAM.

3.3 Discussions About Methodology and Data

The Coastal Cultural Heritage Vulnerability Assessment Model is a newly developed method to evaluate the conditions and the properties of cultural heritage sites located in coastal areas that can be adversely affected by the outcomes of sea level rise

resulting from climate change. Hence, there are several assumptions and checks made while developing it and identifying the indicators to be utilized in the model for the assessment.

3.3.1 Class Limits of Sensitivity Indicators

The value of the sensitivity component is obtained from the newly developed methodology and selected indicators. The computation of the sensitivity value starts with the assessment of a site based on defined indicators. As stated in Section 3.1.2, the indicators are defined based on the literature review findings. However, the limits of indicator classes are determined based on the grouping of the study database obtained by using the Jenks method on the heritage layer in ArcGIS Pro. The Jenks method aims to generate groups in the data where within-group variance is the minimum and between-group variance is the maximum, hence, it provides a grouping based on natural breaks in the data (Jenks, 1967). Hence, when the methodology is followed with a different dataset, it is recommended that the naturally formed groups within the data should be checked first and compared to the classes generated by the CCHVAM methodology for the sensitivity indicators.

3.3.2 The Impact of Weights on the Computation of Sensitivity Value

The computation process of the sensitivity value of each site is developed by checking the results obtained from consecutive trial assessments made with the input data. For initial trials, all the indicators are assumed to have equal weights, and the overall sensitivity is computed by taking the arithmetic average of the indicator values. However, when the results of this computation are checked, it is seen that some of the sites located further away from the shoreline are assigned to higher sensitivity levels than those located closer to the shoreline because they interact with a much shorter shoreline segment. Then, it is decided that different weights should

be assigned to the indicators, providing information about the dominance of an indicator over the other.

After the AHP application, the impact of weights is checked through a series of schematic views. In those, different combinations of possible indicator conditions are presented, as shown in Figure 3.23. Then, each site on these views is assessed twice; equal weights are used in the first assessment, and different weights are used in the second assessment.

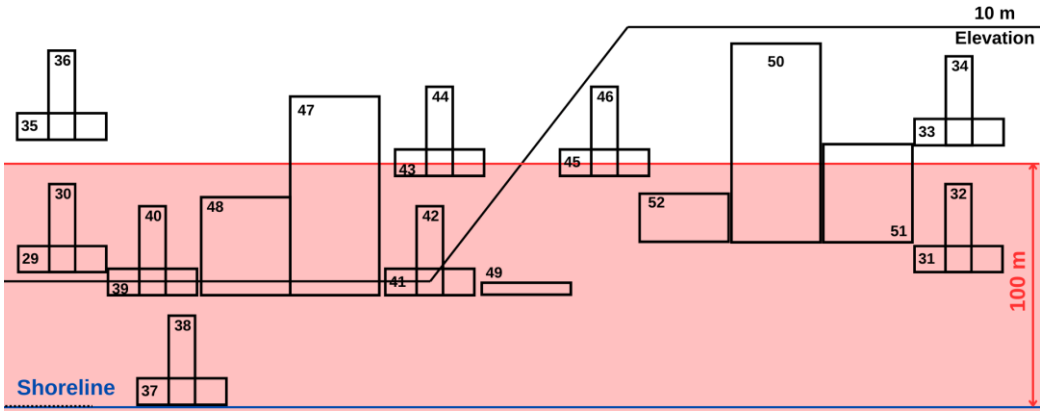


Figure 3.23. Schematic view where representative heritage sites with different positions along the coastline are shown.

In the sample assessment done on the sites shown in the above schematic view, when the indicators are assumed to have equal dominance over the sensitivity, the sensitivity values of Site-31 and Site-38 are obtained as shown in Table 3.15.

Table 3.15. Computation of the sensitivity values of Site-31 and Site-38.

	Site-31	Site-38	Site-31	Site-38
Elevation	5	5	5*0.31	5*0.31
Area	5	5	5*0.15	5*0.15
Proximity	3	5	3*0.51	5*0.51
Interaction Length	5	3	5*0.03	3*0.03
Sensitivity	**18**	**18**	**3.98**	**4.94**

As given in Table 3.13, when equal weights are assumed, both sites get the same sensitivity value. This results from the fact that Site-31 is further away from the shoreline but interacts with a longer shoreline segment, whereas Site-38 is directly on the shoreline but interacts with a shorter shoreline segment. When the computation is repeated by using the weights obtained from the AHP with the same indicator values, Site-38 is found to be more sensitive than Site-31, which makes sense because it is directly on the shoreline, and this result is consistent with the assumptions made during the AHP.

Note that the coastline and the beach properties are assumed to be constant along the coastline segment shown in the schematic view. The indicator values assigned to the sites in the given schematic view are provided in Appendix A.

3.3.3 Limit Values of the Sensitivity Classes

The indicator properties of the sites in each sensitivity class are checked to see whether the defined methodology and the indicators provide a well-defined grouping, or not. Then, the sensitivity classes are adjusted after the initial results are checked while the model is being developed.

The initial limit values of the sensitivity classes are as follows: 0 to 1.5, 1.5 to 2.5, 2.5 to 3.5, 3.5 to 4.5, and 4.5 to 5.0. The distribution of sites assigned to the sensitivity classes based on these limit values for the proximity and elevation indicators is checked primarily because in the previous part of the process, those were selected as the two most dominant indicators. As presented in Figure 3.24, the sites assigned to "Low Sensitivity" and "Very Low Sensitivity" classes are separated from the rest, where there is no such clear separation between "Moderate Sensitivity", "High Sensitivity" and "Very High Sensitivity" classes. Hence, the limiting sensitivity values of these classes are re-evaluated.

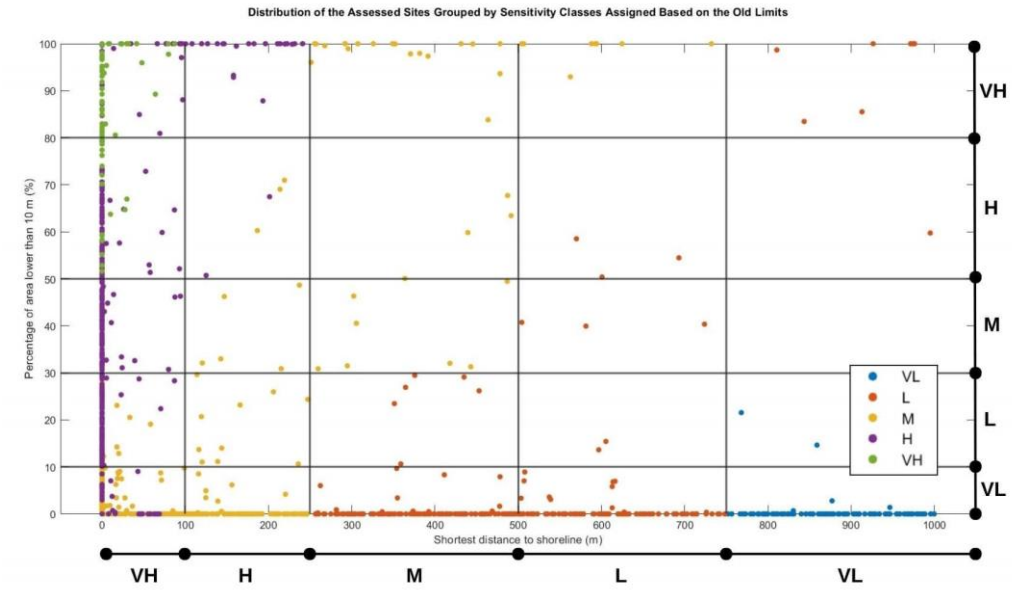


Figure 3.24. Distribution of sites based on their proximity and elevation indicator classes, and they are grouped based on their overall sensitivity values.

In Figure 3.24, the indicator sensitivity classes are presented with the black lines on the chart area and the black labels given on the right and bottom edges. The key points presented in this scatter plot are summarized in Table 3.16. With the initially assigned limit values of the sensitivity classes, it is observed that all the heritage sites

with the “Very Low Sensitivity” indicator class for the proximity, except the ones with a high sensitivity indicator class for the elevation indicator, are assigned to the “Very Low Sensitivity” class. A similar outcome is obtained for the heritage sites in the “Low Sensitivity” class. All the classes with the “Low Sensitivity” indicator class for proximity are assigned to the low sensitivity class, except for the ones with the “Very High Sensitivity” indicator class for elevation. However, as presented in Table 3.16, there are many indicator class combinations assigned to both moderate and high sensitivity classes at the same time, including the ones with “$VL_{elevation}VH_{proximity}$” indicator classes and the ones with “$L_{elevation}VH_{proximity}$” indicator classes.

Table 3.16. Elevation and proximity indicator sensitivity classes observed in sites assigned to each sensitivity class.

Sensitivity Class	**Observed Indicator Sensitivity Combinations**
Very Low (0,1.5)	VL_{elev} VL_{prox} & L_{elev} VL_{prox}
Low [1.5, 2.5)	VL_{elev} M_{prox} - VL_{elev} L_{prox} - L_{elev} M_{prox} - L_{elev} L_{prox} - M_{elev} L_{prox} - H_{elev} L_{prox} - H_{elev} VL_{prox} - VH_{elev} VL_{prox}
Moderate [2.5, 3.5)	VL_{elev} VH_{prox} – VL_{elev} H_{prox} – L_{elev} VH_{prox} – L_{elev} H_{prox} – M_{elev} H_{prox} – M_{elev} M_{prox} – H_{elev} H_{prox} – H_{elev} M_{prox} – VH_{elev} M_{prox} – VH_{elev} L_{prox}
High [3.5, 4.5)	VL_{elev} VH_{prox} – L_{elev} VH_{prox} – M_{elev} VH_{prox} – H_{elev} VH_{prox} – H_{elev} H_{prox} - VH_{elev} VH_{prox} – VH_{elev} H_{prox}
Very High [4.5, 5.0)	H_{elev} VH_{prox} – VH_{elev} VH_{prox}

The scatter plot, given as Figure 3.25, presents the distribution of sites based on their proximity to the shoreline and overall sensitivity values, grouped by elevation indicator sensitivities. In this grouped scatter plot, it can be seen that there are only

the sites with a certain indicator sensitivity class combinations with the overall sensitivity value between 2.5 and 1.5 (low sensitivity class) and below 1.5 (very low sensitivity class), whereas there are sites assigned to multiple sensitivity classes although they have the same indicator sensitivity class combinations, of which the overall sensitivity value is above 2.5 (Moderate, high and very high sensitivity classes), as explained earlier.

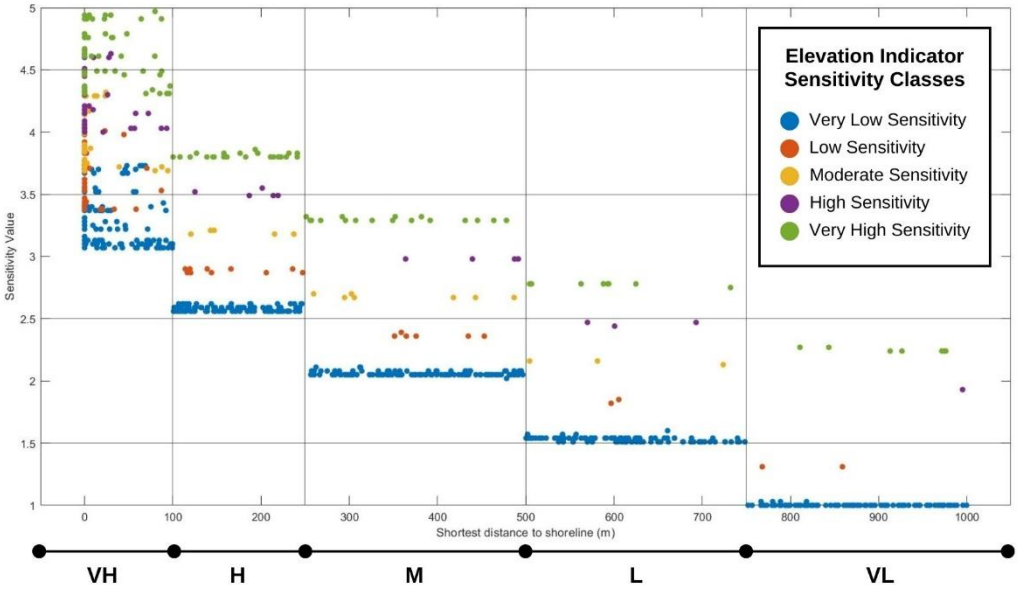


Figure 3.25. Grouped scatter plot showing the distribution of sites based on their proximity parameter and sensitivity values, and grouped by their elevation indicator.

Based on these scatter plots, the limiting values of the sensitivity classes are modified. Then, the plot given in Figure 3.24 is generated with the grouping by the new sensitivity classes, and this plot is provided in Figure 3.26. The differences in these plots can be summarized as follows:

- The new sensitivity class limits provide a more conservative assessment as the majority of the sites with over 30% of their areas below 10 meters

elevation and within 100 m distance of the shoreline are assigned to “Very High Sensitivity” class with the new limits, whereas the sites with a percentage of area below 10 m is between 30% and 50% are all assigned to “High Sensitivity” class even the ones directly on the shoreline with the old limit values. Also, none of the sites that are located directly on the shoreline are assigned to a lower sensitivity class than “High Sensitivity” with the new limit values.

- All the sites with more than 50% of their areas lower than 10 m and with a moderate indicator sensitivity for the proximity are assigned to the “Moderate Sensitivity” class when the old limit values are applied. However, when the new limit values are applied, the sites with over 90% of their areas below 10 m elevation and moderate indicator sensitivity for the proximity are assigned to the “High Sensitivity” class.

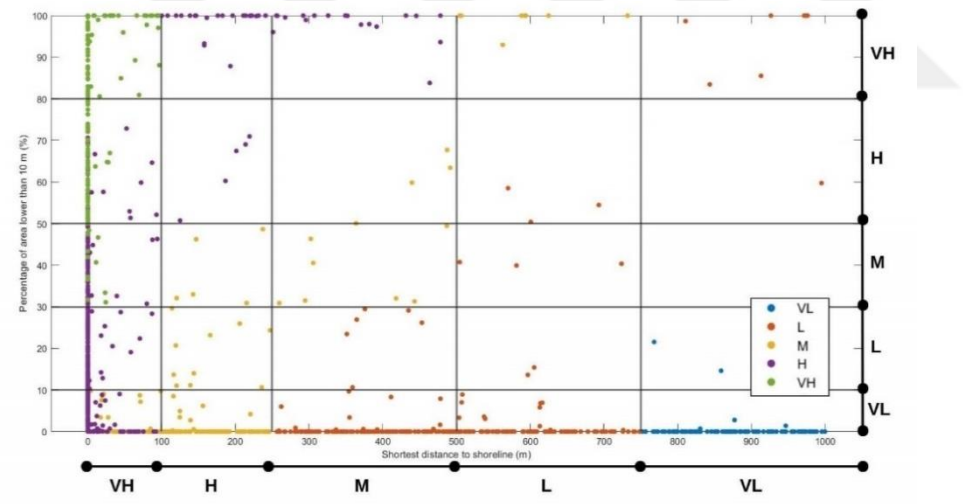


Figure 3.26. Distribution of sites based on their overall sensitivity values and their proximity parameter value after the class limits are modified.

After modifying the sensitivity class limits, the elevation and proximity indicator sensitivity classes observed in each sensitivity class are re-checked and summarized

in Table 3.17. When the new limit values of the sensitivity classes are applied, all the heritage sites with the indicator sensitivity combinations of "$L_{elevation}VH_{proximity}$", "$H_{elevation}H_{proximity}$", and "$VH_{elevation}M_{proximity}$" are moved from the "Moderate Sensitivity" class to the "High Sensitivity" class. Also, all the heritage sites with the indicator sensitivity combinations of "$M_{elevation}VH_{proximity}$", "$H_{elevation}VH_{proximity}$", and "$VH_{elevation}VH_{proximity}$" are moved from the "High Sensitivity" class to the "Very High Sensitivity" class.

Table 3.17. Elevation and proximity indicator sensitivity classes observed in sites assigned to each sensitivity class.

Sensitivity Class	**Observed Indicator Sensitivity Combinations**
Very Low (0,1.5)	VL_{elev} VL_{prox} & L_{elev} VL_{prox}
Low [1.5, 2.5)	VL_{elev} M_{prox} - VL_{elev} L_{prox} - L_{elev} M_{prox} - L_{elev} L_{prox} - M_{elev} L_{prox} - H_{elev} L_{prox} - H_{elev} VL_{prox} - VH_{elev} VL_{prox}
Moderate [2.5, 3.25)	VL_{elev} VH_{prox} – VL_{elev} H_{prox} – L_{elev} H_{prox} – M_{elev} H_{prox} – M_{elev} M_{prox} – H_{elev} M_{prox} – VH_{elev} L_{prox}
High [3.25, 4.25)	VL_{elev} VH_{prox} – L_{elev} VH_{prox} – M_{elev} VH_{prox} – H_{elev} VH_{prox} – H_{elev} H_{prox} – VH_{elev} H_{prox} - VH_{elev} M_{prox}
Very High [4.25, 5.0)	M_{elev} VH_{prox} – H_{elev} VH_{prox} – VH_{elev} VH_{prox}

After the modification of the sensitivity class limits, as presented in Table 3.18, a significant increase is observed in the number of sites assigned to the "High Sensitivity" and "Very High Sensitivity" classes due to the fact that the new limit values apply a more conservative approach while providing a well-grouped distribution of the assessed heritage sites.

Table 3.18. Distribution of the assessed sites based on old and new sensitivity class limits.

Old Limit Values		**New Limit Values**	
Sensitivity Class	# of Sites	Sensitivity Class	# of Sites
Very Low (0.0, 1.5)	109	Very Low (0.0, 1.5)	109
Low [1.5, 2.5)	252	Low [1.5, 2.5)	252
Moderate [2.5, 3.5)	**374**	Moderate [2.5, 3.25)	**232**
High [3.5, 4.5)	**377**	High [3.25, 4.25)	**436**
Very High [4.5, 5.0)	**64**	Very High [4.25, 5.0)	**147**

CHAPTER 4

SHORELINE EVOLUTION MODELING WITH THE DIGITAL SHORELINE ANALYSIS SYSTEM (DSAS)

Rising sea levels have serious impacts on coastal areas, and one of those is coastal erosion, as explained in Chapter 2. Coastal erosion threatens ecosystems, residential and commercial areas, and heritage sites in coastal zones. It is explained in Chapter 3 that the newly developed CCHVAM can assess the vulnerability of coastal heritage sites to coastal erosion when the corresponding impact score is utilized as the exposure component. In the scope of this study, the vulnerability of coastal cultural heritage sites of Türkiye to coastal erosion is assessed with the CCHVAM. Hence, in order to check the accuracy of that, shoreline evolution modeling is performed separately by using the Digital Shoreline Analysis System (DSAS). The change in shoreline positions in the Anemurium Ancient City and the Soli-Pompeiopolis Ancient City is investigated. In this chapter, the input data utilized for this modeling process and the properties of the assessed heritage sites are presented.

As the impacts of climate change started to be observed and studied more, a need for innovative tools to accelerate assessments surfaced. Researchers have always tried to develop more reliable and easy-to-use tools utilizing the technology, data, and knowledge available. Shoreline mapping was one of the methods used to assess the shoreline evolution "as both a scientific and management tool" in the 1980s and early 1990s. However, a standardized method was needed to provide accurate and quantified results on the change in shoreline position over time. Hence, Danforth and Thieler (1992) proposed a new method and tool for applying that.

The DSAS is a geospatial tool developed by the United States Geological Survey (USGS). It is presented as a tool that generates transects at user-defined intervals and computes the rates of shoreline change by utilizing various statistical techniques, including linear regression. This tool utilizes shoreline and baseline data in JSON

format and provides information about the trend observed in shoreline evolution. The first public version of the DSAS was introduced as an extension of ArcView in 2005. Over the years, with enhancements implemented, the DSAS became an extension toolbox of various ArcGIS platforms, including ArcMap and ArcGIS Pro. The latest version of the DSAS (v6.0.168) was released in 2024 as a stand-alone product (U.S. Geological Survey, 2024). The input data are shoreline and baseline prepared in any of the GIS software based on certain attributes as described below in the "Data Preparation" section.

The development of DSAS has significantly enhanced the field of shoreline change analysis because it enables coastal researchers to track erosion, accretion, and long-term shoreline movement trends easily.

4.1 Computation Process in DSAS

As introduced above, DSAS utilizes shoreline data and baseline data to provide insights into the observed change in the shoreline position. It requires this database to be introduced as JSON files, and it casts transects based on the defined spacing and length values. Note that the cast transects can be exported as JSON files, opened, and modified in the ArcGIS Pro environment. Also, a line layer of transects can be imported to the DSAS in JSON format, and it can be utilized for the analysis in the software shown in Figure 4.1. After the transects are introduced to the system, the analysis can be run.

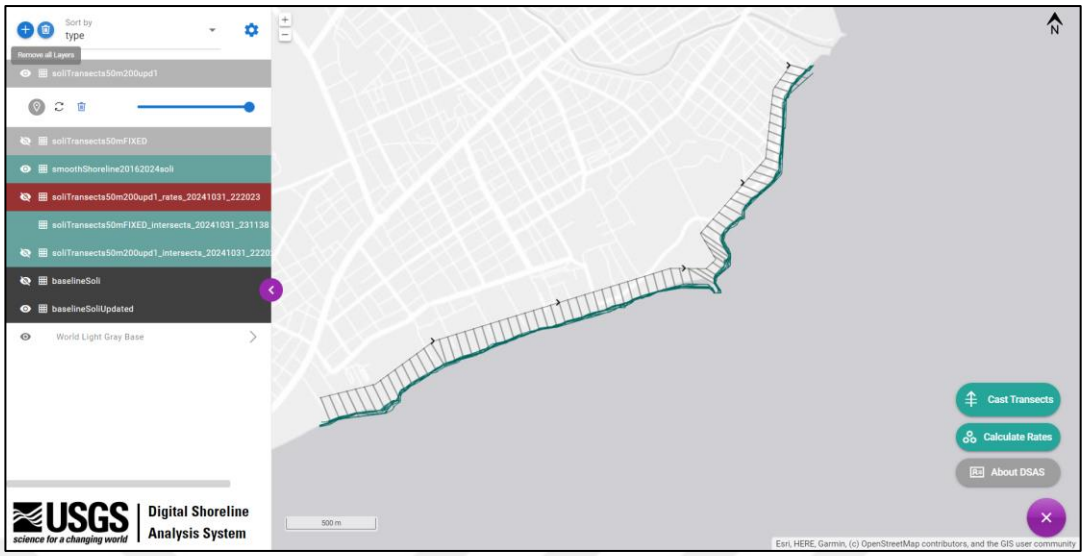


Figure 4.1. The interface of DSAS v6.0.168 with the input data for the analysis of the shoreline segment interacting with the Soli-Pompeiopolis Ancient City loaded.

The output files provided by the DSAS are listed below.

- Line layer of transects with the computed rates and measurements defined as attributes in JSON format.
- Point layer showing the intersection points of shorelines and transects in JSON format.
- Summary report consisting of rates and measurements as a “txt” file.

The distances and rates of the shoreline movement obtained as outputs from the DSAS are:

Shoreline Change Envelope (SCE) - The greatest distance among all the shorelines along a given transect. It is given in meters.

Net Shoreline Movement (NSM) - The distance between the oldest and latest shoreline along a given transect. It is given in meters.

End Point Rate (EPR) - The rate is obtained by dividing the net shoreline movement by the time elapsed between the dates of the oldest and the latest shorelines. This is given in meters per year.

An illustration explaining how these distance measurements and the rate are obtained is provided in Figure 4.2.

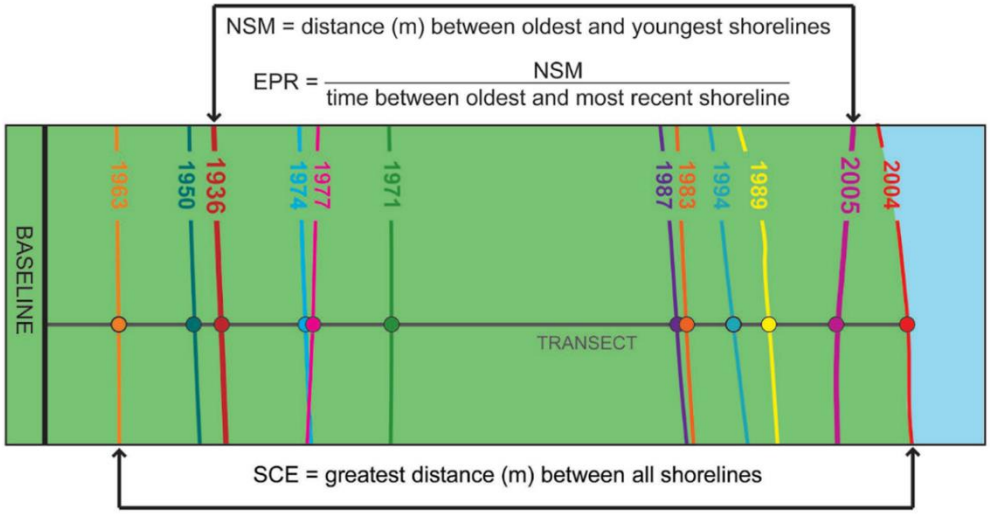


Figure 4.2. The illustration describing how the values of net shoreline movement, shoreline change envelope and end point rate are computed (Himmelstoss, E.A., et al., 2021. Digital Shoreline Analysis System (DSAS) Version 5.1 User Guide).

Linear Regression Rate (LRR) - This rate is obtained by fitting a least-squares line to all the shoreline points along a given transect line. The regression line is cast to minimize the sum of squared residuals, which is computed by getting the square of the offset distance of each data point from the regression line and adding all the squared residuals together. This value is given in meters per year.

4.2 Study Area

The CCHVAM introduced in Chapter 3 is utilized to assess the vulnerability of coastal archaeological heritage sites along the coastline of Türkiye in the scope of this study. Hence, 1176 archaeological heritage sites on the mainland are assessed in total. Among these sites, the shoreline evolution analysis is performed for Soli-Pompeiopolis Ancient City and Anemurium Ancient, marked in Figure 4.3, which were selected as pilot study sites for the TUBITAK Project for enhanced flood mapping. Both sites are located in Mersin, Türkiye, which is one of the largest coastal cities of the country along its Mediterranean coastline, and there are ongoing archaeological excavations in both sites. DSAS is used to analyze the shoreline trend and predict the possible shoreline based on these trends for the future.

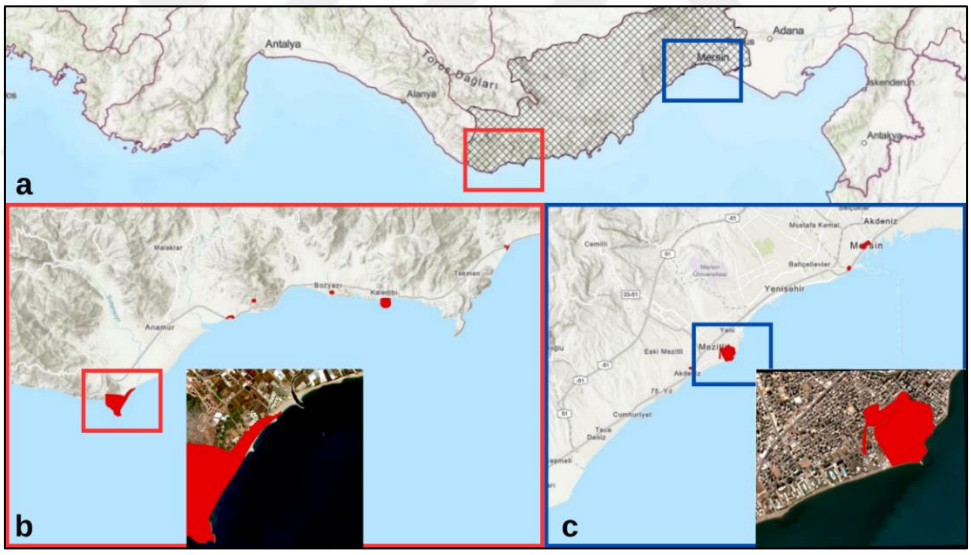


Figure 4.3. a. The Mediterranean coastline of Türkiye where Mersin and the assessed sites are highlighted. b. Location of Anemurium Ancient City in Anamur, Mersin. c. Location of Soli-Pompeiopolis Ancient City in Mezitli, Mersin (Google Earth, 2024).

4.2.1 Anemurium Ancient City

Anemurium Ancient City is located 10 km away from the center of Anamur District. Due to its location and the proximity of the coast to Cyprus, the city provided access to the sea for the other settlements in the inner parts of Anatolia, and it became a center of trade in the region (Doğan, Y. & Tekeli, M., 2024). Although the ancient port has not yet been found, numerous buildings remain, and these were found during the excavations.

Along the city's western border, on the steep slopes of a mountain, there is a necropolis area, which is the largest one in the region. It is reported that there are 350 tombs of different types in this area. On the other hand, the acropolis area of the city is located in the south on a steep and hilly area. The peak of the Anemurium Acropolis is reported to be approximately 149 m high, and it covers an area of 73,000 square meters of the ancient city, which can be seen in Figure 4.4.



Figure 4.4. Necropolis and acropolis of Anemurium Ancient City (Tekocak, M., 2021).

Anemurium is an ancient city lying along a long coastline segment, covering a large area in the coastal zone. The aerial photo of the heritage site area captured by an unmanned aerial vehicle (UAV) on September 21, 2024, (Figure 4.5) during the site visit, provides a detailed view of the Anemurium Ancient City and all the remnant structures in this area. The site is visited to obtain the data on the latest shoreline position and get information about the site from the archaeologists on site.



Figure 4.5. Top view of the Anemurium Ancient City captured by a UAV on September 21, 2024, during the site visit.

In the Acropolis area, there are remains of various public buildings such as churches, baths, and cisterns. Although most parts of the necropolis and acropolis areas are located on and along the steep hills, it can be seen in Figure 4.6 that there are still some structures located directly on the beach.



Figure 4.6. Some of the structures located on the beach of Anemurium Ancient City, photo taken by İremnaz Kösem during the site visit on September 21, 2024.

The archaeological inspections revealed that there are many ancient structures (churches, tombs, basilicas, etc.) either destroyed or deteriorated due to the climatic conditions of the region. Furthermore, Tekocak (2021) stated that it was understood that the destructive impacts keep getting more serious every day, requiring immediate action. Hence, the necessary protection and repair works for the structures in poor physical condition, the mosaic floors and wall frescoes have already started. In addition to the remarks of the archaeological excavation team, the results of wave

action on the structures close to the shoreline are observed and captured as given in Figure 4.7.



Figure 4.7. Some parts of the structures where the coastal material is taken away by the waves leaving gaps in the bottom parts of the structures, photo taken by İremnaz Kösem during the site visit on September 21, 2024.

4.2.2 Soli-Pompeiopolis Ancient City

Soli-Pompeiopolis Ancient City is located 12 km away from the Mersin city center in the Mezitli District. Archaeological evidence shows that the city was founded and developed during the Hellenistic and Roman periods (Akar, T., 2021). Resulting from its location on the coast, the city always had a strategic significance in ancient times. After a period of pirate invasion, the Roman general Pompeius saved the city from the pirates, and the city was named after him. Furthermore, during his trip to Anatolia, the great Roman emperor Hadrian visited the city and made a significant contribution to the construction of its harbor, as shown in Figure 4.8.



Figure 4.8. The ancient harbor of the Soli-Pompeiopolis Ancient City captured on September 20, 2024, by a UAV during the site visit.

After being ruled under major historical figures and serving as a highly strategic border city, Soli-Pompeiopolis is now protected under Law 2863 as a first-degree archaeological site, covering a large area.

Colonnaded Street is one of the major parts of the site, and it is shown in Figure 4.9. Today, 33 columns stand along the street that connects the northern gate of the city to the harbor. Also, some parts of the harbor are still standing.



Figure 4.9. The Colonnade Street of the Soli-Pompeiopolis Ancient City, photo taken by İremnaz Kösem during the site visit on September 20, 2024.

It is known that the harbor has two breakwaters, 200 meters away from each other, as shown in Figure 4.10 and Figure 4.11. The one in the west is clearly in better condition than the other one.



Figure 4.10. The breakwater in the eastern part of the harbor, photo taken by İremnaz Kösem during the site visit on September 20, 2024.



Figure 4.11. The breakwater in the western part of the harbor, photo taken by İremnaz Kösem during the site visit on September 20, 2024.

It is reported that a detailed inspection showed that this breakwater is built by connecting large limestone blocks with iron rivets (Mersin Provincial Directorate of Culture and Tourism, n.d.). A closer look at the breakwater is provided in Figure 4.12.



Figure 4.12. Top of the western breakwater of the harbor, photo taken by İremnaz Kösem during the site visit on September 20, 2024.

The site is still being investigated through archaeological excavations, and especially, in the past ten years, some significant remnants have been found, including the monumental tomb of Aratos, a famous poet, mathematician, and philosopher of his time in Soli-Pompeiopolis (Temiz, G. M., 2022). Additionally, it is reported that there are still ongoing archaeological excavation works on the beach, as shown in Figure 4.13. With two breakwaters acting as groins, as well as a wide sandy beach that filled the ancient port, the site is an interesting heritage area to understand the shoreline trends and future erosion projections.



Figure 4.13. Excavation site on the beach of Soli-Pompeiopolis (IHA, November 2023).

4.3 Input Data

As stated above, the DSAS is a tool that computes the rate of shoreline change by utilizing historical shoreline position and baseline data. To obtain the input data, SENTINEL-2 – MSI L1C satellite imagery is used. The satellite images of both Anemurium and Soli coasts are acquired in September and October of each year from 2016 to 2024. The satellite images are downloaded from the EO Browser of the Copernicus Database as raster datasets in the following URL: [https://apps.sentinel-hub.com/eo-browser/]. The imagery is selected by defining an "Area of Interest" covering all the shoreline segments that are to be analyzed.

The downloaded data includes "Band 3", "Band 8" and "True Color" images in TIFF format, in the WGS-84 coordinate system with a spatial resolution of 10 m, and for

the dates given in Table 4.1 below. It is stated on the EO Browser website in the data characteristics that the error is less than 12 m at 95.5% confidence of Absolute Geolocation, less than 5 m at 95.5% confidence of Multitemporal Registration, and less than 0.3 px at 99.7% confidence of Multispectral Registration. For this study, error is assumed to be less than 5 m among the satellite images used in the assessments due to multitemporal resolution error.

Table 4.1. Dates of the shoreline data utilized in the assessment of Anemurium and Soli-Pompeiopolis shorelines.

Anemurium	**Soli-Pompeiopolis**
September 29, 2016	September 26, 2016
September 29, 2017	October 6, 2017
September 26, 2018	October 6, 2018
September 29, 2019	October 1, 2019
September 28, 2020	October 5, 2020
September 28, 2021	September 25, 2021
September 25, 2022	September 25, 2022
September 28, 2023	September 15, 2023
September 29, 2024	October 4, 2024

All the satellite images downloaded are georeferenced by utilizing the "Georeference" toolset of the ArcGIS Pro and the control points shown in Figure 4.14 and Figure 4.15 below.



Figure 4.14. SENTINEL-2 satellite images of the Soli region from the years 2024 and 2016. The control points are shown with yellow points on these images.



Figure 4.15. Satellite images of Anemurium Ancient City acquired in the years 2024 and 2016. The purple points in those show the control points utilized for georeferencing.

4.3.1 Shoreline Data

DSAS requires the shoreline position as input data. Therefore, the shoreline from each satellite image was extracted following the steps listed below, following the

methodology described in Maglione et al. (2014), El Kafrawy et al. (2017), and Alcaras et al. (2020) studies. With this semi-automated approach, the error is minimized compared to drawing the shoreline through visual inspection.

The layers obtained as a result of each step are presented in Figure 4.16.

- **Generation of Normalized Difference Water Index:** For the detection of water bodies in satellite imagery, the commonly used NDWI index is obtained by using green and near-infrared (NIR) spectral bands (El Kafrawy et al., 2017). The bands in the SENTINEL-2 data are Band 3 for the green and Band 8 for the NIR spectral band. Hence, the index is obtained by the following formula: (Band 3 – Band 8)/(Band 3 + Band 8). The computation is performed by utilizing the "Raster Calculator" tool of ArcGIS Pro.
- **Reclassifying:** The obtained NDWI data is reclassified as water and land by using the "Reclassify" function of ArcGIS Pro to assign "1" as pixel value to the pixels having values lower than 0.2 to define the land and "0" to the rest to define the water.
- **Converting to Polygons:** After reclassifying the pixels, the obtained raster layer is converted to a polygon layer where the pixels with the same value are turned into a single polygon. As a result, a layer is generated that consists of separate polygons for land and water.
- **Obtaining the Shoreline:** The shoreline is obtained by utilizing the "Features to Line" function of ArcGIS Pro, which converts the boundaries of each polygon in a layer to separate lines. However, DSAS requires one continuous line as the shoreline data; hence, the "Merge" function is utilized after redundant line features are eliminated. The obtained shoreline is checked for its accuracy by comparing it with the "True Color" raster data downloaded from the EO Browser.



Figure 4.16. Layers obtained throughout the data preparation process.

This process is repeated for the shoreline observed each year. Then, all the shoreline layers are merged into a single layer, and for each line, the following attribute values are defined: Date and Uncertainty. The date value is entered in mm/dd/yyyy format as required by the DSAS. For the uncertainty, the default value of the DSAS is entered, 10 meters, since it is approximately the average uncertainty of the shoreline data utilized for the latest USGS reports, as stated in the software manual.

4.3.2 Baseline Data

An onshore baseline is defined by creating a line feature in ArcGIS Pro consisting of several segments based on the orientation of each shoreline segment. An ID is defined for each segment so that the ID values are in order, describing the shoreline direction with respect to the sea. The baselines used for the assessments of Anemurium and Soli-Pompeiopolis are shown as a blue line in Figure 4.17. The transects generated by the DSAS are stated to be generated orthogonal to the baseline, and one of the recommended methods to create the baseline, given in the

manual, is to generate a buffer line from the shoreline. In order to have a smoother line, instead of copying the shoreline, a new line feature is created by aiming to match the orientation of the shoreline. Another rule followed while creating the baseline is that it must be “in a projected coordinate system in meters”, again as stated in the manual.



Figure 4.17. The baselines and the latest shorelines obtained for both study areas are shown.

4.3.3 Transects

In this analysis, two sets of transects are utilized with spacing values of 50 m and 100 m. The transects to be utilized for the measurements are automatically generated orthogonally to the baseline by the DSAS. The generated transects are checked and corrected in the ArcGIS Pro environment if they intersect each other, or if the orientation is not accurately representing the shoreline.

The transects utilized for the analysis are checked for their ID numbers and which of those are on the shoreline segment interacting with each cultural heritage site, as shown below in Figure 4.18 and Figure 4.19.



Figure 4.18. ID numbers and locations of the transects along the assessed coastline of Anemurium Ancient City.



Figure 4.19. ID numbers and locations of the transects along the assessed coastline of Soli-Pompeiopolis Ancient City.

CHAPTER 5

SHORELINE EVOLUTION MODELING WITH THE SHORELINE SIMULATION (ShorelineS) MODEL

Accurately modeling shoreline evolution is a significant task for providing resilient coastal areas to the expected impacts of climate change. However, it is not easy to model such dynamic subjects as coastlines in which the materials, orientations, and elements like structures along the shoreline are different for each area of interest. Hence, several approaches and tools have been developed, and one of them is the Shoreline Simulation (ShorelineS) Model presented by Roelvink et al. (2018). Their goal in developing this model was to overcome the limitations of existing models, the complexity of grid-based approaches, and geometrically complex reconstruction. In the scope of this study, the evolution of the coastline segment directly interacting with the Anemurium Ancient City, which is described in detail in Section 4.2.1, is modeled by using the ShorelineS Model. This modeling process aims to see the difference in the projection of the shoreline that might be observed in 2050, obtained by using only the observed shoreline trend, from the one obtained by considering the impacts of physical elements of the region and the climate change-induced sea level rise. The input data and the modeling process performed by using the ShorelineS Model are explained in this chapter.

The ShorelineS Model is a set of MATLAB functions for modeling shoreline evolution over long periods of time (Roelvink et al., 2020). The model simulates the movement by considering the shoreline as a string of grid points located along the mean sea level contour that can move around freely. The coastline position is updated by the model at each timestep based on the conservation of sediment, expressed by Equation 5.1, the parameters of which are given in Table 5.1.

$$\frac{\partial n}{\partial t} = -\frac{1}{D_C}\frac{\partial Q_s}{\partial s} - \frac{RSLR}{tan\beta} + \frac{1}{D_C}\sum q_i \qquad [5.1]$$

Table 5.1. Parameters of the equation of sediment conservation.

n	Cross-shore coordinate
s	Longshore coordinate
D_c	Active profile height
Q_s	Longshore transport
tanβ	Average profile slope between the dune and the depth-of-closure
q_i	Source/sink term
RSLR	Rate of sea level rise

The main force enabling the shoreline evolution in the model is "wave-driven longshore transport". Four longshore transport formulae were provided in the model. Two of them, CERC1 and CERC2, are defined in terms of the offshore wave conditions, and the remaining ones, CERC3 and KAMP, are defined in terms of the breaking wave conditions. The choice of formulation for longshore transport allows the model to be calibrated to match the local rates (Roelvink et al., 2018).

Unlike the DSAS, the ShorelineS Model allows the structures located along the shoreline, the foreshore orientation, the impact of sea level rise, and other properties to be defined and considered while modeling the shoreline evolution using numerical modeling, defining physical processes.

5.1 Input Data

The ShorelineS Model utilizes both a set of "txt" files and a set of input parameters defined in the MATLAB code for the shoreline evolution computations. Although the coastline and coastal structures data can be defined as matrix inputs in the code as well, in the scope of this study, they are introduced through "txt" files into the code.

Other input parameters considered during the computations are introduced in the code as variables, such as active profile height, depth-of-closure, the longshore transport formula to be utilized, and other parameters significant for both the computation and the form of output.

5.1.1 Shoreline Data

The same line layers utilized in the modeling process with the DSAS for the shoreline data are used for this modeling process, as well. The line layers obtained for the shorelines observed in 2016 and 2024 are utilized, the generation process of which is described in Section 4.3.1.

Each shoreline is introduced to the model through a "txt" file consisting of the x and y coordinates of equally spaced points along the line, with a spacing value of 50 m. The points are generated along each shoreline by using the "Generate Points Along Line" tool of ArcGIS Pro. The x and y coordinates of the points are obtained in the WGS1984 UTM 36N coordinate system.

Another key point to which attention is paid while preparing the shoreline data is the order of the points. The xy coordinates of the points are ordered in such a way that the points propagate in a direction along the shoreline, that the sea is on the left and the land is on the right. The analyzed and modeled part of the shoreline segment interacting with the Anemurium Ancient City can be seen in Figure 5.1.



Figure 5.1. Points of which the coordinates are utilized as the input for the shoreline observed on September 29, 2024.

5.1.2 Structures Along the Coastline

Unlike the DSAS, the ShorelineS Model simulates the coastline evolution by performing specific computations considering the local properties, including coastal structures. Along the 2.9 km long shoreline segment, three structures are affecting the shoreline evolution.

The first one is the long jetty shown in Figure 5.2a, the second one is the jetties on both sides of the narrow canal shown in Figure 5.2b, and the last one is the skewed groin given in Figure 5.2c.

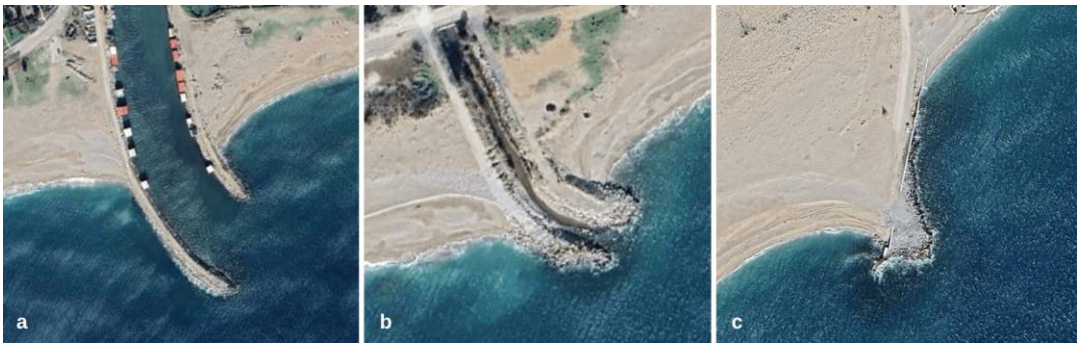


Figure 5.2. a. The jetty on the west edge of the large canal, b. Jetties on both edges of the narrow canal, c. The angled groin located in the middle of the assessed shoreline segment.

While introducing the structures located along the assessed coastline segment, a couple of assumptions are made:

- There is a narrow channel on the east side of the coastline. However, the satellite images showing the shoreline evolution between 2016 and 2024 are checked, and it is assumed that the impact of the discharge from the channel on the sediment transport along the shoreline is negligible, and it is neglected. Hence, the groins on both sides of the channel are assumed to be a single wide groin, shown as Groin-2 in Figure 5.3.
- The fill installed in front of the other groin along the shoreline is taken as part of the groin, shown as Groin-3. It is because the fill provides a solid section along the coastline, working together with the groin and affecting the sediment transport.

Similar to the process followed while generating the shoreline data, the lines on the outer edges of the structures are created as separate line layers on the satellite image recorded in September 2024 by using ArcGIS Pro. Then, the coordinates of the points along these lines are obtained in the WGS1984 UTM 36N coordinate system, and they are introduced to the model through a “txt” file which consists of the xy coordinates of these points on the outer edges of all the structures along the coastline together as a [Nx2] matrix.



Figure 5.3. The structures located along the assessed shoreline, and the close-up view of Groin-3.

The effect of the Anamur (Dragon) stream located in the east of Groin 1, shown in Figure 5.3, on the sediment transport along the assessed shoreline is neglected in the scope of this study. Alakopru Dam on this stream started to regulate the river discharge in 2015 (DSİ, 2021) and through the historical satellite images used in this study, it is seen that this river does not cause a significant sediment accretion since 2016.

5.1.3 Wave Conditions

The ERA5 data of hourly significant wave height (m), peak wave period (sec) and mean wave directions (degrees from the North in clockwise direction, where the North is 0 degrees) for the years between 1974 and 2024 are utilized in the scope of this study. The data for the point shown in Figure 5.4 is acquired from the "ERA5 Hourly Data on Single Levels From 1940 to Present" dataset from the Copernicus database (https://cds.climate.copernicus.eu).



Figure 5.4. The point at which the data of wave conditions is acquired from the Copernicus database.

The wave conditions are introduced to the model through two sets of data for separate runs: wave time-series and wave climate. The wave time-series data is utilized for calibrating the chosen longshore sediment transport method, which is explained in detail in the following parts, and the wave climate data is utilized to generate a shoreline that might be observed in 2050.

5.1.3.1 Wave Time-Series

A “txt” file consisting of the following four columns of data is utilized.

- Date as YYYYMMDDhhMM
- Significant wave height in meters
- Peak wave period in seconds
- Wave direction in nautical convention (degrees from the North in clockwise direction)

The raw hourly time-series data has a temporal coverage from January 1st, 1974, to November 11th, 2024. The part of this data dated between September 29th, 2016, and September 29th, 2024, is utilized for the calibration of the longshore sediment transport formula. As presented in Figure 5.5, the monthly mean significant wave heights observed in the studied period show a descending trend, while the maximum and minimum hourly significant wave heights observed are 1.22 m and 0.35 m, respectively.

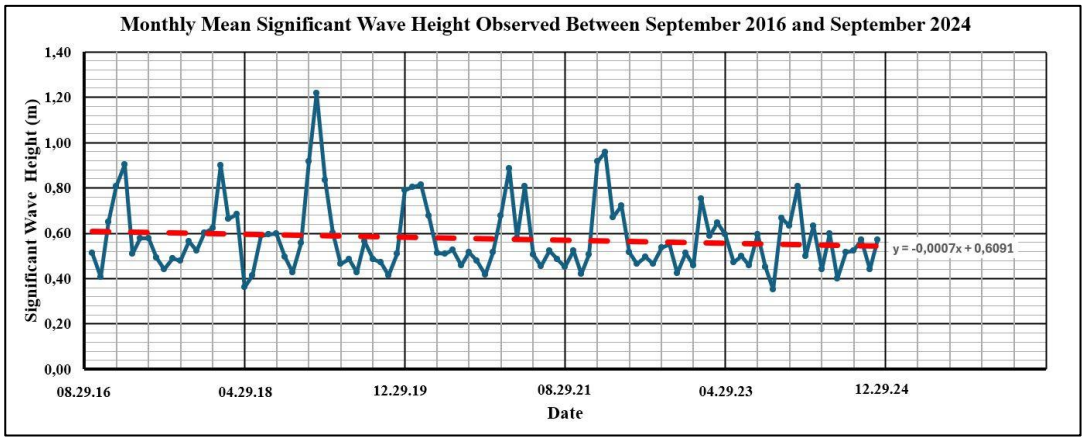


Figure 5.5. The monthly mean significant wave height observed in each month from September 2016 to September 2024, and the trendline with a slope of -0.0007.

The dominant wave direction observed between September 2016 and September 2024 is SSW as presented in Figure 5.6. With this time-series dataset, three separate runs are made after the calibration of the longshore sediment transport formula is completed. The difference between these runs is the monthly, daily, and 3-hour timesteps. The model applies the average wave condition in each timestep. Hence, the accuracy of the generated shoreline increases as the timestep gets smaller, whereas the run-time gets longer.

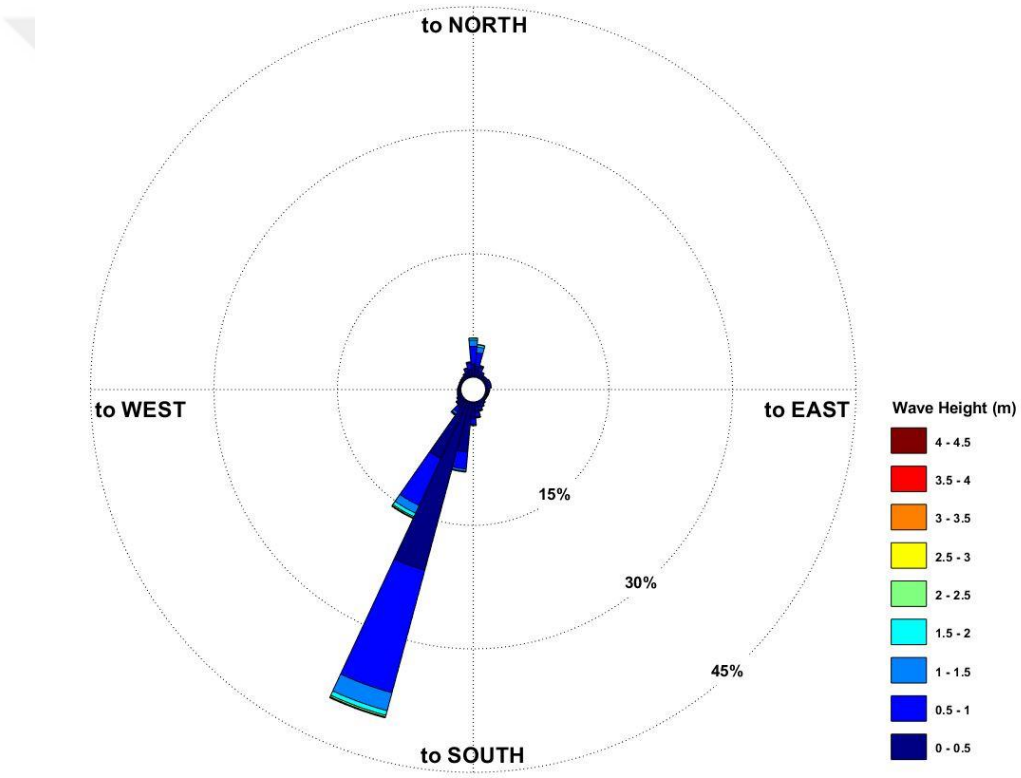


Figure 5.6. The wave rose obtained by utilizing the wave conditions observed between September 2016 and September 2024.

5.1.3.2 Wave Climate

For the modeling of the shoreline that might be observed in 2050, wave climate data is utilized instead of time-series data. A “txt” file is prepared consisting of the following four columns of data by utilizing the same dataset with the temporal coverage between January 1974 and November 2024, described in the previous section. Unlike the wave time-series data, the wave climate data includes probability data as well. The data in each column of the “txt” file is listed below.

- Significant wave heights in meters
- Peak wave period in seconds
- Wave direction in nautical convention (degrees from the North in clockwise direction)
- Probability

Roelvink et al. (2020) recommend the use of wave climate data that consists of a probability distribution of a number of wave direction bins that each has equal total energy flux with a wave height class per direction. When the described distribution is applied, the bins are obtained as presented in Figure 5.7. Additionally, the complete wave climate data is given in Appendix B.

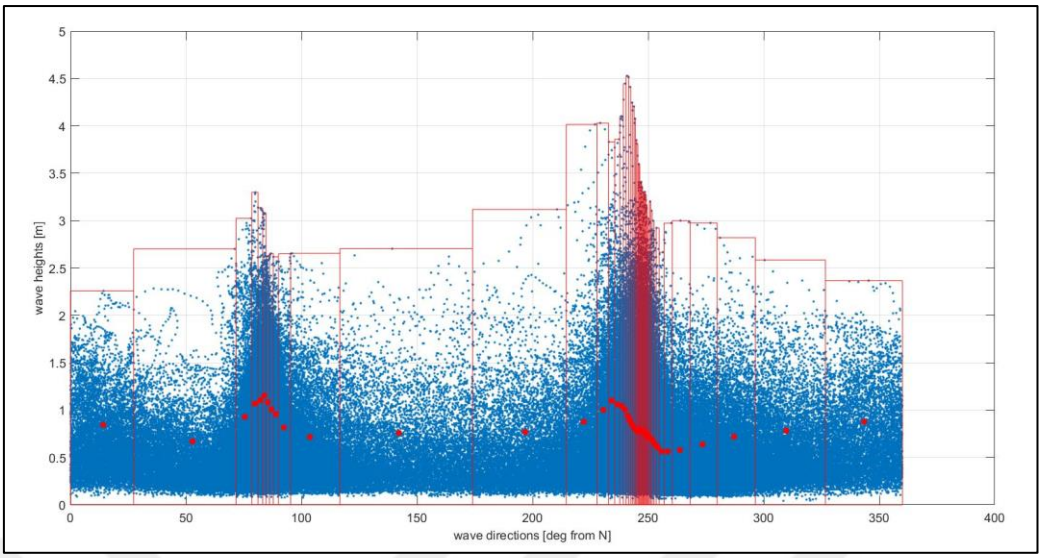


Figure 5.7. The distribution of the waves in wave direction bins with equal total energy flux with a wave height class per direction.

The dataset covering the last 50 years shows that the dominant wave direction is WSW, from which over 30% of the observed waves are coming, as presented in Figure 5.8.

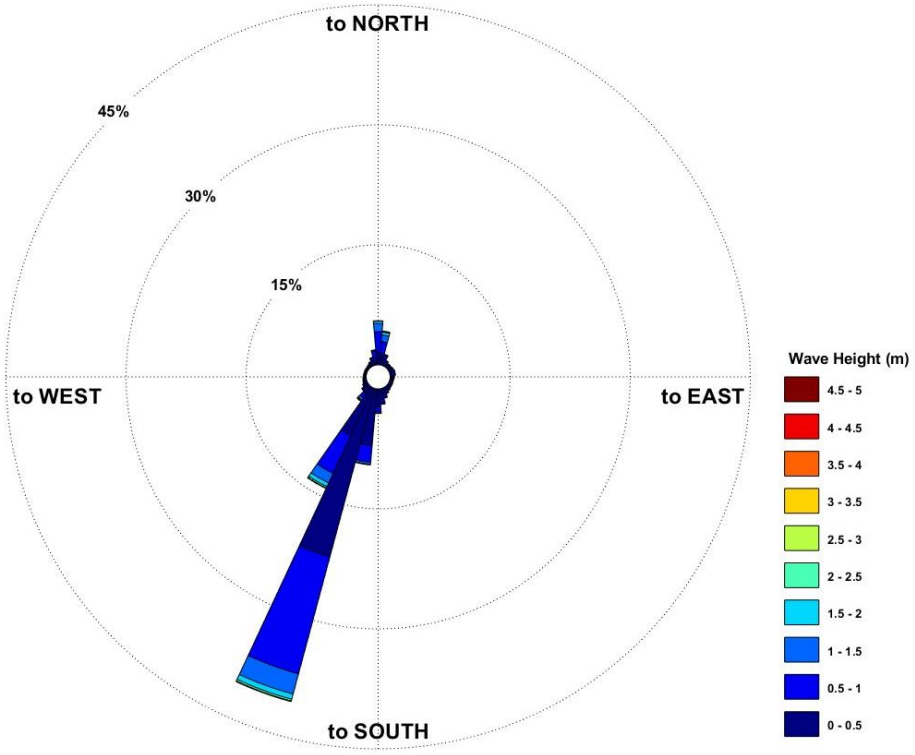


Figure 5.8. Wave rose created by using the hourly significant wave height data with the temporal coverage between January 1974 and November 2024, obtained at (36 N, 33E) from the Copernicus database (https://cds.climate.copernicus.eu).

5.1.4 Foreshore Orientation

The model requires the foreshore orientation parameter to be defined for the wave refraction from the offshore to the nearshore depth-of-closure, which can be estimated based on the depth-of-closure, as stated in the ShorelineS Technical Reference (2015). Hence, the data from the EMODnet Digital Bathymetry (DTM) dataset (http://www.emodnet-bathymetry.eu) is obtained in NetCDF format. As shown in Figure 5.9, a contour layer is created by using the bathymetry data, and orientation is determined as 140 degrees from the North by using the transects generated perpendicular to the contours.

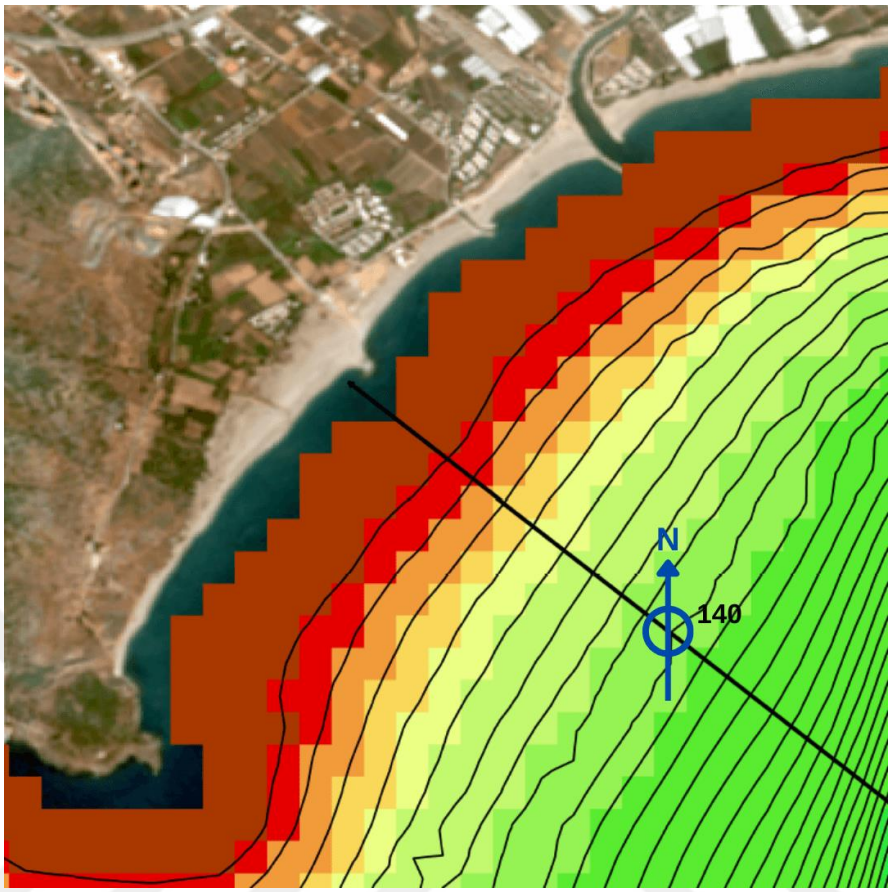


Figure 5.9. The contour lines generated using bathymetry data across the foreshore area, and the transect line showing the orientation angle, determined as 140 degrees from the North.

5.1.5 Offshore Depth and Nearshore Depth

The ShorelineS Model computes shoreline evolution by interpolating wave conditions on the grid points at every timestep, and for this purpose, the model provides two interpolation methods: alongshore mapping and weighted distance. The alongshore mapping method projects the wave location on the coast and interpolates it alongshore, whereas the weighted distance method uses a weighted average of the nearest two wave locations. For the wave transformation process, the model applies

wave refraction in the nearshore direction, depth-induced breaking, and shoaling based on the considered depth.

For these wave transformation and interpolation processes, two different depth values are utilized: offshore depth and nearshore depth.

It is stated in the ShorelineS Technical Reference (2015) that the offshore depth is the depth at which the wave conditions data is acquired. Hence, the offshore depth is determined as 570 m at the point shown in Figure 5.4, in Section 5.1.3. The nearshore depth is estimated based on the inner depth-of-closure.

The inner depth-of-closure value is computed by using the formula given in Equation 5.2, derived by Hallermeier (1981).

$$h_{in} = 2.28H_{12h/y} - 68.5\left(\frac{H_{12h/y}^2}{gT_{12h/y}^2}\right) \quad [5.2]$$

This formula computes the inner depth-of-closure by using the effective wave height exceeded for 12 hours per year ($H_{12h/y}$), the wave period associated with $H_{12h/y}$, and the gravitational acceleration, g.

5.1.5.1 Long-Term Wave Statistics (LTWS)

For computing the depth-of-closure, the dominant wave direction and required wave parameters in that direction are determined by LTWS. For this process, the same hourly wave data with temporal coverage between 1974 and 2024, which is described in the previous sections, is utilized.

In this part of the study, the frequency (in hours) and significant wave height values for each direction are determined, and the depth-of-closure value is computed for each direction by using Equation 5.2, as presented in Table 5.2 and Table 5.3, respectively.

Table 5.3. Frequency table showing the frequency (in hours) and significant wave height observed in each direction over the last 50 years.

Wave Height (m)	Wave Direction															
	NNE	NE	ENE	E	ESE	SE	SSE	S	SSW	SW	WSW	W	WNW	NW	NNW	N
0-0.5	2867	3238	7756	14024	5720	2327	1972	2159	3183	8597	143375	27846	7069	2929	1973	1984
0.5-1.0	3051	1973	4227	19593	2866	1242	1049	1149	1651	4977	96069	7996	3605	2227	1869	2277
1.0-1.5	726	319	1355	8004	710	351	332	400	535	2244	17970	1511	970	581	745	1036
1.5-2.0	130	39	344	2727	208	77	59	107	95	881	5257	405	237	184	196	302
2.0-2.5	32	14	215	659	25	16	23	32	29	321	1851	57	42	15	13	11
2.5-3.0	0	0	41	106	2	1	4	3	7	122	502	8	7	0	0	0
3.0-3.5	0	0	1	18	0	0	0	0	4	40	122	0	0	0	0	0
3.5-4.0	0	0	0	0	0	0	0	0	0	12	24	0	0	0	0	0
4.0-4.5	0	0	0	0	0	0	0	0	0	2	14	0	0	0	0	0
4.5-5.0	0	0	0	0	0	0	0	0	0	0	2	0	0	0	0	0
5.0-5.5	0	0	0	0	0	0	0	0	0	0	0	0	0	0	0	0
5.5-6.0	0	0	0	0	0	0	0	0	0	0	0	0	0	0	0	0
6.0-6.5	0	0	0	0	0	0	0	0	0	0	0	0	0	0	0	0

Table 5.2. The deep-water wave parameters and the depth-of-closure values computed for each direction.

Direction	N	NNE	NE	ENE	E	ESE	SE	SSE	S	SSW	SW	WSW	W	WNW	NW	NNW
$H_{12h/y}$ (m)	1,010	1,03	0,80	1,35	1,92	1,02	0,79	0,77	0,85	0,95	1,76	2,47	1,31	1,23	0,95	0,94
$T_{12h/y}$ (sec)	7,700	7,78	6,88	8,91	10,63	7,75	6,82	6,74	7,08	7,50	10,19	12,07	8,79	8,51	7,50	7,46
Depth-of-closure (m)	2,186	2,229	1,743	2,926	4,162	2,214	1,715	1,673	1,847	2,071	3,827	5,366	2,849	2,669	2,072	2,050

The dominant wave direction is determined as WSW after checking the relation between deep-water significant wave height and cumulative exceedance probability for each direction, as presented in Figure 5.10. Considering the orientation of the coastline, the results for only the directions between ENE and W are shown in the plot below.

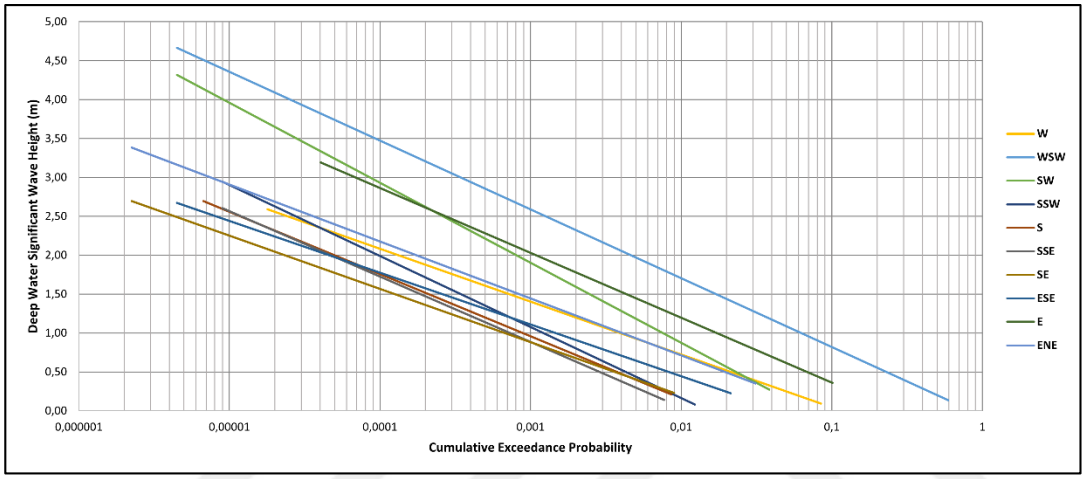


Figure 5.10. The relation of deep-water significant wave height and cumulative exceedance probability in each direction, determined by the LTWS.

After determining that the dominant wave direction is WSW, the effective wave height exceeded for 12 hours per year ($H_{12h/y}$) and the corresponding wave period are computed as 2.47 m and 12.1 sec, respectively. Then, the inner depth-of-closure is computed as 5.37 m by using Equation 5.2 given earlier.

5.1.6 Active Profile Height

A part of the profile moving with the coastline is described as an active profile in the ShorelineS Technical Reference, and its height is defined as the vertical distance between the depth-of-closure and the level of the dune toe. The vertical distance is

determined by taking profile views at every 100 m along the coastline in ArcGIS Pro, as presented in Figure 5.11.



Figure 5.11. The transects along which the profile views are created in ArcGIS Pro.

The height of the dune toe is determined as 2 m after checking the profile views given in Figure 5.12a and Figure 5.12b. Then, the sum of the height of the dune toe and the depth-of-closure is taken as the active profile height, 7.40 m. Additionally, the beach slope is determined as 0.032 based on the created profile views.

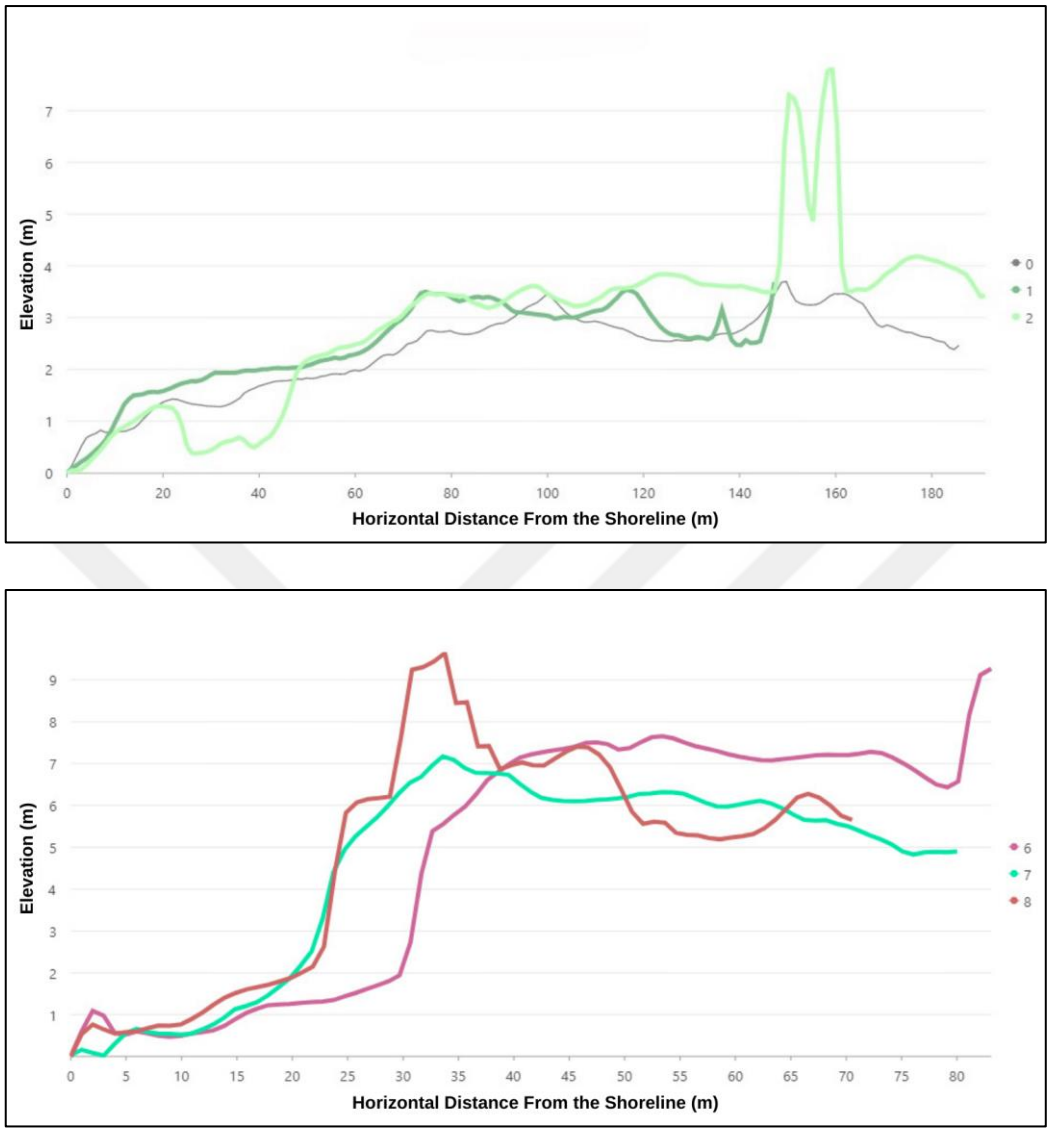


Figure 5.12. a. The elevation plots generated along the transects numbered 0, 1, and 2 in ArcGIS Pro. b. The elevation plots generated along the transects numbered 6, 7, and 8 in ArcGIS Pro.

5.1.7 Boundary Conditions

The movement at the start and end points of the coastline can be controlled while the coastline evolution over the years is modeled using the ShorelineS Model. In the scope of this study, boundary conditions at both ends of the coastline are assigned as

“Fixed”, which means that the positions of the endpoints are kept constant throughout the modeling process.

5.1.8 Climate Change Parameters

For the projection runs, the ShorelineS Model allows three parameters to be introduced to the model, including the rate of sea level rise (SLR), the rate of change in wave height, and the rate of change in wave direction. In the scope of this study, three separate runs are performed:

- None of the climate change parameters are entered.
- The rate of SLR is entered as 0.012 m/year is introduced to the model, which is obtained from the Sea Level Projection Tool of the National Aeronautics and Space Administration (https://sealevel.nasa.gov/ipcc-ar6-sea-level-projection-tool) for the Anamur region.
- The rate of SLR and the rate of change in wave height are introduced to the model

The wave conditions are introduced to the model in these runs by using the wave climate data described in Section 5.1.3.2. The rate of change in hourly significant wave height observed between the years 1974 and 2024 is introduced to the model as the climate change parameter. However, the yearly maximum significant wave heights in this dataset, with the temporal coverage of January 1, 1974 to November 11, 2024, show that there is only a slight increase at the rate of 0.0033 m/yr, as presented in Figure 5.13. Hence, in addition to the obtained rate of change in wave height, the value of 0.01 m/yr is introduced to the model as an input parameter in a separate run as a worst-case scenario of future conditions.

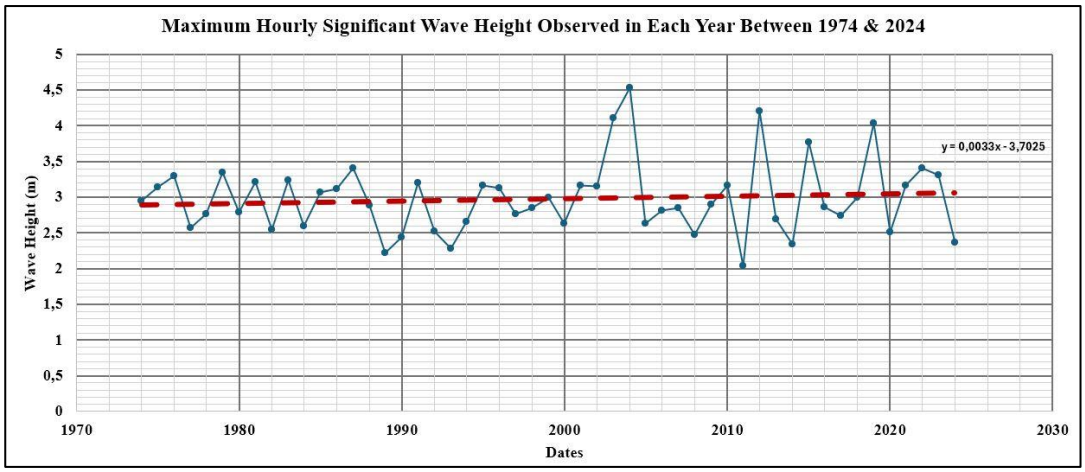


Figure 5.13. Maximum hourly significant wave heights observed in each year between January 1, 1974 and November 11, 2024.

5.2 Calibration of the Longshore Sediment Transport Formula

Wave-driven longshore sediment transport is the main source of coastline evolution, and the ShorelineS Model provides a few formulae for the computation of this sediment transport. In the scope of this study, the simplified version of the longshore sediment transport formula given in the Shore Protection Manual (USACE, 1984) is utilized, as given in Equation 5.3, which is referred to in the ShorelineS Model code as CERC1.

$$Q_s = bH_{s0}^{5/2} \sin 2(\emptyset_{ioc}) \qquad [5.3]$$

The formula computes the amount of sediment transport by considering the significant wave height at the offshore location (H_{s0}) and the relative angle of wave incidence for waves offshore. Since the formula consists of a calibration factor (b), several test runs are performed. In these test runs, the observed shoreline of 2016 is used, and the deviation of the generated shoreline from the observed shoreline of 2024 is checked. For this process, the net deviation between the observed and

generated shoreline positions (biascm) and the root-mean-square difference between those (rmscm) are compared for each tested value of the calibration factor, as recommended by Roelvink et al. (2020). The biascm and the rmscm values are computed by using the formulae given in Equation 5.4 and Equation 5.5, respectively.

$$biascm\,(t) = \frac{1}{L}\int_0^L dist_{comp(t)-meas(t)}\,ds \qquad [5.4]$$

$$rmscm\,(t) = \sqrt{\frac{1}{L}\int_0^L dist^2_{comp(t)-meas(t)} ds} \qquad [5.5]$$

The net deviation of the generated shoreline from the one observed in 2024 is computed at transects placed along the shorelines with a spacing of 50 m, as presented in Figure 5.14.



Figure 5.14. The transect layer utilized to check the consistency of the generated shoreline with the calibration factor of b=2.5e4 with the shoreline observed in September 2024 (ArcGIS Pro).

For determining the calibration factor, a series of test runs is made by using various values of the factor, and as presented in Table 5.4, the value of b = 4.5e4 generates a shoreline with the smallest RMSE value when it is compared with the shoreline observed on September 29, 2024. In the test runs, the wave conditions are introduced to the model by using the time-series data, and the timestep is set as daily, 1/365.

Table 5.4. The biascm, RMSE, and the average value of the absolute distances between the generated and observed shorelines along the transects, which are obtained using the given calibration factors.

DAILY			
b	Abs. Mean Error	rmscm	biascm
2,00E+04	11,42	14,37	-5,49
2,50E+04	11,61	14,35	-5,41
2,60E+04	11,66	14,38	-5,44
3,00E+04	11,86	14,34	-5,23
3,50E+04	12,17	14,42	-5,07
4,00E+04	12,34	14,38	-4,82
4,50E+04	12,39	14,31	-4,41
5,00E+04	12,59	14,57	-4,59
5,50E+04	12,66	14,62	-4,36
6,00E+04	12,91	14,90	-4,35
6,50E+04	12,94	14,88	-4,00
6,80E+04	12,92	14,86	-3,8
7,00E+04	13,20	15,16	-4,01
7,50E+04	13,15	15,15	-3,54
8,00E+04	13,43	15,55	-3,5
8,50E+04	13,48	15,66	-3,36
9,00E+04	13,88	16,32	-3,39
9,50E+04	14,03	16,52	-3,21
1,00E+05	14,10	16,59	-3,00

The generated shorelines by using different values of the calibration factor are presented in Figure 5.15, including the one generated by the selected value of the factor.

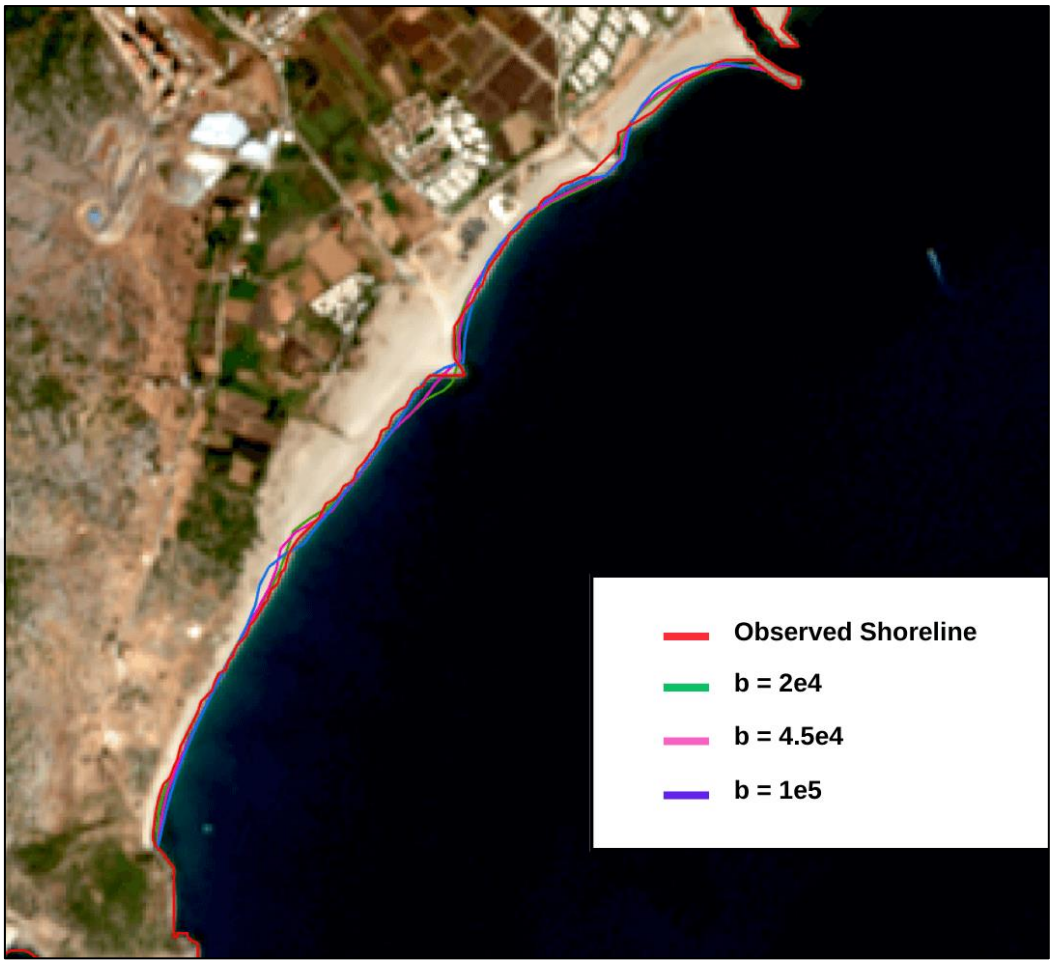


Figure 5.15. Shorelines generated by using the following values of the calibration factor; 1e5, 4.5e4, and 2e4, and the shoreline observed on September 29, 2024 (ArcGIS Pro).

CHAPTER 6

RESULTS & DISCUSSIONS

The results obtained from the application of CCHVAM on the coastal archaeological heritage sites are presented in the first section of this chapter. In these results, four different applications are given; two applications for each exposure component, CVI and coastal erosion impact score, one is with the exposure values obtained from the FCVAM results based on the SSP2-4.5 emission scenario, and the other is the application of the model based on the SSP5-8.5 scenario.

The next two sections of this chapter present the obtained results on the shoreline evolution in the Anemurium and Soli-Pompeiopolis coastlines obtained from the DSAS and the ShorelineS Model.

6.1 Vulnerability Assessment of the Coastal Archaeological Heritage Sites of Türkiye

The newly developed Coastal Cultural Heritage Vulnerability Assessment Model evaluates each heritage site by integrating three main components: sensitivity, exposure, and adaptive capacity. Hence, in addition to the vulnerability class assigned to a site, the results of this model also provide an insight into the properties of the site, making it both open to get adversely affected by the rise in sea levels and resilient against them. Furthermore, the model analyzes the conditions of both the site and the shoreline segment interacting with it, which cause and exacerbate the threats faced.

In the scope of this study, the 1176 coastal archaeological heritage sites of Türkiye that are located within a kilometer distance of the shoreline and partially or fully below 10 meters elevation are assessed. The assessment is repeated four times in

total with four sets of exposure component values. The exposure component of the CCHVAM describes the level of threats to which the shoreline segment interacting with the site is subjected, as introduced in Section 3.1.2. Hence, in the first two assessments, the CVI values, which are obtained by the aggregation of the coastal erosion, surge, and inundation impact scores, are used; whereas, in the last two assessments, the coastal erosion impact scores are used as the exposure component values. The data of the SSP2-4.5 and the SSP5-8.5 scenarios are utilized separately to obtain the CVI values and coastal erosion impact scores. Sensitivity and adaptive capacity values are constant as they are independent of climate change scenarios.

6.1.1 Sensitivity Values of the Assessed Heritage Sites

The sensitivity value is obtained from the sum of weighted values of the following indicators: proximity, elevation, area, and interaction length. The results revealed that 37% of the coastal archaeological sites along the coastline of Türkiye have high sensitivity to the sea level rise and its impacts, and 10% of all the assessed sites have very high sensitivity. As shown in Figure 6.1, they are mostly located along the Mediterranean and Aegean coastlines.

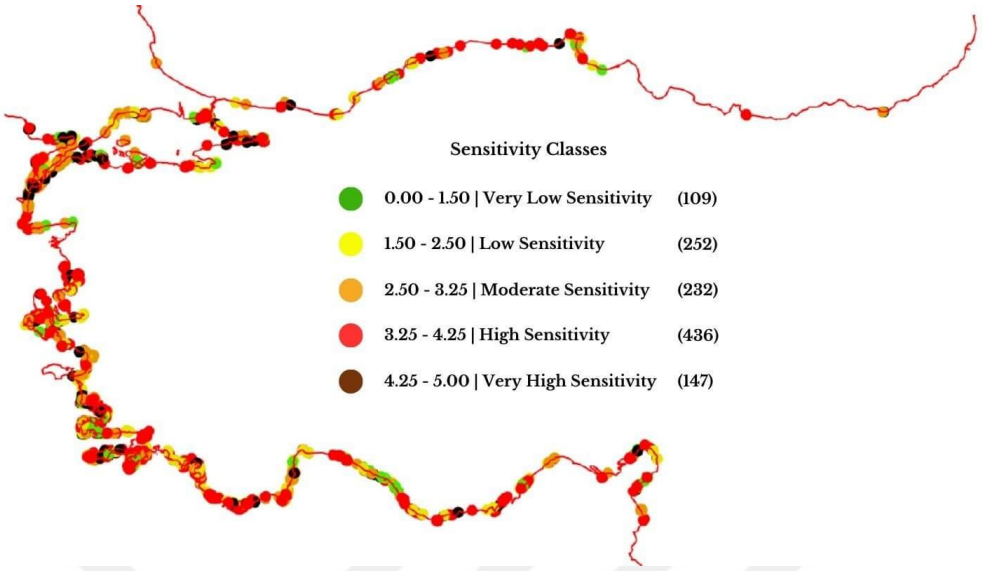


Figure 6.1. Distribution of the heritage sites with very high, high, moderate, low, and very low sensitivity along the coastline of Türkiye.

When the results are checked on a regional scale, it is clearly seen that most of the heritage sites located along the Mediterranean and the Aegean coasts have either very high or high sensitivity, and this ratio is much less in the Black Sea region, as presented in Table 6.1.

The assessment reveals that 39.4% of the sites with “High Sensitivity” are located along the Mediterranean coastline of Türkiye, whereas 51% of the sites with “Very High Sensitivity” are located along the Aegean coastline. Additionally, it is seen that 33.5% of the coastal archaeological sites located in the Marmara region and 40.2% of the sites located along the Black Sea coastline have “High Sensitivity”.

Table 6.1. Regional distribution of the assessed heritage sites with sensitivity levels ranging from very high to very low.

Sensitivity	Mediterranean	Aegean	Marmara	Black Sea	Total
Very Low (0, 1.50)	38	44	16	11	**109 (9.3%)**

Table 6.1 (continued) Regional distribution of the assessed heritage sites with sensitivity levels ranging from very high to very low.

Low [1.50, 2.50)	109	92	32	19	**252 (21.4%)**
Moderate [2.50, 3.25)	77	98	36	21	**232 (19.7%)**
High [3.25, 4.25)	172	167	54	43	**436 (37%)**
Very High [4.25, 5.00)	36	75	23	13	**147 (12.5%)**
Total	**432**	**476**	**161**	**107**	**1176**

On the other hand, the sites directly located on the shoreline are checked in detail. The regional distribution of the heritage sites that are located directly on the shoreline and the percentage of the sites located directly on the shoreline for each region are presented in Table 6.2, separately. It is seen that 41.7% of the sites along the Mediterranean coastline and 40.7% of the sites along the Aegean coastline are located on the shoreline. Regional distribution of the sites located on the shoreline can be seen in Figure 6.2, as well.

Table 6.2. Regional distribution of the assessed heritage sites that are located directly on the shoreline, where the shortest distance to the shoreline (x) is equal to zero for each of these sites.

	Mediterranean	**Aegean**	**Marmara**	**Black Sea**
Number and percentage of the sites located directly on the shoreline (x = 0)	180	194	59	35
	41.7%	40.7%	36.7%	32.7%

It is also found that the least sensitive sites that are located directly on the shoreline have “Moderate Sensitivity” based on the CCHVAM. The consistency between the number of sites located on the shoreline and the fact that the model assigned either “Very High Sensitivity” or “High Sensitivity” to the majority of those is an aimed outcome because the interaction between the impacts on the shoreline and the heritage site increases as the site gets closer to the shoreline. This goal is accomplished by assigning the weights determined by the AHP, as described in Section 3.1.2.

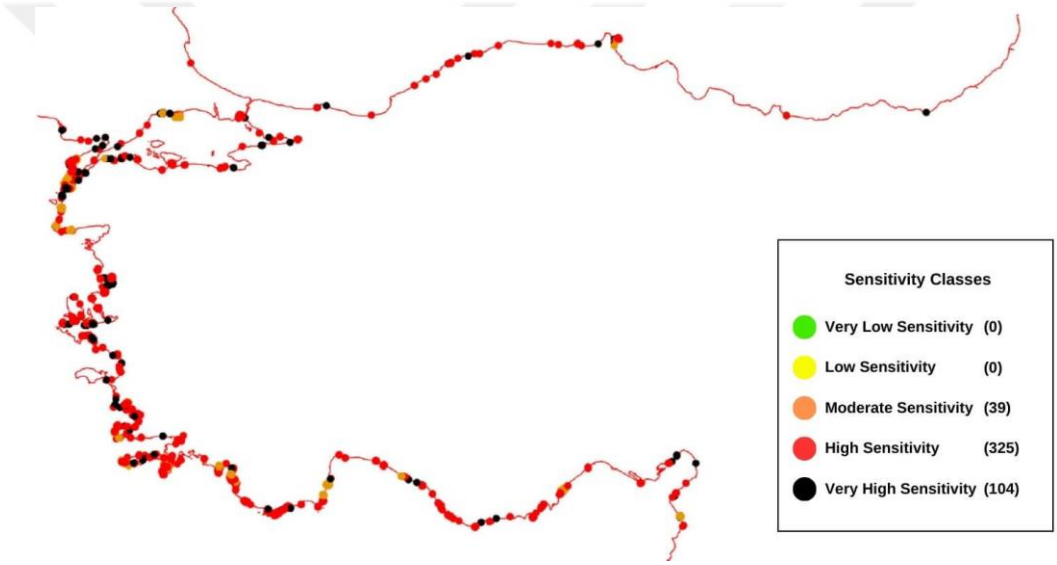


Figure 6.2. Regional distribution of the sites located on the shoreline.

6.1.1.1 Properties of the Sites in Each Sensitivity Class

The sensitivity component of the CCHVAM aims to provide insights into the properties and conditions of each site that make it prone to getting affected by the sea level rise and its impacts. In other words, the sensitivity value of a site describes its interaction with the shoreline.

The general properties of the sites assigned to each sensitivity class are summarized below.

- Very Low Sensitivity [0.00, 1.50):
    - Less than 10% of the areas of these sites are lower than 10 m.
    - These sites have no parts within 100 m distance of the shoreline.
    - The shortest distances of these sites to the shoreline is between 750-1000 m.
    - The length of the coastline segments that directly interact with these sites is between 0 – 2200 m.
- Low Sensitivity [1.5, 2.5):
    - The majority of these sites have less than 10% of their areas lower than 10 m.
    - These sites have no parts within 100 m distance of the shoreline.
    - For the majority of the sites in this class, the shortest distance to the shoreline is between 250-750 m.
    - The length of the coastline segments that directly interact with these sites is between 77 – 6000 m.
- Moderate Sensitivity [2.5, 3.25):
    - The majority of these sites have less than 10% of their areas lower than 10 m.
    - Less than 10% of the areas of most sites are within 100 m distance of the shoreline.
    - The shortest distances of the majority of these sites to the shoreline is between 0-250 m.
    - The length of the coastline segments that directly interact with these sites is between 1000 – 12000 m
- High Sensitivity [3.25, 4.25):
    - Most sites in this class have less than 70% of their areas lower than 10 m. However, there are 39 sites that have more than 90% of their areas lower than 10 m.

    - Most sites in this class have less than 50% of their areas within 100 m distance of the shoreline. However, there are 18 sites that have more than 90% of their areas within 100 m distance of the shoreline.
    - The shortest distance of most sites in this class to the shoreline is shorter than 50 m.
    - The length of the coastline segments that directly interact with these sites is between 2000 – 12000 m.
- Very High Sensitivity [4.25, 5.00]:
    - There are no sites in this class that have less than 30% of their areas lower than 10 m.
    - Most sites in this class have more than 30% of their areas within 100 m distance of the shoreline.
    - The shortest distance of most sites in this class to the shoreline is shorter than 35 m.
    - The length of the coastline segments that directly interact with these sites is between 2000 – 9000 m.

The histograms showing the distribution of sites in the "Very High Sensitivity Class" based on elevation, area, proximity, and interaction length indicators are provided in Figure 6.3. The indicator histograms of the other sensitivity classes are provided in Appendix C.

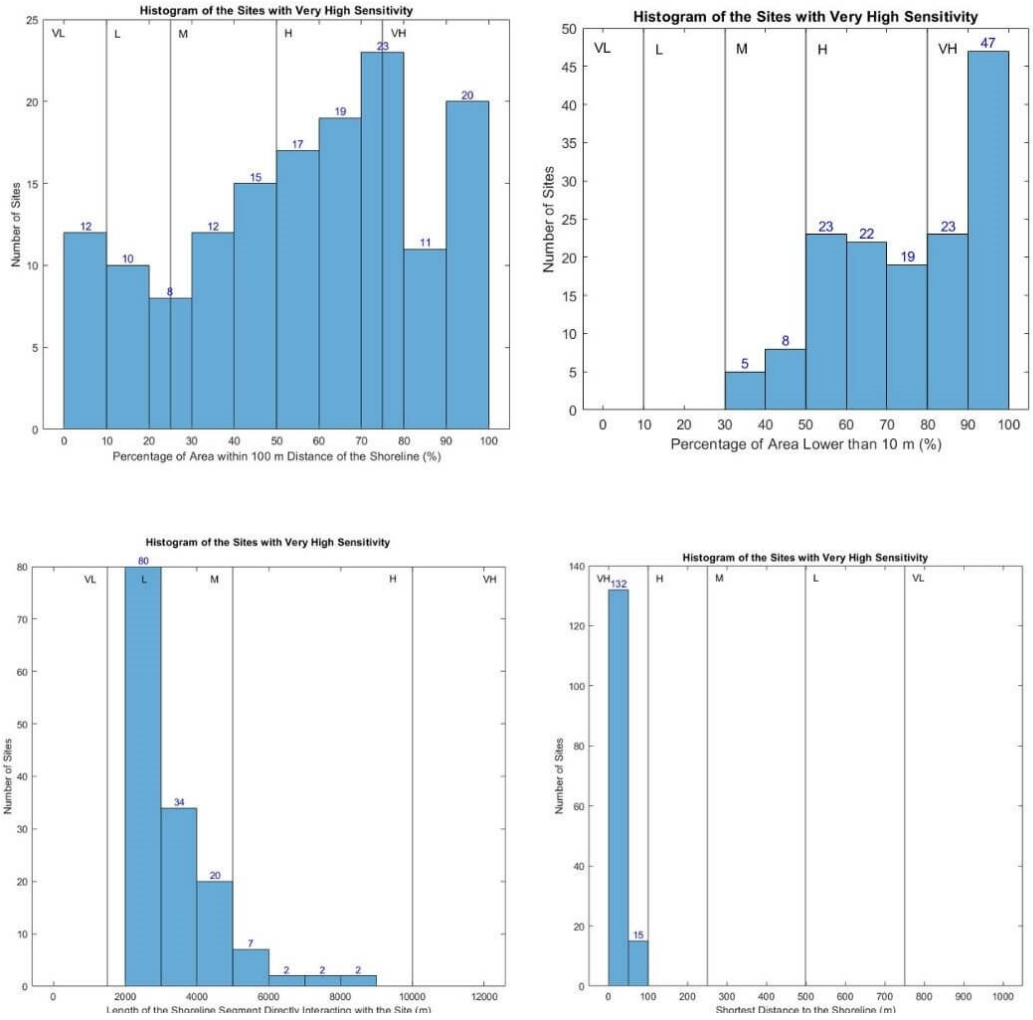


Figure 6.3. Histograms of the sites with very high sensitivity based on proximity, elevation, area, and interaction length indicators.

6.1.2 Adaptive Capacity of the Coastal Archaeological Sites of Türkiye

The adaptive capacity of the CCHVAM assesses the level of resilience of each coastal archaeological site against the sea level rise and its impacts. In the scope of this model, the adaptive capacity is assessed by using two indicators, the degree of protection and urbanization. The degree of protection evaluates the level of protection assigned and provided by the law, and the urbanization indicator evaluates

the percentage of the urbanized area within a one-kilometer distance of the site boundary, which directly interacts with the site.

The distribution of the assessed sites based on their adaptive capacity classes is presented in Figure 6.4. Utilizing the CCHVAM, it is found that 54.3% of the coastal archaeological sites of Türkiye have “Moderate Adaptive Capacity” and 20.3% of the assessed sites have “Low Adaptive Capacity”.

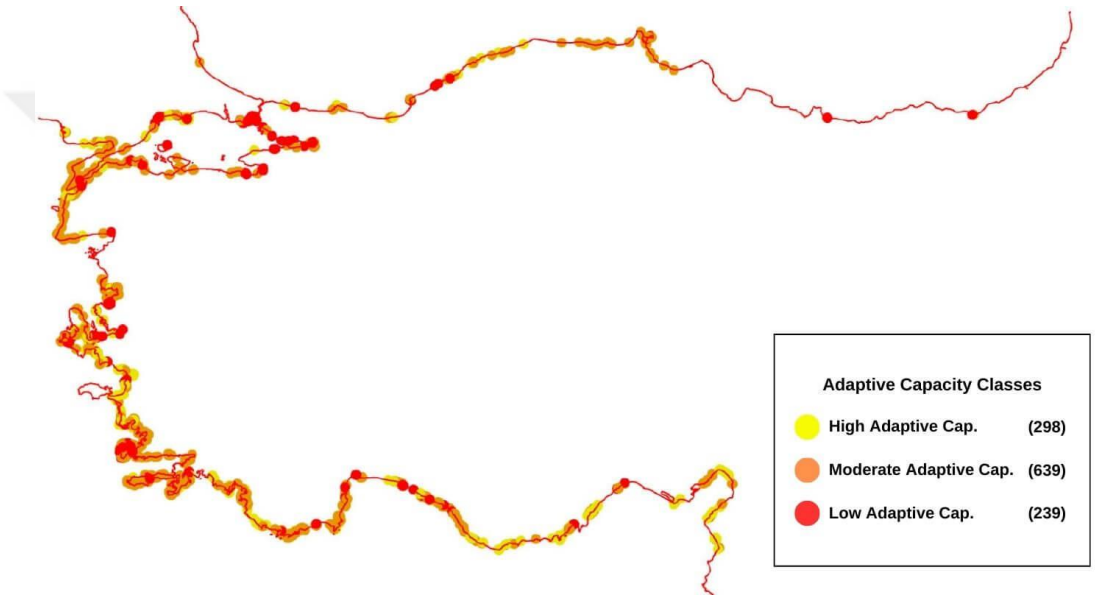


Figure 6.4. The distribution of the coastal archaeological sites of Türkiye based on their adaptive capacity classes.

It is also found that 49.7% of the sites with “High Adaptive Capacity” are located along the Mediterranean coastline, and 41% of the sites with “Low Adaptive Capacity” are located along the Aegean coastline. The regional distribution of the sites grouped by their adaptive capacity classes can be seen in Table 6.3.

Table 6.3. The regional distribution of the sites grouped by their adaptive capacity classes.

Adaptive Capacity	Mediterranean	Aegean	Marmara	Black Sea	Total
Low	35	98	70	36	**239 (20.3%)**
Moderate	249	266	72	52	**639 (54.3%)**
High	148	112	19	19	**298 (25.4%)**

6.1.3 Vulnerability Assessment for the Conditions of SSP2-4.5 Scenario

The initial assessment is performed by utilizing the CVI values obtained from the assessment of the shoreline segments based on the conditions of the SSP2-4.5 emission scenario as the exposure values. Details about the exposure component data are provided in Section 3.2.2, as stated above.

6.1.3.1 Values of Potential Impact

The CCHVAM has three main stages: first, the sensitivity and the exposure component values are obtained; then, these values are combined, and the potential impact class is determined; lastly, the potential impact and adaptive capacity components are combined, and the vulnerability class is assigned.

The potential impact class of each site is determined based on the numerical values of its sensitivity and the exposure components. By utilizing these classes in a decision matrix, a potential impact class is assigned to each site. Hence, the potential impact of a site is not a numerical value, but it is a potential impact class.

The potential impact describes the threat caused by both external and internal factors, and the potential impact class defines the level of this threat. When the exposure values, obtained from the data of the SSP2-4.5 scenario, are utilized, it is found that 40.9% of the coastal archaeological sites of Türkiye have “Moderate Potential Impact” and 35.2% of the sites have “Low Potential Impact” as it is shown in Figure 6.5.

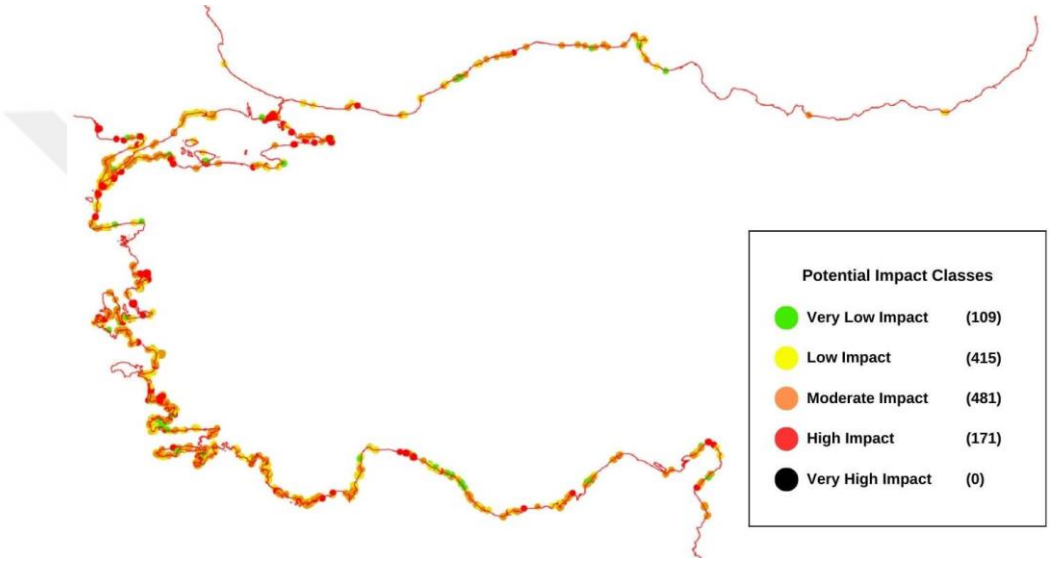


Figure 6.5. Distribution of the coastal archaeological sites based on their potential impact classes.

Furthermore, the regional distribution of the assessed heritage sites grouped by their potential impact classes is provided in Table 6.4. It is found that 54.9% of the sites with “High Potential Impact” are located along the Aegean coastline. On the other hand, 39.5% of the sites with “Moderate Potential Impact” are located along the Mediterranean coastline, and 40.4% of the sites with “Very Low Potential Impact” are located along the Aegean coastline.

Table 6.4. Regional distribution of the assessed heritage sites grouped by their potential impact classes obtained by using the CVI values based on the data of the SSP2-4.5 scenario.

Impact	Mediterranean	Aegean	Marmara	Black Sea	Total
Very Low	38	44	16	11	**109 (9.3%)**
Low	169	160	49	37	**415 (35.2%)**
Moderate	190	178	59	54	**481 (40.9%)**
High	35	94	37	5	**171 (14.6%)**
Very High	0	0	0	0	**0**
Total	**432**	**476**	**161**	**107**	**1176**

The distribution of the assessed sites based on their exposure and sensitivity classes and grouped by their potential impact classes is checked, and it is found that all the sites with “High Potential Impact” have “Moderate Exposure”, and all the sites with “Very Low Sensitivity” have “Very Low Potential Impact”. All the sites with “High Exposure” are found to have “Low Sensitivity” and “Moderate Potential Impact”.

6.1.3.2 Vulnerability Classes

Similar to the potential impact, a vulnerability class is assigned to each site rather than a numerical value.

As can be seen in Figure 6.6, 36.4% of the assessed coastal archaeological heritage sites of Türkiye have “High Vulnerability”, and there are 52 sites with “Very High

Vulnerability". Also, it is seen that 29.2% of all the assessed sites have "Low Vulnerability".

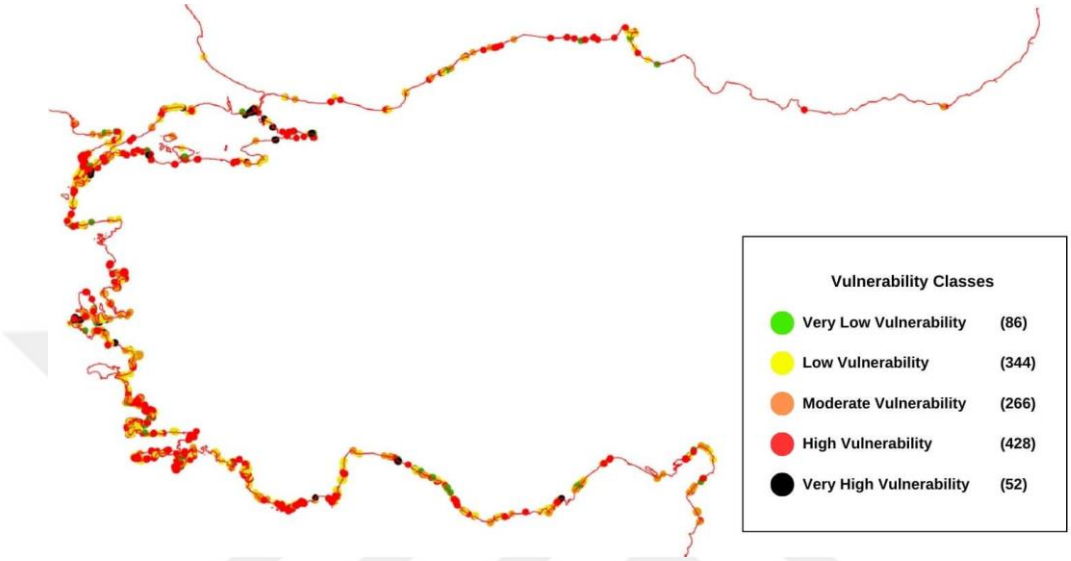


Figure 6.6. Distribution of the coastal archaeological sites of Türkiye based on their vulnerability classes.

When the regional distribution of the sites grouped by their vulnerability classes is checked, as given in Table 6.5, it is found that 41.1% of the sites with "High Vulnerability" are located along the Aegean coastline, and 45.9% of the sites with "Low Vulnerability" are located along the Mediterranean coastline. Additionally, it is found that only 15.4% of the sites with "Very High Vulnerability" are located along the Mediterranean coastline of Türkiye.

Table 6.5. The regional distribution of the coastal archaeological sites of Türkiye grouped by their vulnerability classes obtained by using the data of the SSP2-4.5 scenario.

Vulnerability	Mediterranean	Aegean	Marmara	Black Sea	Total
Very Low	35	32	11	8	**86 (7.3%)**
Low	158	137	28	21	**344 (29.2%)**
Moderate	87	109	39	31	**266 (22.6%)**
High	144	176	61	47	**428 (36.4%)**
Very High	8	22	22	0	**52 (4.5%)**

Furthermore, the distribution of the assessed cultural heritage sites based on their vulnerability classes and proximity indicator values is checked and presented in Figure 6.7. It is seen that there are 468 sites located directly on the shoreline, 61.5% of which have “High Vulnerability” and 26.3% of the sites have “Moderate Vulnerability”. Also, it is noticed that 7.3% of the sites directly on the shoreline have “Low Vulnerability”.

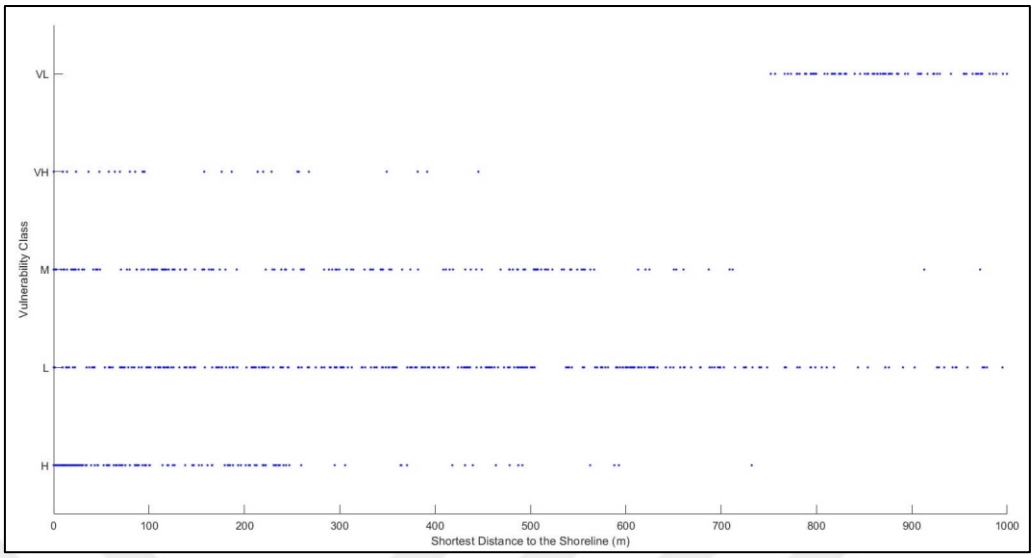


Figure 6.7. Distribution of the coastal archaeological sites of Türkiye based on vulnerability classes and proximity indicator values.

The sites with “Low Vulnerability” based on the exposure values obtained from the data based on the SSP2-4.5 scenario and located directly on the shoreline are checked in detail, and the following properties of these sites are found:

- None of these sites has more than 10% of their areas lower than 10 m. Also, none of these sites has more than 20% of their areas within 100 m distance of the shoreline. It means that the elevation and area indicator sensitivity values of these sites are either “Very Low” or “Low.
- Overall sensitivity values of all of these sites are “Moderate Sensitivity”, and all of them have “Low Exposure”, resulting in “Low Potential Impact”.
- All of these sites have either “Moderate Adaptive Capacity” or “High Adaptive Capacity”.

On the other hand, 78.3% of the sites with “Very High Vulnerability” are located on the shoreline, and they have more than 40% of their areas lower than 10 m. All of these sites have “High Potential Impact” and “Low Adaptive Capacity”.

These findings reveal that although proximity to the shoreline is the most significant indicator when determining the sensitivity of a site, the whole framework of the CCHVAM provides a comprehensive assessment since it integrates the impacts, the conditions enhancing sensitivity, and the resilience.

6.1.4 Vulnerability Assessment for the Conditions of SSP5-8.5

The second assessment is performed by utilizing the exposure component values obtained from the assessment of the shoreline segments based on the conditions of the SSP5-8.5 emission scenario. Details about this exposure component data are provided in Section 3.2.2.

6.1.4.1 Values of Potential Impact

When the exposure values obtained from the data of the SSP5-8.5 scenario are utilized, it is found that 40.6% of the coastal archaeological sites of Türkiye have "Moderate Potential Impact" and 34.5% of the sites have "Low Potential Impact" as it is shown in Figure 6.8.

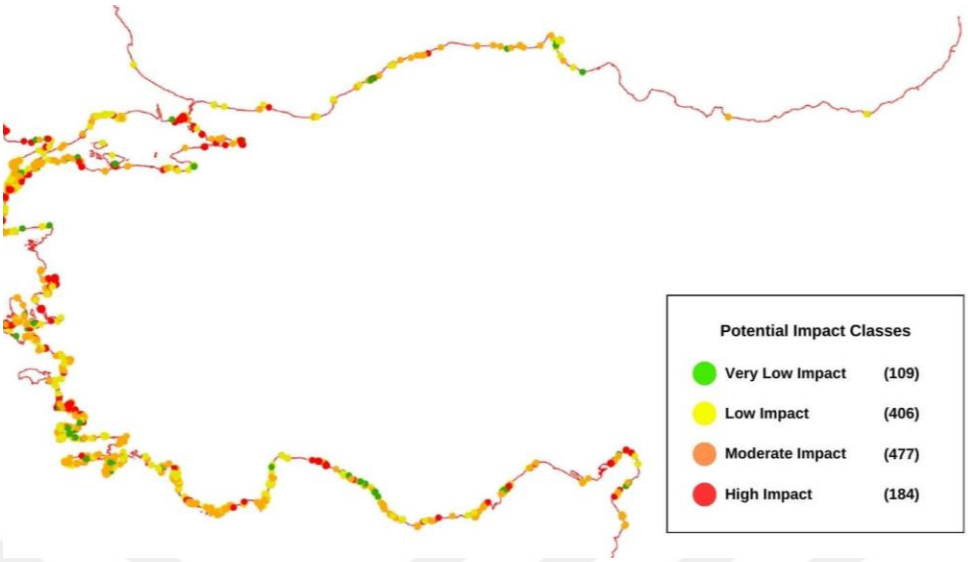


Figure 6.8. Distribution of the coastal archaeological sites of Türkiye based on their potential impact classes determined by the CCHVAM for the SSP5-8.5 scenario.

The regional distribution of the sites in each potential impact class is checked and presented in Table 6.6. It is seen that 23.4% of all the sites with "High Potential Impact" are located along the Mediterranean coastline, and 53.8% are located along the Aegean coastline. Similarly, 36.3% of the sites with "Moderate Potential Impact" are located along the Aegean coastline, and 39.8% are located along the Mediterranean coastline.

Table 6.6. Regional distribution of the coastal archaeological sites of Türkiye grouped by their potential impact classes determined by the CCHVAM using the CVI values obtained from the data of the SSP5-8.5 scenario.

Potential Impact	**Mediterranean**	**Aegean**	**Marmara**	**Black Sea**	**Total**
Very Low	38	44	16	11	**109 (9.3%)**
Low	161	160	49	36	**406 (34.5%)**

Table 6.7. Regional distribution of the coastal archaeological sites of Türkiye grouped by their potential impact classes determined by the CCHVAM using the CVI values obtained from the data of the SSP5-8.5 scenario.

Moderate	190	173	59	55	**477 (40.6%)**
High	43	99	37	5	**184 (15.6%)**

It is seen that the sites with “High Potential Impact” have “Moderate Exposure”, and either “High Sensitivity” or “Very High Sensitivity”. Also, it is seen that 50.5% of the sites with “Very Low Potential Impact” have “Moderate Exposure”, and the rest of the sites have “Low Exposure”.

6.1.4.2 Vulnerability Classes

It is presented in Figure 6.9 that 36.7% of the coastal archaeological sites of Türkiye have “High Vulnerability” and 28.7% of the sites have “Low Vulnerability”. It is noticed that there are 10 sites, of which the vulnerability classes are different when the SSP5-8.5 scenario is followed than the classes obtained from the data of the SSP2-4.5 scenario. Four of these sites are moved from “Low Vulnerability” to “Moderate Vulnerability”, and the classes of two sites are switched from the “Low Vulnerability” class to the “High Vulnerability” class. Lastly, there is one site that moved from the “High Vulnerability” to the “Very High Vulnerability”. These sites are discussed in detail in the following parts of this chapter.

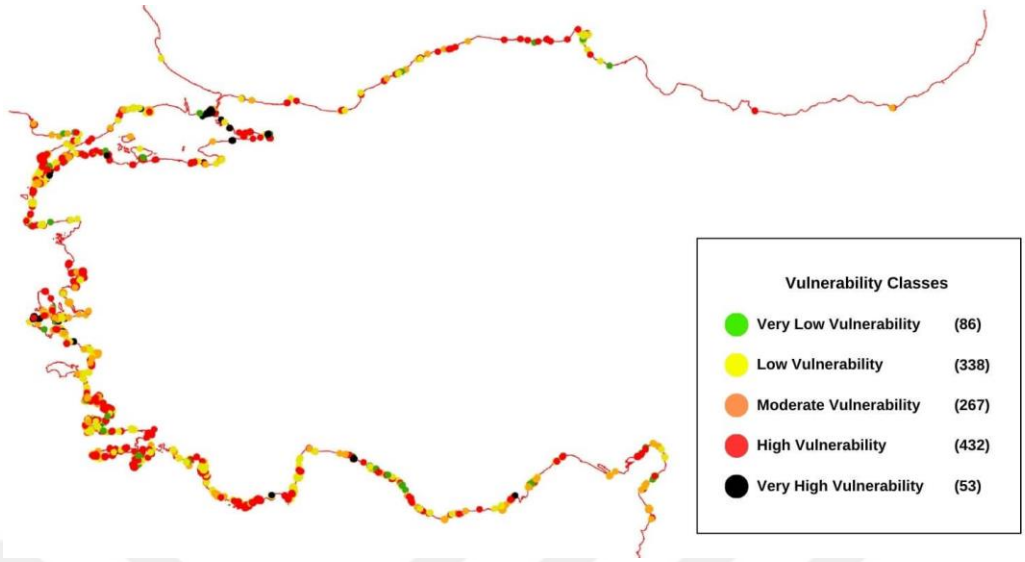


Figure 6.9. Distribution of the coastal archaeological sites of Türkiye based on their vulnerability classes, when the exposure data is obtained from the CVI values based on the SSP5-8.5 scenario.

It is also seen that 43.4% of the sites with "Very High Vulnerability" and 40.5% of the sites with "High Vulnerability" are located along the Aegean coastline of Türkiye, where 45% of the sites with "Low Vulnerability" are located along the Mediterranean coastline. The regional distribution of the assessed heritage sites grouped by their vulnerability classes is provided in Table 6.7.

Table 6.8. Regional distribution of the coastal archaeological sites of Türkiye grouped by their vulnerability classes determined by the CCHVAM using the CVI values obtained from the data of the SSP5-8.5 scenario.

Vulnerability	Mediterranean	Aegean	Marmara	Black Sea	Total
Very Low	35	32	11	8	**86 (7.3%)**
Low	152	137	28	21	**338 (28.7%)**

Table 6.7 (continued) Regional distribution of the coastal archaeological sites of Türkiye grouped by their vulnerability classes determined by the CCHVAM using the CVI values obtained from the data of the SSP5-8.5 scenario.

Moderate	89	109	39	30	**267 (22.7%)**
High	148	175	61	48	**432 (36.7%)**
Very High	8	23	22	0	**53 (4.6%)**

When the proximity indicator of the sites in each vulnerability class is checked through a scatter plot given in Figure 6.10, it is seen that there are a number of sites located directly on the shoreline and have "Low Vulnerability" and "Moderate Vulnerability".

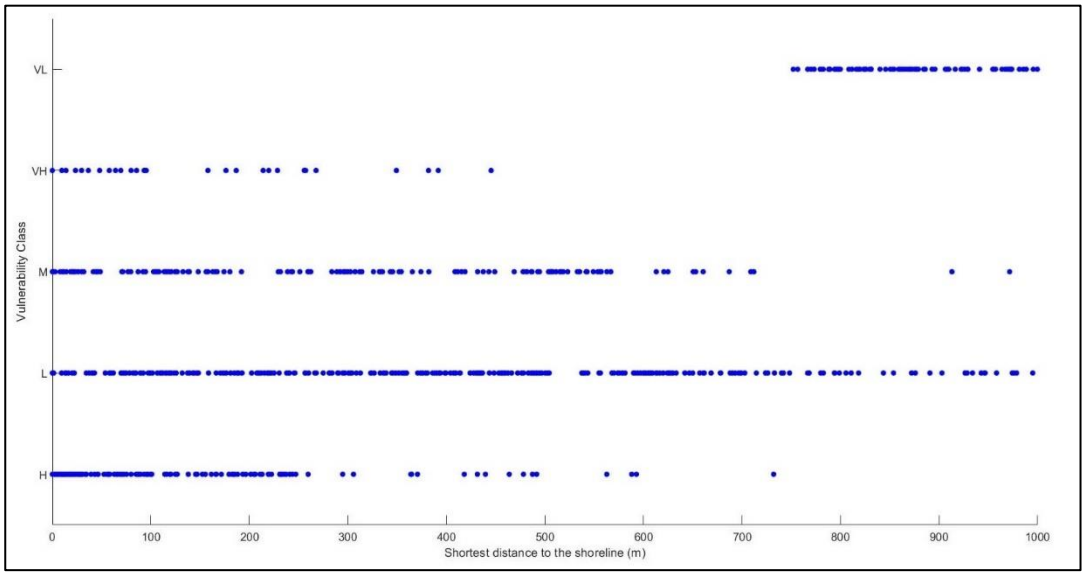


Figure 6.10. The shortest distances of the assessed coastal archaeological sites of Türkiye in each vulnerability class, assigned by the CCHVAM.

When the sites with “Low Vulnerability” and located directly on the shoreline are checked in detail, the following properties of these sites are found:

- None of these sites has more than 10% of their areas lower than 10 m. Also, none of these sites has more than 20% of their areas within 100 m distance of the shoreline. It means that the elevation and area indicator sensitivity values of these sites are either “Very Low” or “Low.
- Overall sensitivity values of all of these sites are “Moderate Sensitivity”, and all of them have “Low Exposure”, resulting in “Low Potential Impact”.
- None of these sites has “Low Adaptive Capacity”.

Since the CCHVAM integrates all these components when assigning a vulnerability class to a site, the sites with these properties have “Low Vulnerability” although they are located directly on the shoreline.

6.1.5 Vulnerability Assessment with the Coastal Erosion Impact Scores Based on SSP2-4.5 Scenario

As it provides insights into an existing threat on the shoreline segment, the erosion impact score obtained from the modified version of FCVAM (Ince, 2024) can also be utilized as the exposure component of the CCHVAM. In this part of the study, the vulnerability assessment with the CCHVAM is done by using the erosion impact score obtained with the data of SSP2-4.5 as the exposure component value of each coastal cultural heritage site, instead of the CVI value, which combines the erosion impact score with surge and inundation impact scores.

6.1.5.1 Values of Potential Impact

When the erosion impact scores obtained from the data of the SSP2-4.5 scenario are utilized as exposure values, it is found that 41.3% of the coastal archaeological sites

of Türkiye have “Moderate Potential Impact” and 35.5% of the sites have “Low Potential Impact” as it is shown in Figure 6.11.

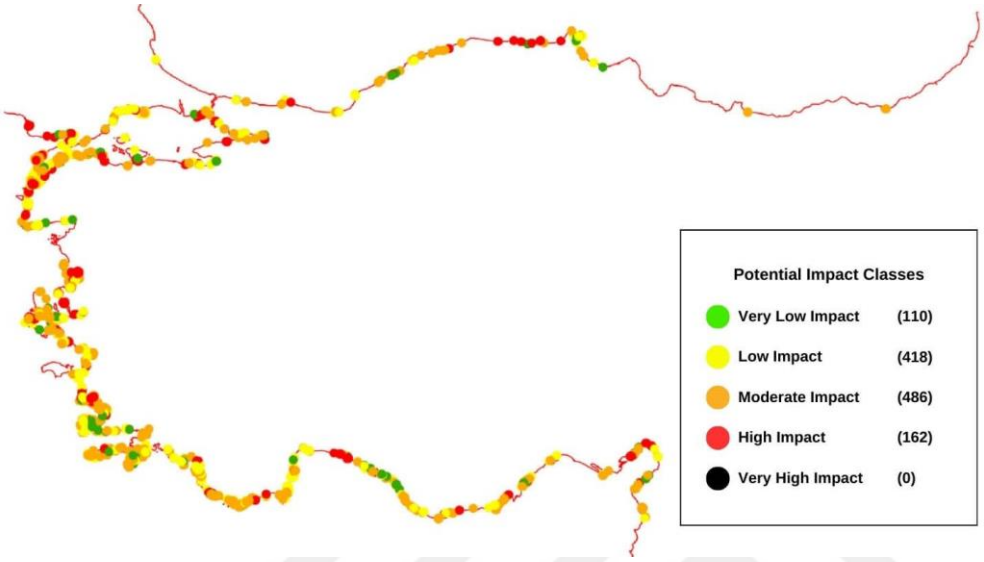


Figure 6.11. Distribution of the coastal archaeological sites of Türkiye based on their potential impact classes determined by the CCHVAM for the SSP2-4.5 scenario.

The regional distribution of the sites in each potential impact class is presented in Table 6.8. It is seen that 51.8% of all the sites with “High Potential Impact” are located along the Aegean coastline, and 23.4% are located along the Mediterranean coastline. On the other hand, 39.3% of the sites with “Moderate Potential Impact” are located along the Mediterranean coastline and 37.7% are located along the Aegean coastline.

Table 6.9. Regional distribution of the coastal archaeological sites of Türkiye grouped by their potential impact classes determined by the CCHVAM using the erosion impact scores obtained from the data of the SSP2-4.5 scenario.

Potential Impact	Mediterranean	Aegean	Marmara	Black Sea	Total
Very Low	38	45	16	11	**110 (9.4%)**
Low	165	164	54	35	**418 (35.5%)**
Moderate	191	183	64	48	**486 (41.3%)**
High	38	84	27	13	**162 (13.8%)**

When the sites in each potential impact class are checked, it is seen that the sites with "High Potential Impact" have "Moderate Exposure", and either "Very High Sensitivity" or "High Sensitivity". Also, it is seen that 42.7% of the sites with "Very Low Potential Impact" have "Moderate Exposure". However, all of these sites with "Moderate Exposure" and "Very Low Potential Impact" have "Very Low Sensitivity". The majority of these sites have no parts lower than 10 m, and their shortest distances to the shoreline are greater than 780 m.

6.1.5.2 Vulnerability Classes

It is presented in Figure 6.12 that 37.3% of the coastal archaeological sites of Türkiye have "High Vulnerability" and 29.2% of the sites have "Low Vulnerability". When these results are compared with the results obtained by using the CVI value of each site, it is noticed that the erosion impact scores of most sites are lower than their CVI values. The differences are discussed in detail in the following parts.

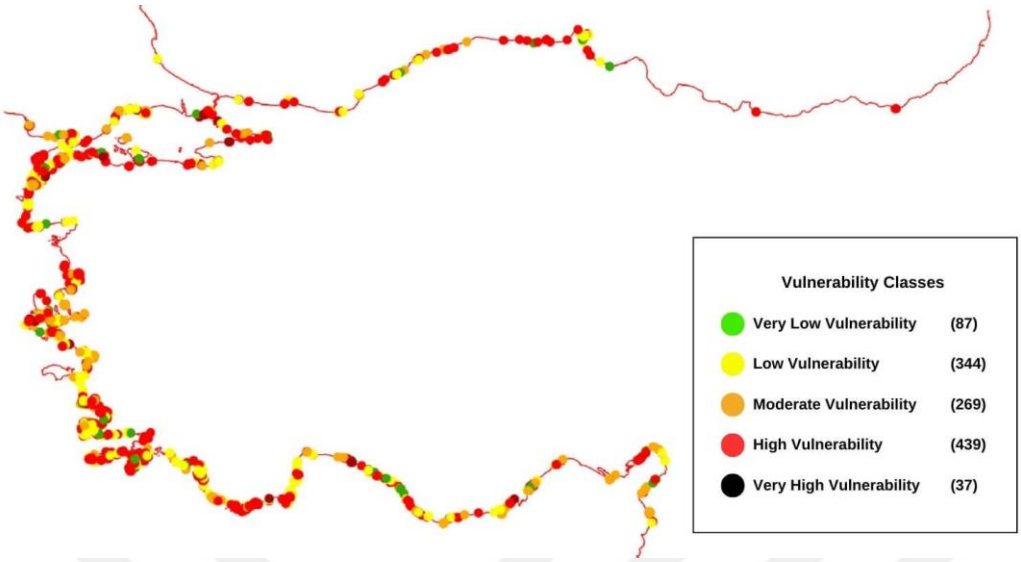


Figure 6.12. Distribution of the coastal archaeological sites of Türkiye based on their vulnerability classes, when the exposure values are the erosion impact scores obtained from the data of the SSP2-4.5 scenario.

It is also seen that 45.9% of the sites with "Very High Vulnerability" and 40.5% of the sites with "High Vulnerability" are located along the Aegean coastline of Türkiye, where 45% of the sites with "Low Vulnerability" are located along the Mediterranean coastline. The regional distribution of the assessed heritage sites grouped by their vulnerability classes is provided in Table 6.9.

Table 6.10. Regional distribution of the coastal archaeological sites of Türkiye grouped by their vulnerability classes determined by the CCHVAM using the erosion impact scores obtained from the data of the SSP2-4.5 scenario.

Vulnerability	Mediterranean	Aegean	Marmara	Black Sea	Total
Very Low	35	33	11	8	**87 (7.4%)**
Low	155	138	31	20	**344 (29.2%)**

Table 6.9 (continued) **R**egional distribution of the coastal archaeological sites of Türkiye grouped by their vulnerability classes determined by the CCHVAM using the erosion impact scores obtained from the data of the SSP2-4.5 scenario.

Moderate	88	110	41	30	**269 (22.9%)**
High	149	178	63	49	**439 (37.3%)**
Very High	5	17	15	0	**37 (3.2%)**

When the proximity indicator of the sites in each vulnerability class is checked, a similar plot is obtained. It is seen that there are a number of sites with “Low Vulnerability” and “Moderate Vulnerability” located directly on the shoreline, in addition to the sites with “High Vulnerability” and “Very High Vulnerability”. The corresponding scatter plot is shown in Figure 6.13.

The sites with “Low Vulnerability”, although they are located directly on the shoreline, are inspected again. It is seen that although the proximity indicator is prioritized in the computation of the sensitivity component, overall, the model provides a comprehensive result considering all the other indicators of threats, impact, and adaptive capacity together.

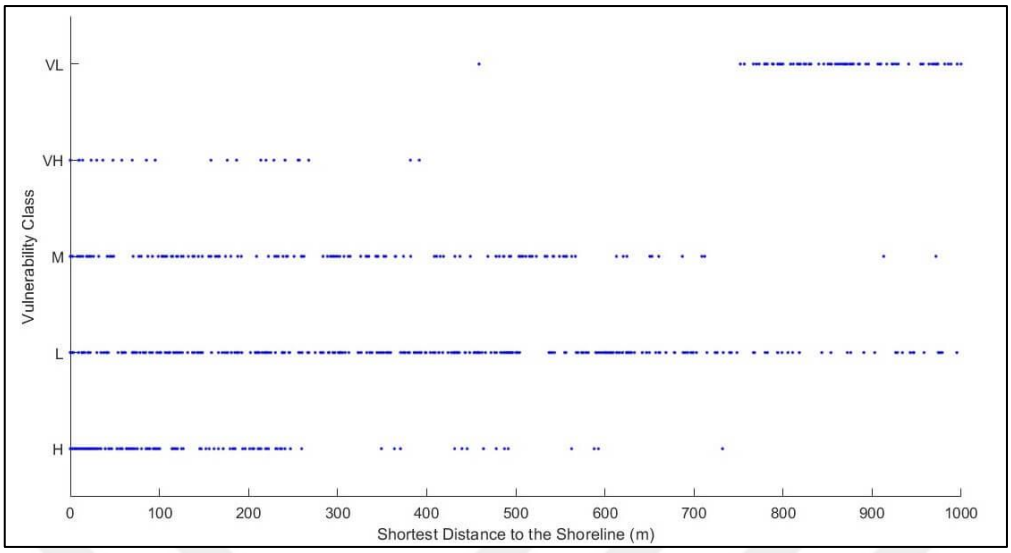


Figure 6.13. The shortest distances of the assessed coastal archaeological sites of Türkiye in each vulnerability class, assigned by the CCHVAM.

6.1.6 Vulnerability Assessment with the Coastal Erosion Impact Scores Based on SSP5-8.5 Scenario

The coastal erosion impact scores are obtained from the data of two emission scenarios as described earlier, and the second scenario, the SSP5-8.5, represents the worst case. Hence, the assessment with the erosion impact score is repeated by using the data of this case, as well.

6.1.6.1 Values of Potential Impact

When the erosion impact scores obtained from the data of the SSP5-8.5 scenario are utilized, it is found that 33.2% of the coastal archaeological sites of Türkiye have “Moderate Potential Impact” and 30.6% of the sites have “Low Potential Impact” as it is shown in Figure 6.14.

When the CVI values are utilized, the change in the scenario causes only minor changes in the number of classes in each potential impact class. However, when the erosion impact scores are utilized, considerable differences are observed among the results of the two scenarios. This can be explained by the fact that the CVI values are obtained from the combination of coastal erosion, surge, and inundation impact scores. Although considerable differences are observed in the impact scores obtained from the data of different scenarios, their combination may result in a smaller difference.

It is noticed that 31.7% of the sites with "Moderate Potential Impact" based on the data of the SSP2-4.5 scenario are moved to the "High Potential Impact" class when the data of the SSP5-8.5 scenario is utilized. Also, 13.9% of the sites with "Low Potential Impact" are switched to the "Moderate Potential Impact Class" when the worst-case scenario is studied.

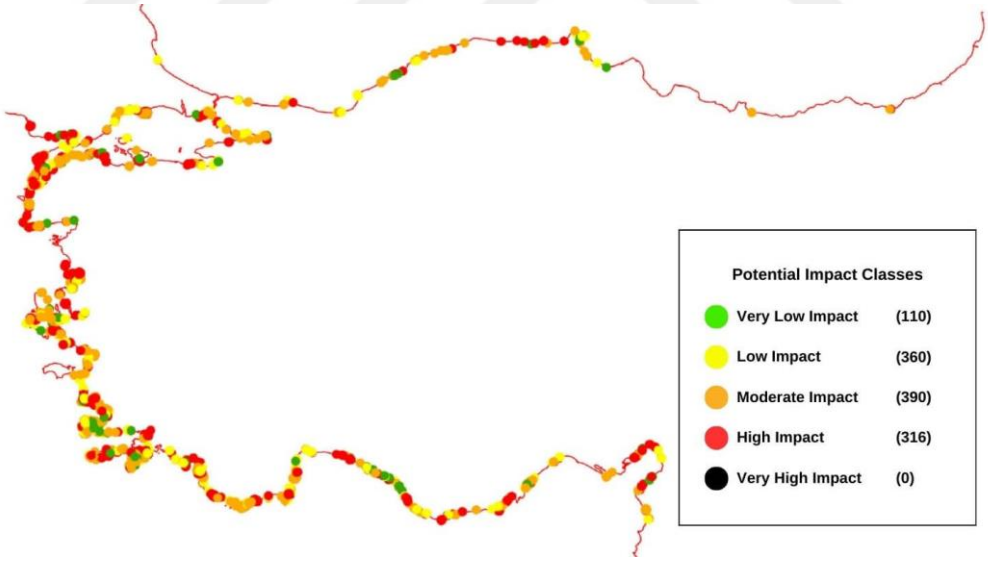


Figure 6.14. Distribution of the coastal archaeological sites of Türkiye based on their potential impact classes determined by the CCHVAM using the coastal erosion impact scores obtained from the data of the SSP5-8.5 scenario.

The regional distribution of the sites in each potential impact class is presented in Table 6.10. It is seen that 46.2% of all the sites with “High Potential Impact” are located along the Aegean coastline, and 35.8% are located along the Mediterranean coastline. On the other hand, 37.9% of the sites with “Moderate Potential Impact” are located along the Aegean coastline, and 39.7% of the sites with “Low Potential Impact” are located along the Mediterranean coastline.

Table 6.11. Regional distribution of the coastal archaeological sites of Türkiye based on their potential impact classes determined by the CCHVAM using the coastal erosion impact scores obtained from the data of the SSP5-8.5 scenario.

Potential Impact	**Mediterranean**	**Aegean**	**Marmara**	**Black Sea**	**Total**
Very Low	38	45	16	11	**110 (9.4%)**
Low	143	137	46	34	**360 (30.6%)**
Moderate	138	148	60	44	**390 (33.2%)**
High	113	146	39	18	**316 (26.8%)**

When the exposure and sensitivity classes of the sites in each potential impact class are checked, it is seen that 61.8% of the sites with “Very Low Potential Impact” have “Moderate Exposure”. This rate is obtained as 42.7% when the data of the SSP2-4.5 scenario is utilized. It is also known that the number of sites in this potential impact class is the same for both scenarios. However, there are 12 sites detected, of which the exposure class has changed.

6.1.6.2 Vulnerability Classes

By using the potential impact class determined based on the SSP5-8.5 scenario and the adaptive capacity class, each site is assigned to a vulnerability class. It is presented in Figure 6.15 that 40.1% of the coastal archaeological sites of Türkiye have “High Vulnerability” and 24.7% of the sites have “Low Vulnerability”.

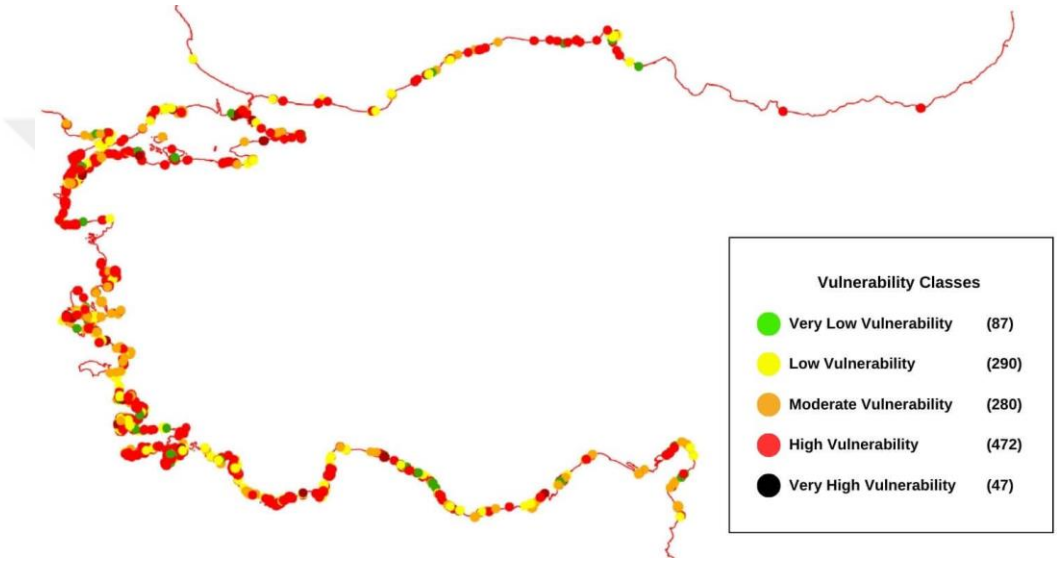


Figure 6.15. Distribution of the coastal archaeological sites of Türkiye based on their vulnerability classes, when the coastal erosion impact scores are obtained from the data of the SSP5-8.5 scenario.

It is also seen that 48.9% of the sites with “Very High Vulnerability” and 40.7% of the sites with “High Vulnerability” are located along the Aegean coastline of Türkiye, where 46.2% of the sites with “Low Vulnerability” are located along the Mediterranean coastline. The regional distribution of the assessed heritage sites grouped by their vulnerability classes is provided in Table 6.11.

Table 6.12. Regional distribution of the coastal archaeological sites of Türkiye based on their vulnerability classes determined by the CCHVAM using the coastal erosion impact scores obtained from the data of the SSP5-8.5 scenario.

Vulnerability	Mediterranean	Aegean	Marmara	Black Sea	Total
Very Low	35	33	11	8	**87 (7.4%)**
Low	134	112	25	19	**290 (24.7%)**
Moderate	93	116	41	30	**280 (23.8%)**
High	164	192	67	49	**472 (40.1%)**
Very High	6	23	17	1	**47 (4%)**

When the proximity indicator of the sites in each vulnerability class is checked, it is seen that there are a number of sites with “Low Vulnerability” and “Moderate Vulnerability” located directly on the shoreline, in addition to the sites with “High Vulnerability” and “Very High Vulnerability”, as shown in Figure 6.16.

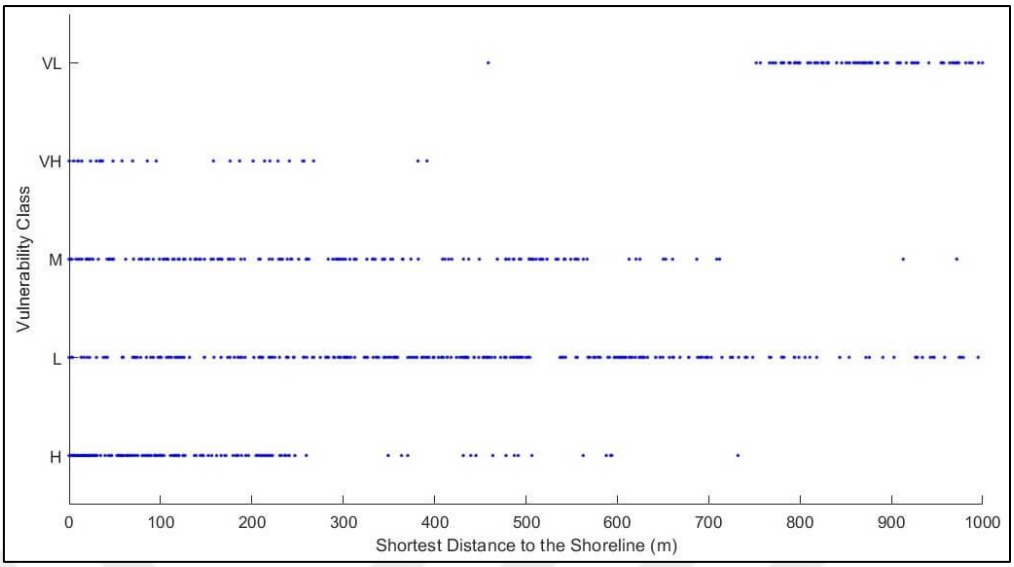


Figure 6.16. The shortest distances of the assessed coastal archaeological sites of Türkiye in each vulnerability class, assigned by the CCHVAM.

6.1.7 Comparison of the Vulnerability Classes Determined Based on SSP2-4.5 and SSP5-8.5 Scenarios

In the scope of this study, the coastal cultural heritage sites of Türkiye are assessed by using the CCHVAM for the conditions of the SSP2-4.5 and the SSP5-8.5 scenarios. Then, the potential impact and vulnerability class of each site are checked to see the differences in the results of CCHVAM due to the change in the level of impacts presented in these scenarios.

Initially, the CVI value of each site is used as the exposure component value. It is noticed that there are 30 sites, of which the exposure class switches from “Low Exposure” to “Moderate Exposure” when the scenario is changed from SSP2-4.5 to SSP5-8.5. The change in their exposure classes is the reason for the change in the potential impact and vulnerability classes of these sites.

As it is presented in Table 6.12, only minor changes occur in the number of sites in each potential impact class. Three sites are moved from the “Low Potential Impact”

class to the “Moderate Potential Impact” class, and 13 sites are moved from the “Moderate Potential Impact” class to the “High Potential Impact” class.

Table 6.13. Comparison of the number of sites in each potential impact class obtained when the SSP2-4.5 and SSP5-8.5 scenarios are followed in the computation of CVI values.

SSP2-4.5		**SSP5-8.5**	
Potential Impact Class	**Number of Sites**	**Potential Impact Class**	**Number of Sites**
Very Low	109	**Very Low**	109
Low	415	**Low**	406
Moderate	481	**Moderate**	477
High	171	**High**	184
Very High	0	**Very High**	0

The number of sites in each vulnerability class based on the two scenarios can be seen in Table 6.13. It is seen that two sites are switching from “Low Vulnerability” to “High Vulnerability” resulting from the change in exposure class and “Moderate Adaptive Capacity”, and four sites are switching from “Low Vulnerability” to “Moderate Vulnerability” resulting from the same change in exposure class but with “High Adaptive Capacity”. Additionally, it is found that three sites are switching from “Moderate Vulnerability” to “High Vulnerability”, resulting from the change in exposure class and “Low Adaptive Capacity”. Another site with “Low Adaptive Capacity” is seen to switch from “High Vulnerability” to “Very High Vulnerability”.

Table 6.14. Comparison of the number of sites in each vulnerability class obtained when the SSP2-4.5 and SSP5-8.5 scenarios are followed for the CVI values.

SSP2-4.5		**SSP5-8.5**	
Vulnerability Class	**Number of Sites**	**Vulnerability Class**	**Number of Sites**
Very Low	86	**Very Low**	86
Low	344	**Low**	338
Moderate	266	**Moderate**	267
High	428	**High**	432
Very High	52	**Very High**	53

The same comparison is made for the potential impact and vulnerability classes of the assessed sites obtained from the use of coastal erosion impact scores as the exposure component values.

When the coastal erosion impact scores computed based on the data of SSP5-8.5 are used instead of the ones obtained from the data of the SSP2-4.5 scenario, it is seen that 31.7% of the sites with “Moderate Potential Impact” based on the conditions of SSP2-4.5 have “High Potential Impact” when the erosion impact scores from the SSP5-8.5 are utilized in the assessment. Also, 58 sites are moved from the “Low Potential Impact” class to the “Moderate Potential Impact” class. The resulting difference in the number of sites in each potential impact class is presented in Table 6.14.

Table 6.15. Comparison of the number of sites in each potential impact class obtained when the SSP2-4.5 and SSP5-8.5 scenarios are followed for the erosion impact scores.

SSP2-4.5		**SSP5-8.5**	
Potential Impact Class	**Number of Sites**	**Potential Impact Class**	**Number of Sites**
Very Low	110	**Very Low**	110
Low	418	**Low**	360
Moderate	486	**Moderate**	390
High	162	**High**	316
Very High	0	**Very High**	0

A similar change is observed for the vulnerability classes, as well. From the “Low Vulnerability” class, 15 sites are moved to the “Moderate Vulnerability” class, and 39 sites are moved to the “High Vulnerability” class. From the “Moderate Vulnerability” class, four sites are moved to the “High Vulnerability” class, and lastly, ten sites are moved from the “High Vulnerability” class to the “Very High Vulnerability” class. The comparison of the results obtained from the SSP2-4.5 and the SSP5-8.5 scenarios is presented in Table 6.15.

Table 6.16. Comparison of the number of sites in each vulnerability class obtained when the SSP2-4.5 and SSP5-8.5 scenarios are followed for the erosion impact scores.

SSP2-4.5		**SSP5-8.5**	
Vulnerability Class	**Number of Sites**	**Vulnerability Class**	**Number of Sites**
Very Low	87	**Very Low**	87
Low	344	**Low**	290
Moderate	269	**Moderate**	280
High	439	**High**	472
Very High	37	**Very High**	47

Finally, when CVI values and the coastal erosion impact scores obtained from the data of the same emission scenario are used as the exposure component values, the number of sites in each vulnerability class is compared in Table 6.16. It can be clearly seen that 37 sites are assigned to the "Very High Vulnerability" class when the coastal erosion impact scores are used. However, there are 52 sites in the same class when the CVI values are used. It proves that a site can be highly vulnerable to the other impacts (surge and inundation) assessed, but not equally vulnerable to coastal erosion. Therefore, in order to understand the actual threat to a site, the impact scores should be checked as well.

Table 6.17. The distribution of sites based on their vulnerability classes determined by the CCHVAM using CVI values and the coastal erosion impact scores as exposure values, separately.

CVI - SSP2-4.5		Coastal Erosion – SSP2-4.5	
Vulnerability Class	**Number of Sites**	**Vulnerability Class**	**Number of Sites**
Very Low	86	**Very Low**	87
Low	344	**Low**	344
Moderate	266	**Moderate**	269
High	428	**High**	439
Very High	52	**Very High**	37

6.2 Shoreline Evolution with the DSAS

The latest version of the DSAS as a stand-alone software is utilized for this modeling process. As explained in Section 4.1, the DSAS uses a series of observed shorelines, a baseline, and generated transects along the baseline as input data to provide the rates and distance of the observed shoreline movement.

The coastline segments interacting with two of the assessed coastal archaeological sites are analyzed in this part of the study: the Anemurium Ancient City and the Soli-Pompeiopolis Ancient City. For both coastline segments, shoreline data from each year between 2016 and 2024 are utilized, and two sets of transects are generated with spacing values of 50 m and 100 m. All the details about the computation process of DSAS, the input data, and the output data obtained from DSAS are provided in Section 4.1 and Section 4.3.

The results obtained from the CCHVAM and the results obtained from the DSAS using the two sets of transects for both sites are given in the following sections.

6.2.1 Anemurium Ancient City

Based on the results obtained from the CCHVAM, where the CVI values are used as the exposure component values, the site has a high sensitivity to the impacts of sea level rise on the interacting shoreline segment, high adaptive capacity, and low exposure based on both the SSP2-4.5 and SSP5-8.5 scenarios. With these component values, the CCHVAM determines that the site has a moderate vulnerability. The indicator values utilized in the exposure, sensitivity, and adaptive capacity modules of the assessment model are given in Table 6.17, Table 6.18, and Table 6.19, respectively. Additionally, all the components of the vulnerability assessment model and the final vulnerability value of Anemurium Ancient City are given in Table 6.20.

Table 6.18. The CVI values and the coastal erosion impact scores obtained from the FCVAM and utilized as the exposure component of the CCHVAM.

Exposure Component Value		**Exposure Class**
CVI (SSP2-4.5)	2.18	Low Exposure
CVI (SSP5-8.5)	2.22	Low Exposure
Coastal Erosion (SSP2-4.5)	2.48	Low Exposure
Coastal Erosion (SSP5-8.5)	2.52	Moderate Exposure

The CVI value indicates that the coastline segment directly interacting with the site has low vulnerability to sea level rise and its impacts as computed from the modified version of the FCVAM (Ince, 2024). However, the coastal erosion impact scores are also checked, and it is seen that the vulnerability of the coastline segment to coastal erosion is higher than its overall vulnerability determined by the combination of coastal erosion, surge, and inundation impact scores.

Table 6.19. The indicator values assessed to obtain the sensitivity component of the CCHVAM.

Sensitivity		
Indicator		**Indicator Sensitivity Class**
Elevation (%)	20.1	Low Sensitivity
Area (%)	21.2	Low Sensitivity
Proximity (m)	0	Very High Sensitivity
Interaction (m)	6075.8	High Sensitivity
Sensitivity Value		**Sensitivity Class**
3.59		High Sensitivity

As described in the previous part of this chapter, these sensitivity indicators provide insight into the interaction of Anemurium Ancient City with the shoreline and the impacts of sea level rise affecting the shoreline. These indicator values describe a site located along a long coastline segment, starting directly from the coastline and covering a large area in the landward direction, and laying on a steep land where the elevation starts rising at a close distance to the coastline. Comparing this description based on the indicator values with the site photos provided in Section 4.2.1, it can be said that the sensitivity module of the CCHVAM provided accurate results for Anemurium Ancient City.

Table 6.20. The indicator values assessed to obtain the adaptive capacity component of the CCHVAM.

Adaptive Capacity		
Indicator		**Adaptive Capacity Class**
Degree of Protection	1	High Adaptive Capacity
Urbanization (%)	4.4	High Adaptive Capacity

The site has a high adaptive capacity, as expected, because it has the highest level of protection provided by Law 2863. Also, it is found that the level of urbanization is very low in the area with which the site directly interacts. Although the site has a high sensitivity value, it is not expected to have a high vulnerability because its adaptive capacity is high and its exposure is low.

Table 6.21. Values obtained from the CCHVAM for each vulnerability component and the final vulnerability value of Anemurium Ancient City.

Exposure	*Low*
Sensitivity	*High*
Potential Impact	Moderate
Adaptive Capacity	High
Vulnerability	**Moderate**

6.2.1.1 Results Obtained From the DSAS

As explained in Section 4.1, the DSAS provides four separate values at each transect: shoreline change envelope (SCE), net shoreline Movement (NSM), end point rate (EPR), and linear regression rate (LRR). These values are obtained from the DSAS as attributes of each transect line in a JSON file and studied in ArcGIS Pro. As an example, the raw layer of results can be seen in Figure 6.17, where the transects are colored based on the LRR values at each of them.

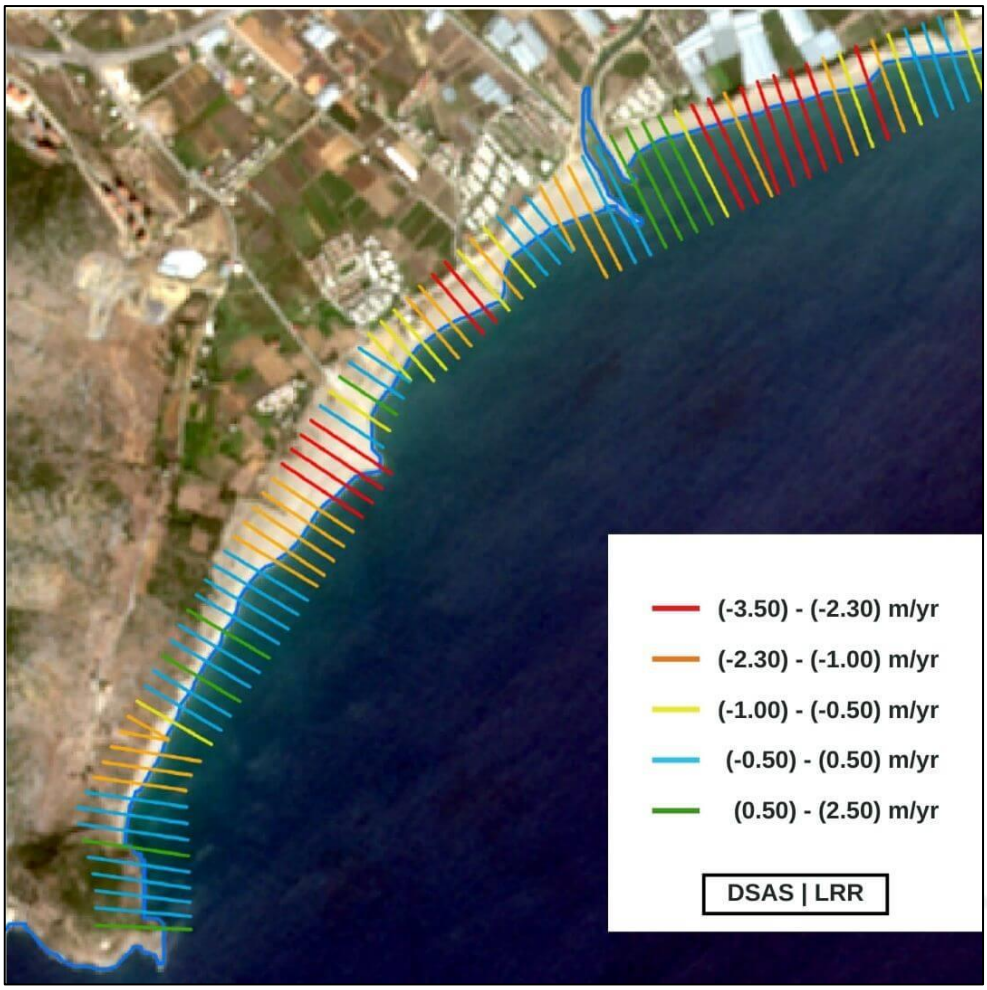


Figure 6.17. The transect layer with 50-m spacings exported from the DSAS, providing the analysis results, and grouped based on the LRR values computed at each of them.

The shoreline change envelope is the longest distance over which the shoreline moved along a transect throughout the time passed between the earliest and the latest shoreline. Statistics of the shoreline change envelope measured at each transect show that the average value of the longest distance that the assessed shoreline moved is over 20 m between 2016 and 2024, as presented in Table 6.21.

Table 6.22. Shoreline change envelope values obtained from both transects with 50 m spacing and transects with a spacing of 100 m.

	Results for Transects with a Spacing of 50 m	**Results for Transects with a Spacing of 100 m**
Number of Transects	79	40
Average Change	21.5 m	20.7 m
Maximum Change	162.6 m, at Transect-22	49.4 m, at Transect-24
Minimum Change	5.2 m, at Transect-63	5.2 m, at Transect-32

On the other hand, net shoreline movement (NSM) is the distance between the intersection points of a transect with the earliest shoreline and the latest shoreline. The statistical values of all the NSM distances measured at the transects, presented in Table 6.22, show that the average distance between the shoreline observed in 2016 and the one observed in 2024 is approximately 5.0 m, and the dominant behavior is shoreline retreat since the average value is negative. Also, when the results obtained from the two transect layers are compared, it is seen that utilizing a finer transect layer results in capturing more accretional areas along the studied coastline segment. Also, the shoreline positions observed in 2016 and 2024 are shown in Figure 6.18.

Table 6.23. Net shoreline movement values obtained from both transects with 50 m spacing and transects with a spacing of 100 m.

	Results for Transects with 50 m Spacing	**Results for Transects with 100 m Spacing**
Average movement (m)	-4.96	-5.23
Percentage of all transects having an erosional movement	57.35%	57.14%

Table 6.22 (continued) Net shoreline movement values obtained from both transects with 50 m spacing and transects with a spacing of 100 m

The largest erosional movement (m)	-42.55, at Transect-47	-42.55, at Transect-24
Average of all erosional movements (m)	-15.56	-15.96
Percentage of all transects having an accretional movement	42.65%	42.86%
The largest accretional movement (m)	45.17, at Transect-22	31.41, at Transect-11
Average of all accretional movements (m)	9.29	9.08

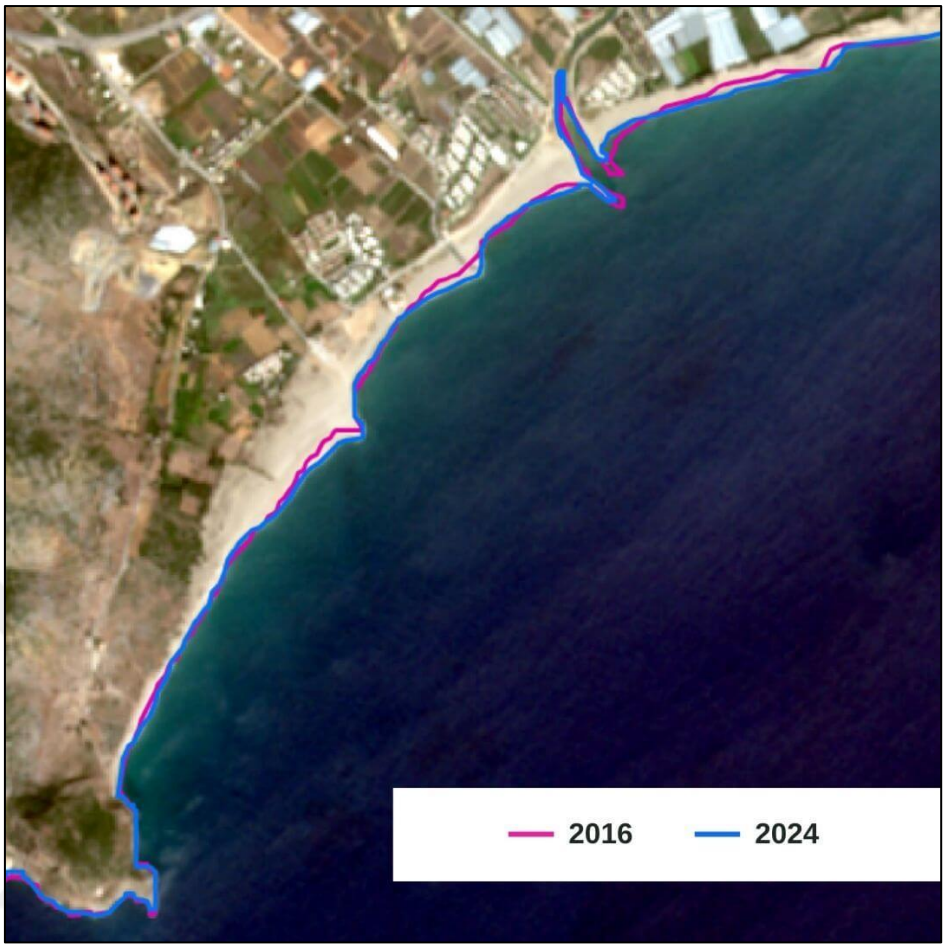


Figure 6.18. The shorelines observed in 2016 and 2024 obtained from the SENTINEL-2 satellite imagery in ArcGIS Pro.

Based on the NSM values, a yearly rate of shoreline movement is computed by the DSAS, which is called the end-point rate (EPR). Based on the total distance measured at each transect between the shorelines observed in only the years 2016 and 2024, the average erosional rate is approximately 2 m/yr, where the average accretional rate is approximately 1.15 m/yr. The overall rate computed by using the rates measured at all the transects is -0.62 m/yr. Additionally, the maximum erosional EPR computed is 5.32 m/yr, which shows that there is a part of the assessed shoreline where a significant erosional behavior is observed, as presented in Table 6.23.

Table 6.24. Statistical values of the endpoint rate at each transect obtained from both the transects with a spacing of 50 meters and the transects with a spacing of 100 meters.

	Results for Transects with 50 m Spacing	**Results for Transects with 100 m Spacing**
Average rate	-0.62 m/yr	-0.65 m/yr
Percentage of all transects at which erosion is observed	57.35%	57.14%
Percentage of all transects with statistically significant erosion	29.41%	22.86%
Maximum erosional rate	-5.32 m/yr, at Transect-47	-5.32 m/yr, at Transect-24
Average erosional rate	-1.95 m/yr	-1.99 m/yr
Percentage of all transects at which accretion is observed	42.65%	42.86%
Percentage of all transects with statistically significant accretion	5.88%	5.71%
Maximum accretional rate	5.65 m/yr, at Transect-22	3.93 m/yr, at Transect-11

Table 6.23 (continued) Statistical values of the endpoint rate at each transect obtained from both the transects with a spacing of 50 meters and the transects with a spacing of 100 meters.

Average accretional rate	1.16 m/yr	1.14 m/yr

Unlike the EPR, while computing the linear regression rate (LRR) values, the shoreline of each year in the shoreline dataset is considered, not only the earliest and the latest ones. The average shoreline movement rate obtained from linear regression across the analyzed coastline segment is -0.88 m/yr, as given in Table 6.24. Although the average rate and the average erosional rate are obtained the same for both transect layers, the average accretional rate obtained from each transect layer is different; it is 0.73 m/yr in the transects with 50 m-spacing, and 0.80 m/yr in the transects with 100 m-spacing.

Table 6.25. Statistical values of the linear regression rate at each transect obtained from both the transects with a spacing of 50 meters and the transects with a spacing of 100 meters.

	Results Obtained From Transects with 50 m Spacing	**Results Obtained From Transects with 100 m Spacing**
Average rate (m/yr)	-0.88	-0.88
Percentage of all transects at which erosion is observed	82.28%	82.50%
Maximum erosional rate (m/yr)	-3.34, at Transect-48	-3.28, at Transect-24

Table 6.24 (continued) Statistical values of the linear regression rate at each transect obtained from both the transects with a spacing of 50 meters and the transects with a spacing of 100 meters

Average of all erosional rates (m/yr)	-1.23	-1.24
Percentage of all transects at which accretion is observed	17.72%	17.50%
Maximum accretional rate (m/yr)	2.53, at Transect-21	2.53, at Transect-11
Average of all accretional rates (m/yr)	0.73	0.80

When the LRR value computed at each transect is matched with the adjacent shoreline segment along the assessed coastline, it is seen that the erosional trend is more dominant in the east of the river mouth than it is on the west side, which can be seen in Figure 6.18. The heritage site is located on the west of the river mouth, and it is seen that in most parts of the shoreline in that area, the shoreline movement rate is less than 0.50 m/yr. However, there are some parts where the rate is between 1.00 m/yr and 2.30 m/yr. In Figure 6.19, it can also be seen that along the coastline where the structures are located on the beach, the erosional rates are higher than 1 m/yr.

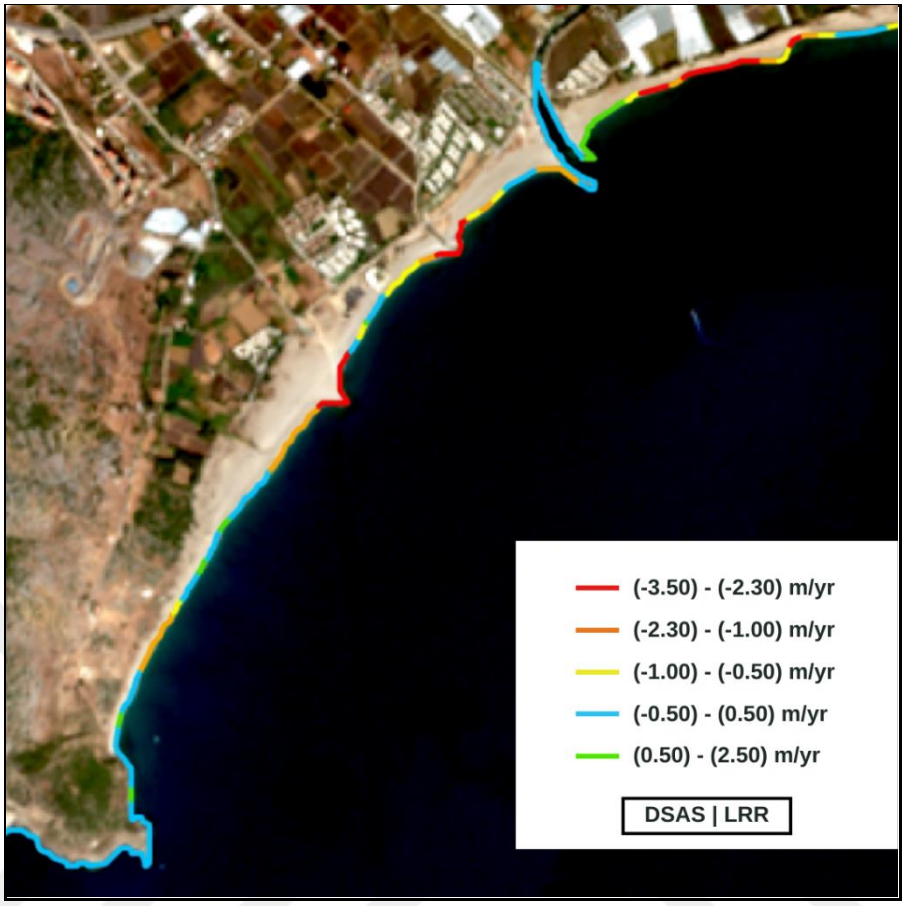


Figure 6.19. The linear regression rate of shoreline movement observed between the years 2016 and 2024, obtained from the transects with equal spacings of 50 m.

6.2.1.2 Projection of the Shoreline Movement Between 2016 and 2024 by Using the LRR Values

The performance of using the LRR values computed by the DSAS for predicting the future shoreline is checked by projecting the shoreline of 2024 and comparing it with the actual shoreline of 2024. The projected shoreline movement is obtained by multiplying the LRR value computed at each transect by the number of years between 2016 and 2024, which is eight. Then, the intersection point of each transect

and the shoreline observed in 2016 is moved to the distance computed by the corresponding LRR value.

The described process is performed for both transect layers, with spacing values of 50 m and 100 m. The projected shoreline by using the transects with 50-meter spacing is shown in Figure 6.20.



Figure 6.20. The shoreline observed in 2024 and the one projected by using the LRR values computed at the transects with 50 m spacing.

The projected shoreline movement and the net shoreline movement computed by the DSAS at each transect line are compared on the graph presented in Figure 6.21. The average net shoreline movement between 2016 and 2024, projected by using the LRR values, is -7.35 m, whereas the DSAS measures the original net shoreline movement as -4.93 m. These average values are -6.55 m and -4.17 m along the heritage site area, which is covered with a red rectangle, respectively.

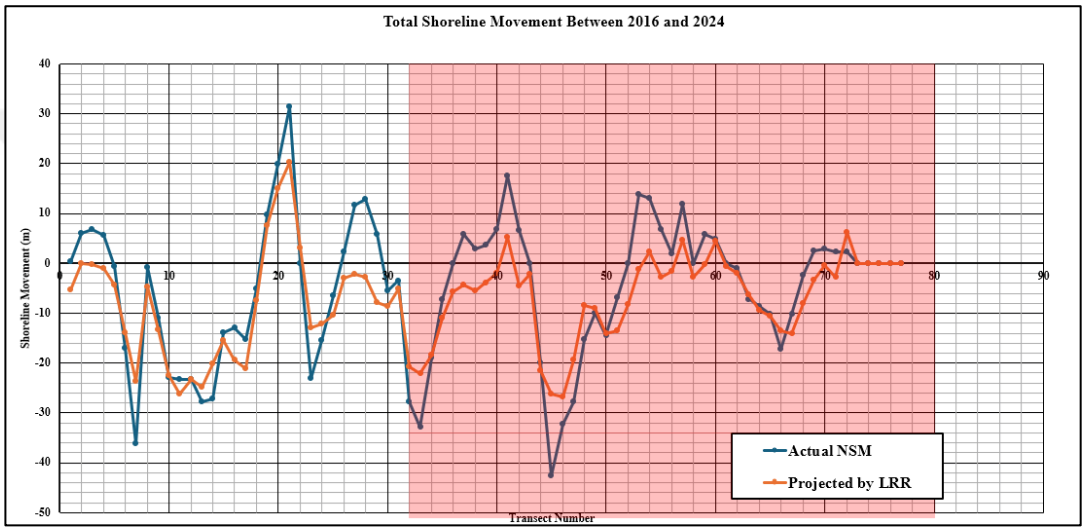


Figure 6.21. Comparison of the net shoreline movement measured and the net shoreline movement between the projected 2024 shoreline and the 2016 shoreline, where the transects overlaying the heritage site area are highlighted with the red area.

The average distance between the projected shoreline and the original shoreline observed in 2024 is measured as 5.4 m. Also, along the assessed shoreline, at 15.6% of all the transects, the distance between the original and the projected shoreline is less than one meter. The average difference between the projected and the original shoreline of the year 2024 at the transects over the heritage site area is 5.33 m, whereas it is 5.50 m for the rest of the assessed shoreline. The change in the distance between the projected and the actual shoreline along the assessed shoreline segment can be seen in Figure 6.22.

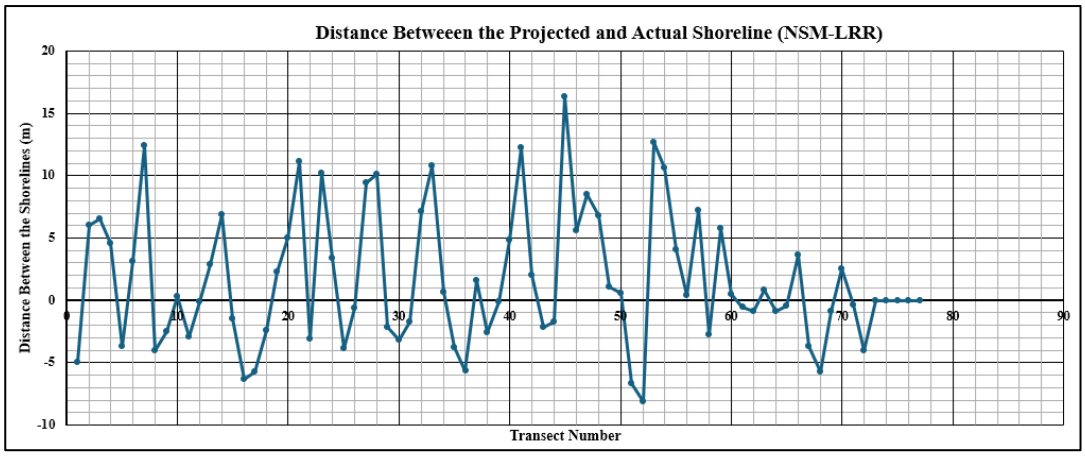


Figure 6.22. Distance between the shoreline observed in 2024 and the projected one by using the LRR values at transects with 50 m spacing.

Since the LRR values obtained at the transects with equal spacings of 100 m are very similar to the ones obtained at the transects with 50 m spacings, the net shoreline movement values obtained from those are also close to the ones given above.

Furthermore, the error in the projection made by using the LRR values is investigated. A certain amount of error is expected since the LRR values are obtained from the shoreline data for an eight-year period only. To investigate the error, a scatter plot is obtained showing the actual values of shoreline movement on the horizontal axis and the projected movement on the vertical axis, as presented in Figure 6.23. The R-square value is obtained as 0.853 from the generated plot. Also, the average difference between the actual and the projected movement is determined as 1.6 m, where the mean absolute error is computed as 5.2 m.

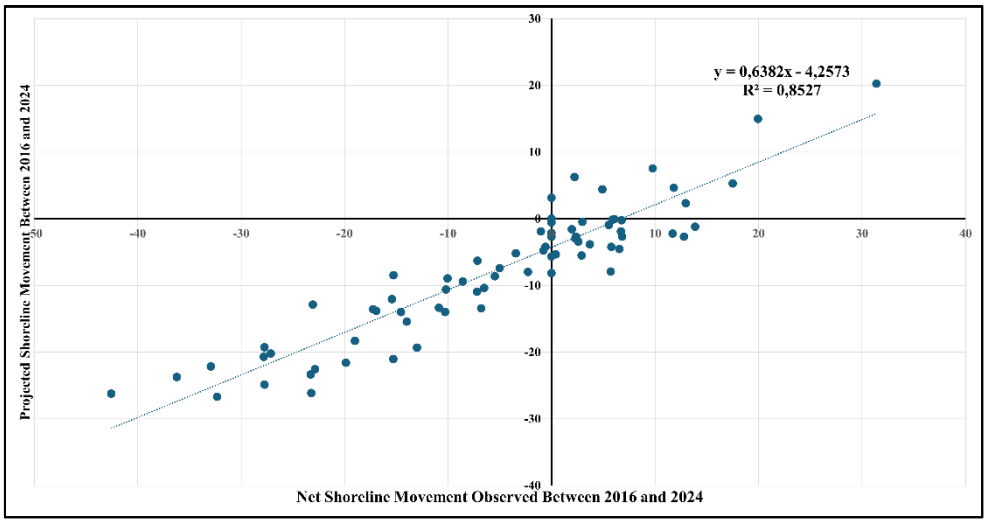


Figure 6.23. Comparison of the actual and projected shoreline movements between 2016 and 2024.

6.2.1.3 Projected Shoreline for the Year 2050

The shoreline position that might be observed in 2050 is projected by following the same process described above using the LRR values.

The projection is made by using both transect layers with spacing values of 50 m and 100 m. The projected shoreline movement using the transects with equal spacings of 50 m is presented in Figure 6.24.

There are significant losses in the beach area projected at various parts of the assessed coastline segment, where there are a number of ancient buildings, as shown in the figures presented in Section 4.2.1. The average distance between the shoreline observed in 2024 and the projected one for the year 2050 is computed as -24.1 m. Also, it is seen that on the east side of the river mouth, significant amounts of erosion are projected by the year 2050 based on the LRR values, which are obtained from the observed shoreline movement between 2016 and 2024.

On the other hand, there are important limitations encountered in this projection process, and they are listed as follows:

- The LRR values utilized to determine the amount of shoreline movement by 2050 are obtained from the observed shoreline movement of a specific eight-year period only, and this results in a considerable amount of error, as discussed in the previous section. However, the reason of the corresponding time period being selected is that there are groins placed at the river mouth in 2016, and this change is assumed to alter the trend observed before this construction.
- The projection is made by moving the shoreline observed in 2024 along the transects over the distances computed by using the LRR values. However, while moving the shoreline, the structures located on the land that should limit the shoreline movement are neglected.



Figure 6.24. The projected 2050 shoreline (purple) and the shoreline observed in September 2024 (red) along the Anemurium Ancient City, obtained from the transects with equal spacings of 50 m.

In most parts of the assessed shoreline segment, the LRR values obtained from both transect layers are similar, therefore, the deviation between the projected shorelines for the year 2050 is minimal, as shown in Figure 6.25. The difference between the average shoreline movement obtained from the transects with 50 m spacing and the one obtained from the transects with 100 m spacing is computed as 0.45 m. However, there are a few parts where shoreline movement is detected only by one of the layers, resulting in a considerable deviation.

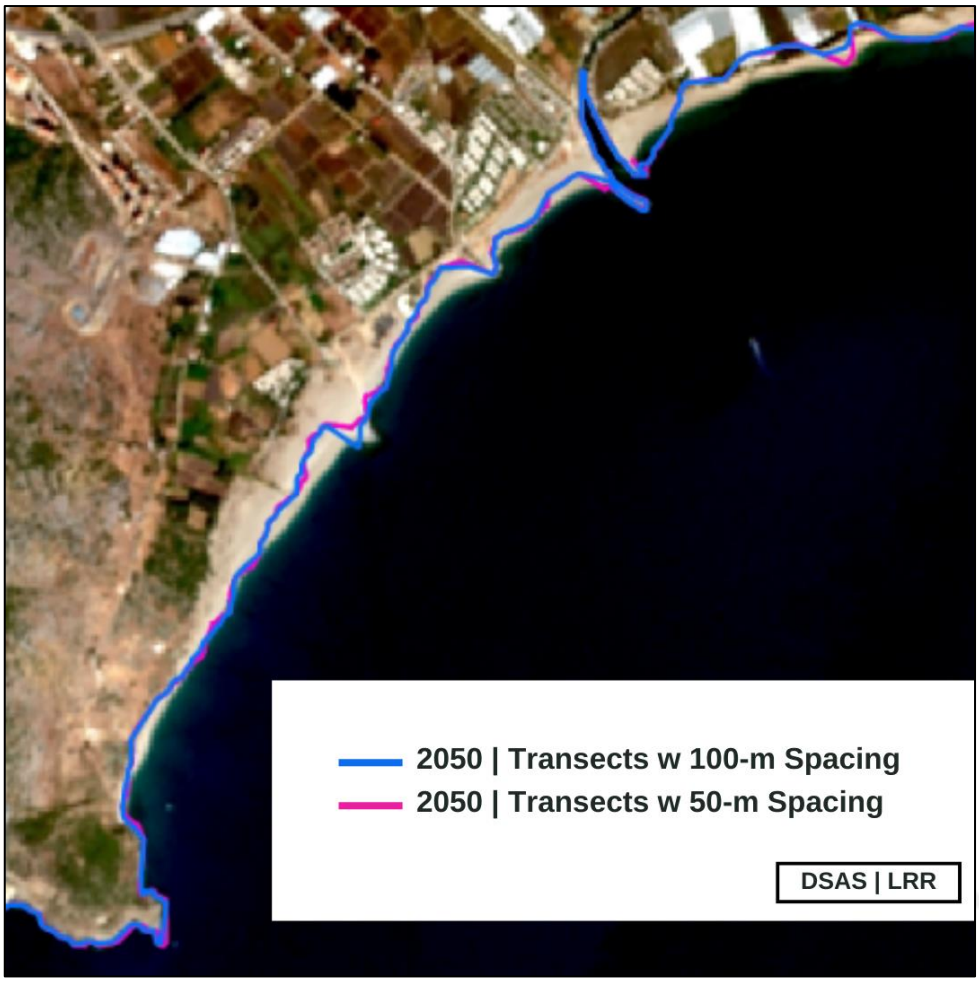


Figure 6.25. The shoreline positions projected to be observed by 2050 by using the LRR values obtained from the transects with 50 m-spacing and the transects with equal spacings of 100 m.

The same process is repeated with the EPR values obtained from the same transect layers. The deviation between the shoreline observed in 2024 and the projected ones is presented in Figure 6.26. It can be clearly seen that at some transects, the EPR values are greater than the LRR values. The average shoreline movement projected by using the LRR values is -24.1 m, whereas the average shoreline movement projected with the EPR values is -16.0 m. However, the average movement projected at the transects where the rate indicates an erosional behavior is -32.9 m when the LRR values are considered, and it is -51.6 m. It is an expected outcome because the

EPR value at a transect is the rate of shoreline movement computed using only the latest and the earliest shoreline positions.



Figure 6.26. Projected shorelines for the year 2050 by utilizing the LRR and the EPR are compared with each other and the shoreline observed in 2024.

The projection done by using the LRR values results in a complete loss of beach in multiple parts of the assessed shoreline. Also, a significant amount of accretion is projected to occur at the east side of the river mouth. Towards the acropolis, the shoreline movement rates get minimal, so the minimum change in shoreline position is projected around the headland. Overall, based on this projection, an erosional shoreline movement is expected in most parts of the assessed shoreline segment by the year 2050. Although there are some parts where small accretional changes are

projected along the shoreline of the heritage site area, the largest accretion is expected to occur on the east side of the river mouth, as shown in Figure 6.27.



Figure 6.27. The parts of the assessed shoreline that are projected to be eroded and accreted by the year 2050 are based on the rates computed by utilizing the transects with 50-meter spacing.

6.2.1.4 Projected Shoreline for the Year 2100

The shoreline position that might be observed in 2100 is also projected with the same LRR values utilized for the previous projections. Hence, the limitations resulting

from the computation of LRR values are valid for this process as well. In addition, there is another significant limitation resulting from the number of shoreline observations used for the computation of the LRR values.

The LRR values are computed by the DSAS using the shoreline position of each year between 2016 and 2024. However, the projected shoreline is supposed to be an outcome of a process taking 76 years, during which significant changes in climate are expected. However, these changes in the climate cannot be reflected in the rates used for the projection because, unlike the Shoreline S Model, there is no input space to define the impact of climate change in DSAS.

The process of obtaining the shoreline of 2100 is the same as the one followed for the projection of the 2050 shoreline. The distance at each transect line is computed by using the LRR values and the existing shoreline is moved over those. Therefore, the limitation resulting from the structures existing on the land is valid for this projection, as well.

In other words, the projection of the 2100 shoreline should be considered as an insight into the expected trend based on the recently observed behavior of the shoreline, rather than a numerically likely projection.

The projected shoreline by using the LRR values is shown in Figure 6.28. It can be seen clearly that when the trend observed between 2016 and 2024 continues, and when the changes in climate are neglected, in most parts of the assessed shoreline, a complete loss of the beach area is projected.

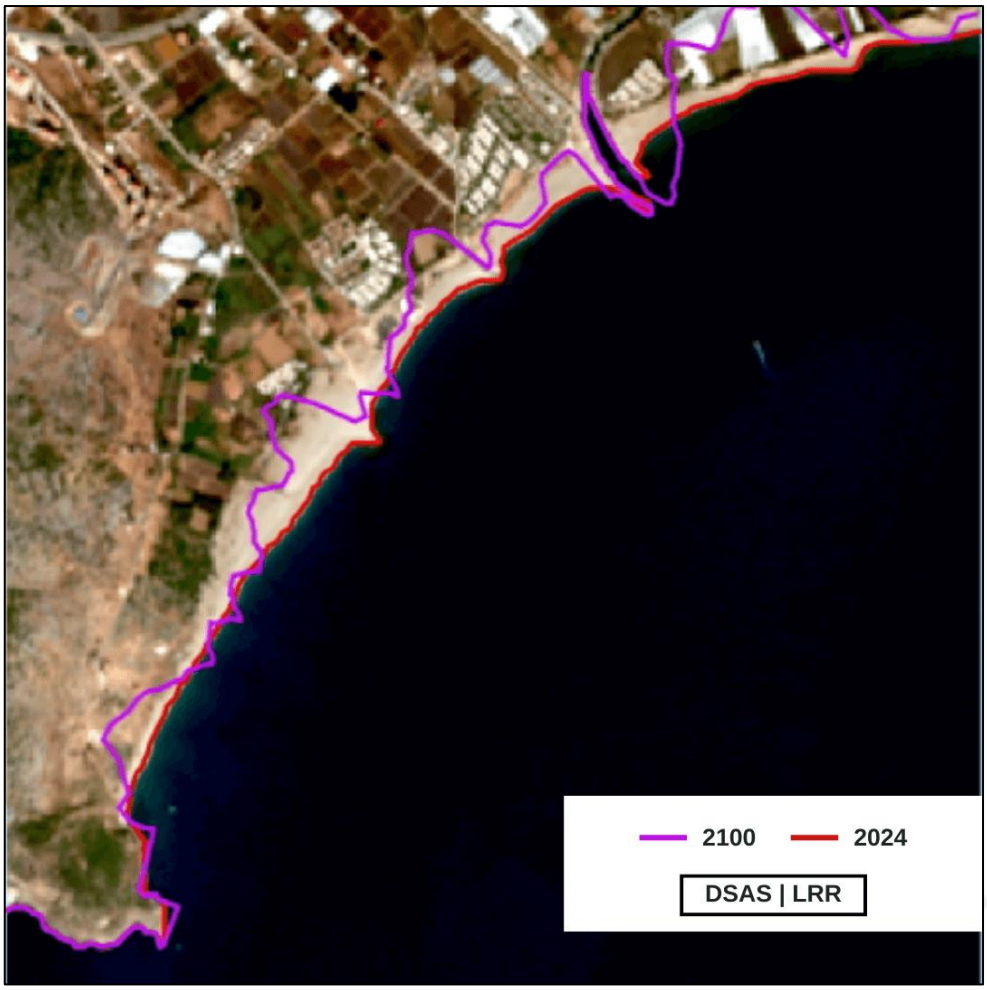


Figure 6.28. The projected 2100 shoreline (purple) and the shoreline observed in September 2024 (red) along the Anemurium Ancient City, obtained from the transects with equal spacings of 50 m.

As stated above, when the urbanized area and dunes on the land and beach area are neglected, there are large areas where shoreline retreat is projected, as presented in Figure 6.29. Also, there are some parts of the shoreline segment at which considerable accretional change is projected for 2100, which are not visible in the projection of the shoreline of 2050.



Figure 6.29. The parts of the assessed shoreline that are projected to be eroded and accreted by the year 2100 are based on the rates computed by utilizing the transects with 50-meter spacing.

Overall, the observed movement and the projected change based on the existing trend of the shoreline are presented in Figure 6.30, where the observed shorelines in 2016 and 2024, and the one projected for the year 2050 by using the LRR values are shown together.

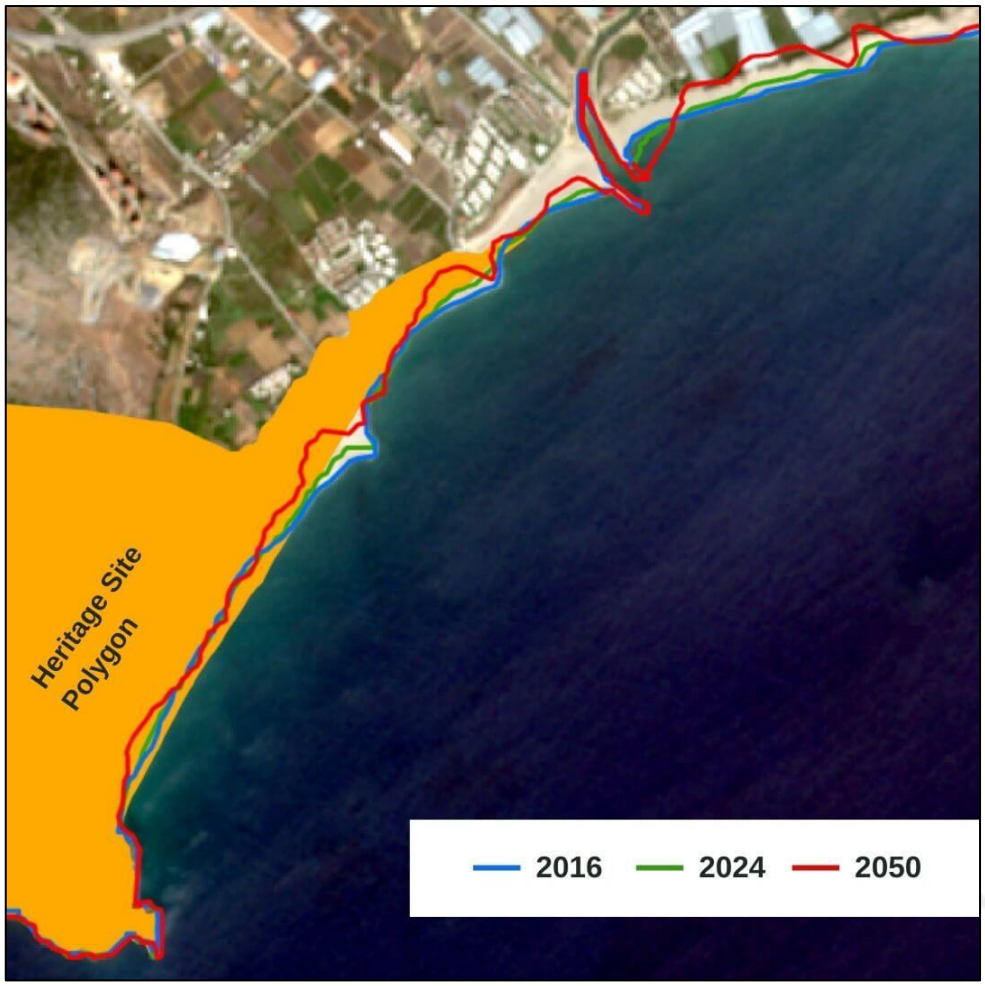


Figure 6.30. The shorelines observed in 2016 and 2024, and the projected one for the year 2050 by using the transects with 50-meter spacings.

6.2.2 Soli-Pompeiopolis Ancient City

Once a significant port city, Soli-Pompeiopolis is now one of the major archaeological heritage sites of Türkiye. However, it is also under a serious threat resulting from the climate change-induced sea level rise. Based on the results obtained from the CCHVAM, the Soli-Pompeiopolis Ancient City has a high vulnerability. The indicator values utilized in the exposure, sensitivity, and adaptive

capacity modules of the CCHVAM are given in Table 6.25, Table 6.26, and Table 6.27, respectively.

Table 6.26. The coastal vulnerability indices obtained from the FCVAM and utilized as the exposure component of the CCHVAM.

Exposure Component Value		Exposure Class
CVI (SSP2-4.5)	2.82	Moderate Exp.
CVI (SSP5-8.5)	3.01	Moderate Exp.
Coastal Erosion (SSP2-4.5)	2.88	Moderate Exp.
Coastal Erosion (SSP5-8.5)	2.96	Moderate Exp.

The CVI value indicates that the coastline segment directly interacting with the site has moderate vulnerability to sea level rise and its impacts as computed from the modified version of the FCVAM (Ince, 2024). When the coastal erosion impact scores are also checked, it is seen that the vulnerability of the coastline segment to surge and inundation is similar to its vulnerability to coastal erosion, because the impact score and the CVI value obtained by the aggregation of the three impact scores are not so different.

Table 6.27. The indicator values assessed to obtain the sensitivity component of the CCHVAM.

Sensitivity		
Indicator		**Indicator Sensitivity Class**
Elevation (%)	70.6	High Sensitivity
Area (%)	20.1	Low Sensitivity
Proximity (m)	0	Very High Sensitivity
Interaction (m)	3304.8	Moderate Sensitivity

Table 6.26 (continued) The indicator values assessed to obtain the sensitivity component of the CCHVAM.

Sensitivity Value	Sensitivity Class
4.18	High Sensitivity

These indicator values describe a site located along a long coastline segment, but it is not as long as the one along which Anemurium Ancient City is located. The heritage area of Soli-Pompeiopolis starts directly from the coastline as well, and it covers a large area in the landward direction. However, unlike Anemurium, it lies on land where the slope is not as steep as the one in Anamur. Comparing this description based on the indicator values and the site photos provided in the figures given in Section 4.2.2, it can be said that the sensitivity module of the CCHVAM provided accurate results for the Soli-Pompeiopolis Ancient City.

Table 6.28. The indicator values assessed to obtain the adaptive capacity component of the CCHVAM.

Adaptive Capacity		
Indicator		**Adaptive Capacity Value**
Degree of Protection	1	High Adaptive Capacity
Urbanization (%)	44.6	Moderate Adaptive Capacity

The site has moderate adaptive capacity because the level of urbanization is higher in the surrounding area than it is in the surrounding area of Anemurium, although it has the highest level of protection provided by Law 2863. It is consistent with reality, considering that the Soli-Pompeiopolis is much closer to the city center than Anemurium is.

As described in Chapter 4, the potential impact and vulnerability classes are determined by the CCHVAM by using separate decision matrices. It is found that, resulting from component classes, the CCHVAM determines that the Soli-Pompeiopolis Ancient City has a high vulnerability to sea level rise and its impacts, as summarized in Table 6.28.

Table 6.29. Values obtained from the CCHVAM for each vulnerability component and the final vulnerability value of Soli-Pompeiopolis Ancient City.

Exposure	*Moderate*
Sensitivity	*High*
Potential Impact	High
Adaptive Capacity	Moderate
Vulnerability	**High**

6.2.2.1 Results Obtained From the DSAS

Similar to the process followed for the analysis of the shoreline segment interacting with the Anemurium Ancient City, two layers of transect lines with spacing values of 50 m and 100 m are utilized in the shoreline evolution analysis of the coastline segment directly interacting with the Soli-Pompeiopolis Ancient City.

The shoreline change envelope is the longest distance between the shorelines observed in each year between 2016 and 2024 along a transect line as defined in the previous part. Based on the statistics of the SCE values obtained at all the transects, which are provided in Table 6.29, it is determined that between 2016 and 2024, an average change in shoreline position of 18.8 m is observed.

Table 6.30. Shoreline change envelope values obtained from both transects with 50 m spacing and transects with a spacing of 100 m.

	Results for Transects with a Spacing of 50 m	**Results for Transects with a Spacing of 100 m**
Number of Transects	74	37
Average Change	18.80 m	18.80 m
Maximum Change	39.80 m, at Transect-1	39.80 m, at Transect-1
Minimum Change	5.39 m, at Transect-33	9.04 m, at Transect-23

On the other hand, net shoreline movement (NSM) provides very summarized information about the shoreline movement because it is the distance between the intersections of the earliest and latest shoreline with a transect line. The NSM is measured at each transect line by the DSAS, and the statistical values shown in Table 6.30 are provided in the summary report file.

The measured NSM values show that a significant erosional trend is observed along the analyzed shoreline segment, as the average NSM value obtained from both transect layers is -8.50 m. On the other hand, it is seen that there are transect lines at which an accretional shoreline movement is observed. However, the average of the accretional NSM values is 3.03 m and 4.11 m, where the average of the erosional NSM values is 9.47 m and 9.23 m, obtained from the transect layers with 50 m spacing and 100 m spacing, respectively. Additionally, the shoreline positions observed in 2016 and 2024 are presented in Figure 6.31.

Table 6.31. Net shoreline movement values obtained from both transects with 50 m spacing and transects with a spacing of 100 m.

	Results for Transects with 50 m Spacing	**Results for Transects with 100 m Spacing**
Average movement (m)	- 8.46	- 8.51
Percentage of all transects having an erosional movement	91.89%	94.59%
The largest erosional movement (m)	-33.40, at Transect-22	-33.40, at Transect-11
Average of all erosional movements (m)	-9.47	-9.23
Percentage of all transects having an accretional movement	8.11%	5.41%
The largest accretional movement (m)	4.40, at Transect-34	4.40, at Transect-17
Average of all accretional movements (m)	3.03	4.11



Figure 6.31. The shoreline positions observed in 2016 and 2024.

When the rate of shoreline movement is computed by using only the distance between shorelines observed in 2016 and 2024, which is called the endpoint rate (EPR), it is found that at more than 90% of the transects, there is an erosional trend. Also, it is noticed that utilizing a finer transect layer allows more accretional areas to be detected. However, no major differences are observed in the extreme values obtained from the two transect layers, as given in Table 6.31.

Based on the total distance measured at each transect between the shorelines observed in only 2016 and 2024, the average erosional rate is approximately 1.15 m/yr, the average accretional rate is approximately 0.45 m/yr, and the overall rate is computed as -1.05 m/yr.

Table 6.32. Statistical values of the endpoint rate at each transect obtained from both the transects with a spacing of 50 meters and the transects with a spacing of 100 meters.

	Results for Transects with 50 m Spacing	**Results for Transects with 100 m Spacing**
Average rate	-1.05	-1.06
Percentage of all transects at which erosion is observed	91.89%	94.59%
Percentage of all transects with statistically significant erosion	18.92%	21.62%
Maximum erosional rate	-4.16, at Transect-22	-4.16, at Transect-11
Average erosional rate	-1.18	-1.15
Percentage of all transects at which accretion is observed	8.11%	5.41%
Percentage of all transects with statistically significant accretion	0%	0%
Maximum accretional rate	0.55, at Transect-34	0.55, at Transect-17

Table 6.31 (continued) Statistical values of the endpoint rate at each transect obtained from both the transects with a spacing of 50 meters and the transects with a spacing of 100 meters.

Average accretional rate	0.38	0.51

While the NSM and EPR values are obtained from the shoreline data of the years 2016 and 2024 only, the linear regression rate (LRR) is obtained from the shoreline data of each year over this period.

When the LRR values are compared to the EPR values, it is seen that the values of both the accretional and the erosional rates are larger when the shoreline movements between all the consecutive years are considered.

The average shoreline movement rate obtained from linear regression across the analyzed coastline segment is approximately -1.25 m/yr, as can be seen in Table 6.32.

Table 6.33. Statistical values of the linear regression rate at each transect obtained from both the transects with a spacing of 50 meters and the transects with a spacing of 100 meters.

	Results Obtained From Transects with 50 m Spacing	**Results Obtained From Transects with 100 m Spacing**
Average rate (m/yr)	-1.27	-1.25
Percentage of all transects at which erosion is observed	90.54%	91.89%

Table 6.32 (continued) Statistical values of the linear regression rate at each transect obtained from both the transects with a spacing of 50 meters and the transects with a spacing of 100 meters.

Maximum erosional rate (m/yr)	-4.25 at Transect-22	-4.25 at Transect-11
Average of all erosional rates (m/yr)	-1.44	-1.39
Percentage of all transects at which accretion is observed	9.46%	8.11%
Maximum accretional rate (m/yr)	0.88 at Transect-34	0.88 at Transect 17
Average of all accretional rates (m/yr)	0.33	0.37

The LRR value obtained at each transect line is assigned to an adjacent shoreline segment. It can be seen that in the harbor area, the rate of shoreline movement is between -2.0 and -1.0 m/year, as shown in Figure 6.32.

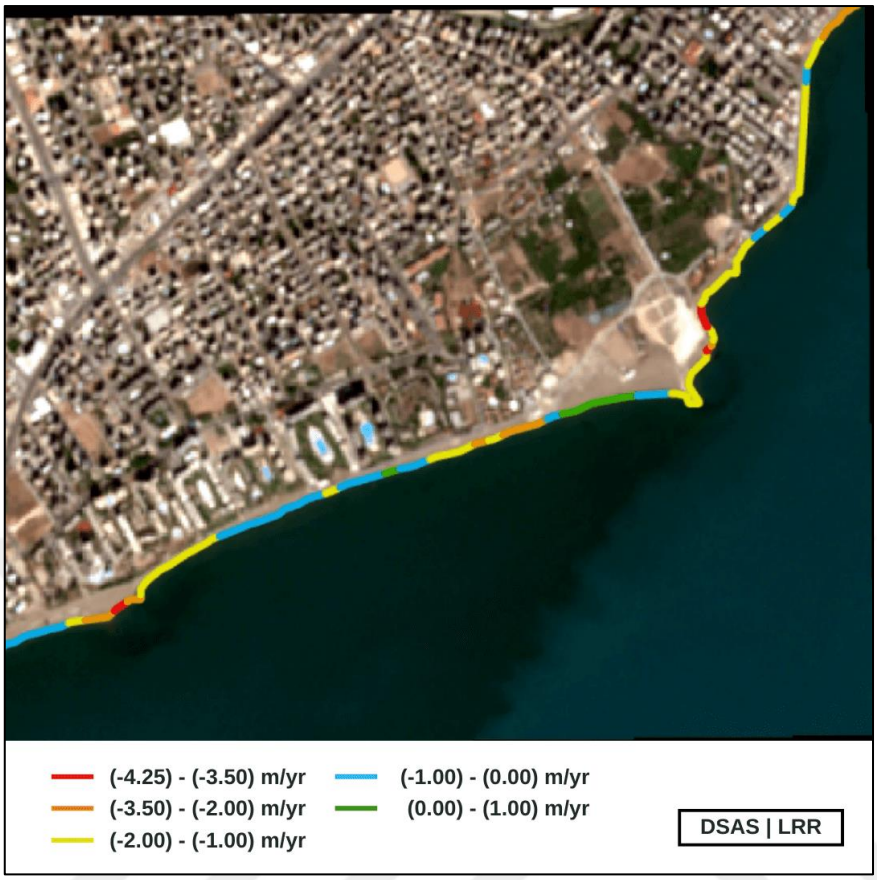


Figure 6.32. The linear regression rate of shoreline movement observed between the years 2016 and 2024, obtained from the transects with equal spacings of 50 m.

6.2.2.2 Projection of the Shoreline Movement Between 2016 and2024 by Using the LRR Values

The accuracy of the LRR values computed by the DSAS is controlled by projecting the shoreline observed in 2024. The projection is made by multiplying the LRR value obtained at each transect line by eight and moving the shoreline observed in 2016 over the distance computed by this multiplication. Then, the actual shoreline captured in September 2024 and the projected shoreline are compared by using the net shoreline movement values, taking the shoreline observed in 2016 as a reference. The shoreline observed in 2024 and the projected one are shown in Figure 6.33.



Figure 6.33. The shoreline position observed in 2024 and the projected one using the LRR values computed at transects with 50 m of spacing.

The comparison of the NSM values of the actual and projected shorelines is shown in the graph presented in Figure 6.34. It is clearly seen that both the erosional and the accretional movements computed by using LRR are larger than the ones actually observed. Also, it is interesting that both extremes are observed at the transects located over the heritage site area. Noting that the transects are numbered starting from east to west, the erosional movements determined by using the LRR values on the east side of the analyzed shoreline segment are larger than those observed at the same transects. However, on the west side, the exact opposite case is observed.

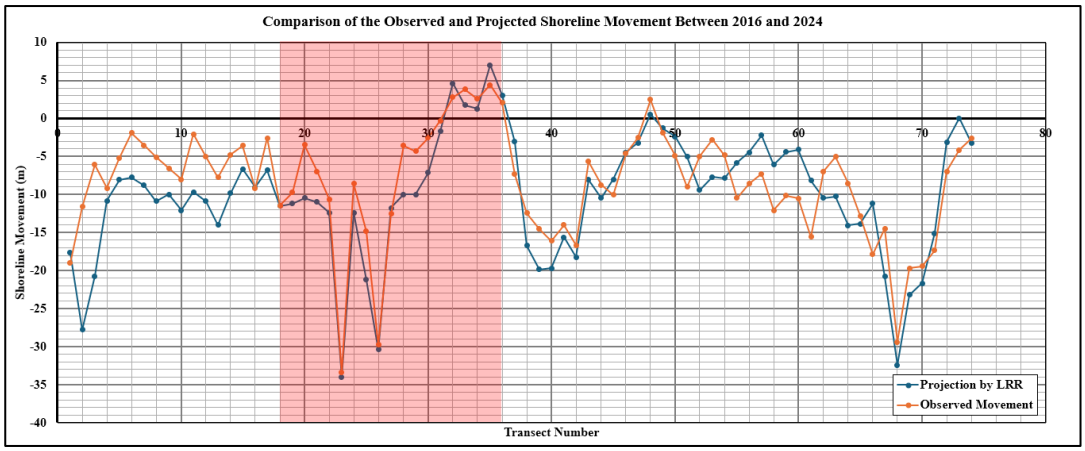


Figure 6.34. Comparison of the net shoreline movement measured and the net shoreline movement between the projected 2024 shoreline and the 2016 shoreline, where the transects overlaying the heritage site area are highlighted as the red area.

The average shoreline movement observed between 2016 and 2024 is -8.45 m, whereas the average movement projected by the LRR values is -10.19 m. Also, it is found that the average distance between the observed and the projected shorelines is 1.7 m. However, the average distance between these shorelines over the heritage site area is 2.15 m. The distance between the observed and the projected shoreline at each transect line can be seen in Figure 6.35.

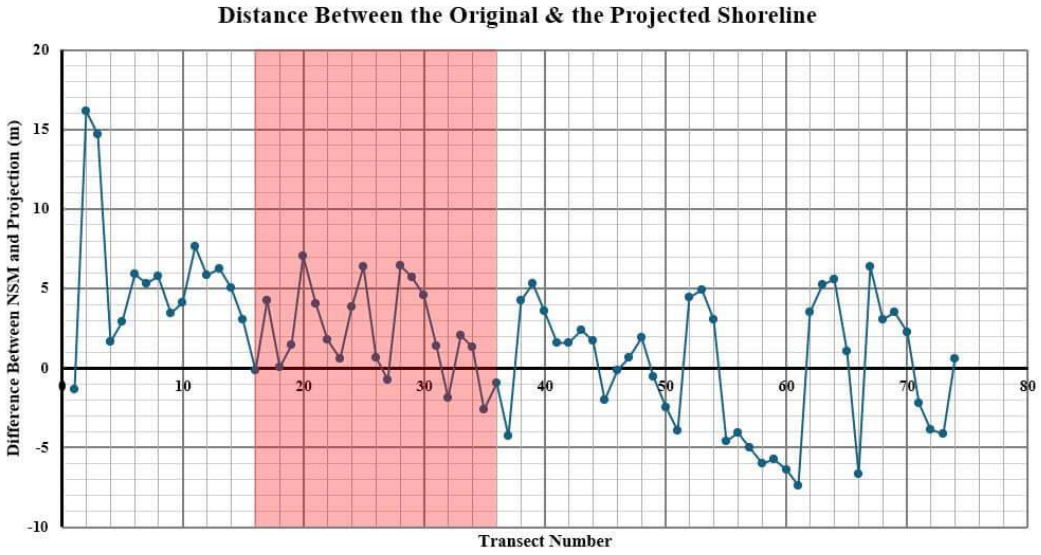


Figure 6.35. The distance between the original shoreline and the projected shoreline for the year 2024 is calculated at each transect. The heritage site area along the analyzed shoreline is highlighted with the red rectangle.

It is observed that the deviations between the projected shorelines by using the transect layers with the spacing values of 50 m and 100 m result from the fact that the finer layer detects movement at the points that the lines of the other transect layer do not pass, as shown in Figure 6.36. Hence, the comparison of the projected shoreline by using the LRR values of the transects with a spacing of 100 m and the actual shoreline observed in 2024 is not given here, but provided in Appendix D. Additionally, the comparison of the projected and actual shorelines on the satellite image is given in Appendix D, as well.

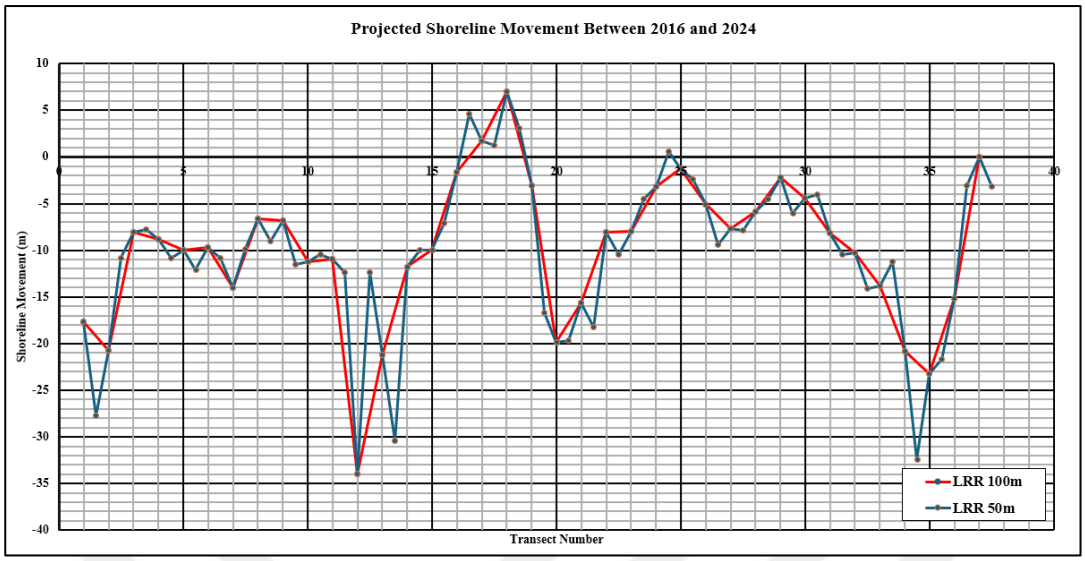


Figure 6.36. Comparison of the projected shoreline movement between 2016 and 2024 by using the LRR values of the transects with spacing values of 50 m and 100 m.

Furthermore, the error in the projection made by using the LRR values is investigated by following the same process described in the previous part. A scatter plot is obtained showing the actual values of shoreline movement on the horizontal axis and the projected movement on the vertical axis, as presented in Figure 6.37. The R-square value is obtained as 0.705 from the generated plot. Also, the average difference between the actual and the projected movement is determined as 1.7 m, whereas the mean absolute error is computed as 3.8 m.

The deviation is greater in the area where the heritage site is located along the shoreline, which can also be seen in the above figures, especially around the ancient breakwater. On the other hand, it is found that the percentage of transects where the difference is less than one meter is only 13.5%.

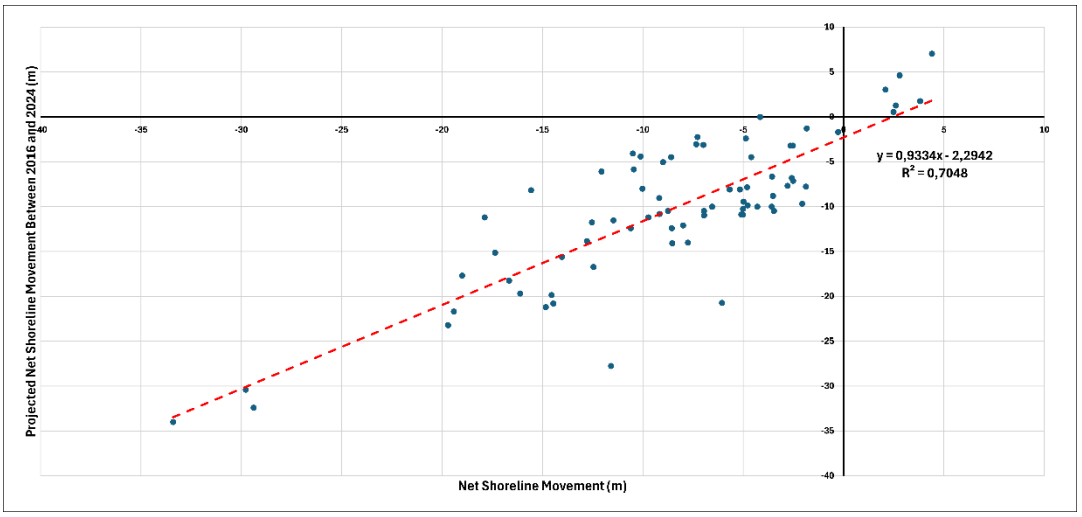


Figure 6.37. Comparison of the actual and projected shoreline movements between the years 2016 and 2024.

6.2.2.3 Projected Shoreline for the Year 2050

The process described above in the projection of the shoreline movement between 2016 and 2024 is utilized to project the 2050 shoreline, as well. The process is repeated for both transect layers with the spacing values of 50 m and 100 m. The projected shoreline using the transects with equal spacings of 50 m is presented in Figure 6.38.

The limitations of the projection process explained in the previous section are valid for this part, as well. In most parts of the assessed coastline, there are structures including vertical walls and residential buildings. However, while moving the shoreline to generate over the distances calculated by the rates, these structures are neglected. The shoreline is moved as if it were completely a beach without any built structure which would limit the shoreline movement and act like a barrier. It is seen that the rate of erosion is already higher in some parts of the shoreline where there are no buildings than it is in the parts where there are buildings.



Figure 6.38. The projected 2050 shoreline (blue) and the shoreline observed in 2024 (red) along the Soli-Pompeiopolis Ancient City, obtained from the transects with equal spacings of 50 m.

The average shoreline movement between 2024 and 2050 is -33.1 m based on the projection made using the LRR values.

The only part of the analyzed shoreline segment where major accretion is projected is on the west side of the breakwater. This can be explained by the impact of the breakwater on the wave action over this shoreline segment. Furthermore, the fact that along the rest of the shoreline erosional behavior is projected implies that the area is subjected to a significant threat. The areas projected to erode can be seen clearly in Figure 6.39.



Figure 6.39. The parts of the assessed shoreline that are projected to be eroded and accreted by the year 2050 are based on the rates computed by utilizing the transects with 50-meter spacing.

The projection is repeated with the other transect layer with a spacing value of 100 m. It is found that there is only a small difference between the projections made by using the two transect layers, as can be seen in Figure 6.40. The average shoreline movement is -33.1 m when the transects with a spacing of 50 m are used, whereas the average value becomes -32.5 m when the coarse transect layer is used for the analysis.

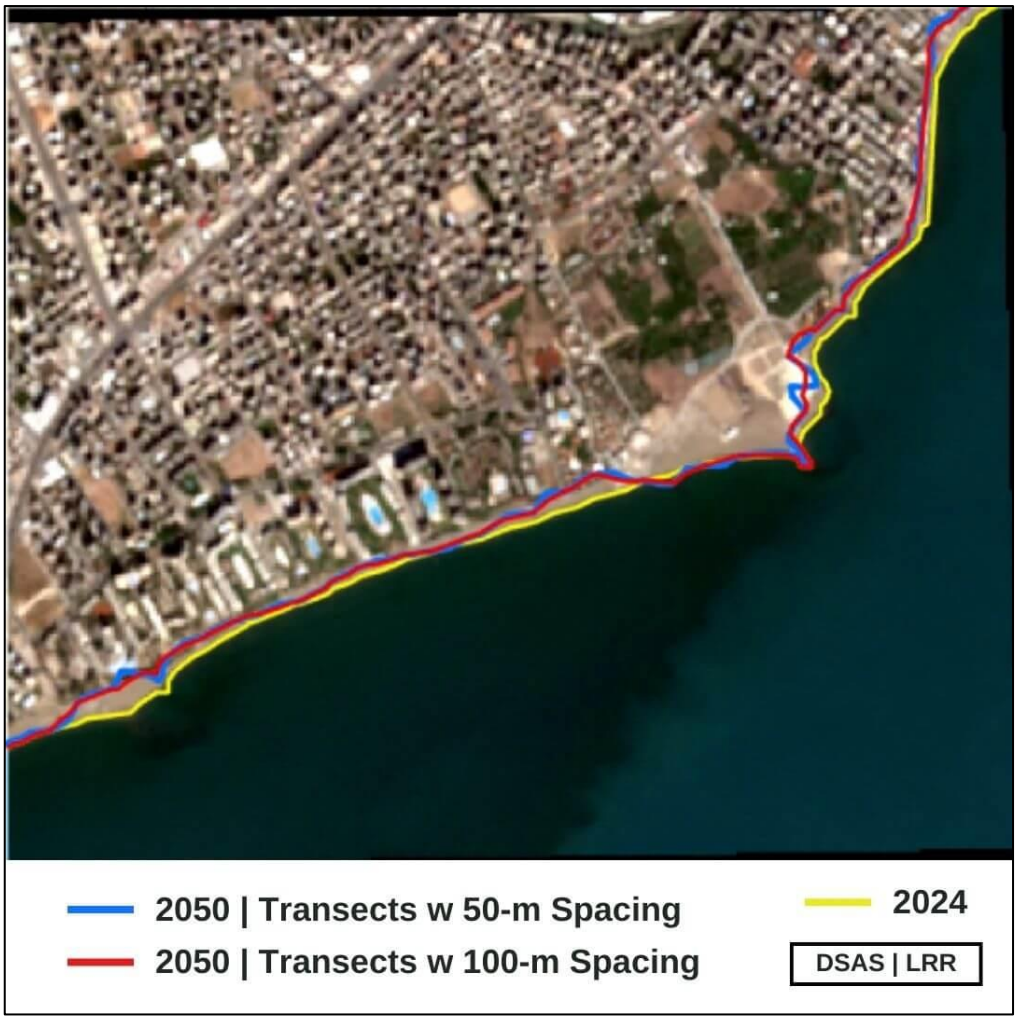


Figure 6.40. The shorelines projected for the year 2050 by using the LRR values at the transects with the spacing values of 50 m (blue) and 100 m (red).

On the other hand, the projection is repeated by using the EPR values, which is the rate of shoreline movement computed from the distance between the shorelines observed in 2016 and 2024 only. It can be seen in Figure 6.41 that on the east side of the breakwater, LRR values project larger erosional movements than the EPR values do, however, in the other part of the assessed shoreline segment, there are some parts where the EPR values project larger erosional and accretional movements than the LRR values do.

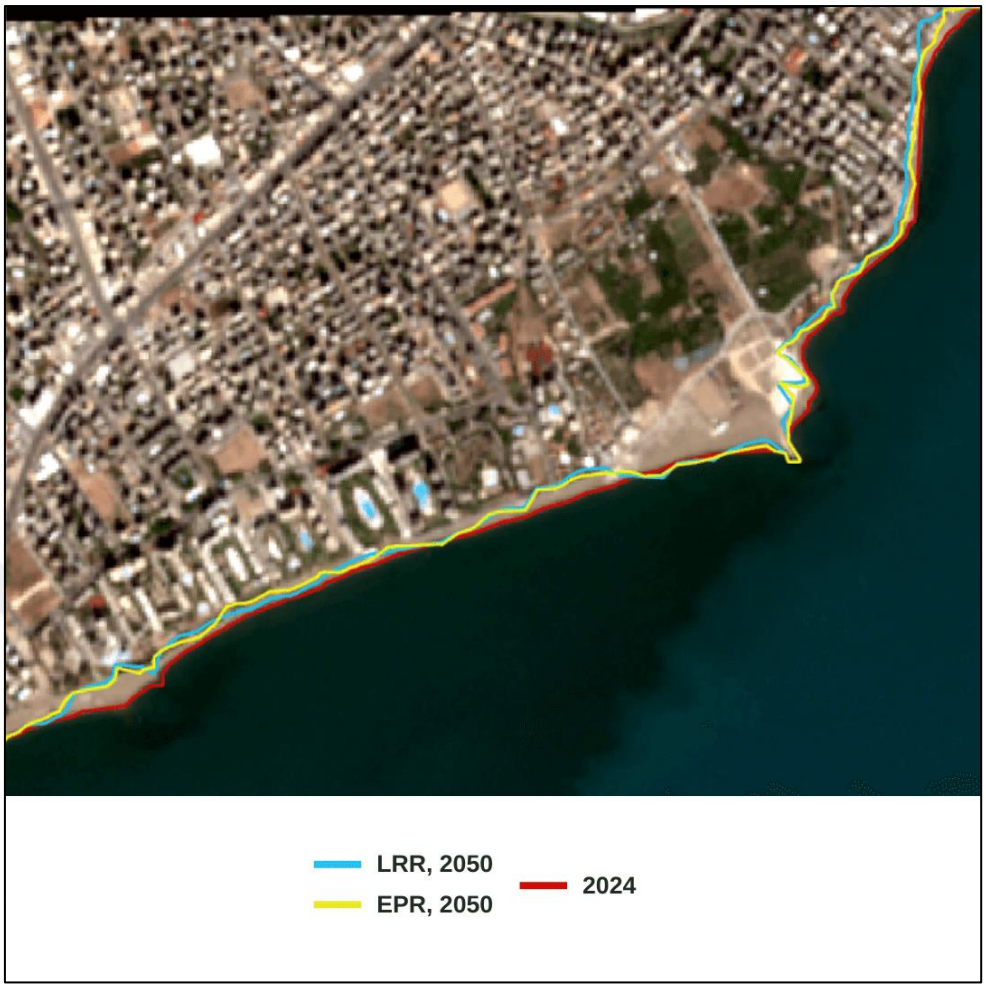


Figure 6.41. Projected shorelines for the year 2050 by utilizing the LRR and the EPR are compared with each other and the shoreline observed in 2024.

The NSM between 2024 and 2050 calculated for the projected shorelines by using the LRR and the EPR values at each transect is checked, and it is found that the average NSM obtained from the LRR values is -33.1 m, whereas the average NSM resulting from the EPR values is -27.4 m. Similarly, the average value of NSM measured at the transects located across the heritage site area is -29.9 m in the shoreline projected from LRR values, and it is -22.9 m in the shoreline projected from EPR values.

6.2.2.4 Projected Shoreline for the Year 2100

The shoreline of 2100 is projected by following the same process: multiplying the number of years between 2024 and 2100 by the LRR values obtained at the transects and moving the intersection points of the transects and the 2024 shoreline to the NSM values obtained by this multiplication. When the line is moved to the projected distance, the residential buildings and the vertical walls are neglected during this projection process, as well.

The shoreline is projected to move over the beach area in front of the residential buildings by 2050, however, it is found that this erosional behavior of the assessed coastline results in a complete loss of the beach in front of the residential buildings and a major loss of land in the beach of Soli-Pompeiopolis Ancient City by 2100. The described retreat of the shoreline is shown in Figure 6.42.

The distance between the shoreline observed in 2024 and the projected 2100 shoreline is checked, and it is found that the average NSM value is -96.8 m. Additionally, this average distance is found to be -87.4 m over the shoreline segment at the heritage site area.



Figure 6.42. The projected 2100 shoreline (blue) and the shoreline observed in 2024 (red) along the Soli-Pompeiopolis Ancient City, obtained from the transects with equal spacings of 50 m.

The parts of the shoreline where significant amounts of erosion and accretion are projected as presented in Figure 6.43. By looking at the projected shoreline movement, it can be said that if there were no buildings in this area, a huge amount of land would have been lost due to shoreline retreat, where the only part of the shoreline that accretion is projected is the east side of the ancient breakwater.



Figure 6.43. The parts of the assessed shoreline that are projected to be eroded and accreted by the year 2100 are based on the rates computed by utilizing the transects with 50-meter spacing.

It should be noted that all the figures showing the projected shorelines and the graphs are generated by using the data obtained from the transects with a spacing of 100 m, as well, and they are provided in Appendix D.

Overall, it can be said that the urbanized area in front of the heritage site area and the vertical wall on the east of the breakwater provide significant protection, considering the projected erosion is the most critical in that area, as shown in Figure 6.44. Furthermore, it should be noted that the projected changes in the sea level for the future resulting from climate change in various scenarios are not considered in this

assessment. However, those have a great possibility to make the projected erosion even more critical. Considering that the archaeologists are still investigating the site, providing significant insights into all the civilizations that have ruled the region throughout centuries, it is important to make additional assessments to see the possible impacts of climate change over the region and take immediate action to provide protection.

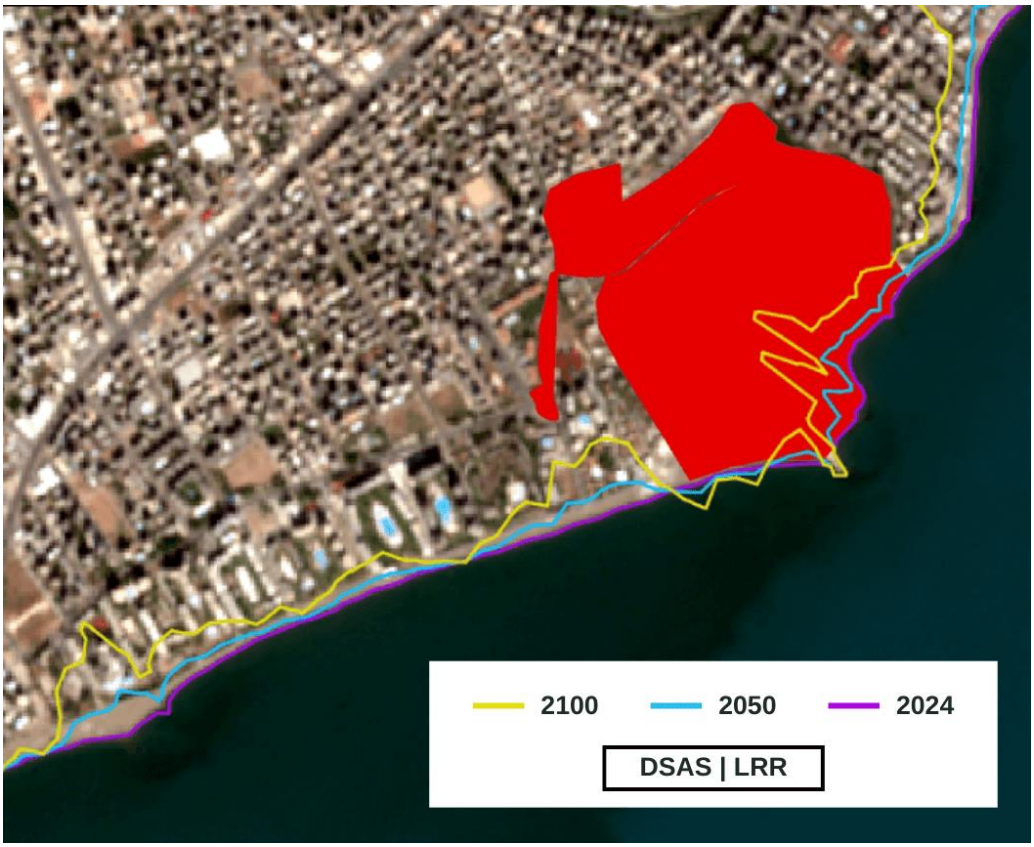


Figure 6.44. Comparison of projected shorelines for the years 2100 and 2050 to the shoreline recorded in 2024 along the assessed shoreline and over the heritage site (red).

6.3 Shoreline Evolution Modeling with the Shoreline Simulation (ShorelineS) Model

ShorelineS Model simulates the coastline evolution over long periods of time, such as years and decades, utilizing a set of MATLAB functions and data on the coastline, coastal structures, wave conditions, and other physical parameters affecting the coastline evolution. In the scope of this study, the expected change by 2050 in the shoreline that directly interacts with the Anemurium Ancient City is modeled by using the ShorelineS Model.

In this modeling process, the CERC formula (USACE, 1984) is utilized for longshore sediment transport. In addition to the wave parameters, the formula consists of a calibration factor (b). Hence, before simulating the coastline evolution by 2050, the value of the calibration factor is determined by making test runs. As explained in Section 5.2, in these test runs, the wave time-series data consisting of the observed wave conditions between January 1, 2016, and November 11, 2024, is utilized, and the calibration factor resulting in the generation of a shoreline which has the minimum deviation from the shoreline observed on September 29, 2024, is determined as 4.5e4. The assumptions made in this modeling process are explained in Section 5.1 in detail.

In the scope of this study, three separate simulations are performed as described below.

- Generation of the shoreline that might be observed in 2050 by using the existing wave conditions only
- Generation of the shoreline that might be observed in 2050 by considering the rate of sea level rise (RSLR) based on the SSP5-8.5 scenario in addition to the existing wave conditions
- Generation of the shoreline that might be observed in 2050 by considering the observed rate of change in wave height in the last 50 years in addition to the RSLR and the existing wave conditions

6.3.1 Projected Shoreline for the Year 2050

The shoreline evolution by 2050 is simulated by using the calibrated longshore sediment transport formula and the wave climate data described in Section 5.1.3. During this simulation, no additional climate change input is introduced to the model. Hence, the shoreline presented in Figure 6.45 is obtained by the wave conditions observed in the last 50 years only.

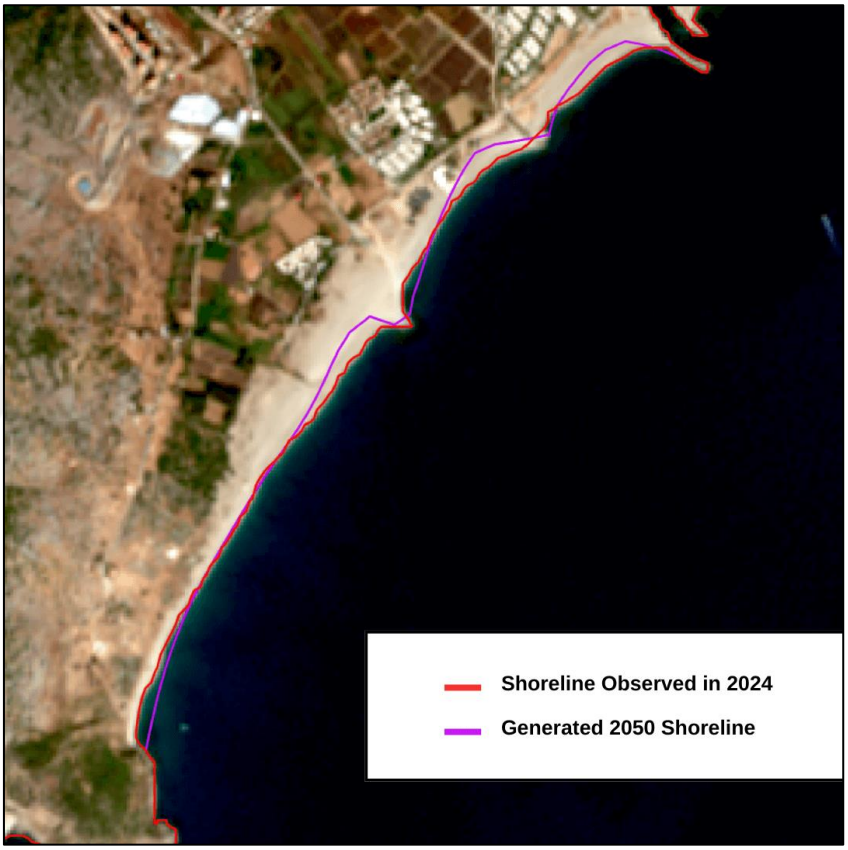


Figure 6.45. Shoreline resulting from the simulated shoreline evolution by 2050 and the shoreline observed on September 29, 2024 (ArcGIS Pro).

Net shoreline movement (NSM) is computed for the generated shoreline at transects placed with a spacing of 50 m along the assessed shoreline. The NSM is the distance

between the observed and generated shorelines along a transect. Based on this computation, the average NSM is 5.46 m in the landward direction. In total 51 transects are inserted, and it is found that at 54.9% of all transects, coastline retreat is measured. On the other hand, at the transects where accretional change is computed, the average NSM is 16.2 m.

The areas along the shoreline where erosional and accretional changes are projected are presented in Figure 6.46. The areas of these polygons are computed in the ArcGIS Pro, and it is found that the total area where accretional change is projected is 0.017 km^2, and the total area where erosional change is projected is 0.032 km^2.

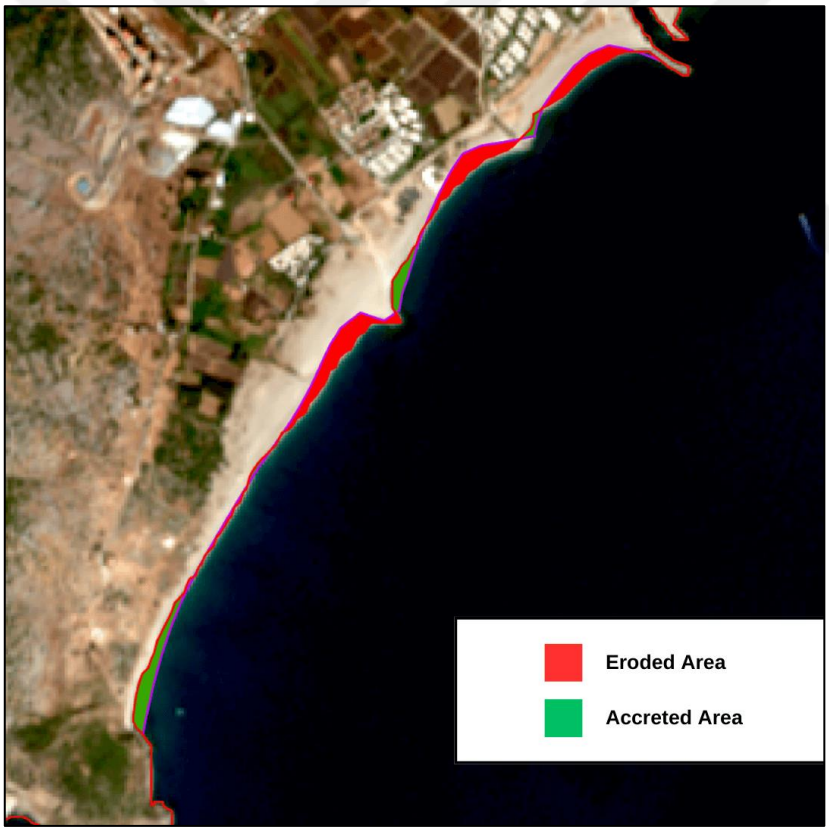


Figure 6.46. Based on the 2050 projection, the areas where the erosional and accretional changes are measured.

6.3.2 Projected Shoreline Evolution by 2050 Considering the Impact of Climate Change

6.3.2.1 Projection Considering the RSLR Only

The ShorelineS Model allows the impacts of climate change to be considered while simulating the shoreline evolution. In the scope of this simulation, the rate of sea level rise (ccSLR) is introduced to the model as an input parameter, in addition to the wave climate data obtained from the ERA5 dataset with a temporal coverage between January 1, 1974, and November 11, 2024.

Net shoreline movement (NSM) is computed for the generated shoreline, presented in Figure 6.47, at transects placed with a spacing of 50 m along the assessed shoreline. The average NSM is computed as 16.10 m in the landward direction. In total 51 transects are inserted, and it is found that at 72.5% of all transects, coastline retreat is measured. On the other hand, at the transects where accretional change is computed, the average NSM is 14.68 m.

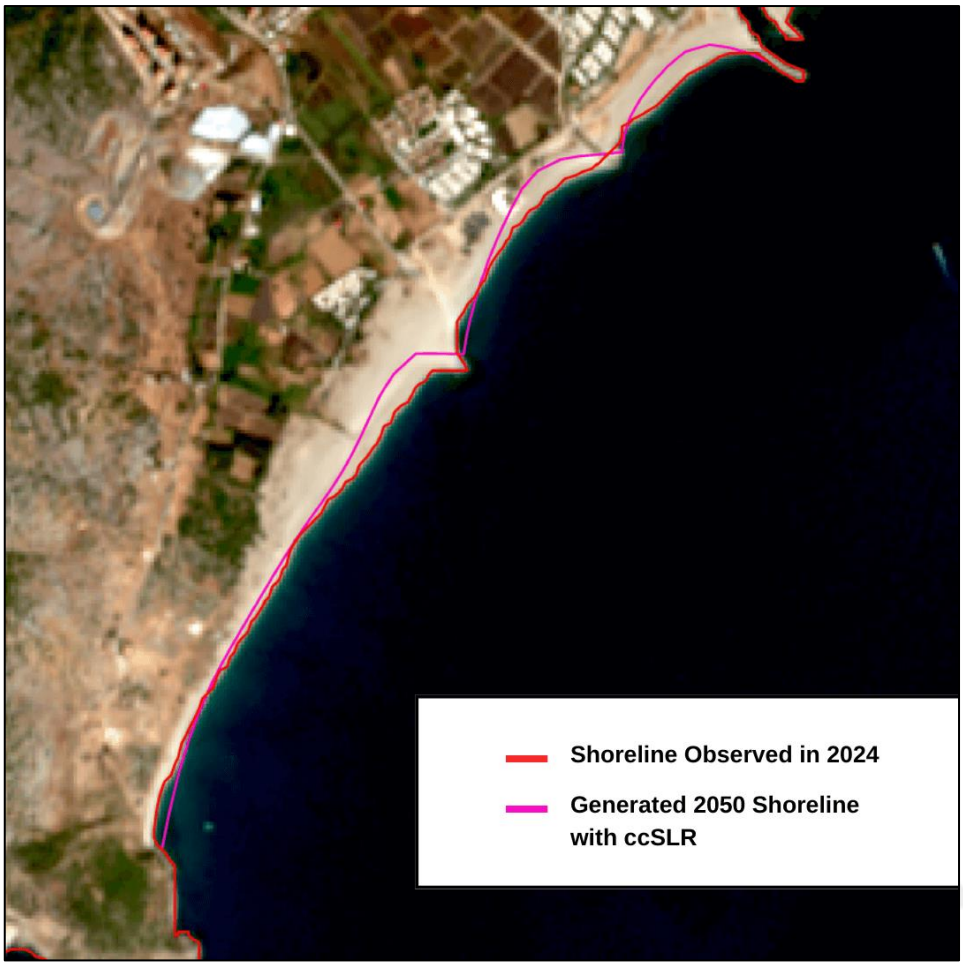


Figure 6.47. Shoreline resulting from the simulated shoreline evolution by 2050 with the RSLR input parameter (ccSLR), and the shoreline observed on September 29, 2024 (ArcGIS Pro).

The areas along the shoreline where erosional and accretional changes are projected are presented in Figure 6.48. The areas of these polygons are computed in the ArcGIS Pro, and it is found that the total area where accretional change is projected is 0.010 km^2, and the total area where erosional change is projected is 0.050 km^2.

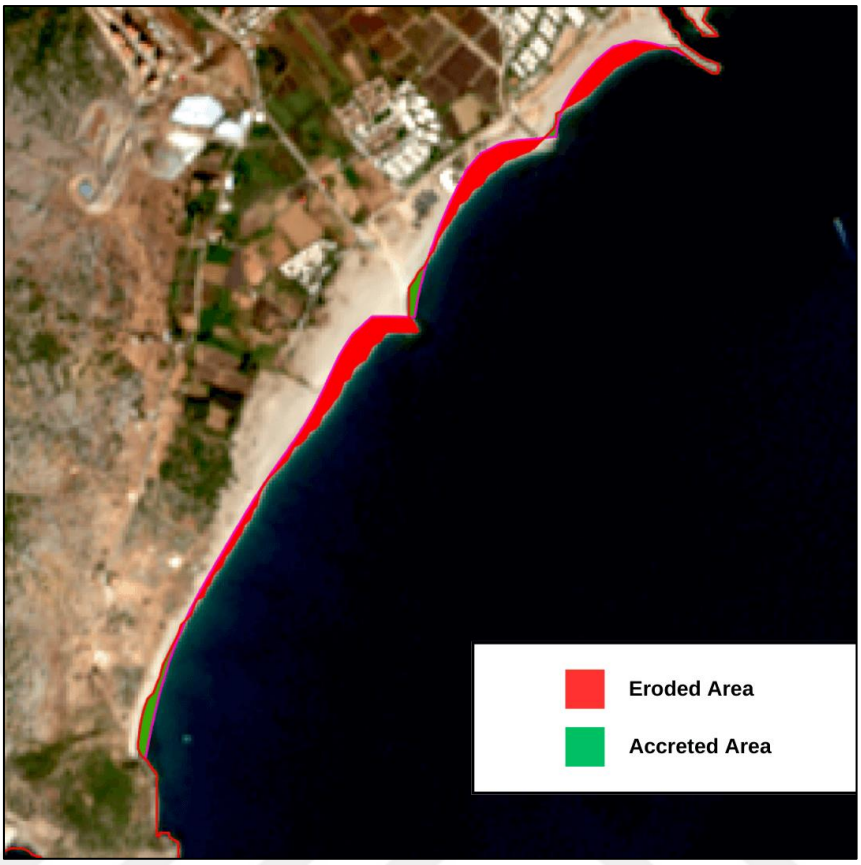


Figure 6.48. Based on the 2050 projection with the RSLR input parameter, the areas where the erosional and accretional changes are measured.

6.3.2.2 Projection Considering the RSLR and the Change in Wave Height

In this simulation, the rate of change in wave height (ccHS) is introduced to the model as an input parameter, in addition to the RSLR and the wave climate data.

The generated shoreline is presented in Figure 6.49, and at the transects placed with a spacing of 50 m along the assessed shoreline, the average NSM is computed as 16.33 m in the landward direction. In total 51 transects are inserted, and it is found that at 72.5% of all transects, coastline retreat is measured. On the other hand, at the transects where accretional change is computed, the average NSM is computed as 13.55 m.

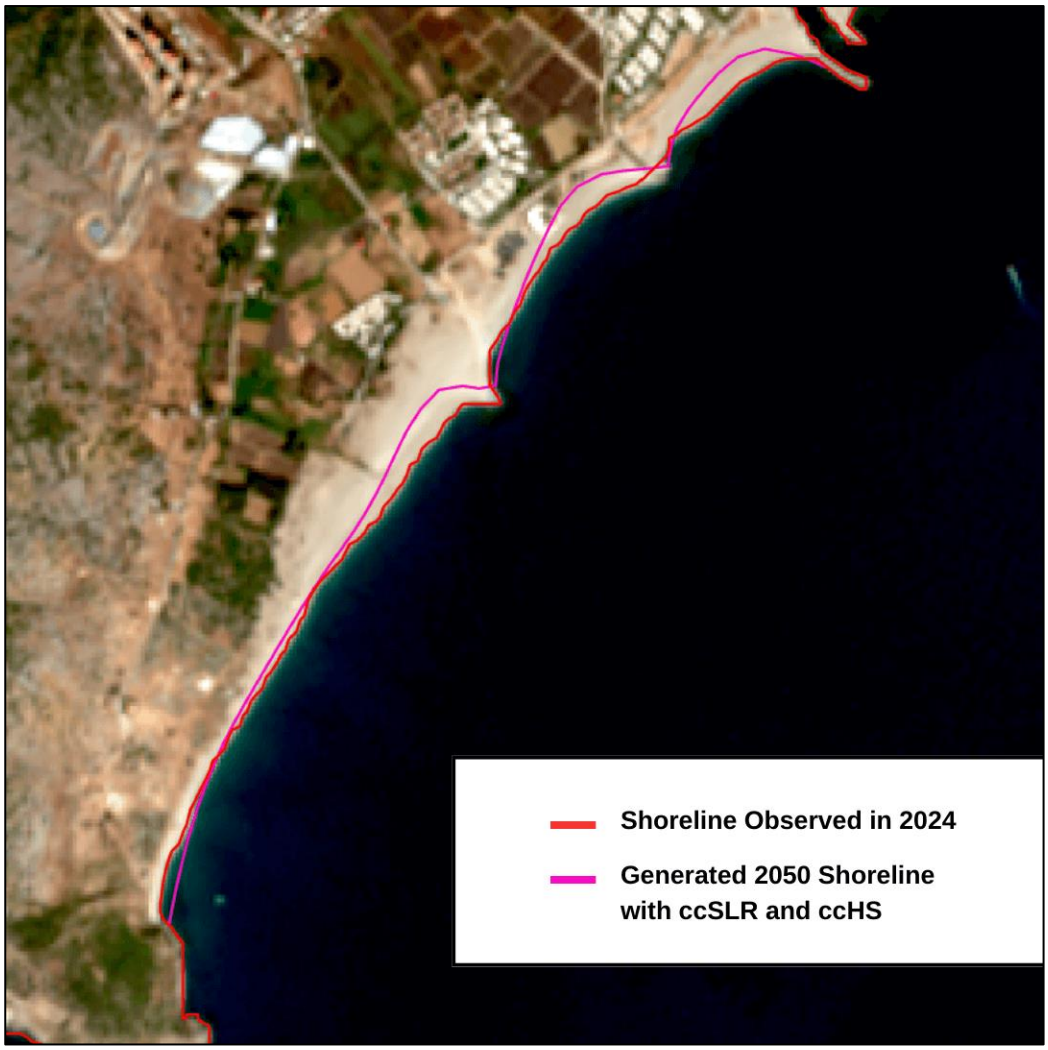


Figure 6.49. Shoreline resulting from the simulated shoreline evolution by 2050 with the RSLR (ccSLR) and rate of change in wave height (ccHS) input parameters, and the shoreline observed on September 29, 2024 (ArcGIS Pro).

The areas along the shoreline, where erosional and accretional changes are projected, are presented in Figure 6.50. The areas of these polygons are computed in the ArcGIS Pro, and it is found that the total area where accretional change is projected is 0.009 km^2, and the total area where erosional change is projected is 0.05 km^2.

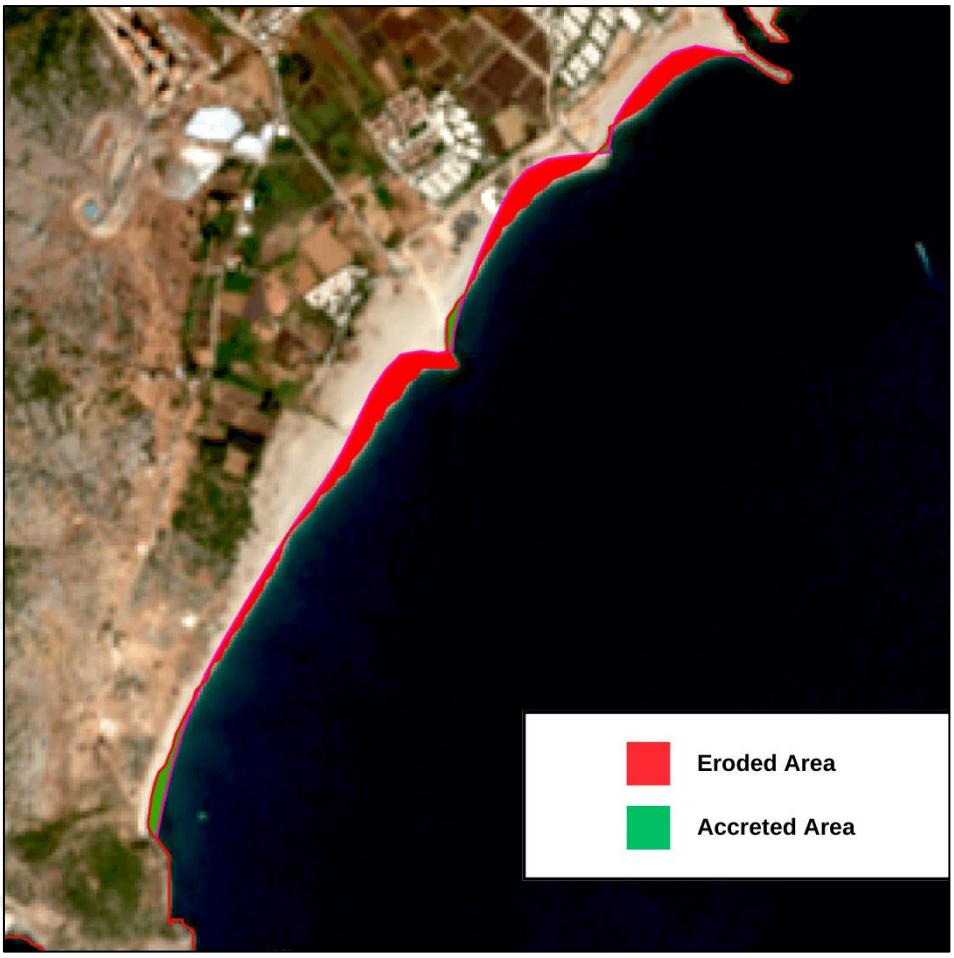


Figure 6.50. Based on the 2050 projection with the RSLR (ccSLR) and rate of change in wave height (ccHS) input parameters, the areas where the erosional and accretional changes are measured.

6.4 Discussions on the 2050 Projections

In the first part of this study, the CCHVAM is applied to assess the vulnerability of the coastal cultural heritage sites of Türkiye, including Anemurium Ancient City, to sea level rise. The assessment is performed twice. In the first one, the overall CVI value is utilized as the exposure component of the model, and in the second assessment, the coastal erosion impact score of each site is utilized as the exposure component.

As stated in Section 6.2.1., the coastline directly interacting with the Anemurium Ancient City has moderate exposure and moderate vulnerability to coastal erosion. In the second part of this study, the coastline evolution of the shoreline is modeled with the DSAS and the ShorelineS Model. In both modeling processes, it is found that the site is under the threat of coastal erosion. However, there are some parts where the two projections show different trends, as presented in Figure 6.51.

The main difference between the two projection processes is their methods. The first projection is done by using the linear regression rates obtained from the DSAS by using only the observed shoreline evolution from 2016 to 2024. The second projection is done by simulating the coastal evolution by using the ShorelineS Model which uses the wave climate data acquired from the wave conditions observed in the last 50 years and the physical parameters of the assessed coastline.

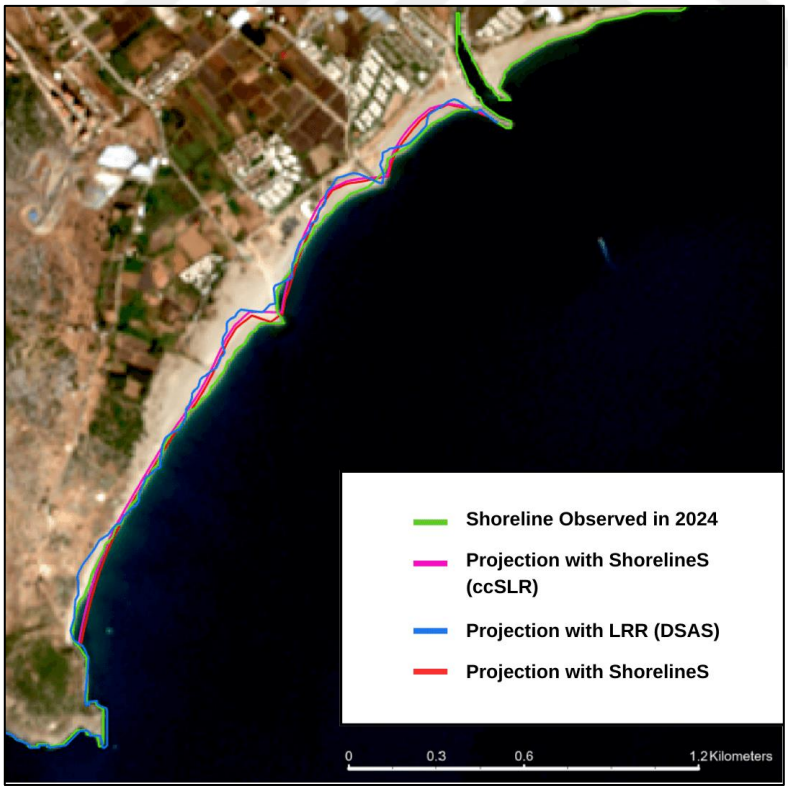


Figure 6.51. The shorelines obtained from the 2050 projections performed by using the results of the DSAS and the simulations performed with the ShorelineS Model.

The simulation with the ShorelineS Model is repeated as explained in the previous section; the first simulation is done by using the wave climate data only, but in the second simulation, the RSLR input is introduced to the model in addition to the wave climate. As provided in Table 6.33, the projected shoreline obtained from the simulation with the RSLR input is similar to the one generated by using the LRR values obtained from the DSAS. Although especially in the southern part of the coastline, the simulation and the projection with the LRR values result in contradicting projections, where the initial one projects an accretional change and the latter projects an erosional change, the average erosional shoreline movement values of both are over 27 m, and the total area projected to be lost to coastal erosion is found almost the same.

Table 6.34. The average net shoreline movement, average erosional and accretional shoreline movement, and the total areas where erosional and accretional changes are projected by the LRR values and the simulations performed with the ShorelineS Model.

	Average NSM	**Avg. Erosion**	**Avg. Accretion**	**Total Erosion**	**Total Accretion**
LRR (DSAS)	-20.4 m	27.9 m	10.4 m	0.059 km^2	0.007 km^2
ShorelineS	-5.5 m	23.2 m	16.2 m	0.032 km^2	0.017 km^2
ShorelineS (RSLR)	-16.1 m	27.7 m	14.7 m	0.050 km^2	0.010 km^2

As presented in the above figure and table, there are differences in numerical values and the shoreline evolution trends at some parts of the assessed shoreline. However, the key finding of these coastline evolution simulations and modeling is that in the part of the assessed shoreline, where there are ancient buildings close to the

shoreline, a significant erosional behavior is observed and projected, which can be seen in Figure 6.52. Hence, it can be said that the result obtained from the CCHVAM is consistent with the findings of the projections.

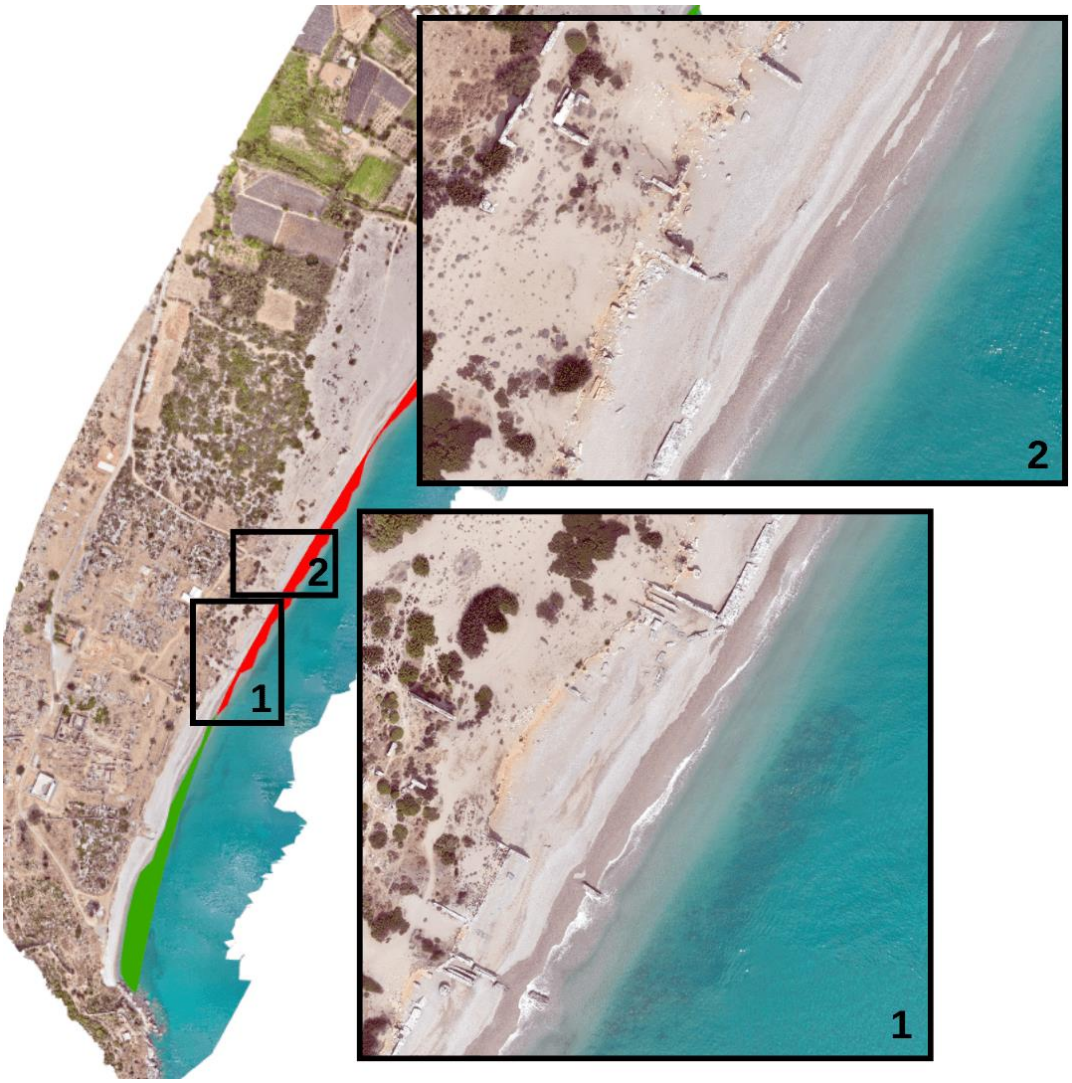


Figure 6.52. The remainings of the Anemurium Ancient City located on the shore where erosional change is projected in the ShorelineS Model simulation with the RSLR input.

CHAPTER 7

CONCLUSION

This study primarily aims to develop a new methodology to assess the vulnerability of coastal cultural heritage sites to sea level rise resulting from climate change. For this purpose, the coastal cultural heritage vulnerability assessment model (CCHVAM) is developed and utilized to assess the vulnerability of the coastal cultural heritage sites of Türkiye. Then, based on the findings of the literature review and to investigate the accuracy of the results obtained from the CCHVAM on coastal erosion, the coastline evolution in two of these sites is modeled: Soli Pompeiopolis and Anemurium ancient cities. Finally, the study concludes with the projection of coastline evolution by 2050 in the Anemurium Ancient City, which contributes to the assessment of the performance of different tools, providing insights into the coastline evolution.

The CCHVAM is developed based on both the findings of the literature review and expert evaluations. The indicators of the exposure, sensitivity, and adaptive capacity components of the CCHVAM are determined. Then, the framework of the model is constructed with decision matrices. Through this framework, the CCHVAM assigns a vulnerability class to each assessed site based on internal and external factors, making the site vulnerable, and the conditions enhancing its resilience. After the model is developed, it is utilized, and the vulnerability of 1176 coastal cultural heritage sites in Türkiye is assessed. They are divided into 5 classes from very high vulnerability to very low vulnerability. The assessment is done four times. In these assessments, two sets of CVI values and coastal erosion impact scores are taken as exposure values; one set is based on the SSP2-4.5 scenario and the other is based on the SSP5-8.5 scenario. It is found that there are 52 sites with very high vulnerability to sea level rise when the CVI values based on the SSP2-4.5 scenario are taken as the exposure component. Furthermore, 36.4% of all the assessed sites are found to

have high vulnerability. When the scenario is switched to SSP5-8.5, it is seen that ten sites are moved to a higher vulnerability class. There are four sites moved from the ”Low Vulnerability” class to the “Moderate Vulnerability” class, two sites are moved from the “Low Vulnerability” class to the “High Vulnerability” class, three sites are moved from the “Moderate Vulnerability” class to the “High Vulnerability” class, and one site is moved from the “High Vulnerability” class to the “Very High Vulnerability” class.

These applications show that the model provides comprehensive insights into the characteristics and conditions of the coastal cultural heritage sites and their vulnerability to sea level rise, as the characteristics of the sites in each sensitivity, potential impact and vulnerability class can be checked separately. Also, it is seen that the model allows a rapid assessment of a large set of heritage sites to be performed at once, as it was aimed.

Additionally, it is seen that when the coastal erosion impact scores are utilized as the exposure component data, instead of the overall CVI values, the majority of the assessed sites are assigned to higher vulnerability classes. The number of sites in “Moderate Vulnerability” and “High Vulnerability” classes increased considerably when the coastal erosion impact score is used instead of CVI values, based on SSP2-4.5 scenario. The percentage of sites assigned to the “High Vulnerability” class rose to 37.3%. Furthermore, when the scenario is switched to SSP5-8.5, it is seen that 23.8% of all the assessed sites are assigned to the “Moderate Vulnerability” class, and 40.1% of the sites are assigned to the “High Vulnerability” class. Hence, the possible use of simple shoreline prediction tools is discussed through coastal erosion analyses performed in the scope of this study.

Two of the assessed sites are selected as pilot sites in the scope of the TÜBİTAK-funded research project, the ancient cities of Soli-Pompeiopolis and Anemurium, and these sites are visited for both data collection and having meetings with the archaeologists working on these sites. The results obtained from the CCHVAM for these sites are checked in detail, and the shoreline evolution observed in the last eight

years in these sites is investigated by using the DSAS. The analyses in the DSAS are performed with two sets of transects with spacings of 50 m and 100 m for both sites. As the first step of this coastal evolution analysis, the shoreline behavior observed between 2016 and 2024 is checked, and it is seen that the average net shoreline movement observed in the shoreline directly interacting with the Anemurium Ancient City is around 5 m landward and in the shoreline directly interacting with the Soli-Pompeiopolis Ancient City is around 8.50 m landward.

Furthermore, using the LRR values obtained from this analysis, the shoreline that might be observed in 2050 is generated for both sites after checking the accuracy of the LRR values by generating the shoreline of 2024 and comparing it with the observed one through R-square values. As a result of these 2050 projections, it is found that the average distance between the shoreline observed in 2024 and the generated 2050 shoreline is 24.1 m landward in the coastline of Anemurium Ancient City, and it is 33.1 m landward in the coastline of Soli-Pompeiopolis Ancient City. Additionally, it is seen that a coastal area of 0.059 km^2 is projected to get lost due to coastal erosion along the shoreline of Anemurium Ancient City, and it is a coastal area of 0.115 km^2 along the shoreline of Soli-Pompeiopolis Ancient City.

In addition to the 2050 projections, the coastline evolution by 2100 is also projected by using the same LRR values. This projection result presented the fact that if the coastline evolution keeps going in the same trend, the remaining ancient buildings on the coasts of these regions are under a serious threat of getting damaged or destroyed. On the other hand, especially along the coastline directly interacting with the Soli-Pompeiopolis Ancient City, there are many parts where the beach in front of the residential buildings is found to be completely threatened by coastal erosion.

In the last part of this study, the coastline evolution in the Anemurium Ancient City region is investigated even further with the ShorelineS Model to analyze the effect of climate change on the coastline evolution. Comparison of the projected shoreline for the year 2050 is used to analyze the difference in the results obtained from a numerical model and a tool utilizing historical shoreline data only. DSAS analyzes

the observed trend and computes the coastline movement rate by using only the observed shorelines, whereas the ShorelineS Model generates shoreline by using an initial shoreline and the input parameters including the wave conditions, coastal structures, foreshore orientation, beach slope, RSLR, the rate of change in wave height, and more. For this projection, the model is calibrated by using the wave time-series data and simulating the coastline evolution between 2016 and 2024. Then, by using the calibrated model, the 2050 shoreline is projected. Three simulations are made: with the observed wave climate over the last fifty years only, with the wave climate and the RSLR, and with the wave climate, the RSLR, and the rate of change in wave height.

The key findings of these simulations and their comparison with the projection made with the LRR values obtained from the DSAS are listed below.

- The part of the beach where there are multiple ancient buildings and their remains is under threat of getting damaged or destroyed due to coastal erosion.
- When the observed wave climate is utilized and the RSLR is introduced as an input, the projected shoreline movement is similar to the one obtained from the projection made with the LRR values. Hence, it can be said that a similar rise in sea level observed between 2016 and 2024 is expected in the SSP5-8.5 scenario.

With the detailed coastline evolution analyses and projections, the scale and meaning of the described threat to the coastal cultural heritage sites are shown through examples. The main limitation of the analysis performed with the DSAS is the fact that the effect of the structures located in the coastal area and the climate change on sediment transport and the change in shoreline position cannot be introduced to the analysis. It only uses historical shoreline positions to provide insights into the observed trend along the assessed shoreline. However, being a numerical model, the ShorelineS Model generates a shoreline position at each time step by using a set of

input parameters describing the wave conditions, the initial coastline position, the structures located along the shoreline, climate change, and more.

The results of these analyses showed that, being a much simpler tool, DSAS projected a similar change in the shoreline position in the Anemurium Ancient City to the one projected with the ShorelineS Model when the climate change-related parameters are introduced to the model. However, there are some assumptions made while the projected shoreline is generated with the ShorelineS Model. The major assumption is that the effect of the regulated river on the east side of the assessed shoreline segment is neglected. It is because the satellite images of the last three decades are checked, and it is seen that the overall trend along the shoreline is erosion, and the river has not caused any major change in the shoreline position. On the other hand, the projection made with the ShorelineS Model can be improved by using spatially varying parameters as input to minimize the assumptions.

Overall, this study shows that the newly developed CCHVAM enables the vulnerability assessment of coastal cultural heritage sites to be performed quickly and efficiently, providing a systematic output describing the characteristics and conditions of the assessed sites. Also, the model makes the rapid assessment on a national scale possible. However, the major challenge encountered while developing this vulnerability assessment model is the data availability. In the literature review, it is found that there are a number of indicators recommended to assess the sensitivity and adaptive capacity of the coastal heritage sites. However, most of them require a site-specific approach, and the model introduced in this study aims to provide an assessment on a national scale. Hence, in future studies, the development of a detailed and up-to-date dataset on the heritage sites is the primary recommendation for the additional indicators recommended in the literature, such as the budget for the conservation of heritage sites and the level of public awareness about the heritage sites and climate change, then the framework of the model can be improved with the new indicators. It is also recommended that investigating other possible indicators, conducting surveys asking for experts' opinions, and creating comprehensive datasets are recommended for a comprehensive and more detailed assessment.

Finally, the improvement and use of the CCHVAM are recommended for enhancing the resilience of the assessed cultural heritage sites. The output of the model can accelerate the planning stage of the actions for the conservation of the coastal heritage sites, and it can also be utilized as a guide for detailed site-specific assessments. This will enable the heritage of ancient civilizations to endure for future generations, allowing them to get inspired by the knowledge and experience that these ancient cities possess.

REFERENCES

Akar, T. 2021. Kent içinde arkeolojik miras: Mersin-Mezitli'de kaya mezarları rölöve ve konservasyon projesi. *Çukurova Araştırmaları*, 7(2), 262-276. https://dx.doi.org/10.29228/cokar.515530

Alcaras, E., Errico, A., Falchi, U., Parente, C., Vallario, A. 2020. Coastline extraction from optical satellite imaginery and accuracy evaluation. R3 in Geomatics: Research, Results and Review. R3GEO 2019. *Communications in Computer and Information Science*, vol 1246. Springer, Cham. https://doi.org/10.1007/978-3-030-62800-0_26

Anderson, D. G., Bissett, T. G., Yerka, S., Wells, J. J., Kansa, E., Kansa, S. W., Myers, K. N., DeMuth, R. C., White, D. 2017. Sea-level rise and archaeological site destruction: An example from the southeastern United States using DINAA (Digital Index of North American Archaeology). PLOS ONE, 12(11). Doi: 10.1371/journal.pone.0188142

Ashmore, P. 1994. Archaeology and the Coastal Zone. *Toward a Historic Scotland Policy*, Edinburgh: Historic Scotland.

C3S. (2018). *ERA5 hourly data on single levels from 1940 to present* [Dataset]. Copernicus Climate Change Service (C3S) Climate Data Store (CDS). https://doi.org/10.24381/CDS.ADBB2D47

Carslaw, K. S. 2022. *Aerosols and Climate*. Elsevier:https://doi.org/10.1016/B978-0-12-819766-0.09989-2

Cassar, J. 2016. Climate change and archaeological sites: Adaptation strategies. InR.-A. Lefèvre & C. Sabbioni (Eds.), Cultural heritage from pollution to climate change. pp.119–127. Edipuglia srl.

Causes of Climate Change. n.d. European Commission: Energy, Climate, Environment. Retrieved from https://climate.ec.europa.eu/climate-change/causes-climate-

change_en#:~:text=The%20main%20driver%20of%20climate,space%20and%20causing%20global%20warming. Data of Access: February 2025

Ciantelli, C., Palazzi, E., von Hardenbeg, J., Vaccaro, C., Tittarelli, F., Bonazza, A. 2018. *Geosciences*. 8, 296, https://doi.org/10.3390/geosciences8080296

CLS & Aviso+ (dist.). 2024. MSS_CNES_CLS18. https://www.aviso.altimetry.fr/

Coastal Erosion. U.S. Climate Resilience Toolkit. Retrieved from https://toolkit.climate.gov/coastal-erosion, last visited in March 2025.

Daire, M. Y., Lopez-Romero, E., Proust, J. N., Regnauld, H., Pian, S., Shi, B. 2012. Coastal Changes and Cultural Heritage (1): Assessment of the Vulnerability of the Coastal Heritage in Western France. *The Journal of Island and Coastal Archaeology*.https://doi.org/10.1080/15564894.2011.652340

Daly, Cathy. 2014. A Framework for Assessing the Vulnerability of Archaeological Sites to Climate Change: Theory, Development, and Application. *Conservation and Management of Archaeological Sites*. 16. 268-282. 10.1179/1350503315Z.00000000086.

Danforth, W.W., Thieler, E.R. 1992. Digital Shoreline Analysis System (DSAS) User's Guide. Version 1.0. Reston, Virginia: *U.S. Geological Survey Open-File Report No. 92-355, 42p.*

Day, J. C., Heron, S. F., Markham, A. 2020. Assessing the climate vulnerability of the world's natural and cultural heritage. *Parks Stewardship Forum*. 36(1). Doi: 10.5070/P536146384

Devlet Su İşleri Generl Müdürlüğü (DSİ) 6. Bölge Müdürlüğü. 2021. DSİ'nin Alaköprü Sulama Projesiyle Yüzler Gülüyor. https://bolge06.dsi.gov.tr/Haber/Detay/4684#

Dogan, Y., Tekeli, M. 2024. The Impact of Local Community Attitudes Towards Sustainable Tourism Development on Tourism Development Support.

Journal of Tourism and Gastronomy Studies, 12 (2), 1089-1104. https://doi.org/10.21235/jotags.2024.1426

Durie, A., Khamis, H. 2025. 'I trust my eyes, not the forecast': Alexandria is sinking. Why don't local fisheries believe it? *Guardian*. Retrieved from https://www.theguardian.com/environment/2025/mar/20/rising-sea-levels-alexandria-egypt-nile-delta-sinking-climate-el-max-fishing?

El-Kafrawy, S., Soliman, A. 2017. Performance evaluation of shoreline extraction methods based on remote sensing data. *Journal of Geography Environment and Earth Science International*. DOI:: 10.9734/JGEESI/2017/36233

EMODnet Digital Bathymetry (DTM 2024) Retrieved from https://emodnet.ec.europa.eu/geonetwork/srv/eng/catalog.search#/metadata/cf51df64-56f9-4a99-b1aa-36b8d7b743a1 Date of access: February 2025.

Esri. *Data classification methods*. ArcGIS Pro Help. Retrieved from https://pro.arcgis.com/en/pro-app/latest/help/mapping/layer-properties/data-classification-methods.html. Accessed on December 5, 2024.

European Commission: Directorate-General for Education, Youth, Sport and Culture. 2022. *Strengthening cultural heritage resilience for climate change: where the European Green Deal meets cultural heritage*. Publications Office of the European Union. https://data.europa.eu/doi/10.2766/44688.

European Commission, Cassar, M., Sabbioni, C., & Brimblecombe, P. (2010). *The atlas of climate change impact on European cultural heritage : scientific analysis and management strategies*, (M. Cassar,editor. C Sabbioni, editor, P.Brimblecombe, editor) Anthem Press. https://data.europa.eu/doi/10.2777/11959

European Environment Agency. (2020). *Coastal Zones Land Cover/Land Use 2018 (vector), Europe, 6-yearly, Feb. 2021* (Version 01.00) [Geopackage]. European Environment Agency. https://doi.org/10.2909/205E2DB2-4E35-4B1B-BF84-271C4A82248C

European Space Agency & Airbus. (2022). *Copernicus DEM* [Dataset]. https://doi.org/10.5270/ESA-c5d3d65

Ezcurra, P., Rivera-Collazo, I. C. 2018. An assessment of the impacts of climate change on Puerto Rico's Cultural Heritage with a case study on sea-level rise. *Journal of Cultural Heritage*. 32, 198-209. Doi: 10.1016/j.culher.2018.01.016.

Forino, G., Mackee, J., von Meding, J. 2016. A proposed assessment index for climate change-related risk for cultural heritage protection in Newcastle. *International Journal of Disaster Risk Reduction*. 19, 235-248. https://doi.org/10.1016/j.ijdrr.2016.09.003.

Fraile Jurado, P., Sánchez Rodríguez, E., Fernández Díaz, M., Pita López, M. F., & López Torres, J. M. 2015. Estimation of the future behaviour of the sea level in the Canary Islands from the analysis of recent records. *Geographicalia, 66,* 79-98. https://doi.org/10.26754/ojs_geoph/geoph.2014661066

Himmelstoss, E.A., Henderson, R.E., Kratzmann, M.G., and Farris, A.S. 2021. Digital Shoreline Analysis System (DSAS) version 5.1 user guide: *U.S. Geological Survey Open-File Report 2021–1091, p. 104*. https://doi.org/10.3133/ofr20211091.

ICOMOS Climate Change and Cultural Heritage Working Group International. 2019. *The Future of Our Pasts: Engaging cultural heritage in climate action Outline of Climate Change and Cultural Heritage (- International Council on Monuments and Sites - ICOMOS & H. Wilson, Eds.).* International Council on Monuments and Sites - ICOMOS. http://openarchive.icomos.org/id/eprint/2459/

Ince, A. 2024. *Application of fuzzy logic based coastal vulnerability model in coastal cultural heritage sites in Turkey*. METU Civil Engineering Department. MSc Thesis.

Intergovernmental Panel on Climate Change. 2014. *Summary for policymakers in Climate Change 2014: Impacts, Adaptation, and Vulnerability. Part A:*

Global and Sectoral Aspects. Contribution of Working Group II to the Fifth Assessment Report of the Intergovernmental Panel on Climate Change. 1-32.

IPCC, 2021. *Climate Change 2021: The Physical Science Basis. Contribution of Working Group I to the Sixth Assessment Report of the Intergovernmental Panel on Climate Change* [Masson-Delmotte, V., P. Zhai, A. Pirani, S.L. Connors, C. Péan, S. Berger, N. Caud, Y. Chen, L. Goldfarb, M.I. Gomis, M. Huang, K. Leitzell, E. Lonnoy, J.B.R. Matthews, T.K. Maycock, T. Waterfield, O. Yelekçi, R. Yu, and B. Zhou (eds.)]. Cambridge University Press. In Press.

Jenks, G. F. 1967. The data model concept in statistical mapping. *International Yearbook of Cartography*. 7. 186-190.

Karaca, M., Nicholls, R.J. 2008. "Potential implications of accelerated sea-level rise for Turkey." *Journal of Coastal Research*. 242: 288-298.

Kratzmann, M.G., & Thieler, E.R. 2010. Digital Shoreline Analysis System (DSAS) version 4.0: An ArcGIS extension for calculating shoreline change. *USGS Open-File Report 2010-1179*.

Kuleli, T. 2010. "City-based risk assessment of sea level rise using topographic and census data for the Turkish coastal zone". *Estuaries and Coasts*. 33: 640-651.

Li, Y., Jia, X., Zhen Liu, Luo Zhao, Zhou, X., & Storozum, M. J. 2022. The potential impact of rising sea levels on China's coastal cultural heritage: A GIS risk assessment. *Antiquity*, 1–16. Doi: 10.15184/aqy.2022.1

Losada, I., Izaguirre, C., & Díaz, P. 2014. Cambio climático en la costa española. *Oficina Española de Cambio Climático, Ministerio de Agricultura, Alimentación y Medio Ambiente: Madrid, Spain*, *133*.

Maglione, P., Parente, C., Vallario, A. 2014. Coastline extraction using high resolution WorldView-2 satellite imagery. *European Journal of Remote Sensing*, 47:1, 685-699. DOI: 10.5721/EuJRS20144739

Marzeion, B., Levermann, A. 2014. Loss of cultural world heritage and currently inhabited places to sea-level rise. *Environmental Research Letters*. Doi: 10.1088/1748-9326/9/3/034001

Mediterranean UNESCO World Heritage at-risk from coastal flooding and erosion due to sea-level rise. 2018. *Nature Communications*. 9. Doi: 10.1038/s41467-018-06645-9

Mersin Provincial Directorate of Culture and Tourism. n.d. *Soli-Pompeiopolis-Mersin*. Retrieved from https://www.kulturportali.gov.tr/turkiye/mersin/gezilecekyer/soli-pompeipolis

Özyurt, G. 2010. *Fuzzy Vulnerability Assessment of Coastal Areas to Sea Level Rise*. METU Civil Engineering Department. PhD Thesis.

Reimann, L., Vafeidis, A. T., Brown, S., Hinkel, J., & Tol, R. S. J. 2018. Mediterranean UNESCO World Heritage at risk from coastal flooding and erosion due to sea-level rise. *Nature Communications*. 9(1), 4161-4161. Doi: 10.1038/s41467-018-06645-9

Roelvink, D., Huisman, B., Elghandour, A. 2018. *Efficient modelling of complex coastal evolution at monthly to century time scales*. Sixth International Conference on Estuaries and Coasts

Roelvink, D., Huisman, B., Elghandour, A., Ghonim, M., Reyns, J. 2020. Efficient Modeling of Complex Sandy Coastal Evolution at Monthly to Century Time Scales. *Frontiers in Marine Science*. 7:535. doi: 10.3389/fmars.2020.00535

Roelvink, D., Huisman, B. 2024. ShorelineS Technical Reference.

Saaty, T. L. 1990. How to make a decision: The analytic hierarchy process. European Journal of Operational Research. 48. p.9-26. http://dx.doi.org/10.1016/0377-2217(90)90057-I

Sánchez, F. G., Sánchez, H. G., Ribalaygua, C. 2020. Cultural heritage and sea level rise threat: Risk assessment of coastal fortifications in the Canary Islands. *Journal of Cultural Heritage*. Volume 44. p.211-217. https://doi.org/10.1016/j.culher.2020.02.005.

Sesana, E., Gagnon, A.S., Bertolin, C., & Hughes, J. J. 2018. Adapting Cultural Heritage to Climate Change Risks: Perspectives of Cultural Heritage Experts in Europe. *Geosciences*. 8(8):305. Doi: 10.3390/geosciences8080305

Sesana, E., Gagnon, A. S., Bonazza, A. & Hughes, J. J. 2020. An integrated approach for assessing the vulnerability of World Heritage Sites to climate change impacts. *Journal of Cultural Heritage*. 41, 211-224. Doi: 10.1016/j.culher.2019.06.013

Sesana, E., Gagnon, A. S., Ciantelli, C., Cassar, J., & Hughes, J. 2021. Climate Change Impacts on cultural heritage: A literature review. *WIREs Climate Change*. 12(4). Doi: 10.1002/wcc.710

Soli Pompeiopolis Antik Kenti'nde Kazı Çalışmaları Devam Ediyor. November 25, 2023. IHA News. Retrieved from https://www.iha.com.tr/mersin-haberleri/soli-pompeipolis-antik-kentinde-kazi-calismalari-devam-ediyor-44526051. Date of Access: November 12, 2024.

Tekocak, M. (2021). Anemurium Antik Kenti'nde Kültürel Mirası Koruma ve Yaşatma Çalışmaları. *Kültürel Miras Araştırmaları*, 2(1), 1-15.

Temiz, G. M. September 7, 2021. Mersin'deki kazılarda gökbilimci ve şair Aratos'un anıt mezarının olduğu değerlendirilen yapının zeminine ulaşıldı. Anadolu Ajansı. Retrieved from https://www.aa.com.tr/tr/kultur-sanat/mersindeki-kazilarda-gok-bilimci-ve-sair-aratosun-anit-mezarinin-oldugu-degerlendirilen-yapinin-zeminine-ulasildi/2357125. Date of Access: November 12, 2024.

The World Meteorological Organization (WMO) . 2024. State of the Climate 2024 – Update for COP29. *Climate Action Report.* Retrieved from https://www.un.org/en/climatechange/reports/sea-level-rise

Thieler, E.R., Himmelstoss, E.A., Zichichi, J.L., & Ergul, A. 2005. Digital Shoreline Analysis System (DSAS) version 2.0: Shoreline Change Measurement Software Extension for ArcView. *USGS Open-File Report 2005-1304*.

Thieler, E.R., Himmelstoss, E.A., Zichichi, J.L., & Ergul, A. 2009. Digital Shoreline Analysis System (DSAS) version 3.0: An ArcGIS extension for calculating shoreline change. *USGS Open-File Report 2008-1278*.

Toimil, A., Camus, P., Losada, I. J., Le Cozannet, G., Nicholls, R. J., Idier, D., & Maspataud, A. 2020. Climate change-driven coastal erosion modelling in temperate sandy beaches: Methods and uncertainty treatment. *Earth-Science Reviews, 202, 103110*. https://doi.org/10.1016/j.earscirev.2020.103110

Turkish Museums. N.D. Anemurium Ancient City. Retrieved from https://www.turkishmuseums.com/museum/detail/2158-mersin-anemurium-archaeological-site/2158/4. Date of Access: November 11, 2024.

Türkiye Kültür Portalı. N.D. Soli Pompeiopolis-Mersin. Retrieved from https://www.kulturportali.gov.tr/turkiye/mersin/gezilecekyer/soli-pompeipolis. Date of Access: November 12, 2024.

UNESCO World Heritage Online Map. Retrieved from https://whc.unesco.org/en/list/?cid=31&l=en&&type=cultural. Date of Access: December 2024.

WTW Natural Catastrophe Review January – June 2024. July 2024. WTW Research Network. Retrieved from https://www.wtwco.com/en-vn/insights/2024/07/natural-catastrophe-review-january-june-2024, Date of Access: March 2025.

Zarley, A., Witte, S. & Burgess, G. 2016. Heritage At-Risk: Vulnerability of Cultural Resources along Florida's Coast to Sea Level Rise and Hurricanes.

APPENDICES

A. Assessment of the Impact of Weights Through the Schematic View

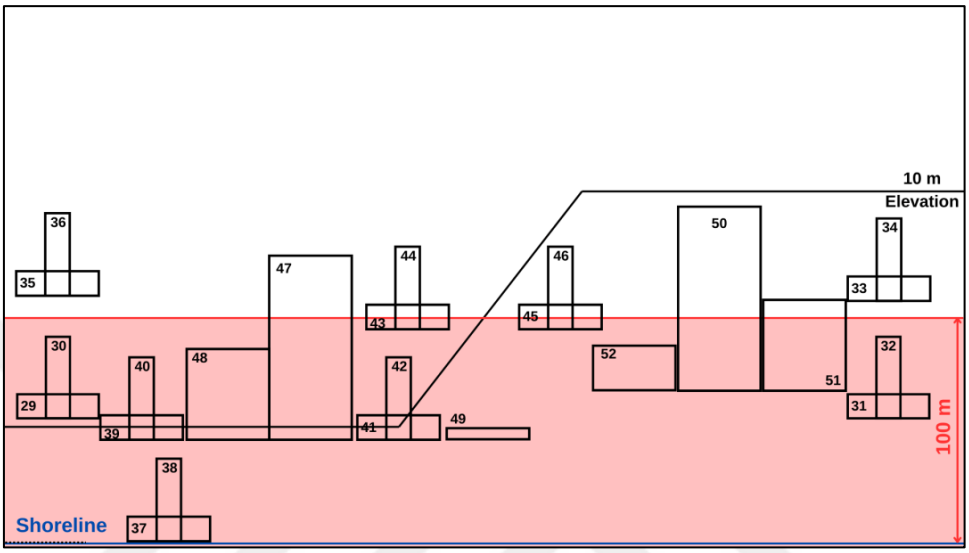


Figure 8.1. Schematic view where representative heritage sites with different positions along the coastline are shown.

The impact of assigning weights to sensitivity indicators is investigated through a sample assessment of the sites shown in the above schematic view. Without the weights, the sensitivity value of a site is computed as shown below. In Table 8.1, the computation matrix used for the assessment of Site 33 is presented.

Table 8.1. Computation matrix utilized to determine the sensitivity value of Site 33, assuming that each indicator has equal weight.

Indicator	**1**	**2**	**3**	**4**	**5**	**Sensitivity Value**	**Total**
Elevation					1	5	**13**
Area	1					1	
Proximity		1				2	
Interaction Length					1	5	

Table 8.2. The sensitivity value of each site shown in Figure 7.5 is computed as described above.

Site ID	Elevation	Area	Proximity	Interaction	Sensitivity	AHP
31	5	5	4	5	19	4,49
32	5	5	4	3	17	4,43
33	5	1	2	5	13	2,87
34	5	1	2	3	11	2,81
35	1	1	2	5	9	1,63
36	1	1	2	3	7	1,57
39	3	5	4	5	17	3,87
41	4	5	4	5	18	4,18
45	5	3	3	5	16	3,68
46	5	2	3	3	13	3,47
47	1	4	4	5	14	3,1
48	2	5	4	5	16	3,56
49	5	5	4	5	19	4,49

The sensitivity values given in the column "AHP" are computed by using the weights determined by following the AHP described in Section 3.1.2. As an example, the computation of the sensitivity value of Site 33 is given below.

Sensitivity = 0.31*Elevation + 0.51*Proximity + 0.15*Area + 0.03*Interaction

Sensitivity = (0.31*5) + (0.51*2) + (0.15*1) + (0.03*5) = 2.87

B. Wave Climate Data

Wave Height (m)	Peak Period (s)	Wave Direction	Prob. of Occ.	Sum EF
8.4468693e-01	5.0598151e+00	1.4190506e+01	6.6747596e+00	2.8884647e+07
6.7020948e-01	4.7009777e+00	5.2814066e+01	1.1435668e+01	2.8945170e+07
9.2920354e-01	4.9898168e+00	7.5453157e+01	5.6041481e+00	2.8941508e+07
1.0689505e+00	5.1949915e+00	7.9905947e+01	4.0706137e+00	2.8964441e+07
1.1040560e+00	5.2963987e+00	8.2202435e+01	3.7442776e+00	2.8975847e+07
1.1538958e+00	5.3337425e+00	8.3909032e+01	3.4032196e+00	2.8970798e+07
1.0821177e+00	5.2647470e+00	8.5377221e+01	3.9209408e+00	2.8974905e+07
1.0082202e+00	5.1988801e+00	8.6952038e+01	4.5695236e+00	2.8946545e+07
9.5773529e-01	5.0685501e+00	8.8841936e+01	5.1952056e+00	2.8952275e+07
8.1620086e-01	4.6981828e+00	9.2346397e+01	7.7118378e+00	2.8932578e+07
7.1536834e-01	4.3369930e+00	1.0364045e+02	1.0875417e+01	2.8933389e+07
7.5915506e-01	5.0183485e+00	1.4215203e+02	8.3481524e+00	2.8941258e+07
7.6885925e-01	5.6570506e+00	1.9684018e+02	7.2202889e+00	2.8943001e+07
8.7639181e-01	5.8085026e+00	2.2215492e+02	5.4242134e+00	2.9007000e+07
1.0022103e+00	5.9493811e+00	2.3057249e+02	4.0624349e+00	2.9099205e+07
1.1001380e+00	6.0904039e+00	2.3427374e+02	3.2903514e+00	2.9072871e+07
1.0590957e+00	5.9016078e+00	2.3667462e+02	3.6641249e+00	2.9074765e+07
1.0450412e+00	5.8568494e+00	2.3851074e+02	3.7892613e+00	2.9052979e+07
1.0051998e+00	5.6622322e+00	2.3989331e+02	4.2382802e+00	2.9066142e+07
9.4100285e-01	5.5178088e+00	2.4104634e+02	4.9694694e+00	2.9104744e+07
8.9080054e-01	5.3675873e+00	2.4203296e+02	5.7022943e+00	2.9113534e+07
8.5689962e-01	5.3085700e+00	2.4285082e+02	6.2371911e+00	2.9142831e+07

Wave Height (m)	Peak Period (s)	Wave Direction	Prob. of Occ.	Sum EF
8.2337806e-01	5.2400423e+00	2.4355061e+02	6.8309757e+00	2.9088501e+07
8.0968901e-01	5.2548646e+00	2.4417173e+02	7.0632550e+00	2.9168100e+07
7.9495014e-01	5.2845582e+00	2.4472389e+02	7.2685441e+00	2.9096526e+07
7.8054814e-01	5.2962010e+00	2.4524347e+02	7.5106381e+00	2.9049986e+07
7.8900908e-01	5.3022103e+00	2.4572765e+02	7.3405180e+00	2.9043764e+07
7.9729166e-01	5.3739396e+00	2.4616571e+02	7.0828842e+00	2.9002979e+07
7.8176253e-01	5.3851813e+00	2.4658544e+02	7.3585115e+00	2.9029880e+07
7.8631966e-01	5.4587812e+00	2.4698913e+02	7.1695801e+00	2.9006338e+07
7.8071023e-01	5.4989204e+00	2.4738187e+02	7.2186532e+00	2.9001374e+07
7.6441038e-01	5.5185594e+00	2.4777809e+02	7.5016414e+00	2.8996155e+07
7.6852013e-01	5.5587916e+00	2.4817503e+02	7.3650546e+00	2.8984919e+07
7.7499179e-01	5.5884775e+00	2.4855772e+02	7.2072028e+00	2.8997442e+07
7.6243152e-01	5.6547866e+00	2.4894321e+02	7.3617830e+00	2.9007223e+07
7.4863939e-01	5.6720702e+00	2.4936130e+02	7.6079664e+00	2.8990837e+07
7.2644133e-01	5.6524206e+00	2.4980644e+02	8.1044226e+00	2.8977631e+07
7.1014185e-01	5.6498184e+00	2.5030021e+02	8.4790140e+00	2.8958448e+07
7.0039031e-01	5.6447968e+00	2.5085021e+02	8.7292868e+00	2.8974274e+07
6.9679735e-01	5.6625183e+00	2.5145561e+02	8.7963534e+00	2.8988818e+07
6.6778527e-01	5.6826224e+00	2.5215313e+02	9.5398108e+00	2.8977937e+07
6.3734407e-01	5.6851829e+00	2.5300348e+02	1.0469746e+01	2.8982359e+07
6.0925749e-01	5.6923064e+00	2.5410464e+02	1.1438122e+01	2.8970099e+07
5.6528173e-01	5.5915128e+00	2.5572369e+02	1.3526182e+01	2.8969413e+07
5.6296580e-01	5.4932472e+00	2.5846200e+02	1.3872966e+01	2.8951276e+07
5.7853850e-01	5.3270420e+00	2.6373255e+02	1.3558080e+01	2.8977043e+07
6.3790670e-01	5.4110162e+00	2.7352178e+02	1.0979288e+01	2.8978279e+07

C. Properties of Each Sensitivity Class

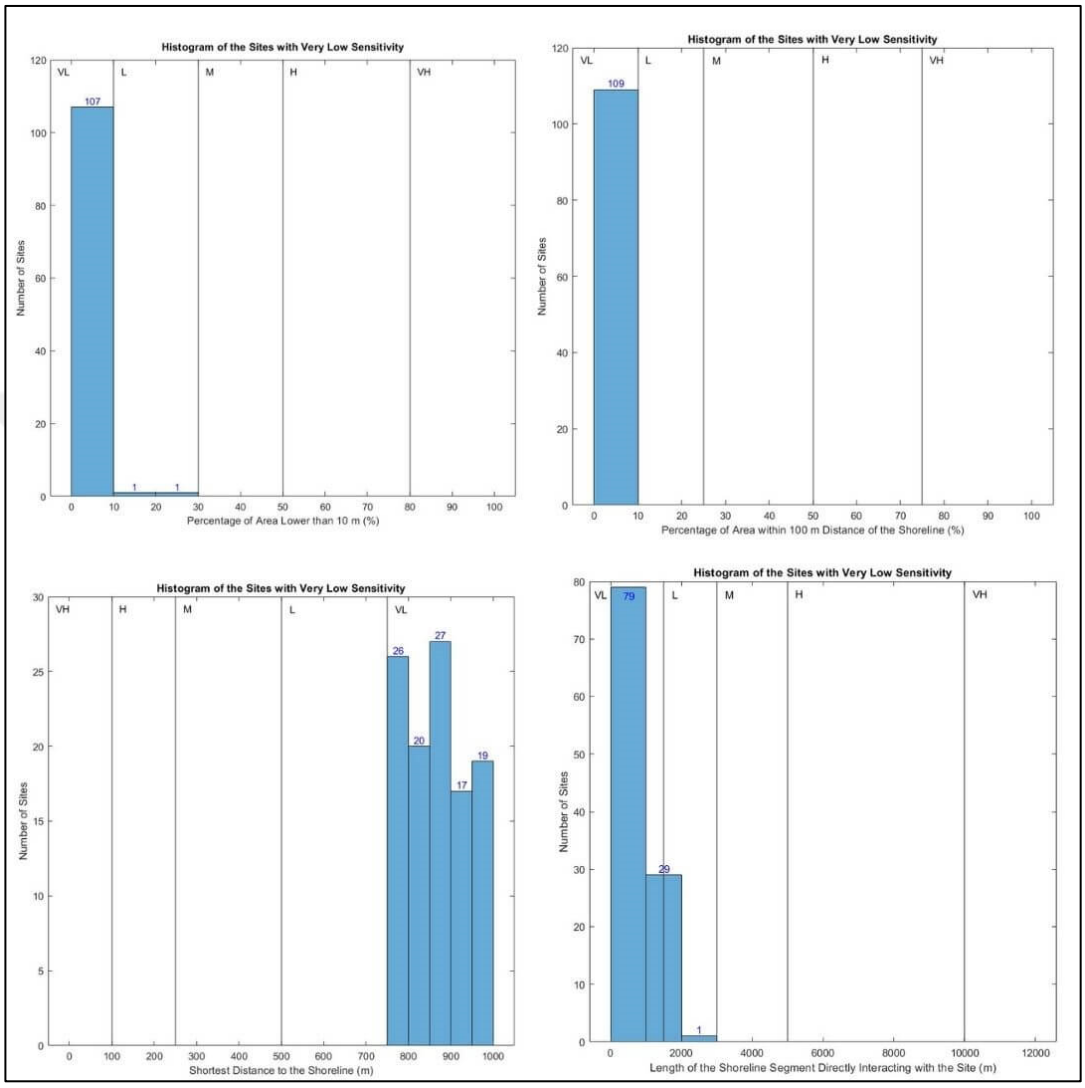


Figure 8.2. Distribution of the sites with very low sensitivity based on indicator values.

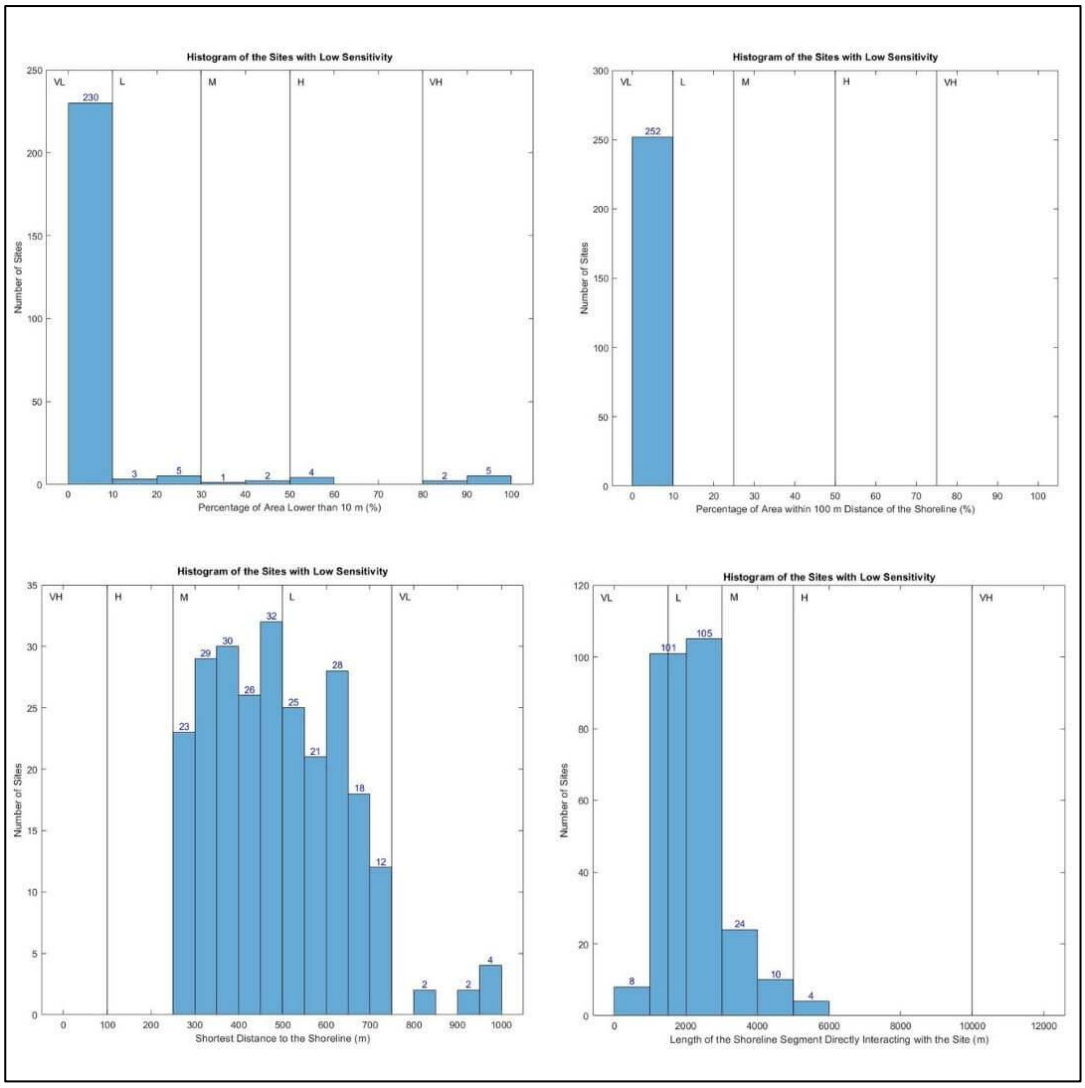


Figure 8.3. Distribution of the sites with low sensitivity based on indicator values.

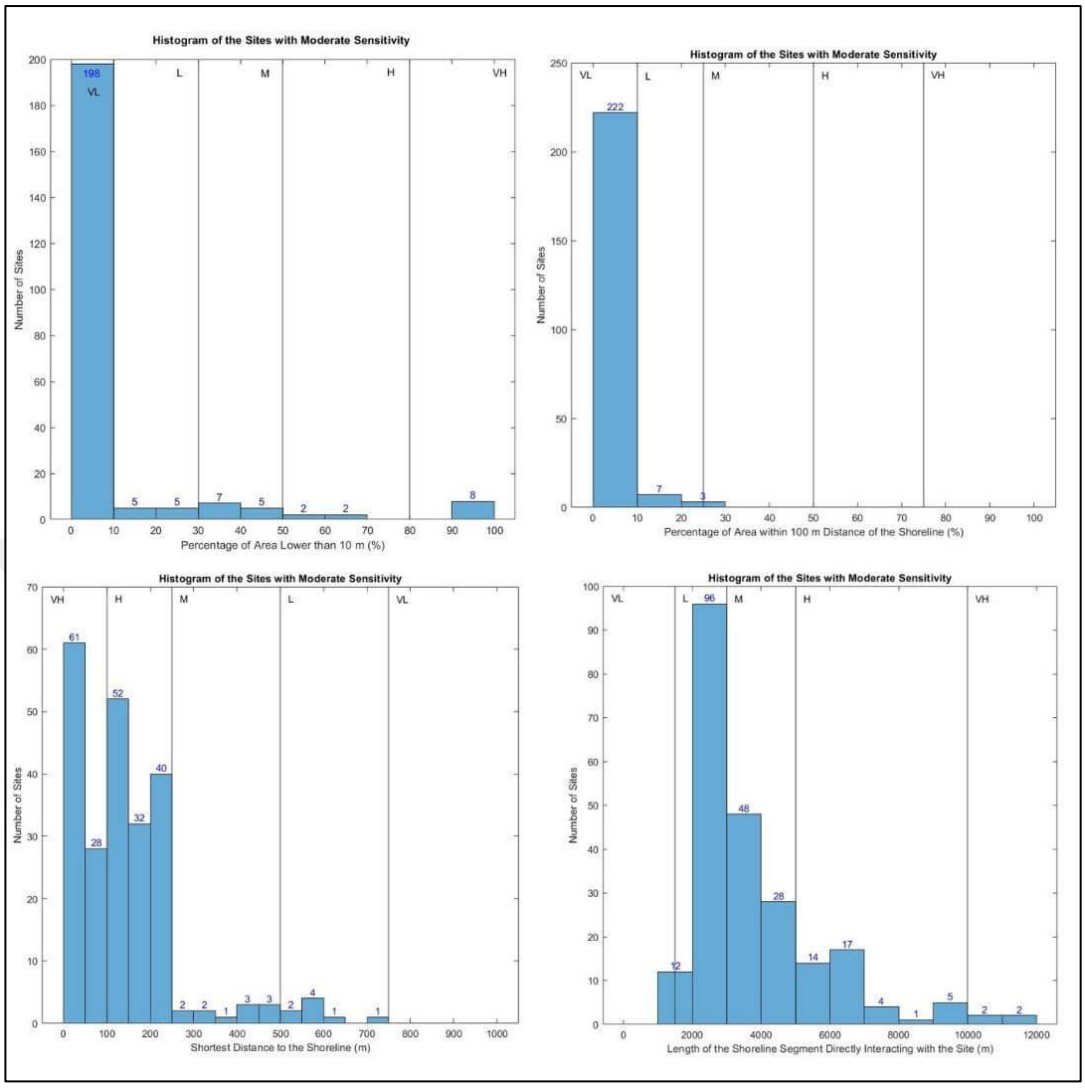


Figure 8.4. Distribution of the sites with moderate sensitivity based on indicator values.

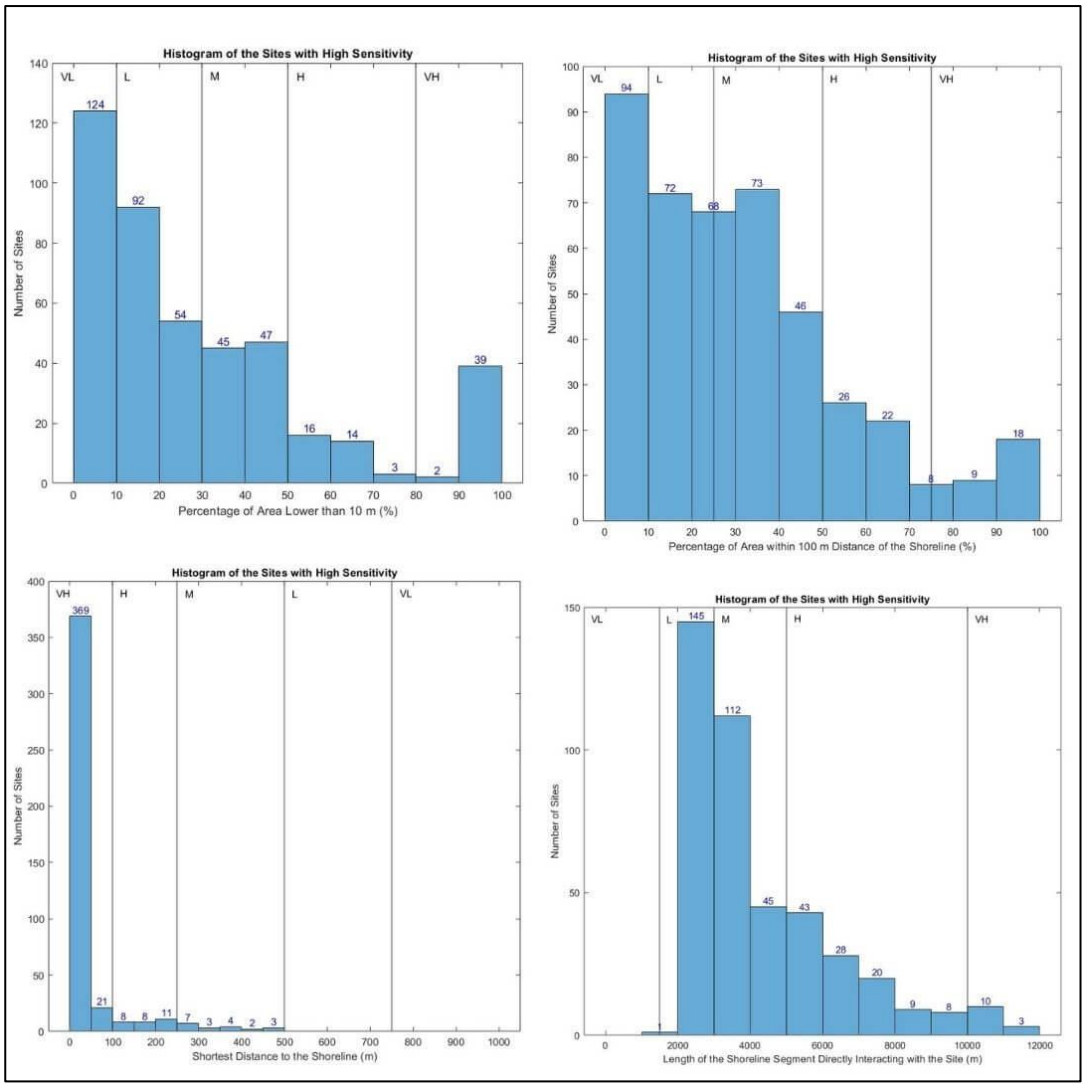


Figure 8.5. Distribution of the sites with high sensitivity based on indicator values.

D. Results of Shoreline Evolution Modeling with DSAS Using Transects with Spacings of 100 m

D.1. Anemurium Ancient City

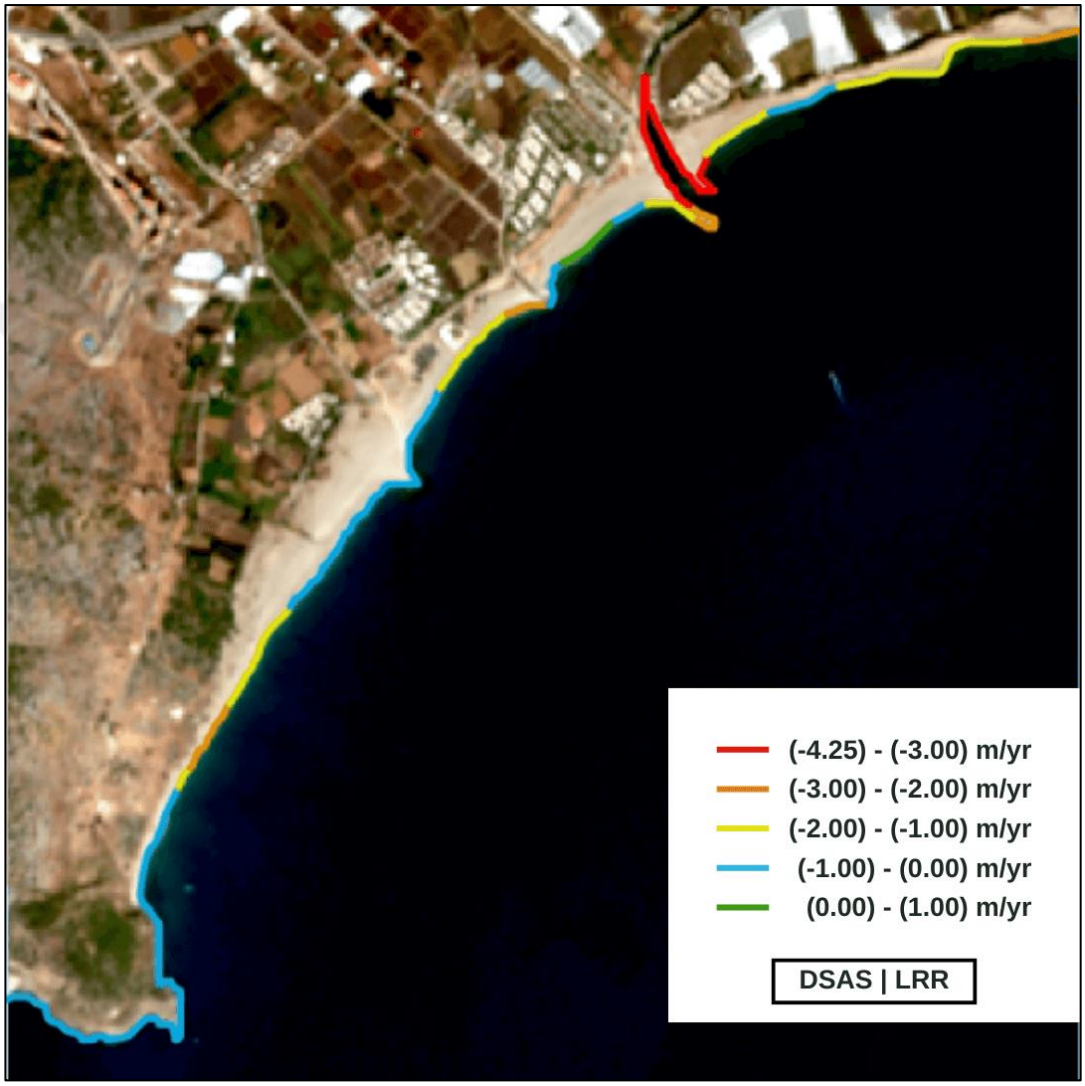


Figure 8.6. The linear regression rate of shoreline movement observed between the years 2016 and 2024, obtained from the transects with equal spacings of 100 m.



Figure 8.7. The shoreline observed in 2024 and the one projected by using the LRR values computed at the transects with 100 m spacing.



Figure 8.8. The projected 2050 shoreline (blue) and the shoreline observed in September 2024 (red) along the Anemurium Ancient City, obtained from the transects with equal spacings of 100 m.



Figure 8.9. The parts of the assessed shoreline that are projected to be eroded and accreted by the year 2050 are based on the rates computed by utilizing the transects with 100-meter spacing.

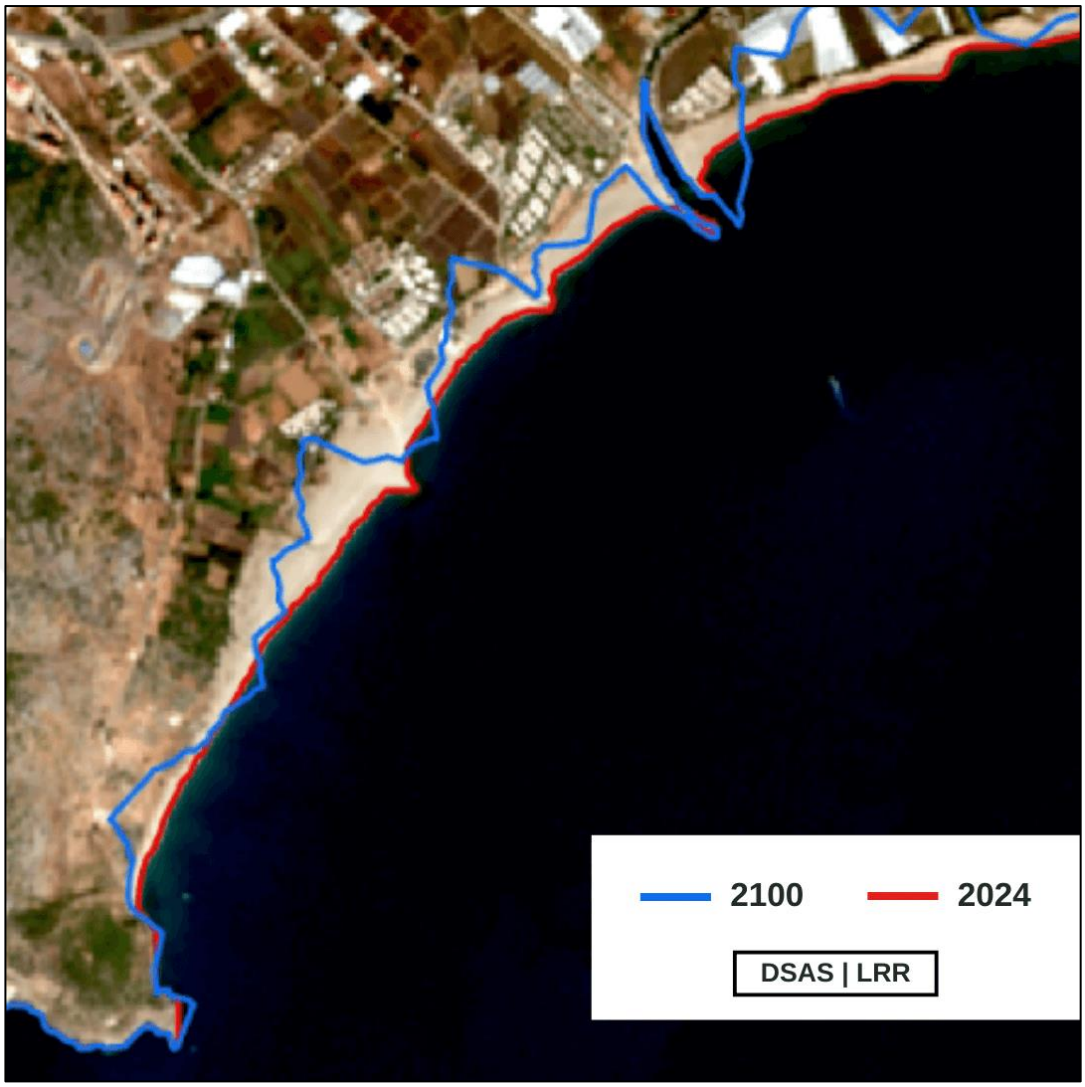


Figure 8.10. The projected 2100 shoreline (blue) and the shoreline observed in September 2024 (red) along the Anemurium Ancient City, obtained from the transects with equal spacings of 100 m.



Figure 8.11. The parts of the assessed shoreline that are projected to be eroded and accreted by the year 2100 are based on the rates computed by utilizing the transects with 100-meter spacing.

D.2. Soli-Pompeiopolis Ancient City



Figure 8.12. The linear regression rate of shoreline movement observed between the years 2016 and 2024, obtained from the transects with equal spacings of 100 m.



Figure 8.13. The shoreline position observed in 2024 and the projected one using the LRR values computed at transects with 100 m of spacing.



Figure 8.14. The projected 2050 shoreline (blue) and the shoreline observed in 2024 (red) along the Soli-Pompeiopolis Ancient City, obtained from the transects with equal spacings of 100 m.



Figure 8.15. The parts of the assessed shoreline that are projected to be eroded and accreted by the year 2050 are based on the rates computed by utilizing the transects with 100-meter spacing.



Figure 8.16. The projected 2100 shoreline (blue) and the shoreline observed in 2024 (red) along the Soli-Pompeiopolis Ancient City, obtained from the transects with equal spacings of 100 m.



Figure 8.17. The parts of the assessed shoreline that are projected to be eroded and accreted by the year 2100 are based on the rates computed by utilizing the transects with 100-meter spacing.